

**Project Report
ATC-122**

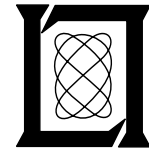
**Ground Clutter Cancellation for the
NEXRAD System**

J. E. Evans

19 October 1983

Lincoln Laboratory

MASSACHUSETTS INSTITUTE OF TECHNOLOGY
LEXINGTON, MASSACHUSETTS



Prepared for the Federal Aviation Administration,
Washington, D.C. 20591

This document is available to the public through
the National Technical Information Service,
Springfield, VA 22161

This document is disseminated under the sponsorship of the Department of Transportation in the interest of information exchange. The United States Government assumes no liability for its contents or use thereof.

1. Report No. ATC-122	2. Government Accession No.	3. Recipient's Catalog No.
4. Title and Subtitle Ground Clutter Cancellation for the NEXRAD System		5. Report Date 19 October 1983
7. Author(s) James E. Evans	6. Performing Organization Code	
9. Performing Organization Name and Address Lincoln Laboratory, M.I.T. P.O. Box 73 Lexington, MA 02173-0073	8. Performing Organization Report No. ATC-122	
12. Sponsoring Agency Name and Address Department of Commerce National Oceanographic and Atmospheric Administration National Weather Service Washington, D.C. 20910	10. Work Unit No.	
	11. Contract or Grant No. NA82AAG03351	
	13. Type of Report and Period Covered Project Report	
	14. Sponsoring Agency Code	

15. Supplementary Notes

The work reported in this document was performed at Lincoln Laboratory, a center for research operated by Massachusetts Institute of Technology, under Air Force Contract F19628-80-C-0002.

16. Abstract

Returns from the ground and associated obstacles surrounding a NEXRAD weather radar (i.e., ground clutter) will contaminate the estimates of weather echo spectral features (e.g., reflectivity, mean velocity, and spectral width). The ground clutter returns are particularly large at low elevation angles and close range (e.g., within 40 km). Additionally, the pulse repetition frequency (PRF) values necessary to obtain the desired weather Doppler features result in ground clutter contamination at ranges that are multiples of the unambiguous range interval (e.g., 115-175 km for a typical NEXRAD). Fortunately, the ground clutter power spectrum is localized around zero velocity so that one can reduce its effect by appropriate Doppler signal processing.

Automatic reduction of clutter contamination is essential if NEXRAD is to achieve the desired automatic weather product generation capability. The results of an analytical/experimental study oriented toward development of a clutter cancellation specification and associated quality assurance tests for the NEXRAD system are described.

17. Key Words Doppler weather radar weather parameter estimation low level wind shear	NEXRAD clutter obscuration	18. Distribution Statement Document is available to the public through the National Technical Information Service, Springfield, Virginia 22161.	
19. Security Classif. (of this report) Unclassified	20. Security Classif. (of this page) Unclassified	21. No. of Pages 182	22. Price

ABSTRACT

Returns from the ground and associated obstacles surrounding a NEXRAD weather radar (i.e., ground clutter) will contaminate the estimates of weather echo spectral features (e.g., reflectivity, mean velocity and spectral width). The ground clutter returns are particularly large at low elevation angles and close range (e.g., within 40 km). Additionally, the pulse repetition frequency (PRF) values necessary to obtain the desired weather Doppler features result in ground clutter contamination at ranges which are multiples of the unambiguous range interval (e.g., 115-175 km for a typical NEXRAD). Fortunately, the ground clutter power spectrum is localized around zero velocity so that one can reduce its effect by appropriate Doppler signal processing.

Automatic reduction of clutter contamination is essential if NEXRAD is to achieve the desired automatic weather product generation capability. This project memorandum describes the results of an analytical/experimental study oriented toward development of a clutter cancellation specification and associated quality assurance tests for the NEXRAD system. Specific topics include:

- (1) experimental measurements illustrating situations in which clutter cancellation will be particularly useful to NEXRAD,
- (2) quantitative criteria for clutter suppression capability based on models for distributed and discrete clutter,
- (3) degradation in weather product accuracy due to clutter,
- (4) hardware tests to demonstrate that the desired clutter cancellation capability can be achieved,
- (5) examples of achievable clutter cancellation using data from the MIT and NSSL S-band weather radar sites, and
- (6) additional clutter suppression features which may be necessary in an operational NEXRAD.

Acknowledgment

The development of the specification and its rationale was aided significantly by animated discussions with J. Anderson, D. Sirmans and K. Glover. The continued support of the NEXRAD Joint System Program Office (JSPO) (especially J. Sowar, R. Jacobsen and T. Durham) was appreciated as the deadlines grew near.

The MIT clutter data was obtained by W.H. Drury with the assistance of R.M. Lang while D. Sirmans and S. Dooley obtained the NSSL data. B.E. Forman and B.J. Gonsalves wrote and used the bulk of the software for analysis of clutter data from the MIT and NSSL sites. The manuscript was ably typed by B. Farino with assistance on the figures from M.A. Dalpe'.

LIST OF ACRONYMS AND ABBREVIATIONS

A/D	Analog to Digital
AGL	Above Ground Level
AP	Anomalous Propagation
ARTCC	Air Route Traffic Control Center
ASR	Airport Surveillance Radar
ATC	Air Traffic Control
COHO	Coherent Local Oscillator
CRPL	National Bureau of Standards Central Radio Propagation Laboratory
dBz	Wavelength Corrected Volume Reflectivity Factor with Respect to $1 \text{ mm}^6/\text{m}^3$
E1	Elevation
FAATC	Federal Aviation Administration Technical Center
FIR	Finite Impulse Response
IF	Intermediate Frequency
IIR	Infinite Impulse Response
JDOP	Joint Doppler Operational Project
JSPO	Joint System Program Office
LLWS	Low Level Wind Shear
LTI	Linear Time Invariant
MA	Massachusetts
MT _s	Maximum Dwell Time
MDS	Minimum Detectable Signal
M/S	Meters Per Second
NEXRAD	Next Generation Weather Radar
NSSL	National Severe Storms Laboratory
NWS	National Weather Service
NTR	NEXRAD Technical Requirements
OK	Oklahoma
PP	Pulse Pair
PRF	Pulse Repetition Frequency
R _c (), R _w ()	Clutter and weather auto-correlation function
RDA	Radar Data Acquisition
RF	Radio Frequency
RFP	Request for Proposal

LIST OF ACRONYMS AND ABBREVIATIONS (Continued)

S/C	Signal-to-Clutter Power Ratio
SNR	Signal-to-Noise Ratio
STALO	Stable Local Oscillator
STC	Sensitivity Time Control
V_a	Unambiguous Velocity
V_{av}	Weather Mean Velocity
V_p	Low Pass Filter Stopband
σ_v	Weather Spectrum Width

CONTENTS

	<u>Page</u>
Abstract	iii
I. INTRODUCTION	1-1
A. Background	1-1
B. Program Tasks	1-3
1. Specification Development	1-3
2. Quality Assurance Section Development	1-4
3. Supporting Analyses	1-4
C. Outline of Remainder of the Report	1-4
II. CLUTTER PROBLEM TO NEXRAD	2-1
III. RELATIONSHIP OF WEATHER PARAMETERS AND CLUTTER SUPPRESSION CAPABILITY TO RADAR PARAMETERS	3-1
A. Weather Parameter Estimation	3-1
B. Relationship of Clutter Characteristics to Radar Parameters	3-5
C. Relationship of Clutter Suppression to Weather Parameter Estimates	3-7
IV. CLUTTER SUPPRESSION CAPABILITY	4-1
A. General Approach to Specification Development	4-1
B. Rationale for Doppler Parameter Specification	4-8
C. Rationale for Reflectivity Estimate Specification	4-8
V. CLUTTER MODELS	5-1
A. Homogeneous Distributed Clutter	5-1
1. Received Power Levels	5-1
2. Amplitude Distribution of Distributed Clutter	5-3
3. Spectral Characteristics of Distributed Clutter	5-7
4. Principal Problems with the Distributed Clutter Model	5-11
B. Discrete Scatterer Model	5-11
C. Recorded Clutter Time Series	5-14
VI. RECOMMENDED HARDWARE TESTS FOR QUALITY ASSURANCE	6-1
A. Digital Simulation Tests	6-1
B. Hardware Tests	6-1

CONTENTS (Continued)

	<u>Page</u>
VII. CLUTTER SUPPRESSION PERFORMANCE OF REPRESENTATIVE FILTERS ON MODEL AND MEASURED CLUTTER DATA	7-1
A. Finite Impulse Response Filter Results for Weather and Clutter Models	7-1
B. Infinite Impulse Response (IIR) Results for Weather and Clutter Models	7-19
C. FIR Filter Results for Measured Clutter Data	7-24
1. MIT Data	7-24
2. NSSL Results	7-54
VIII. SUMMARY AND RECOMMENDATIONS FOR FUTURE WORK	8-1
A. Summary	8-1
B. Recommendations for Future Work	8-4
1. Clutter Environment Characterization	8-4
2. Implementation Issues	8-5
3. Data Editing for Clutter Residue Suppression	8-5
REFERENCES	R-1
APPENDIX A Technical Characteristics of the MIT Radar	A-1

FIGURES

<u>No.</u>		<u>Page</u>
1-1	Approaches to NEXRAD Clutter Suppression	1-5
2-1	Comparison of Rays in the CRPL Reference Refractivity Atmospheres - 1958 and the 4/3 Earth Atmosphere (from [27])	2-3
2-2	Interim Testbed Radar at M.I.T.	2-4
2-3	Relation of Interim Testbed to Boston Area Features	2-5
2-4	View from Interim Testbed Toward Logan International Airport	2-6
2-5	View from Interim Testbed Toward L.G. Hanscom Airport	2-6
2-6	View from Interim Testbed Toward Needham, MA, TV Towers	2-7
2-7	Clutter Amplitude Distributions at 0.36° Elevation Angle of MIT Meteorology Dept. S-band Radar	2-8
2-8	First Trip MIT Site S-band Clutter Above 10 dBz	2-9
2-9	First Trip MIT Site S-band Clutter Above 30 dBz	2-10
2-10	First Trip MIT Site S-band Clutter Above 50 dBz	2-11
2-11	First and Second Trip MIT Site S-band Clutter Above 30 dBz	2-13
2-12	First and Second Trip MIT Site Clutter Above 30 dBz After 20 dB Clutter Suppression	2-14
2-13	First and Second Trip MIT Site Clutter Above 30 dBz After 35 dB Clutter Suppression	2-15
2-14	Illustration of Second Trip Weather Obscuration by NSSL First Trip Clutter	2-16
3-1	Effective Number of Independent Samples For Reflectivity Measurements (from [4])	3-2
3-2	Clutter Spectrum Widths σ_{ca} Due to Antenna Rotation (Scale on Lower Axis) and σ_{cw} Due to Wind Speed (Upper Axis). Dashed Line is Through Two Estimated Data Points (from [1])	3-6
3-3	Time Waveform and Spectrum of Uniform Aperture Scatterer Return	3-8
3-4	Time Waveform and Spectrum of Circular Aperture Scatterer Return	3-9
3-5	Idealized LTI Clutter Filter Velocity Response Used to Bound Weather Parameter Errors	3-11
3-6	Computation of Errors for Idealized LTI Clutter Filter	3-12
3-7a	Reflectivity Estimate Error for Idealized Clutter Filter with 3 m/s Passband	3-13
3-7b	Reflectivity Estimate Error for Idealized Clutter Filter with 3 m/s Passband	3-14

FIGURES (Continued)

<u>No.</u>		<u>Page</u>
3-8a	Mean Velocity Error for Idealized Clutter Filter with 3 m/s Passband	3-15
3-8b	Mean Velocity Error for Idealized Clutter Filter with 3 m/s Passband	3-16
3-9a	Spectrum Width Error for Idealized Clutter Filter with 3 m/s Passband	3-17
3-9b	Spectrum Width Errors for Idealized Clutter Filter with 3 m/s Passband	3-18
3-9c	Spectrum Width Errors for Idealized Clutter Filter	3-19
3-10	Reflectivity Error for 2 m/s Passband	3-20
3-11	Mean Velocity Errors for 2 m/s Passband	3-21
3-12	Spectrum Width Errors for 2 m/s Passband	3-22
3-13	Reflectivity Errors for 1 m/s Passband	3-23
3-14	Mean Velocity Errors with 1 m/s Passband	3-24
3-15	Spectrum Width Errors with 1 m/s Passband	3-25
3-16	Magnitude of the Normalized Velocity Error Versus the Magnitude of the Signal Mean Velocity	3-28
3-17	Biased Spectrum Width When Signal and Clutter are Present	3-29
4-1	Clutter Suppression Capability Characterization for Linear Time Invariant Clutter Filtering	4-7
5-1	Backscatter Coefficients vs. Grazing Angle at 2750 MHz (from [17])	5-4
5-2	Backscatter Coefficient vs. Grazing Angle at 9405 MHz (from [17])	5-4
5-3	Comparison of Weather Return SNR with Clutter Returns	5-5
5-4	σ^* at X-Band for Cultivated Terrain at Different Times of the Year. Depression Angle 1.25° (from [18])	5-8
5-5	Characteristics of X-Band Ground Clutter (from [18])	5-9/10
5-6	Phase Variation As MIT Radar Scans by Radio Tower	5-13
6-1	Instability Residue for C-band Surveillance Radar	6-4
6-2	Instability Residue Spectrum on MIT Meteorology Dept. Radar	6-5
6-3	Envelope from Range Gate with Radio Tower	6-7
6-4	Envelope from Range Gate 0.25 nmi Away From Gate in Fig. 6-3	6-7
6-5	Power Spectrum of Data From NSSL Radar	6-8
7-1	Frequency Response for FIR Filter 1	7-3
7-2	FIR Filter #1 Suppression for Clutter Model A	7-3
7-3	FIR Filter #1 Suppression for Clutter Model B	7-5
7-4	Weather Parameter Errors with FIR Filter #1	7-6/7
7-5	Frequency Response for FIR Filter #2	7-8

FIGURES (Continued)

<u>No.</u>		<u>Page</u>
7-6	FIR Filter #2 Suppression for Clutter Model A	7-8
7-7	FIR Filter #2 Suppression for Clutter Model B	7-9
7-8	Weather Parameter Errors for FIR Filter #2	7-10/11
7-9	FIR Filter #3 Frequency Response	7-12
7-10	FIR Filter #3 Suppression for Clutter Model A	7-12
7-11	FIR Filter #3 Suppression for Clutter Model B	7-13
7-12	Weather Parameter Errors with FIR Filter #3	7-14/15/16
7-13	FIR Filter #3 Weather Parameter Errors Due to Passband Ripples	7-17
7-14	FIR Filter #3 Weather Parameter Errors Due to Passband Ripples	7-18
7-15	Frequency Response for FIR Filter #4	7-20
7-16	FIR Filter #4 Suppression for Clutter Model A	7-20
7-17	FIR Filter #4 Suppression for Clutter Model B	7-21
7-18	Reflectivity Errors with FIR Filter #4	7-22/23
7-19	Frequency Response for IIR Filter #1	7-25
7-20	IIR Filter #1 Suppression for Clutter Model A	7-25
7-21	IIR Filter #1 Suppression for Clutter Model B	7-26
7-22	Reflectivity Error with IIR Filter #1	7-27
7-23	Weather Mean Velocity Error with IIR Filter #1	7-28
7-24	Weather Spectrum Width Error with IIR Filter #1	7-29
7-25	Frequency Response for IIR Filter #2	7-30
7-26	IIR Filter #2 Suppression for Clutter Model A	7-30
7-27	IIR Filter #2 Suppression for Clutter Model B	7-31
7-28	Weather Reflectivity Errors for IIR Filter #2	7-32
7-29	Weather Velocity Errors for IIR Filter #2	7-33
7-30	Weather Spectrum Width Error with IIR Filter #2	7-34
7-31	Frequency Response for IIR Filter #3	7-35
7-32	IIR Filter #3 Suppression for Clutter Model A	7-35
7-33	IIR Filter #3 Suppression for Clutter Model B	7-36
7-34	Reflectivity Error with IIR Filter #3	7-37
7-35	Weather Mean Velocity Error with IIR Filter #3	7-38
7-36	Weather Spectrum Width Error with IIR Filter #3	7-39
7-37a	MIT Point Clutter Suppression by 2.5 m/s Stopband FIR Filter	7-40
7-37b	MIT Point Clutter Suppression by 1.7 m/s Stopband FIR Filter	7-41
7-38	Example of Suppression of Radio Tower Clutter for MIT Radar	7-42/43
7-39	Example of Suppression of Radio Tower Clutter from MIT Radar	7-44/45
7-40	Measured Clutter Suppression in 1.5 nmi Rings at MIT Site	7-51

FIGURES (Continued)

<u>No.</u>		<u>Page</u>
7-41a	Suppression of MIT Site Clutter at 19 km Range	7-55
7-41b	Suppression of MIT Site Clutter at 19 km Range	7-56
7-42	Suppression of MIT Site S-Band Clutter	7-57/58
7-43	Suppression of MIT Site S-Band Clutter	7-59/60
7-44a	NSSL Site Clutter Suppression with Stationary Antenna	7-61
7-44b	NSSL Site Clutter Suppression with Stationary Antenna	7-62
7-45a	Clutter Suppression of NSSL Site Clutter at 15 km	7-64
7-45b	Clutter Suppression of NSSL Site Clutter at 15 km	7-65
7-46a	Results of Filtering NSSL Data at Range of 4.2 km	7-66
7-46b	Results of Filtering NSSL Data at Range of 4.2 km	7-67
A-1	IF Amplifier Characteristic	A-3

TABLES

<u>No.</u>		<u>Page</u>
1-1	August 1981 NEXRAD Technical Requirements Text Associated with Ground Clutter Suppression	1-2
2-1	Altitudes for Some Salient Weather Phenomena	2-1
3-1	Typical Required Averaging Times for Weather Parameter Estimates	3-4
4-1	Recommended Clutter Suppression Capability Specification Text	4-2
4-2	Maximum Allowable Bias in Reflectivity Estimates Due to the Use of Clutter Suppression	4-3
4-3	Clutter Suppression for Radial Velocity and Spectrum Width Estimates	4-4
5-1	Land Clutter Reflectivity (0 to 1.0° Incident Angle) (from [5])	5-6
6-1	Recommended Quality Assurance Test Associated with Clutter Suppression	6-2
7-1	Parameters for Finite Impulse Response Clutter Filters	7-2
7-2	Summary Results on Suppression of Discrete Scatterer Clutter with MIT S-Band Weather Radar	7-46
7-3	Filter Statistics for Range Rings Corresponding to Fig. 7-41	7-48
7-4	Filter Statistics for Range Rings Corresponding to Fig. 7-42	7-49
7-5	Filter Statistics for Range Rings Corresponding to Fig. 7-43	7-50
7-6	Distribution of M.I.T. Clutter Spectrum Widths at Very Close Range	7-52
7-7	Distribution of M.I.T. Clutter Mean Velocities at Very Close Range	7-52
7-8	Distribution of M.I.T. Clutter Spectral Widths at Close Range	7-53
7-9	Distribution of M.I.T. Clutter Mean Velocities at Close Range	7-53
7-10	Results of Filtering NSSL Data at Range of 15 km With Antenna Stationary	7-63
7-11	Results of Filtering NSSL Data at 15 km	7-68
7-12	Results of Filtering NSSL Data at Range of 4.2 km	7-69
8-1	Clutter Suppression Against Theoretical Clutter Models Clutter Suppression (dB)	8-3
8-2	Clutter Suppression Against Measured Point Clutter Data From MIT Site	8-3
A-1	MIT Testbed Radar Characteristics	A-2

I. INTRODUCTION

A. Background

Ground clutter returns from the ground and associated obstacles (e.g., trees and buildings) surrounding a Next Generation Weather Radar (NEXRAD) will contaminate the estimates of weather echo spectral features (e.g., reflectivity, mean velocity and spectral width). These ground clutter returns are particularly large at low elevation angles and close range (e.g., within 40 km). Additionally, the pulse repetition frequency (PRF) values necessary to obtain the desired Doppler features result in ground clutter contamination at ranges which are multiples of the unambiguous range interval (e.g., 125 km - 175 km) for the JDOP (Joint Doppler Operational Project) strawman design. Fortunately, the ground clutter power spectrum is localized around zero velocity so that one can reduce its effects by appropriate Doppler signal processing.

Ground clutter can also be reduced by system siting (including the use of terrain features, trees and/or fences) to minimize the illumination of clutter sources and antenna design (especially sidelobes). These alternate approaches were not considered in this study although they would be available in the total NEXRAD design.

Automatic reduction of clutter contamination is essential if NEXRAD is to achieve the desired weather product quality. The NEXRAD system definition phase Request for Proposal (RFP) specifications (shown in Table 1-1) for the Radar Data Acquisition (RDA) system define a clutter mitigation capability in terms of suppression within certain Doppler velocity regions. This system definition phase RFP clutter performance specification was incomplete in a number of respects:

1. quantitative criteria for suppression capability were not clearly defined,
2. tolerable loss in weather product accuracy was not explicitly addressed,
3. tests/analyses to be performed by the contractor in conjunction with clutter rejection capability demonstration were not defined,
4. the use of site dependent clutter rejection (e.g., as a function of range and elevation angle) was not considered in detail, and
5. the specification implied a certain form of clutter processing (linear time invariant filter followed by pulse pair estimation [1,2]).

Many of the above difficulties were noted by the NEXRAD JSPO and/or the contractors.

TABLE 1-1. AUGUST 1981 NEXRAD TECHNICAL REQUIREMENTS
TEXT ASSOCIATED WITH GROUND CLUTTER SUPPRESSION.

3.7.1.7 Ground Clutter and Overlaid Echo Capability

The requirements for ground clutter suppression and reduction of overlaid echoes are defined in the following sections.

3.7.1.7.1 Ground Clutter Suppression

The RDA shall include ground clutter suppression for the reflectivity channel of 30 dB.

The RDA shall include ground clutter suppression for the Doppler channel with the following characteristics:

1. Ground clutter suppression: 50 dB with a stopband halfwidth of not greater than 3.0 m/s.
2. The stopband halfwidth shall be selectable: 1.0, 2.0, and 3.0 m/s with reduced clutter rejection capability for stopband halfwidths of 2 m/s and below.
3. Passband ripple: ± 1 dB maximum.

3.7.1.7.2 Reduction of Overlaid Echoes

A technique shall be provided to minimize the obscuration effect of overlaid echoes in the mean radial velocity and spectrum width estimates at ranges between 1 and 230 km.

This report describes the results of a six-month program to yield an improved specification in a time frame consistent with issuing the RFP for the validation phase (VP) of the NEXRAD program.

B. Program Tasks

The program had three principal tasks:

1. development of a revised RDA clutter suppression capability specification,
2. delineation of tests to demonstrate that the desired capability has been achieved, and
3. supporting analyses.

Each of these three tasks is described below.

1. Specification Development

The background discussion above identified a number of deficiencies with the System Definition Phase RDA clutter suppression specification. These were resolved via analytical studies, experimental measurements using NEXRAD-like radars and simulation studies.

The resulting clutter suppression capability specification includes quantitative criteria for performance against:

1. a theoretical distributed clutter model similar to that used in the National Severe Storms Laboratory (NSSL) clutter studies [1], and
2. a discrete scatterer clutter model which approximates much of the higher level clutter encountered by land-based radars.

Analytical and/or computer simulation studies were conducted to insure that the criteria developed for each of the clutter types are practically achievable.

The use of a clutter suppression technique necessarily involves a loss of weather return data. Consequently, if the clutter at the current scan's elevation angle and (possibly) range is sufficiently weak, there is no reason to use a clutter suppression technique. Consequently, the clutter suppression can be used on a range-elevation selectable basis.

The relative amount of clutter contamination which can be tolerated for reflectivity estimation is different from that for Doppler products (e.g., velocity and spectrum variance). Moreover, the capability for clutter suppression in the reflectivity channel will differ from that for Doppler data in some (but, not all) system realizations. Thus, it was

necessary to specify the clutter suppression capability separately for the reflectivity and velocity products.

During the system definition phase, it became evident that criteria were needed for clutter rejection techniques (such as spectral domain estimation) which do not use the more common approach (see Fig. 1-1) of a cascade of a linear time invariant filter followed by pulse pair processing. The criteria developed to deal with this contingency consider the degradation in weather return parameter accuracy as well as clutter suppression capability.

2. Quality Assurance Section Development

An important element of the overall specification is the tests to be performed by the contractors to demonstrate that the various performance criteria have been achieved. The digital signal processing portion of the RDA clutter rejection system can readily be assessed by computer simulations using the defined clutter models. Computer data tapes will be provided to insure that all contractors can perform some tests against the same environment.

Criteria were developed to insure that the analog radar hardware [e.g., RF and Intermediate Frequency (IF)] performance is compatible with the desired clutter rejection capability.

3. Supporting Analyses

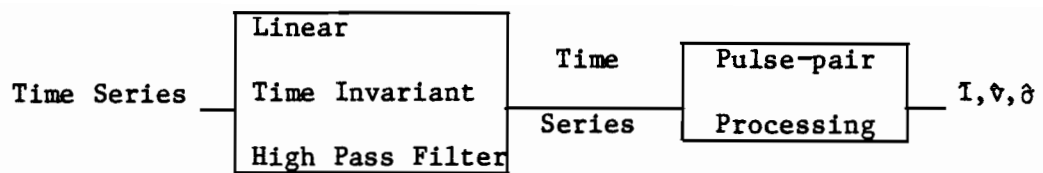
In addition to analyses which directly support the RDA specification and quality assurance material development, studies were carried out on related issues such as:

- a. relation of the clutter rejection specification numerical values to the NEXRAD weather return estimation capability,
- b. relationships/tradeoffs between clutter rejection capability and certain other key RDA parameters such as scan strategy, obscuration avoidance, PRF, desired accuracies, and
- c. definition of follow-on studies/inputs which will be needed to develop the final NEXRAD RDA requirements documents.

C. Outline of Remainder of the Report

The remainder of this report is divided into the following sections:

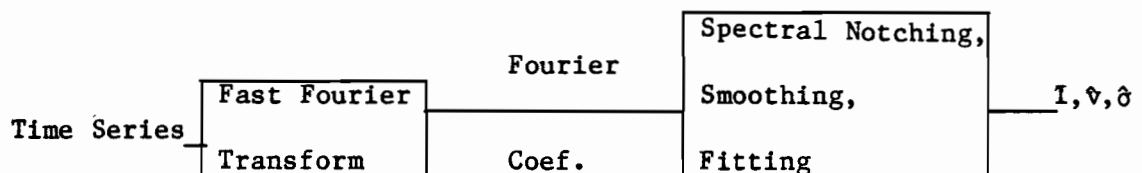
Chapter II. Clutter problems for NEXRAD (supported where possible by quantitative analyses based on measured data). Specific topics include:



Clutter Suppression

Weather Parameter
Estimation

(a) Example of a "Conventional" Clutter Suppression Technique



(b) Example of a "Nonconventional" Clutter Suppression Technique

Fig. 1-1. Approaches to NEXRAD Clutter Suppression.

- a. Obscuration of higher order trip weather by close in clutter
- b. Anomalous propagation
- c. Detectability of Low Level Wind Shear (LLWS) near airports, and
- d. Clutter characteristics for NEXRAD-like applications.

Chapter III. Relation of clutter suppression capability to other key NEXRAD RDA requirements (e.g., data rate, beam width) and the desired weather product accuracies.

Chapter IV. Criteria for clutter suppression capability and the rationale based on (1) and (2).

Chapter V. Defined clutter models for quality assurance tests and the associated rationale. This includes both theoretical models and measured I, Q data.

Chapter VI. Hardware tests for clutter suppression quality assurance and associated rationale.

Chapter VII. Clutter performance capability of representative techniques against the specified clutter models and measured clutter data.

Chapter VIII. Areas requiring additional study to develop the Preproduction Phase RDA clutter suppression specification.

II. CLUTTER PROBLEM FOR NEXRAD

The temporal (or spectral) and spatial characteristics of ground clutter have been discussed in many radar books and papers (see, for example [1,5,6]. Similarly, the effects of ground clutter on weather parameter estimates have been considered in several recent papers [1,4, 9]. In the interest of report brevity, it is assumed that the reader is conversant with the above mentioned references.

The coverage region of NEXRAD in relationship to the weather phenomena of concern is a key factor in understanding the clutter problem for NEXRAD. Figure 2-1 shows values for ray propagation altitude versus range at typical ground level refractive index values (N_s):

- (a) $N_s = 250$ is a near minimum level condition (e.g., Caribou, ME, in March)
- (b) $N_s = 301$ yields the "classical" 4/3 earth model gradient, while
- (c) $N_s = 400$ is a near maximum level (e.g., Lake Charles, LA, in July).

Table 2-1 shows the altitudes associated with some principal weather phenomena of interest for NEXRAD.

TABLE 2-1
ALTITUDES FOR SOME SALIENT WEATHER PHENOMENA

Salient Weather Phenomena	Altitude AGL(kft)
Thunderstorm	2-25
Severe thunderstorm (mesocyclone)	2-35 (2-50)
Stratiform precipitation	0-6 (below "bright band")
Gust front	0-3
Down burst	0-0.5 to 0-1 (region dependent)

If we further assume that:

- (1) the weather phenomena maximum altitude should at least correspond to the NEXRAD beam centroid,

- (2) mainlobe clutter will occur if the clutter source is within 1.0° (the half power beamwidth of the NEXRAD beam) of the beam centroid, and
- (3) typically, a significant number of clutter sources will occur at elevation angles up to $+0.5^\circ$. In hilly or mountainous regions, clutter sources can be found at elevation angles as high as 4° .

It follows from Figure 2-1 and Table 2-1 that a NEXRAD will experience a significant clutter problem in:

- detecting Low Level Wind Shear (LLWS) events such as gust fronts and down bursts in the terminal/airport region,
- estimating Doppler data at the beginning of the second, third, etc. trips (due to obscuration by close-in first trip clutter), and
- accurately estimating stratiform rain rate beyond 50 km in cases where there are hills or mountains.

Additionally, when Anomalous Propagation (AP) or ducting is present, the rays which leave the NEXRAD site at low ($<1^\circ$) elevation angles can intersect the terrain at distances up to several hundred miles, thus causing obscuration in many trips. Note, however, that first trip thunderstorms can generally be measured at elevation angles which do not involve mainlobe clutter.

The other key factors in the NEXRAD clutter problem are:

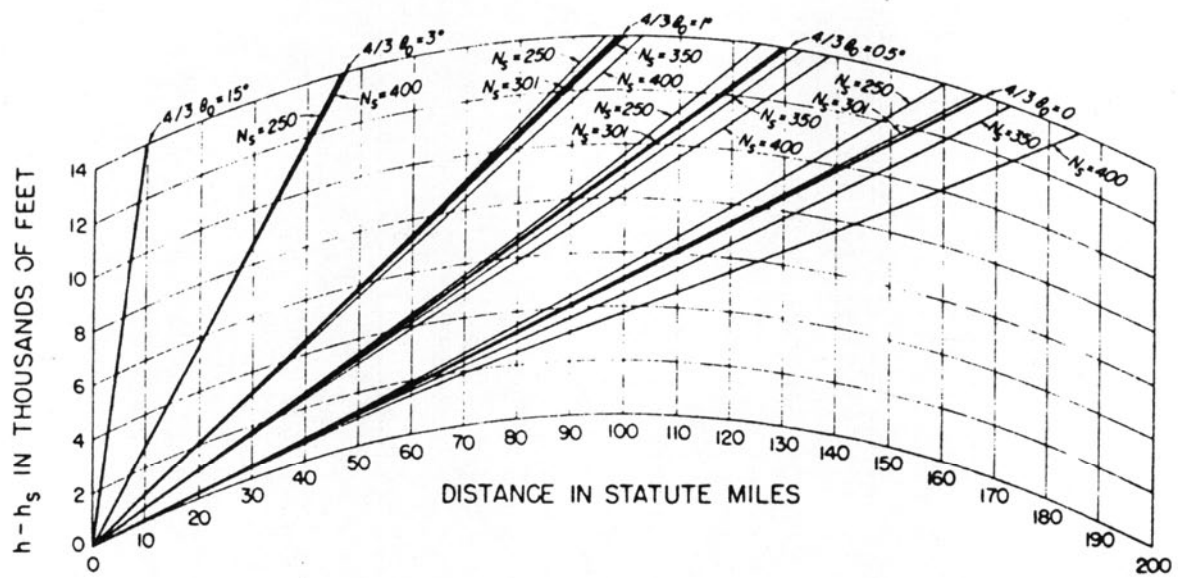
- (1) clutter levels relative to the weather reflectivity*
- (2) spatial distribution of the significant clutter, and
- (3) temporal and spectral characteristics of the clutter.

Examples of each of these for the NSSL site in Norman, OK, are presented in Hamidi and Zrnic'[1]. This site is considered to be a relatively benign clutter environment due to the lack of hills, mountains and extensive urban areas.

Figure 2-2 shows the far more challenging clutter environment of the Doppler weather radar located atop the MIT Meteorology department building in Cambridge, MA. This site is in the center of the Boston metropolitan area (Figure 2-3). Figures 2-4 to 2-6 show panoramic photographs. Clutter arises both from the many man-made structures and the approximately 150-foot-high ridge and hilly region which commences some 6 miles to the west of the radar.

Figures 2-7 to 2-10 show typical clutter levels for this site converted to dBz. We see that much of the clutter at close range has an

*Chapter V discusses clutter levels for idealized distributed clutter sources; however, we consider the results on actual sites to be far more relevant for the operationally oriented users.



N_s = refractive index at surface

θ_0 = elevation angle at NEXRAD site

Fig. 2-1. Comparison of Rays in the CRPL Reference Refractivity Atmospheres - 1958 and the 4/3 Earth Atmosphere (from [27]).

113790-R



2-4

Fig. 2-2. Interim testbed at M.I.T.

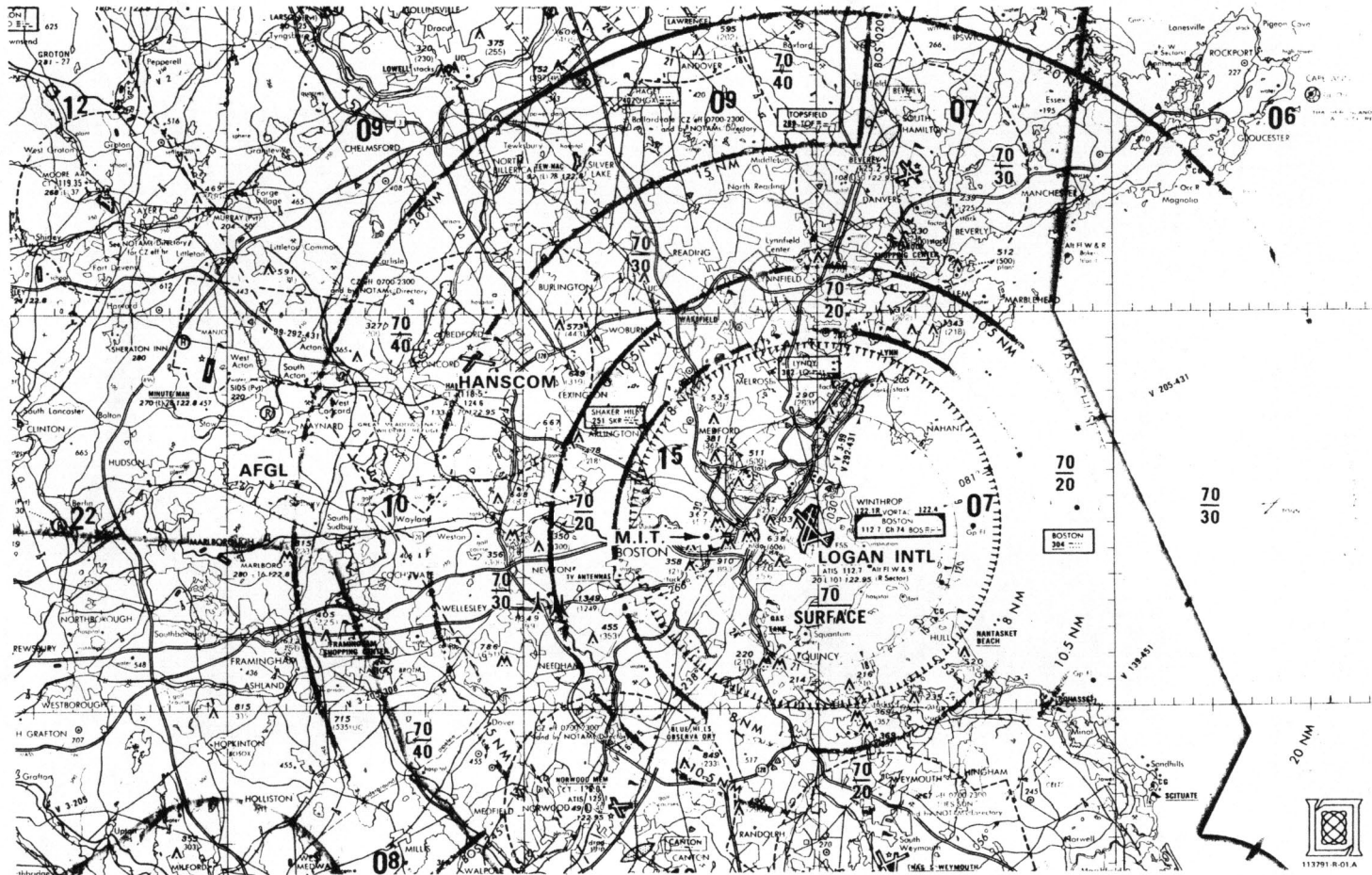


Fig. 2-3. Relation of interim testbed to Boston area features.

113942-R

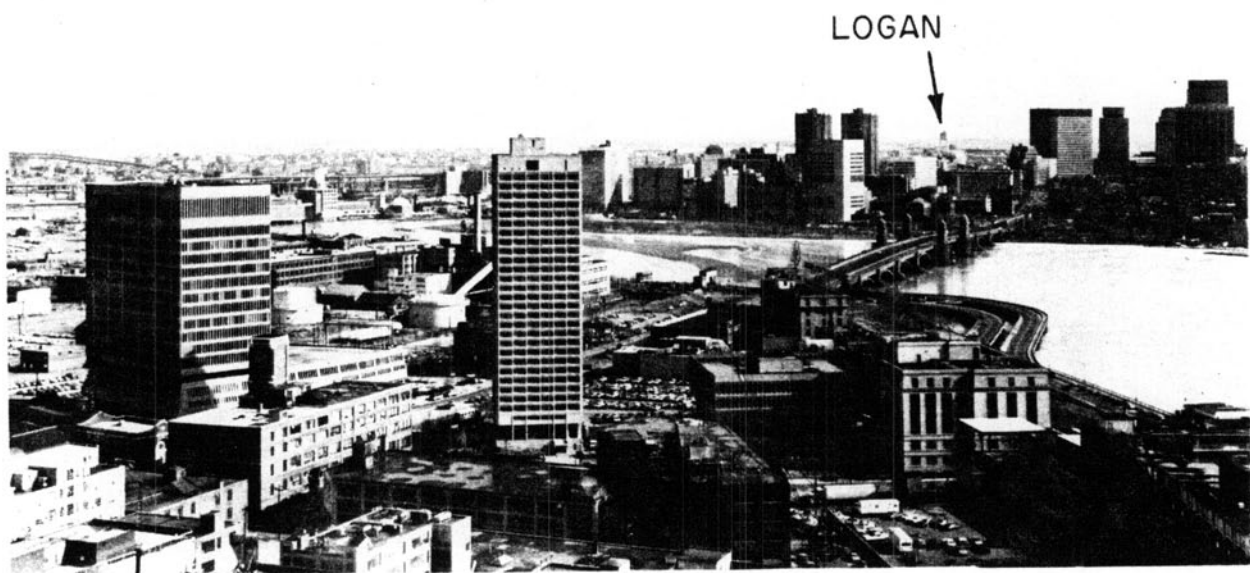


Fig. 2-4. View from interim testbed toward Logan International Airport.

113943-R



Fig. 2-5. View from interim testbed toward L. G. Hanscom Airport.

113944-R

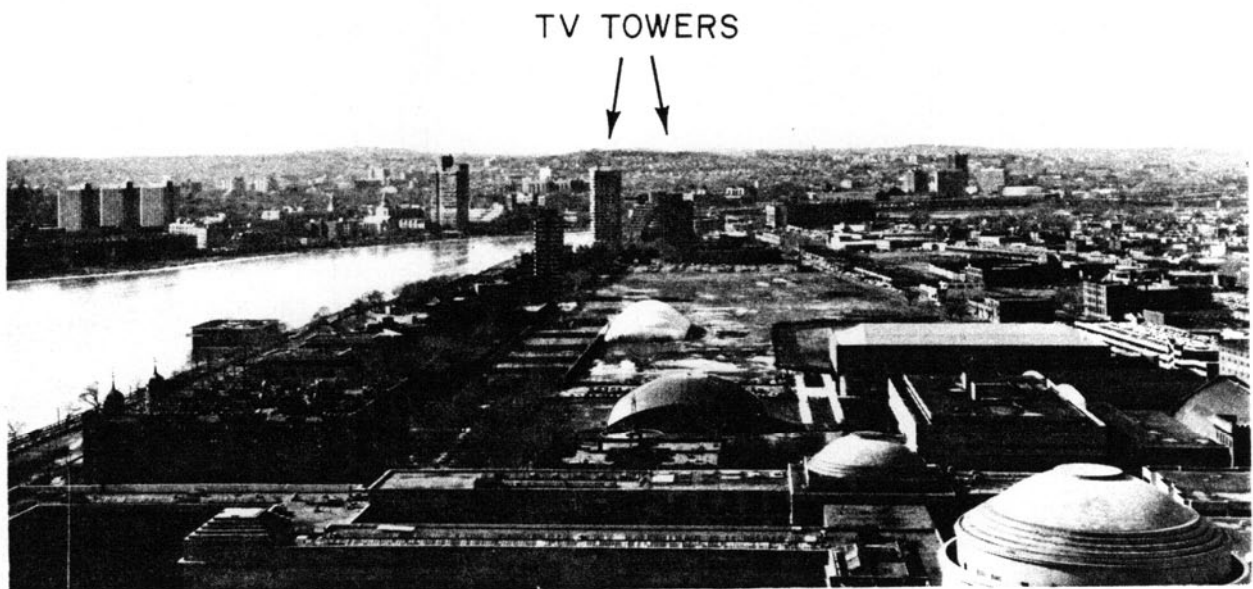


Fig. 2-6. View from interim testbed toward Needham, Massachusetts TV towers.

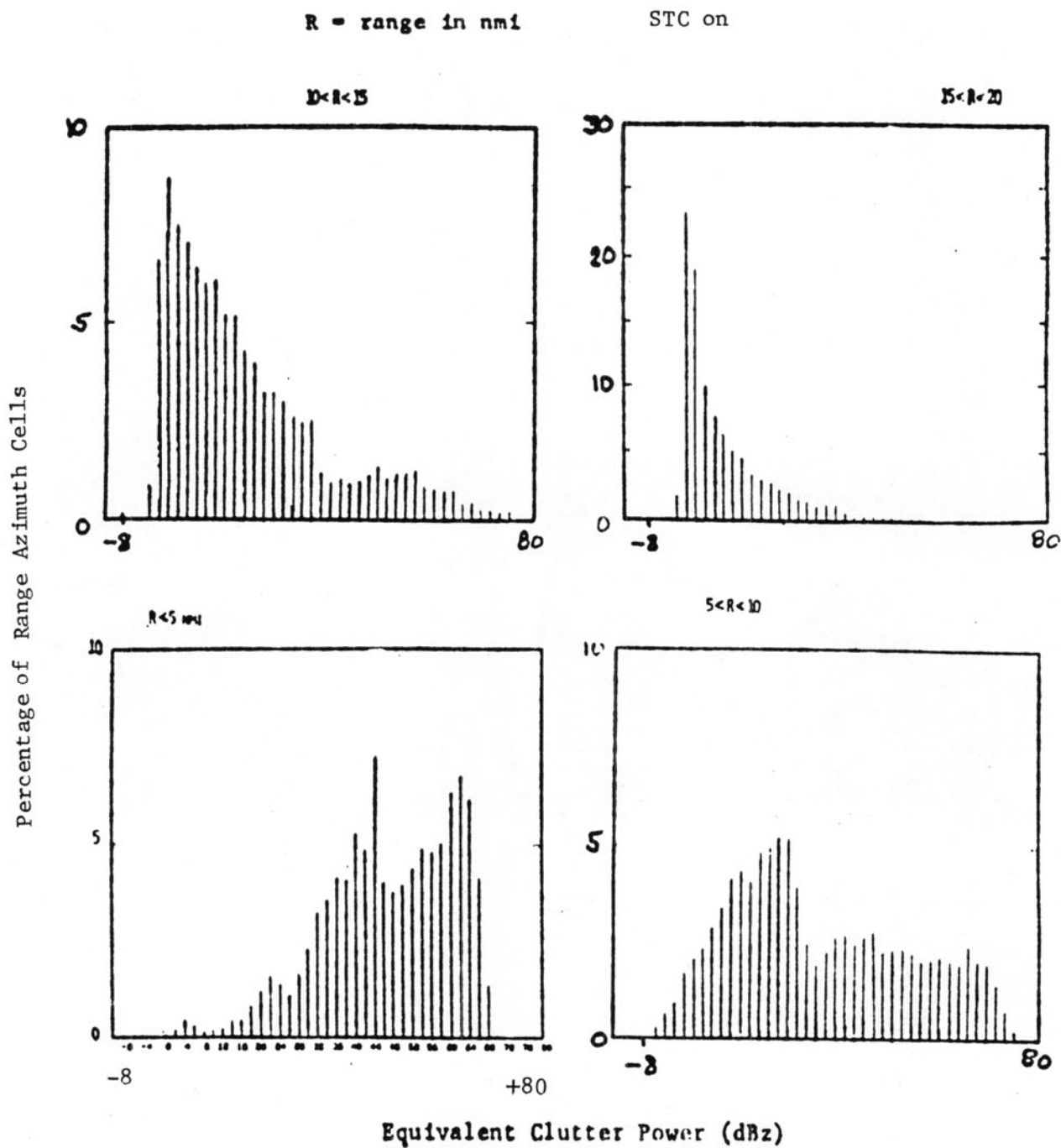


Fig. 2-7. Clutter Amplitude Distributions at 0.36° Elevation Angle
of MIT Meteorology Dept. S-band Radar.

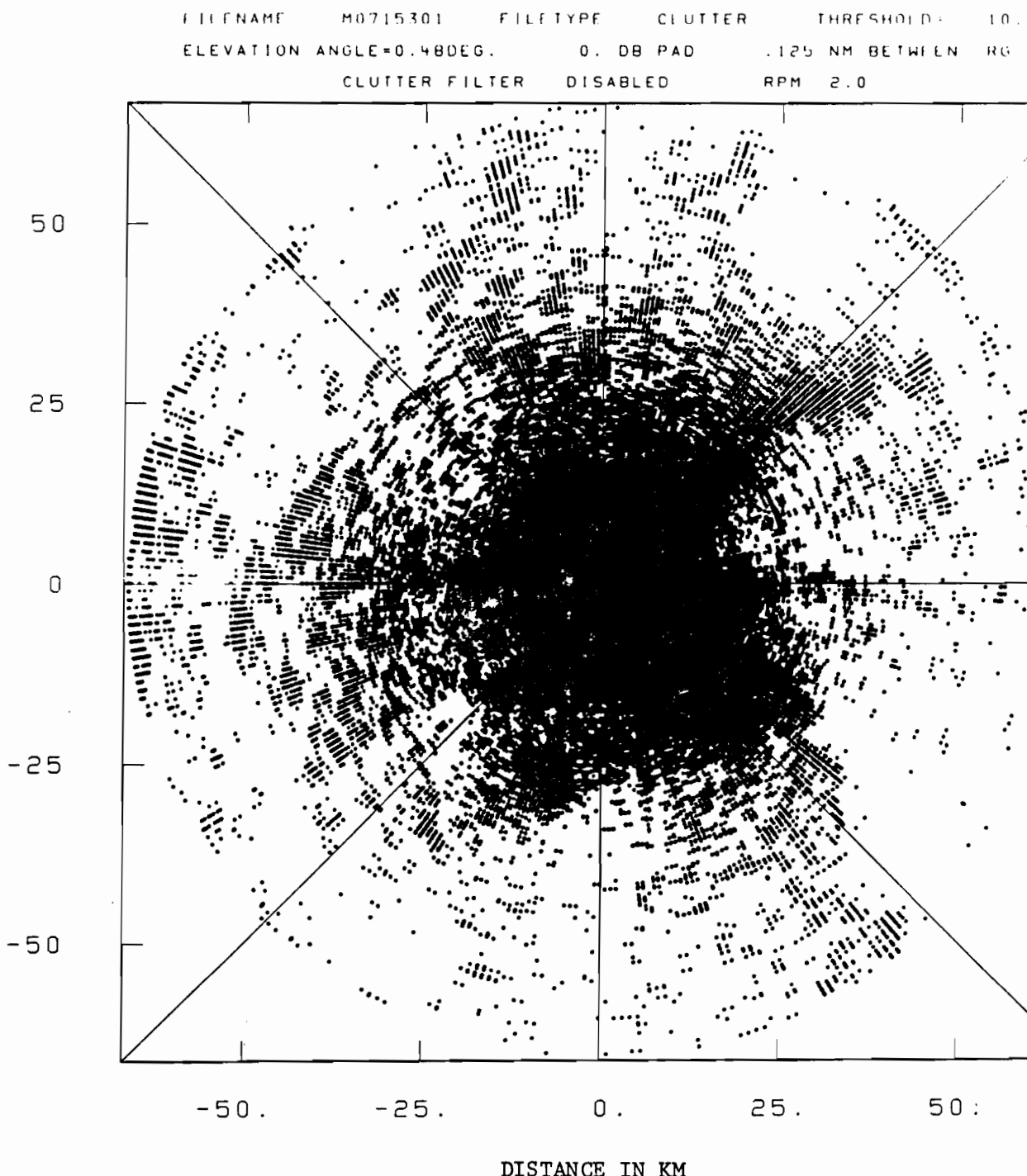


Fig. 2-8. First Trip MIT Site S-Band
Clutter Above 10 dBz.

FILENAME M0715301 FILETYPE CLUTTER THRESHOLD= 30.
ELEVATION ANGLE=0.48DEG. 0. DB PAD .125 NM BETWEEN RG
CLUTTER FILTER DISABLED RPM 2.0

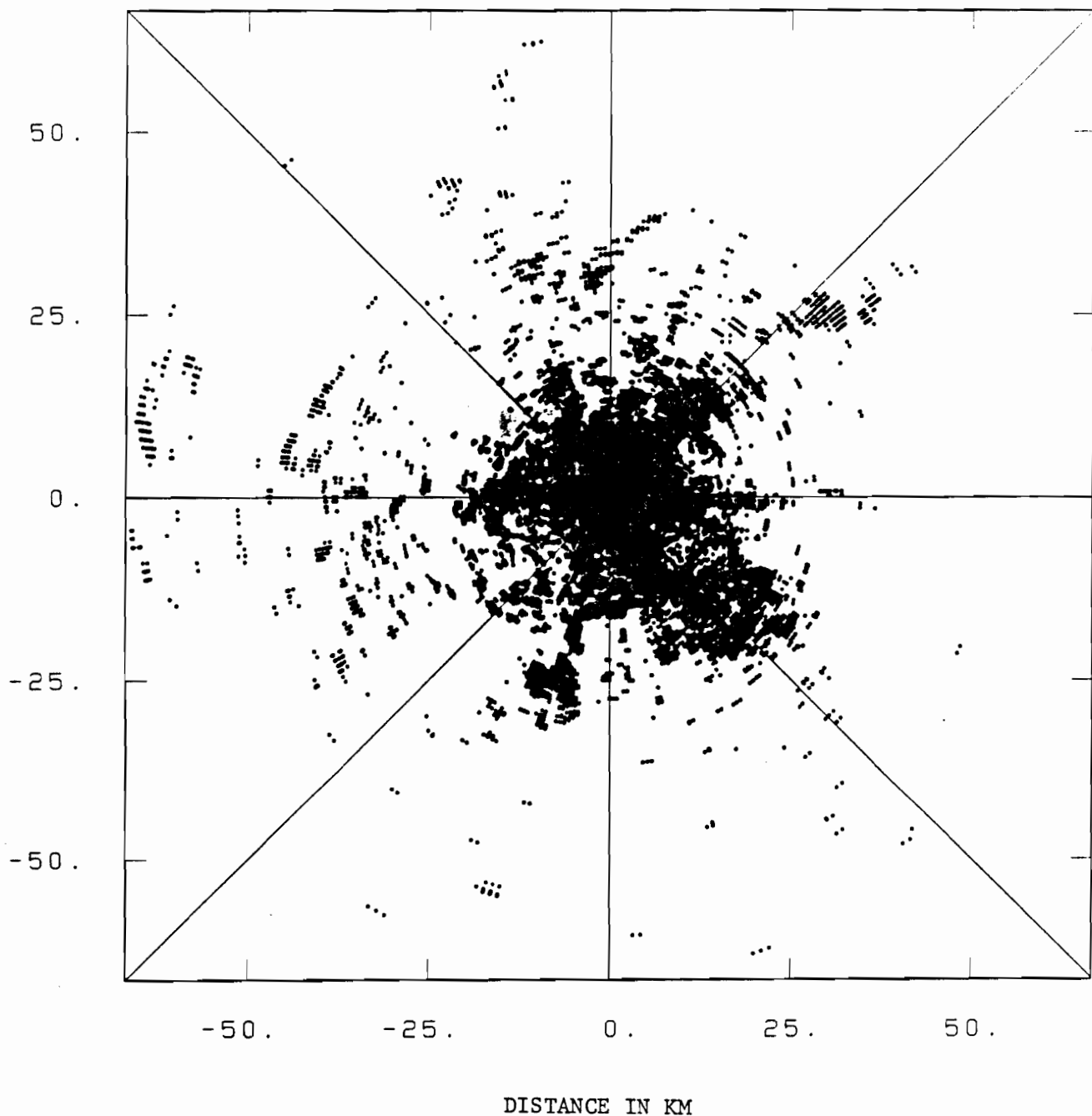


Fig. 2-9. First Trip MIT Site S-band Clutter
Above 30 dBz.

FILENAME M0715301 FILETYPE CLUTTER THRESHOLD= 50.
ELEVATION ANGLE=0.48DEG. 0. DB PAD .125 NM BETWEEN RG
CLUTTER FILTER DISABLED RPM 2.0

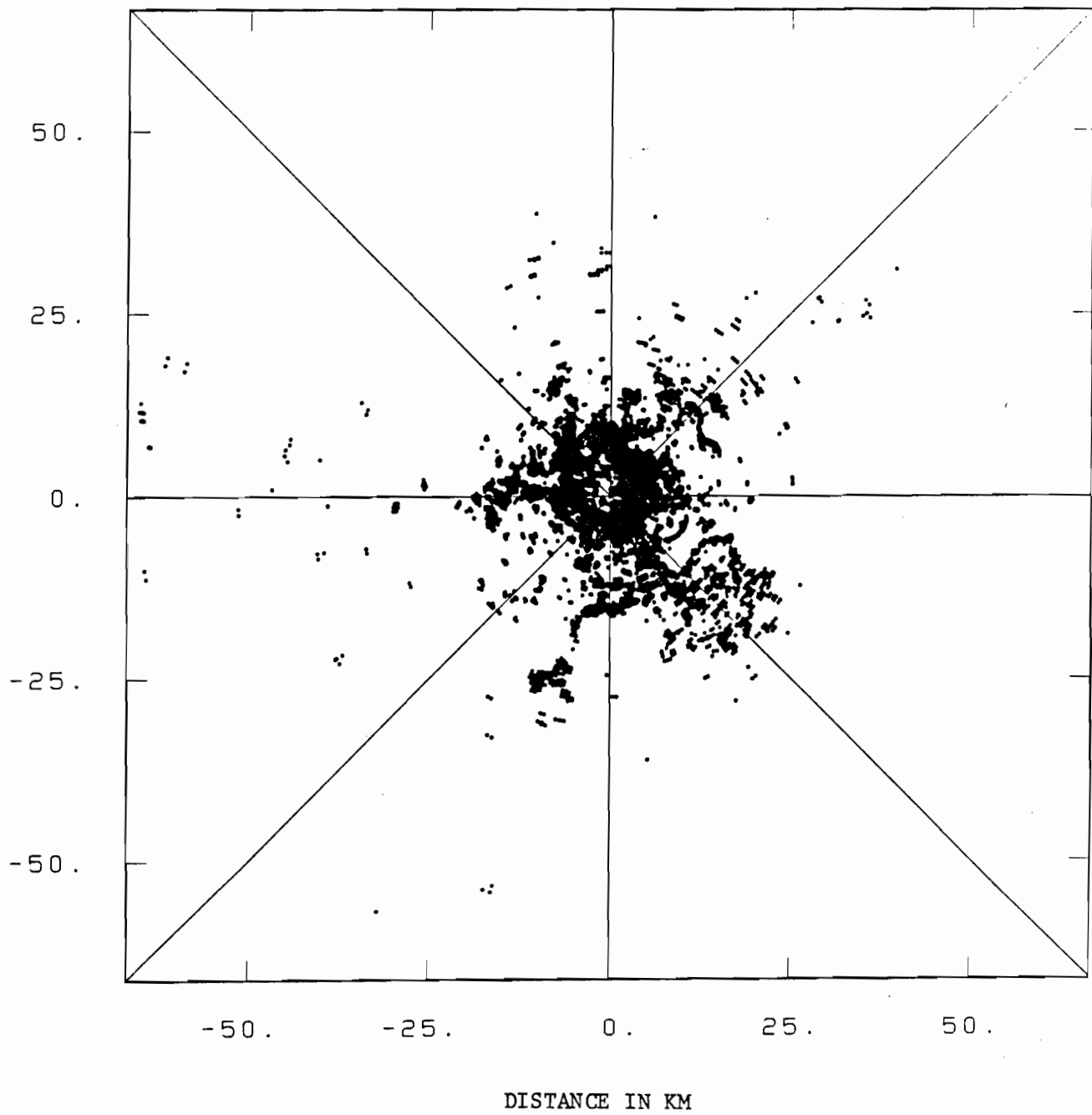


Fig. 2-10. First Trip MIT Site S-band Clutter
Above 50 dBz.

effective reflectivity level above 50 dBz. In such cases, even 50 dB of clutter suppression might not be adequate to yield reliable detection of low reflectivity phenomena in all radar cells below 1.5° elevation angle.

A particularly challenging clutter problem arises when weather from a higher order trip is obscured by the first trip weather. This problem is particularly acute in the Doppler channel since the PRF values needed to give the desired unambiguous Doppler range typically result in the higher order trip weather being of practical concern.

For a given radar reflectivity (e.g., 30 dBz), the received power varies proportionally to R^{-2} . Since weather signals are typically characterized by radar reflectivity levels, an appropriate way of assessing the impact of first trip ground clutter is to determine a second trip reflectivity level which results in the same received power level. Using the R^{-2} law, it is easy to show that the first trip clutter has an effective reflectivity in the second trip which is higher than the first trip reflectivity by:

$$K_{21} = 20 \log_{10} (1 + R_a/R_1) \quad (2-1)$$

where R_1 = range to clutter

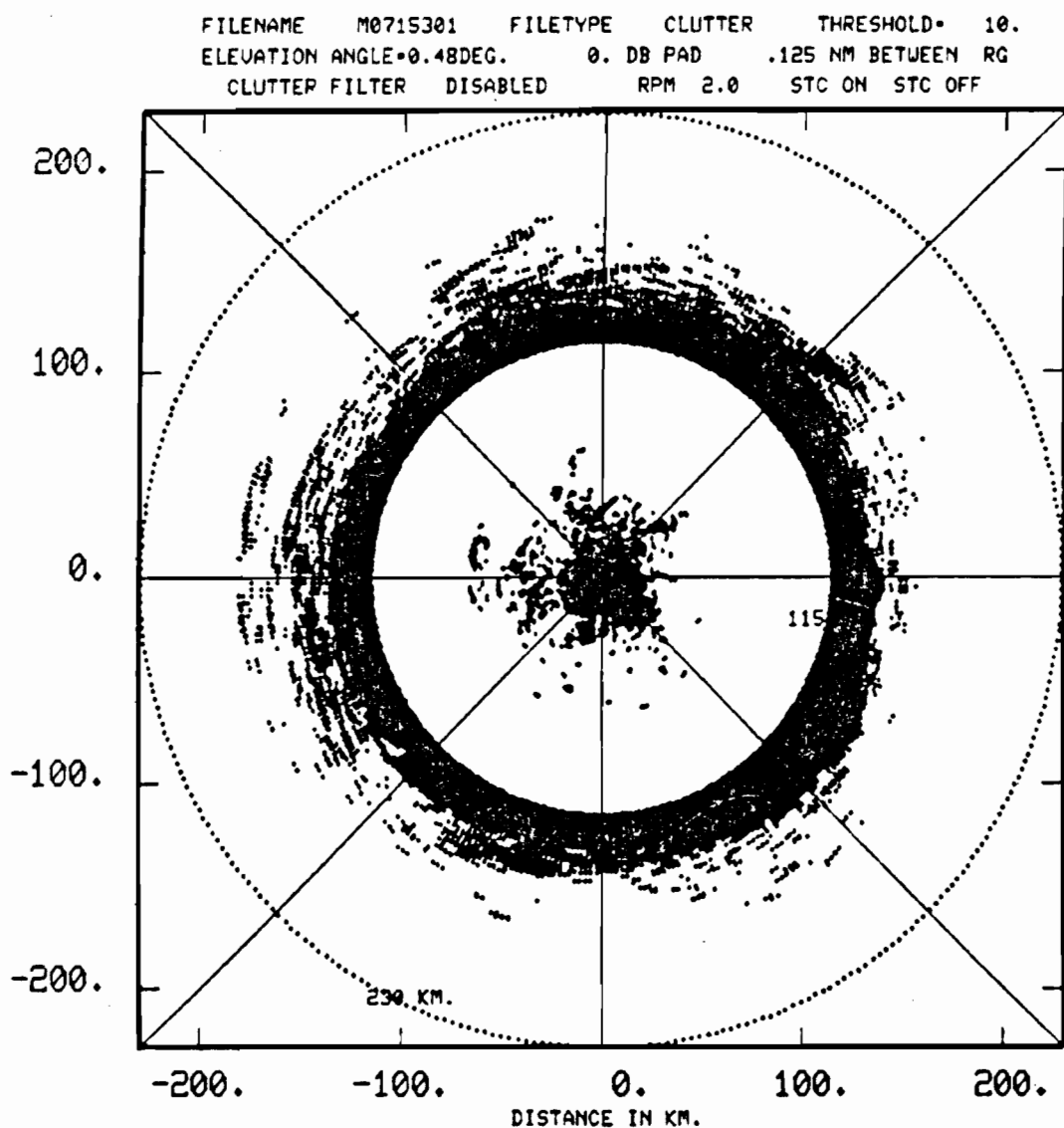
R_a = unambiguous range (e.g., typically 115 km for Doppler data)

The quantity K_{21} is the range factor for converting first trip dBz values to equivalent second trip dBz values.

Figure 2-11 is an example of this range factor increase of effective clutter levels in the second trip for the MIT data. We see that low level (i.e., <30dBz) ground clutter from the first 30km has the potential for obscuring a significant region in the second trip. Since the Doppler parameter errors rise drastically with a signal-to-clutter ratio (S/C) <+10 dB, at this site it will be very difficult to obtain good Doppler data in much of the second trip except in the most intense regions of a convective storm unless clutter filtering is utilized.

Figures 2-12 and 2-13 show how much of the MIT coverage region is recovered by two levels of ideal clutter cancellation. We see that 20 dB of cancellation reduces the area of clutter with effective reflectivity >30 dBz by 40% while 35 dB of clutter rejection recovers some 60% of the area.

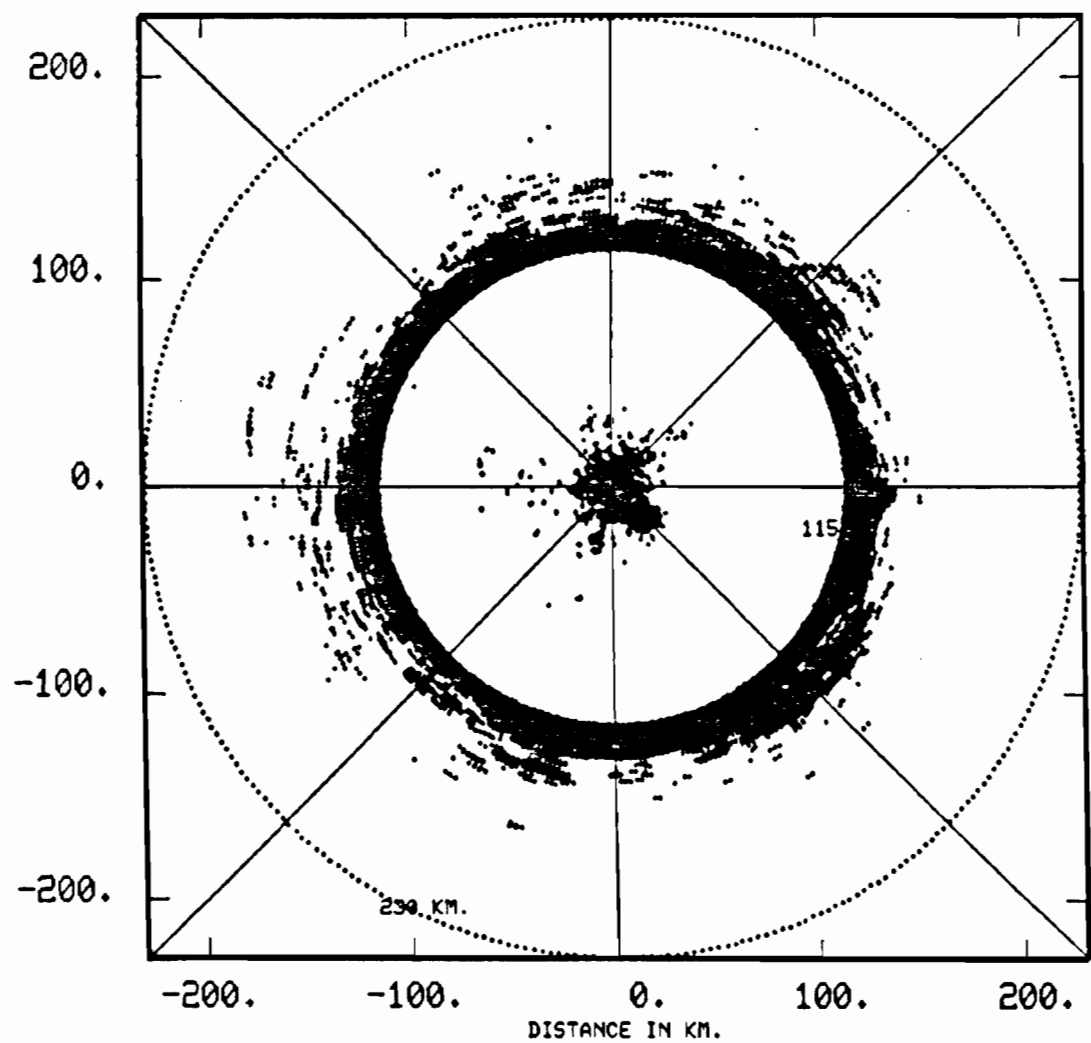
Figure 2-14 is an example of second trip weather obscuration by clutter at NSSL site. We see that the automated range de-aliasing algorithm of Hennington [21] prevented first trip clutter from being interpreted as second trip weather, but could not recover the second trip weather which was overlaid by first trip clutter. It should be emphasized that this problem will occur in most of the scan strategies under consideration for NEXRAD, including:



AREA IN KM THAT EXCEEDS 30 dBz = 20260 km^2
 UNAMBIGUOUS RANGE = 115 km

Fig. 2-11. First and Second Trip MIT Site S-band Clutter Above 30 dBz.

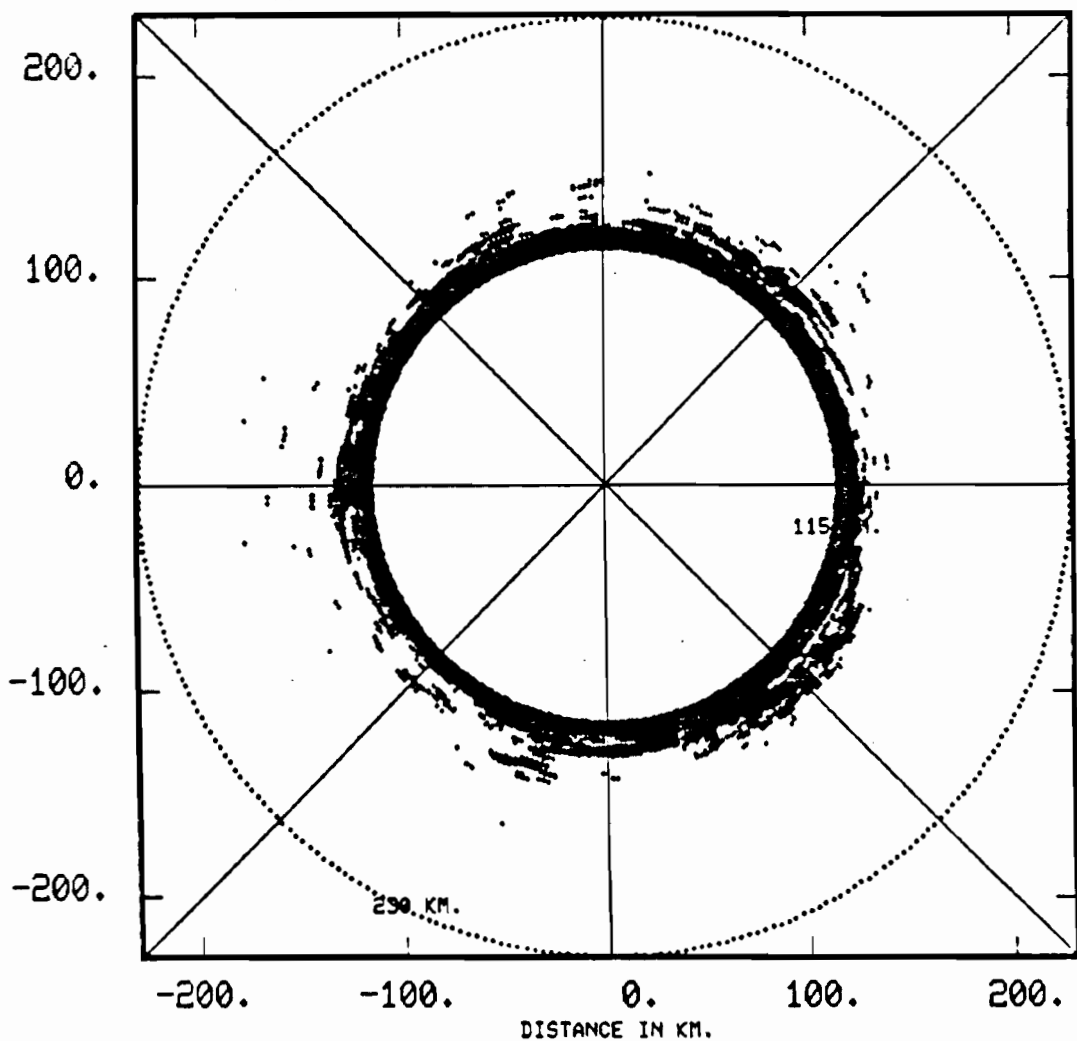
FILENAME M0715301 FILETYPE CLUTTER THRESHOLD= 30.
ELEVATION ANGLE=0.48DEG. 0. DB PAD .125 NM BETWEEN RG
CLUTTER FILTER DISABLED RPM 2.0 STC ON STC OFF



AREA IN KM. THAT EXCEEDS 30.DBZ= 11815.KM**2
20. DB CLUTTER REJECTION

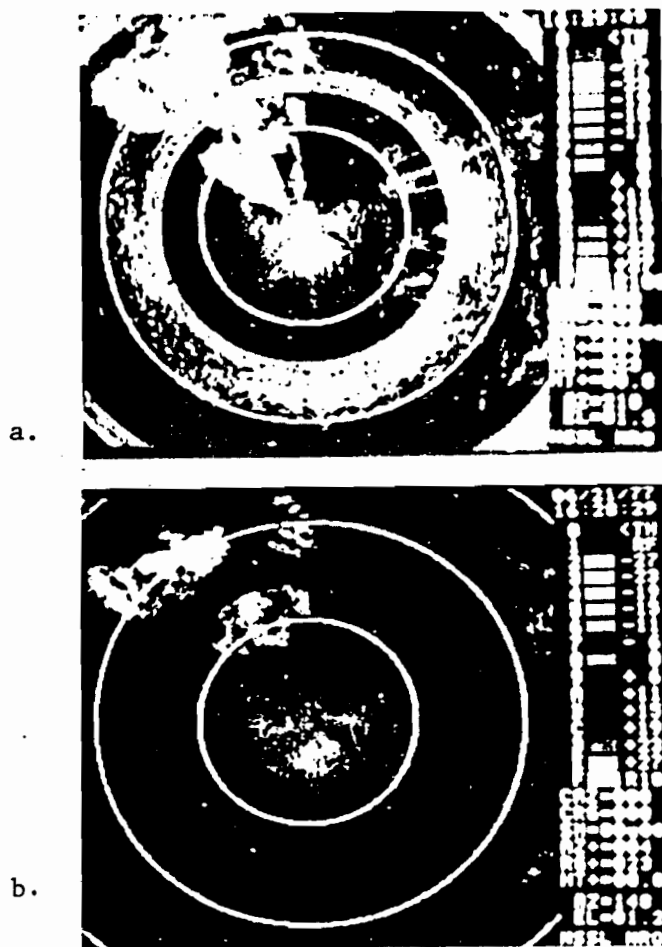
Fig. 2-12. First and Second Trip MIT Site Clutter
Above 30 dBz After 20 dB Clutter Suppression.

FILENAME M0715301 FILETYPE CLUTTER THRESHOLD= 30.
ELEVATION ANGLE=0.48DEG. 0. DB PAD .125 NM BETWEEN RG
CLUTTER FILTER DISABLED RPM 2.0 STC ON



AREA IN KM. THAT EXCEEDS 30.DBZ= 8054.KM**2
35. DB CLUTTER REJECTION

Fig. 2-13. First and Second Trip MIT Site Clutter
Above 30 dBz After 35 dB Clutter Suppression.



"a" shows storm echoes without the range de-aliasing algorithms and "b" with range de-aliasing adjustments.

Note that the first trip clutter obscures a considerable segment of the second trip weather at the beginning of the second trip.

Fig. 2-14. Illustration of Second Trip Weather Obscuration by NSSL First Trip Clutter.

- (i) batch processing ala NSSL [1].
- (ii) use of a constant, but different PRF on separate frequencies for reflectivity and velocity estimation, and
- (iii) use of separate scans (each at a constant PRF) for reflectivity and Doppler estimation at low elevation angles.

The temporal and spectral characteristics of the clutter are of concern for clutter rejection. No general statement is applicable to all clutter situations; however, experience at Lincoln [7-9] and elsewhere [5,6] suggests that the NEXRAD clutter can be considered to be a mixture of:

- (1) reflections from many small scatterers such as tree branches or ocean waves, which often move with the wind, and
- (2) reflections from larger discrete scatterers such as buildings and mountain sides which are little affected by the wind.

The degree to which one or the other dominates in a given radar cell depends on the local geometry, season, and size of the radar cell. Recent Lincoln measurements and analyses of radar clutter in a variety of FAA [7-9] and DOD programs and the experience of others involved in clutter measurements (e.g., Georgia Tech [18]) suggest that discrete scatterers probably generate the higher clutter levels in areas which have many man-made structures.

In the next chapter we will consider how the radar features affect the clutter spectral characteristics and clutter rejection, while Chapter V will consider the types of clutter in greater detail.

III. RELATIONSHIP OF WEATHER PARAMETERS AND CLUTTER SUPPRESSION CAPABILITY TO RADAR PARAMETERS

In this section, we consider how the weather parameter estimates and clutter suppression capability are affected by principal radar parameters. In considering the clutter suppression capability, it is essential that we keep in mind the overall objective of improving the accuracy of weather parameter estimates. Suppression of the clutter will generally result in some degradation of weather parameter accuracy. The net weather parameter error can be viewed as the sum of:

- (1) the error due to the clutter suppression technique, and
- (2) the error due to the residual clutter.

Thus, considerable attention was paid to the tradeoff of these two types of errors.

The section proceeds as follows. First, we will very briefly review some pertinent features of weather parameter estimation. Next, we consider how the clutter characteristics will be affected by the radar parameters. The final section considers weather parameter estimate errors due to spectral notching by an idealized linear time invariant clutter filter and, errors due to the clutter residue with a pulse pair processor.

A. Weather Parameter Estimation

Weather parameter [e.g., reflectivity (I), mean velocity (v), spectrum width (σ)] estimation with Doppler weather radars has been discussed in detail by Zrnic' and Doviak [4, 10], so the discussion here will be terse. The weather return can be modeled as a Gaussian random process, whose decorrelation time is determined by the spectrum shape (typically the width). If we make the further assumption that the weather velocity spectrum is Gaussian with rms width σ_v , the accuracy of the various weather parameter estimates at high signal-to-noise ratio (SNR) is as follows:

$$\text{Var}(I) \sim K_1 (M_i N_{rg})^{-1} \quad (3-1)$$

$$\text{Var}(v) \sim K_2 \sigma_v (M T_s N_{rg})^{-1} \quad (3-2)$$

$$\text{Var}(\sigma) \sim K_3 \sigma_v (M T_s N_{rg})^{-1} \quad (3-3)$$

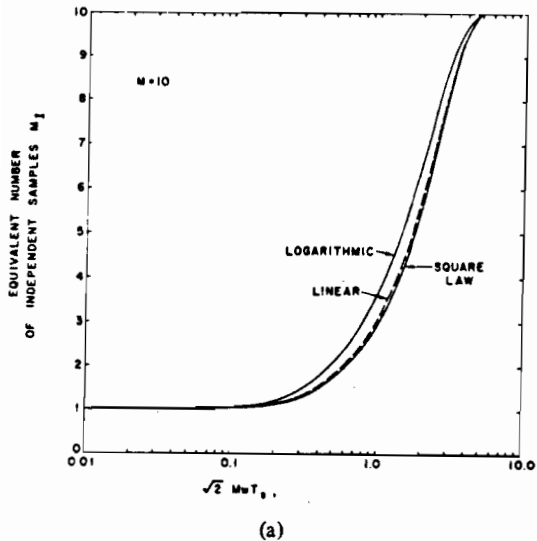
where M = number of pulses used in estimating the parameter,

N_{rg} = number of range gates averaged.

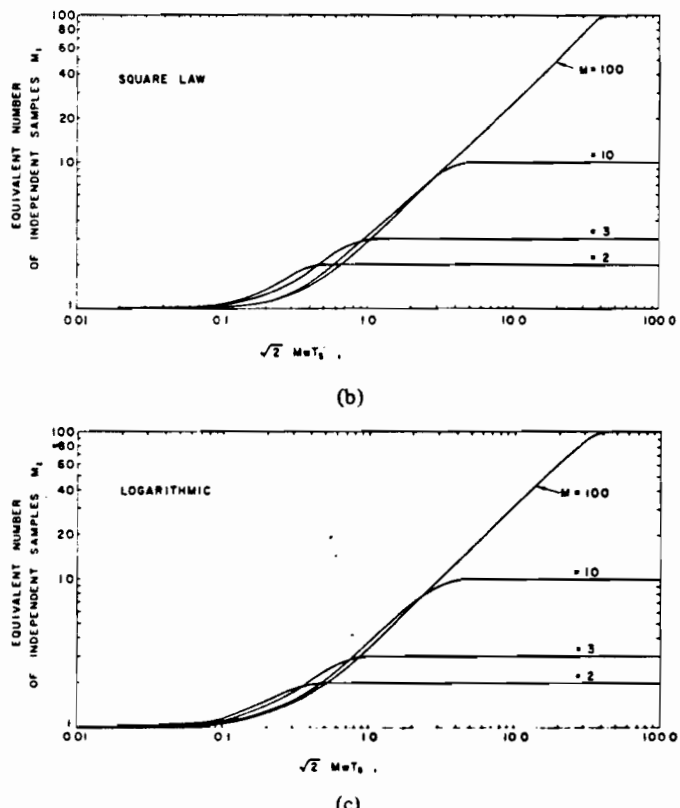
M_i = equivalent number of independent pulses

T_s = pulse repetition period

Figure 3-1 shows the relationship of M_i to the spectrum width, pulse repetition period and number of pulses averaged. The key features to note from Eqs. (3-1) to (3-3) and Figure 3-1 are:



(a)



(c)

(a) Equivalent number of independent samples for the three receiver types. The number of samples is 10 and time or angle averaging parameters of a Gaussian correlation are on the abscissa. (b) Equivalent number of independent samples for the square-law receiver. A very similar graph with slightly more independent samples applies to a linear receiver. (c) Equivalent number of independent samples for the logarithmic receiver.

$$w = 2 \sigma_v / \lambda$$

M = # of samples

T_s = sampling time

Fig. 3-1. Effective Number of Independent Samples For Reflectivity Measurements (from [4]).

- (1) no one weather spectrum width is "worst case" for all three parameters; rather, narrow widths are a problem for reflectivity estimation whereas wide widths cause difficulties in velocity estimation. The NEXRAD specification [11] considers this by specifying a weather spectrum width to be associated with the tolerable weather parameter rms errors as shown in Table 3-1.
- (2) the maximum dwell time (MT_s) typically is less than BW/α where BW is the beamwidth and α the rotation rate to avoid excessive loss of resolution. The "average" NEXRAD rotation rate of 2.8 rpm* with a 1° BW corresponds to $MT_s = 60$ ms.
- (3) range averaging is effective in permitting faster rotation rates, but often will increase the clutter level in a given radar cell. Also, since range resolution is fixed in the NEXRAD specification, range averaging can be improved only by shortening the pulse duration which in turn reduces the SNR.

The relationships above are important in clutter suppression considerations since some forms of clutter cancellation (especially, "batched" linear filtering followed by pulse pair processing) will result in a smaller number of samples being available for weather estimation [1]. Linear filtering can also affect the number of effective independent samples by changing the weather spectrum width. However, this is probably a second order effect relative to the bias errors which will be considered in the last portion of this chapter.

*Corresponding to 14 elevations in 5 minutes.

TABLE 3-1
TYPICAL REQUIRED AVERAGING TIMES FOR WEATHER PARAMETER ESTIMATES

Parameter	Maximum std. deviation	Assumed Weather Spectrum Width (σ_v)	Required value of $M T_s N_{RG}$ at high SNR (ms)
Reflectivity	1 dB	1 m/s	350 ¹
Mean velocity	1 m/s	4 m/s	28 ²
Spectrum rms width	1 m/s	4 m/s	11 ³

Notes:

1. result valid only for $M N_{RG} > 15$
2. result valid only for $M > 16$ at $T_s = 0.001$
3. result valid only for $T_s < 0.002$

B. Relationship of Clutter Characteristics to Radar Parameters

The clutter environment (and consequently) clutter rejection performance will depend on several of the radar parameters. In particular:

1. the beamwidth and range resolution will determine the clutter area and hence clutter levels as well as clutter type. For example, the clutter in a Doppler channel cell with 0.25 km range resolution may have the character of discrete clutter while the corresponding 1 km range resolution reflectivity channel cell may appear to have distributed clutter since more scatterers are contained in the reflectivity channel cell.
2. the rotation rate will change the spectrum characteristics of the clutter. Distributed clutter is typically assumed to be spatially homogenous with a Gaussian spectrum whose rms width given by [1,5]:

$$\sigma_c = [W_1^2 + W_2^2]^{1/2} \quad (3-4)$$

W_1 = rms width due to wind

W_2 = rms width due to rotation = $0.13 \alpha \lambda / \text{BW}$

where λ is the wavelength, α the rotation rate, and BW the one-way beam-width. Figure 3-2 shows the relationship between σ_c and α observed experimentally at NSSL [1].

Discrete clutter is generally considered to be unaffected by the wind, hence, the transform of the time-varying return scales in frequency proportional to α . The width of the discrete clutter return in a weather estimation interval will increase with α , but no precise quantitative expression [e.g., analogous to (3-4)] is possible since the windowed transform is the convolution of a time-shifted window function with the transform of the clutter waveform.

However, some insight can be obtained by considering the spectrum of the clutter waveform. This is surprisingly easy to summarize since the discrete clutter time waveform is simply the two-way antenna pattern*, i.e.,

$$c(t) = A p^2 (\alpha t - \phi_c, E_c) \quad (3-5)$$

*It is assumed that the propagation path to the discrete scatterer doesn't vary over the time period of concern (in particular, that the antenna phase center is at the center of rotation).

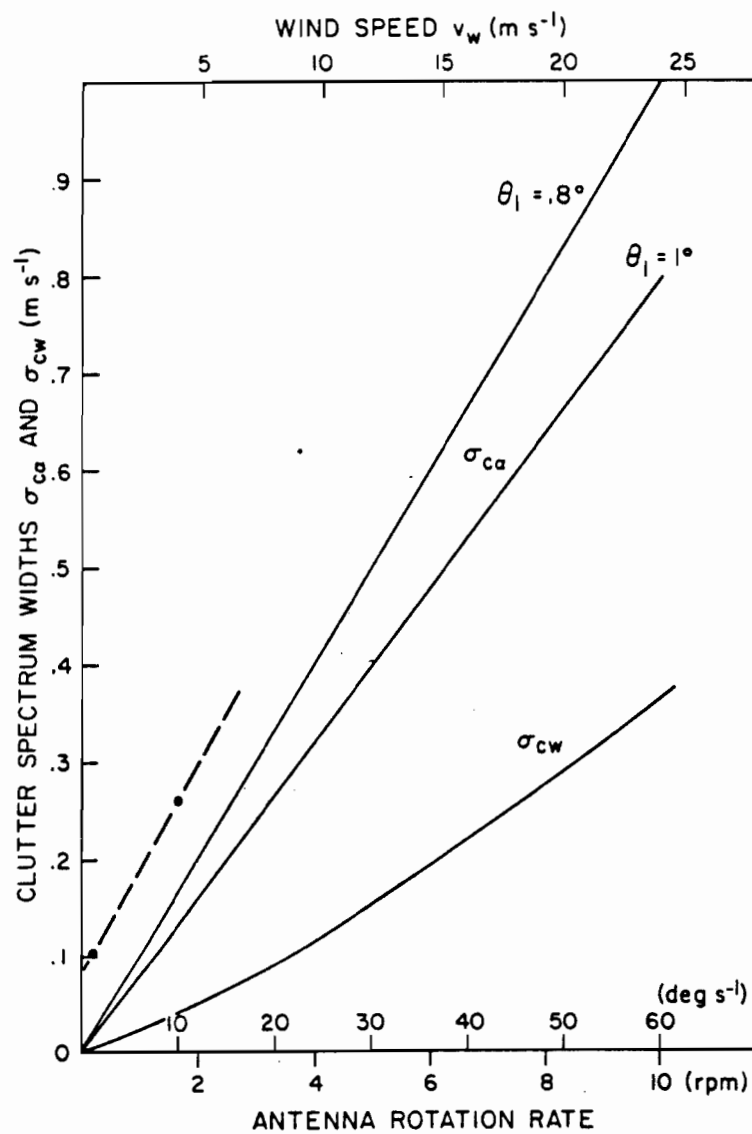


Fig. 3-2. Clutter spectrum widths σ_{ca} due to antenna rotation (scale on lower axis) and σ_{cw} due to wind speed (upper axis). Dashed line is through two estimated data points (from [1]).

where ϕ_c = azimuth at which the scatterer is located
 E_c = elevation at which the scatterer is located
 $p(at-\phi_c, E_c)$ = one-way antenna pattern $\Delta p()$.

Consequently, the transform of $c(t)$ is the convolution of the transform of $p()$. But since $p()$ is the transform of the aperture excitation [12], it follows from Fourier theory that the transform of $c(t)$ is the convolution of the aperture excitation function.

This is an important result since it tells us that the energy spectrum of a discrete scatterer clutter signal is a compact function, i.e., non-zero only over a finite extent. In particular, the spectrum does not have "tails" such as are associated with the distributed clutter model spectra.

Figure 3-3 shows the relationship of aperture excitation function to clutter energy spectrum for a rectangular aperture with uniform excitation. Figure 3-4 shows a much more realistic excitation function for NEXRAD:

$$I(r) = 1 - (r/r_0)^2 \quad (3-6)$$

where r = distance from center of a parabolic aperture
 r_0 = aperture radius

and the corresponding discrete clutter energy spectrum. The tapered excitation of equation (3-4) yields an array pattern of the form

$$P(u) = J_2(u)/u \quad (3-7)$$

where $u = 2\pi r_0 \sin\phi/\lambda$
 ϕ = conical angle with respect to boresight
 J_2 = second-order Bessel function.

This pattern has a -25 dB first sidelobe with the other sidelobes at least -40 dB with respect to the peak. Since this sidelobe characteristic closely emulates the NEXRAD specification [11], the excitation of (3-6) was assumed for all of the discrete scatterer theoretical model simulations.

The relationship of the radar parameters to anomalous propagation (AP) clutter characteristics is unclear at this point due to lack of Doppler measurements on AP. The principal uncertainty here is the phase stability of the refractive index duct. Measurements are essential, but have not been carried out to date due to the lack of AP conditions at the principal weather radar sites which can record time series data.

C. Relationship of Clutter Suppression to Weather Parameter Estimates

In the preceding section, we have seen that the radar rotation rate and the wind condition can change the spectrum width of the clutter signal.

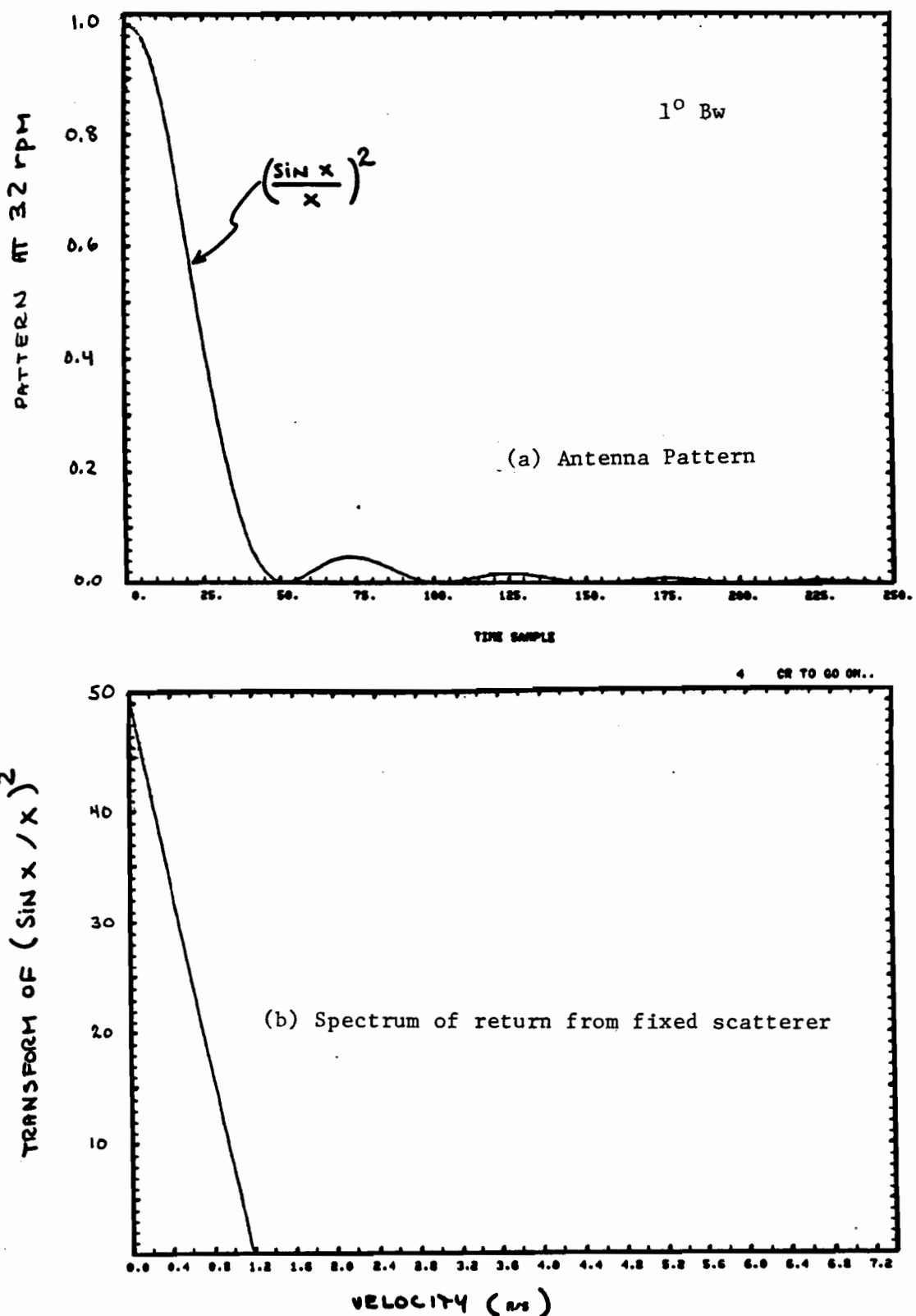


Fig. 3-3. Time Waveform and Spectrum of Uniform Aperture Scatterer Return.

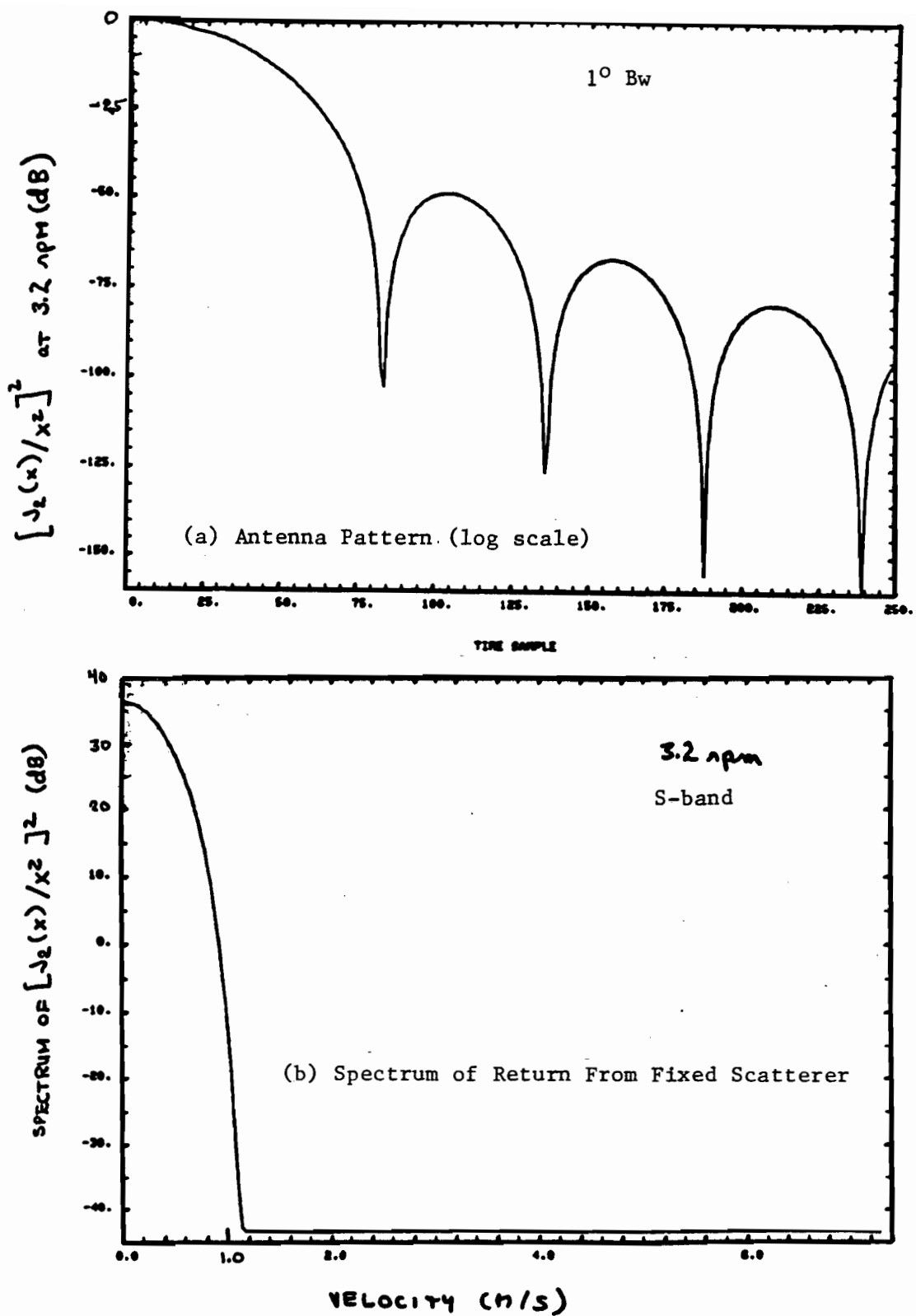


Fig. 3-4. Time Waveform and Spectrum of Circular Aperture Scatterer Return.

In this section, we consider how suppressing clutter which has a wider width may cause errors in the weather parameter estimates and how un suppressed clutter causes weather parameter errors.

The weather parameter bias errors due to clutter suppression are computed for an idealized linear time invariant high-pass clutter filter (of various stopband widths) operating on I, Q samples followed by pulse pair estimation. This particular clutter suppression approach was viewed as appropriate because:

- (1) the original NEXRAD NTR clutter suppression text implicitly assumes such a form of processing, and
- (2) the principal Doppler radar clutter suppression studies to date [1,2] focussed on this approach.

Figure 3-5 shows the transfer function of the idealized filter. This filter does not have the ripples associated with practical filters because our principal objective was to determine the errors due to spectrum truncation with the original passband widths in the NTR clutter suppression section.*

Figure 3-6 summarizes the straightforward approach used to determine the weather parameter errors when no clutter is present†. Figures 3-7 to 3-9 show the parameter errors as a function of weather mean velocity (V_{av}) for weather widths of 1 m/s to 4 m/s when the filter stopband width (V_p) is 3 m/s. Figures 3-10 to 3-15 are the corresponding results at widths of 1 m/s and 4 m/s when V_p is 1 m/s and 2 m/s.

Several comments can be made:

(1) reflectivity estimation

The error at the passband edge ($V_p = V_{av}$) is 3 dB for a weather width $\sigma_v < V_p$ since half of weather power is in the notch. At wide widths ($V_p < \sigma_v$), some of weather power is on either side of the notch when $V_{av} = V_p$. If we define $V_{usable} = V_p + 1$ m/s, the worst error at $V_{av} = V_{usable}$ occurs for large σ_v since this yields the most power in the filter notch.

*Simulations of the weather parameter errors with representative realistic clutter filters (Chapter VII) suggest that the ripples typically have a much smaller effect than do the spectrum notches for representative spectrum widths.

†The simulation also ignores effects of modifying the front-end noise spectrum on the weather parameter estimates on the grounds that such errors are predictable from knowledge of the clutter filter being used.

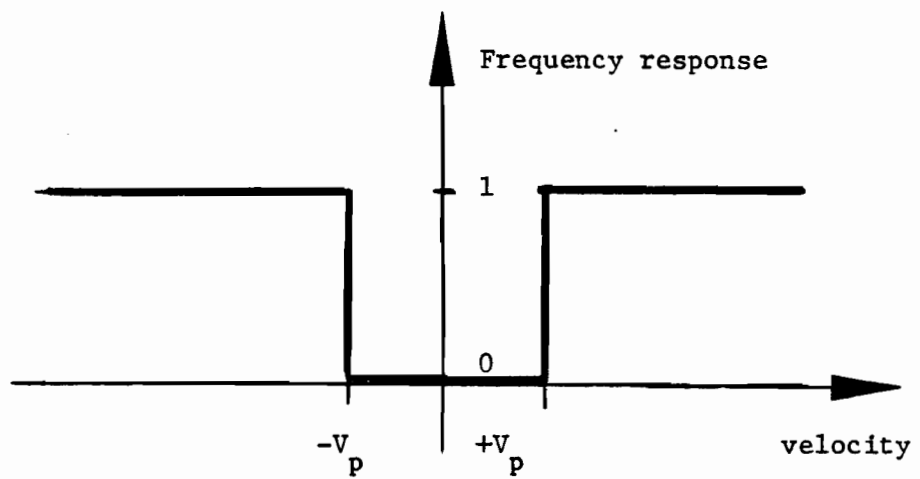


Fig. 3-5. Idealized LTI Clutter Filter Velocity Response Used to Bound Weather Parameter Errors.

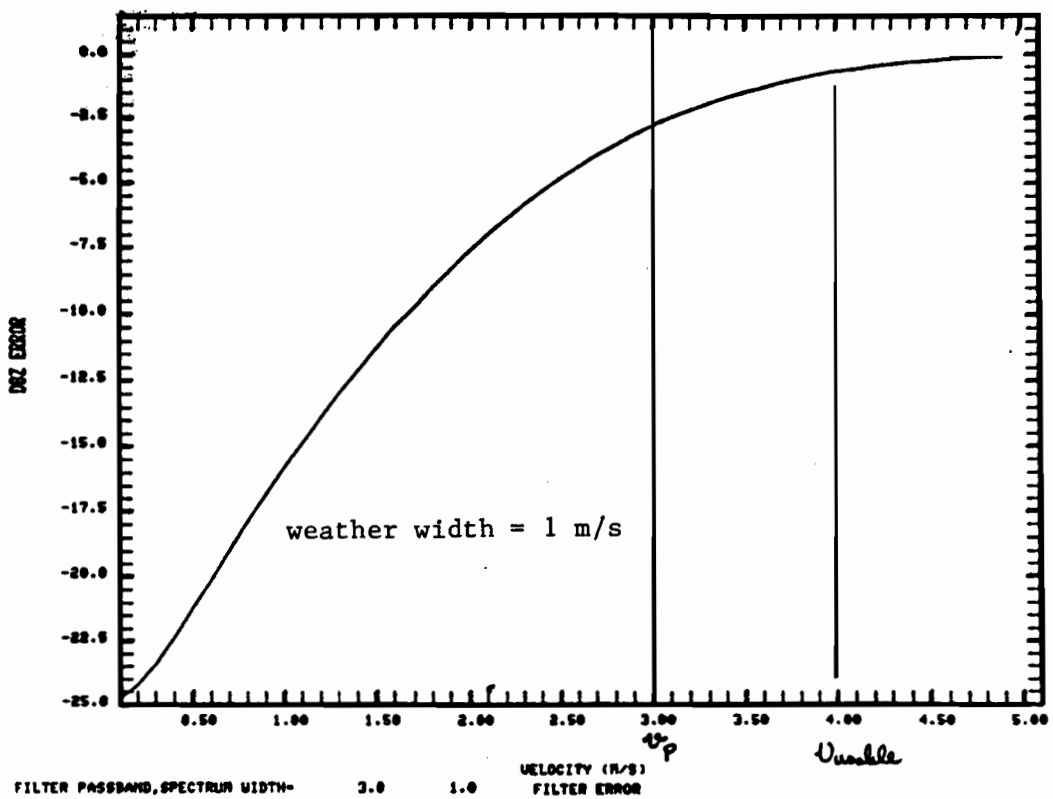
**OBJECTIVE: UNDERSTAND PERFORMANCE DEGRADATION FOR
PERFECT CLUTTER CANCELLATION**

COMPUTATION PROCEDURE

- 1. WEIGHT GAUSSIAN WEATHER SPECTRUM BY IDEALIZED
TRANSFER FUNCTION**
- 2. INVERSE FOURIER TRANSFORM TO GET AUTOCORRELATION**
- 3. APPLY PULSE PAIR ALGORITHMS TO ESTIMATE
WEATHER PARAMETERS**

**PLOT ERROR AS FUNCTION OF WEATHER MEAN VELOCITY FOR FIXED
WEATHER SPECTRUM WIDTH AND CLUTTER FILTER PASSBAND**

**Fig. 3-6. Computation of Errors for Idealized
LTI Clutter Filter.**



horizontal scale is weather mean velocity

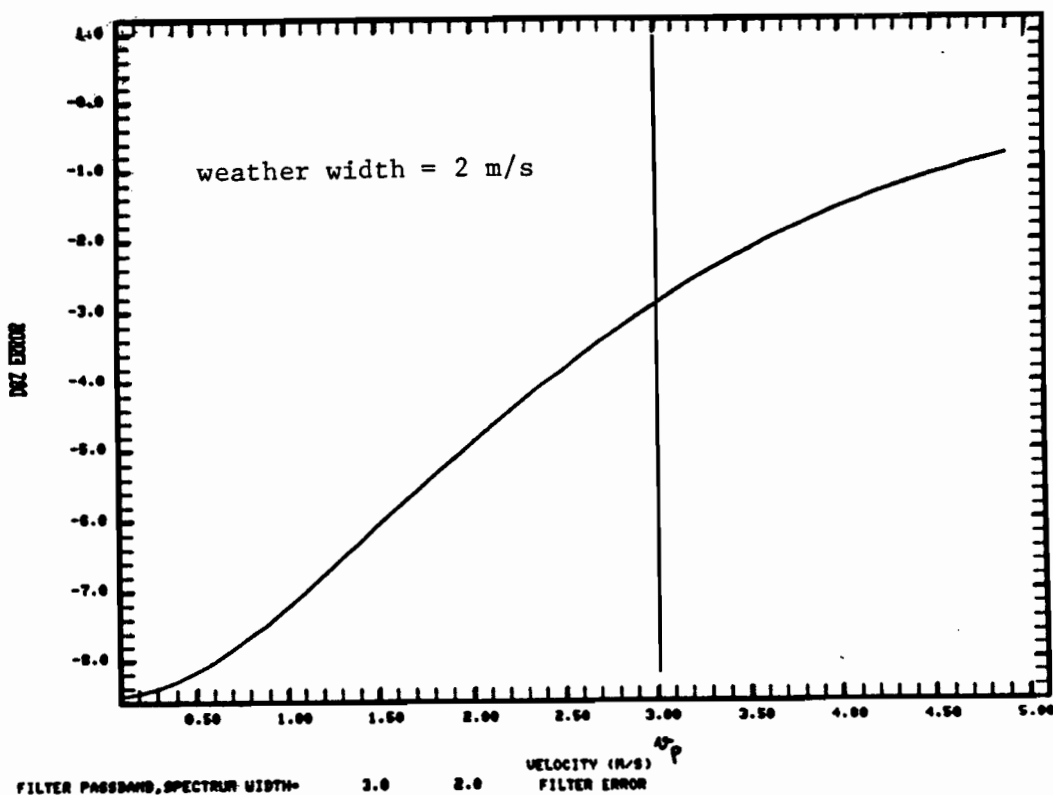
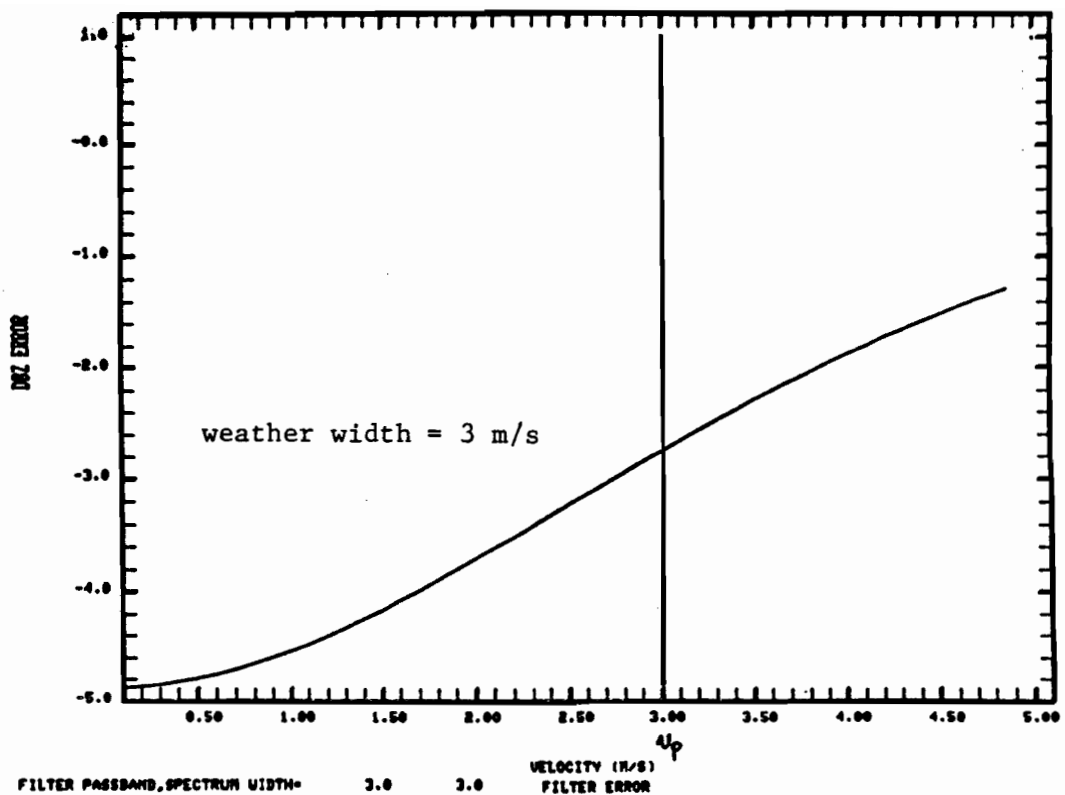


Fig. 3-7a. Reflectivity Estimate Error For Idealized Clutter Filter With 3 m/s Passband.



horizontal scale is weather mean velocity

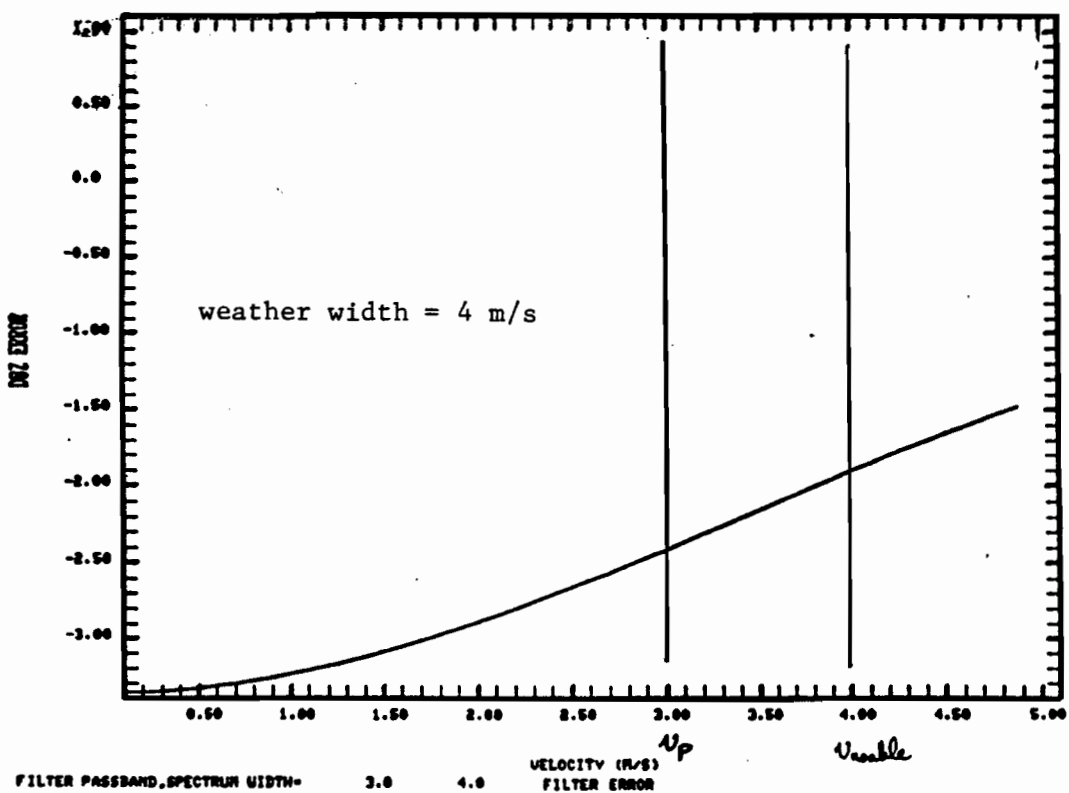
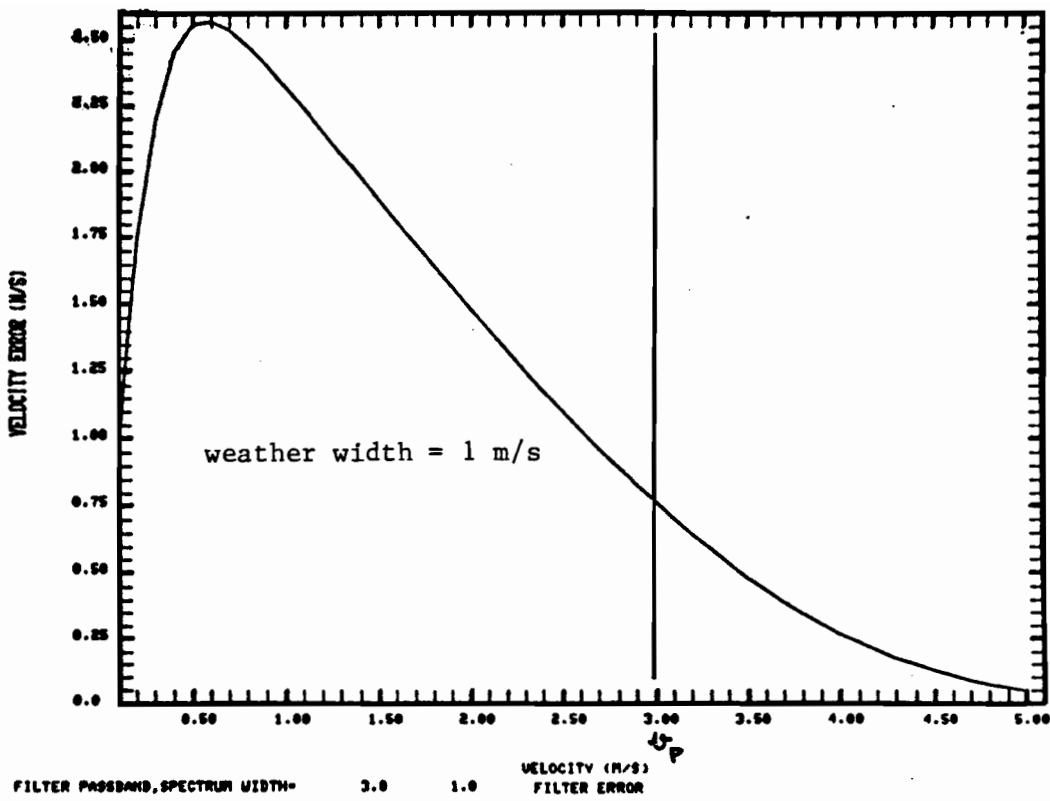


Fig. 3-7b. Reflectivity Estimate Error For Idealized Clutter Filter With 3 m/s Passband.



horizontal scale is weather mean velocity

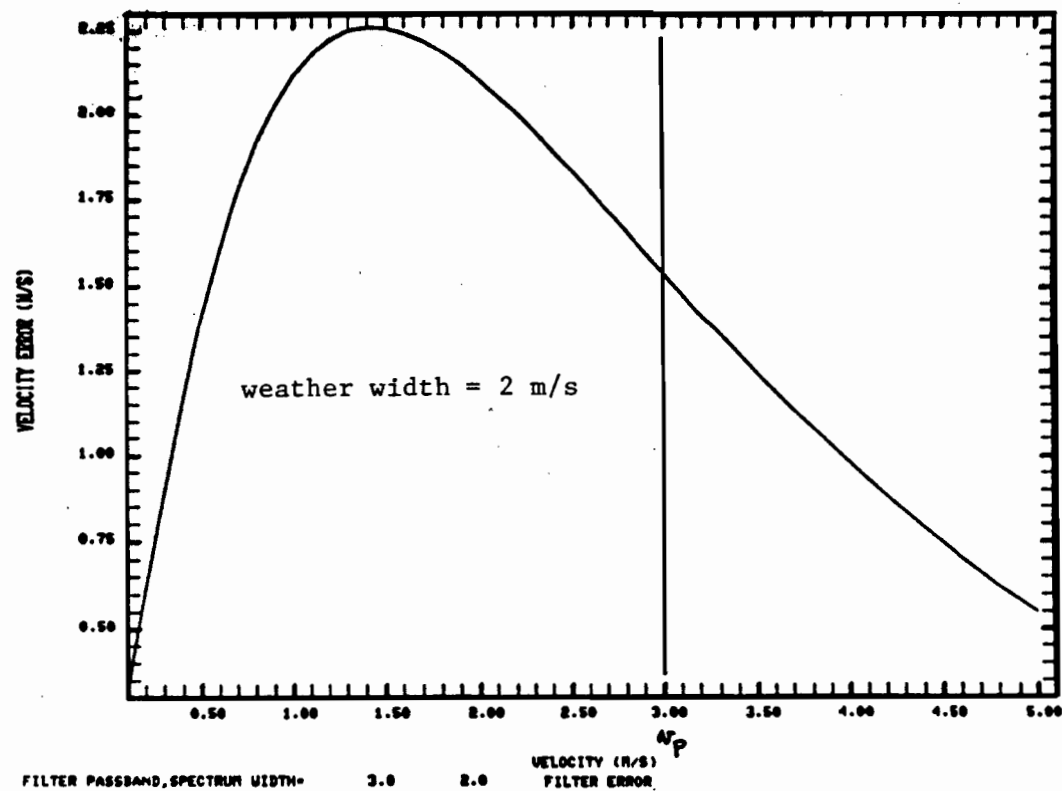
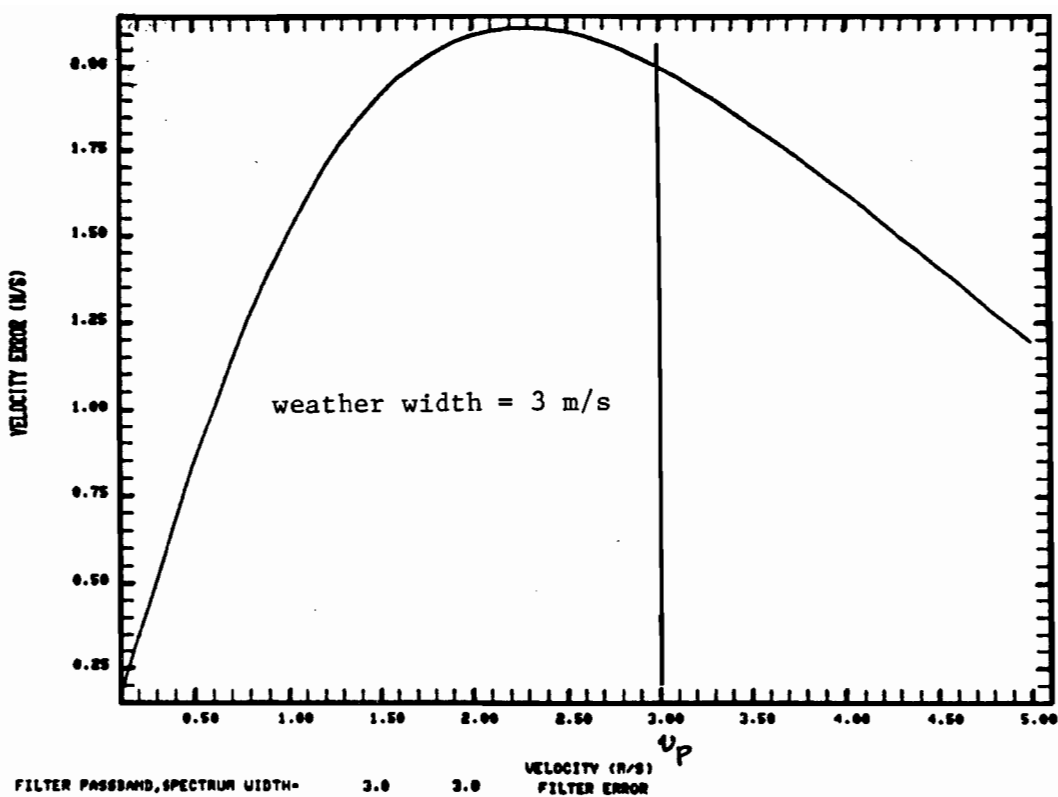


Fig. 3-8a. Mean Velocity Error For Idealized Clutter Filter With 3 m/s Passband.



horizontal scale is weather mean velocity

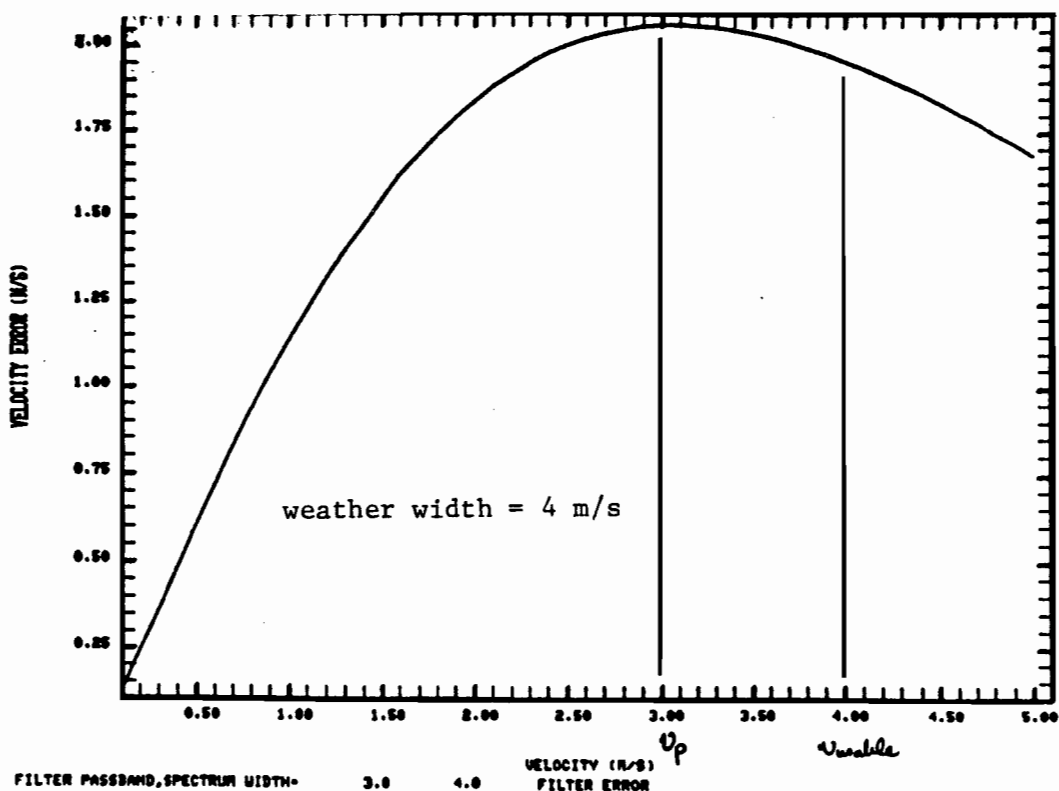
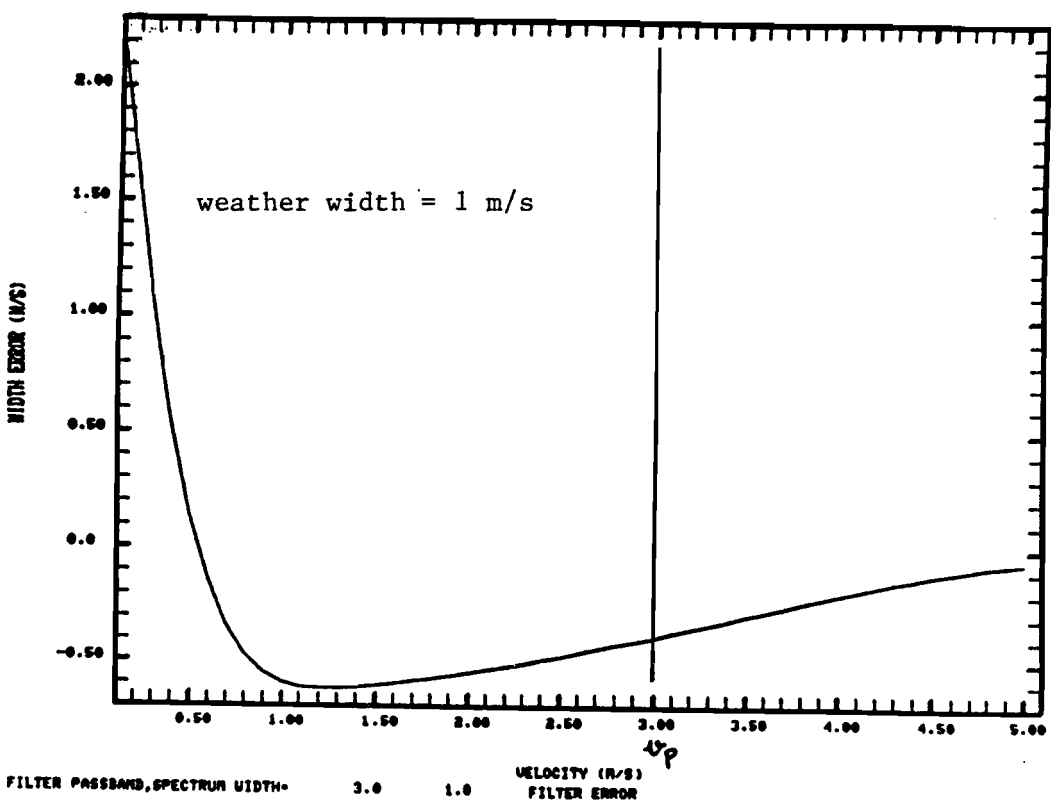


Fig. 3-8b. Mean Velocity Error For Idealized Clutter Filter With 3 m/s Passband.



R(1)/R(2) width estimator

horizontal scale is weather mean velocity

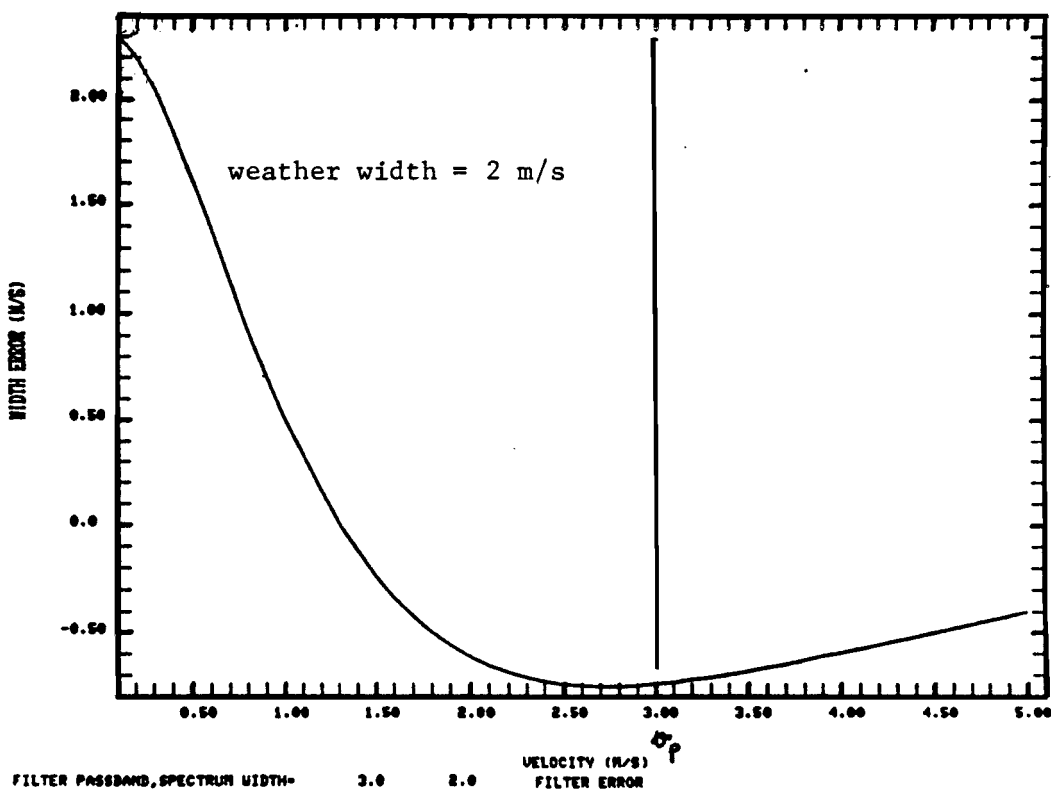
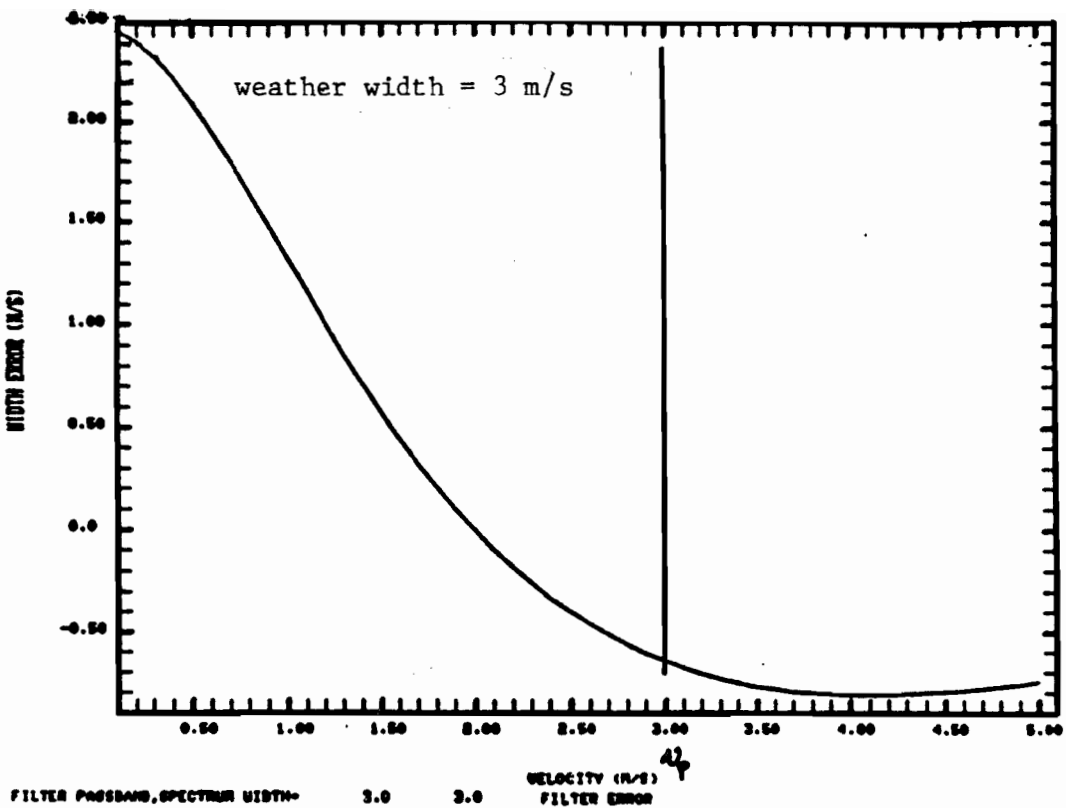


Fig. 3-9a. Spectrum Width Error For Idealized Clutter Filter With 3 m/s Passband.



R(1)/R(2) width estimator

horizontal scale is weather mean velocity

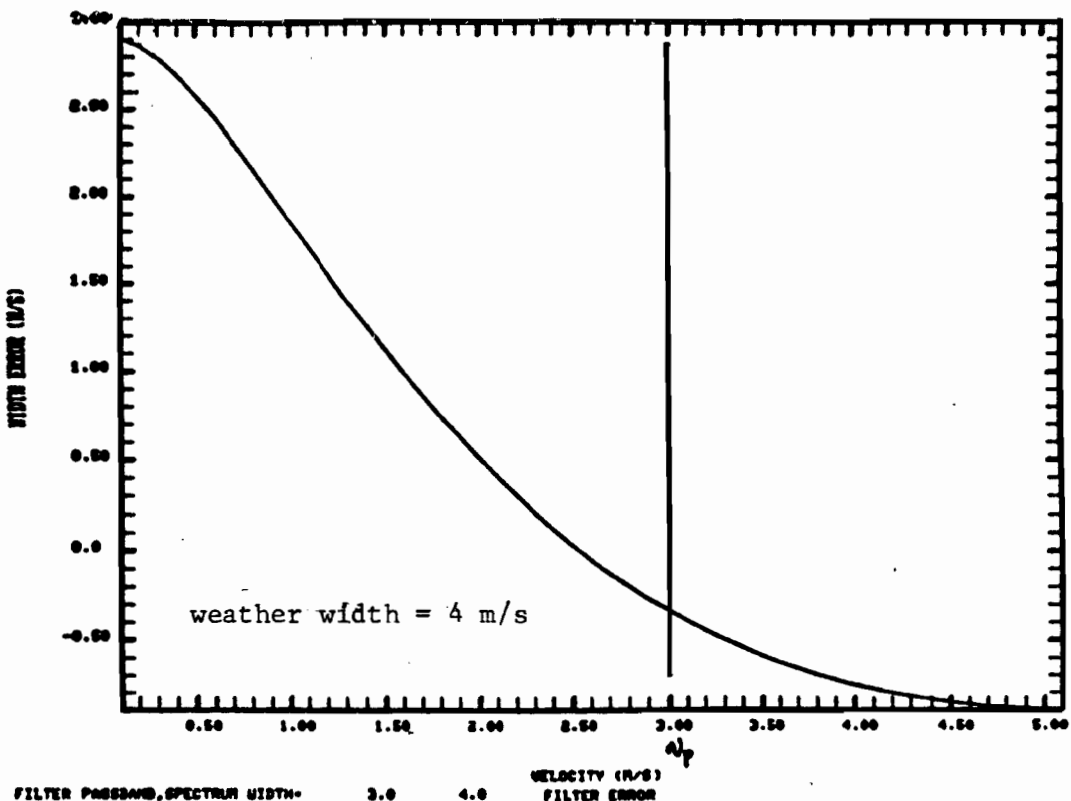
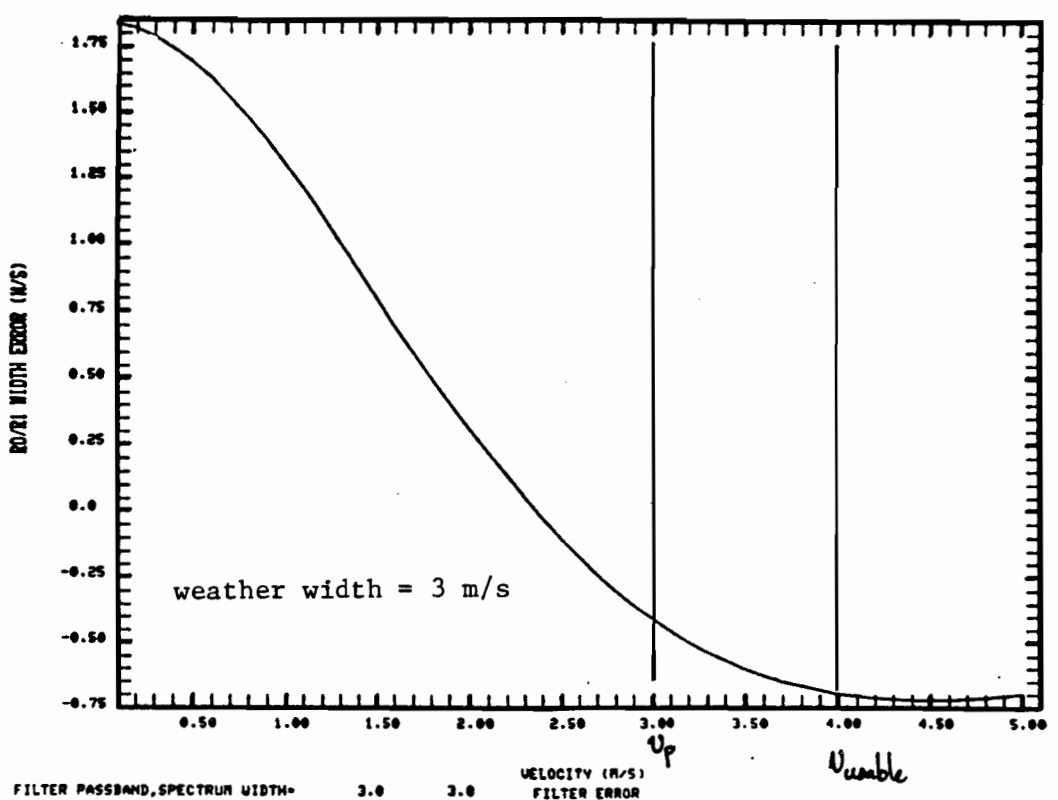


Fig. 3-9b. Spectrum Width Errors for Idealized Clutter Filter with 3 m/s Passband.



R(0)/R(1) width estimator
horizontal scale is weather mean velocity

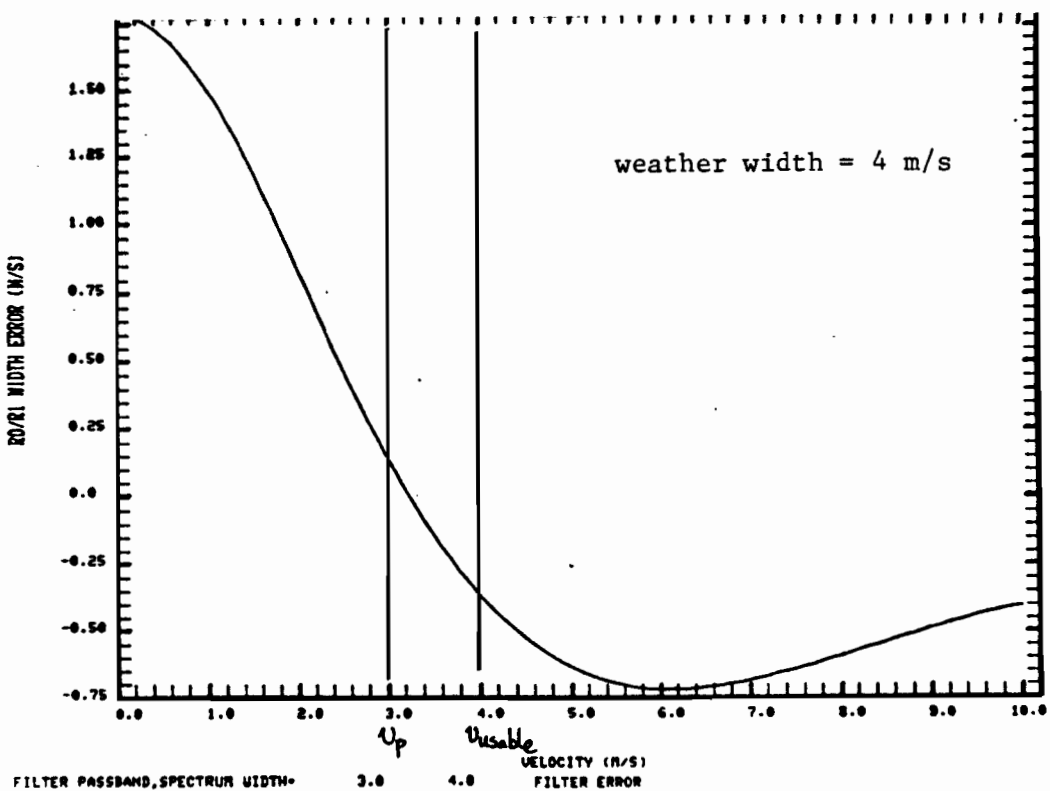


Fig. 3-9c. Spectrum Width Errors for Idealized Clutter Filter.

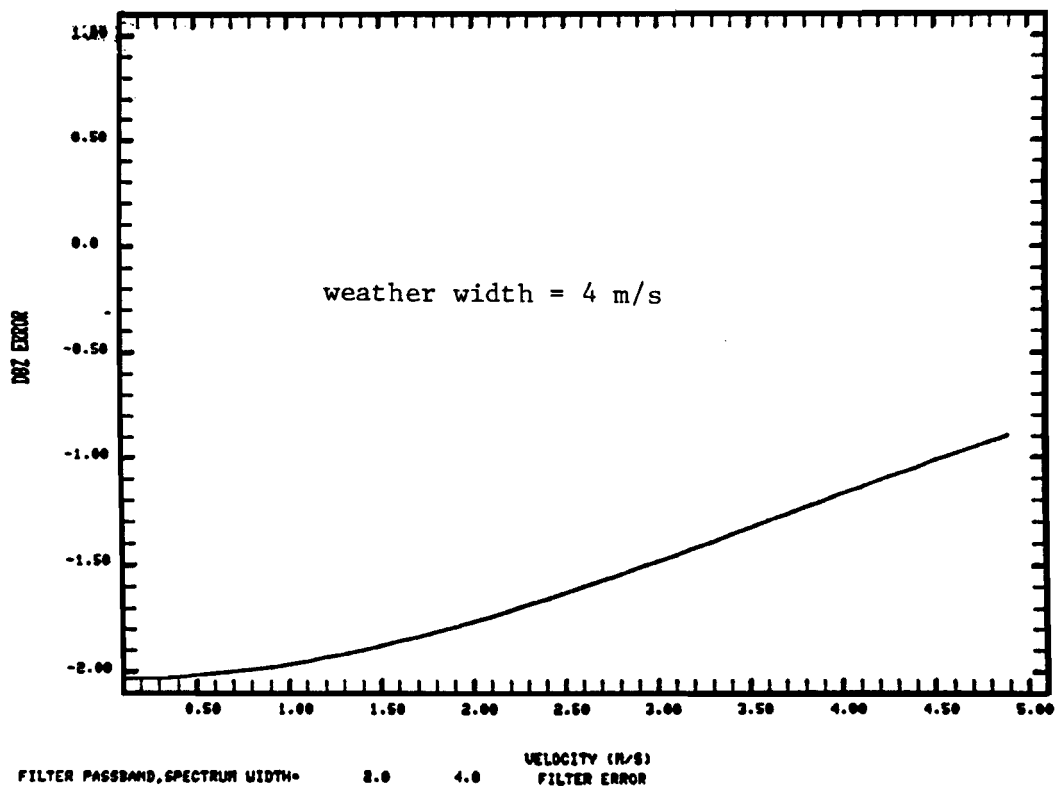
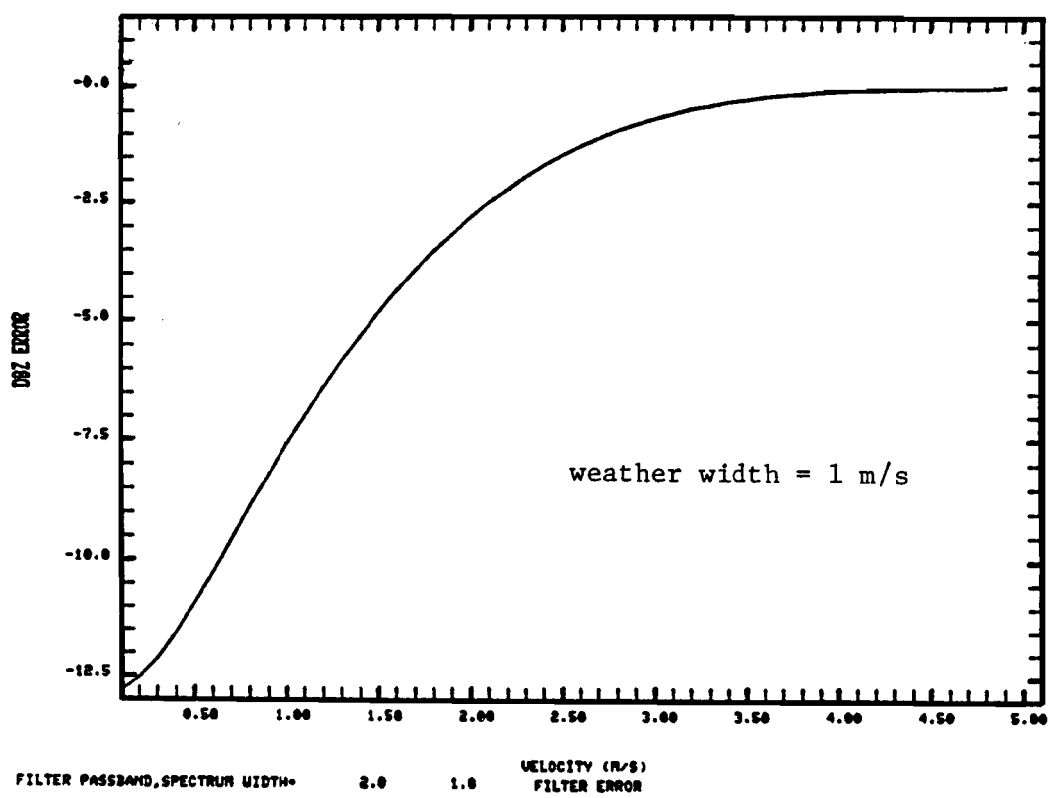


Fig. 3-10. Reflectivity Error for 2 m/s Passband.

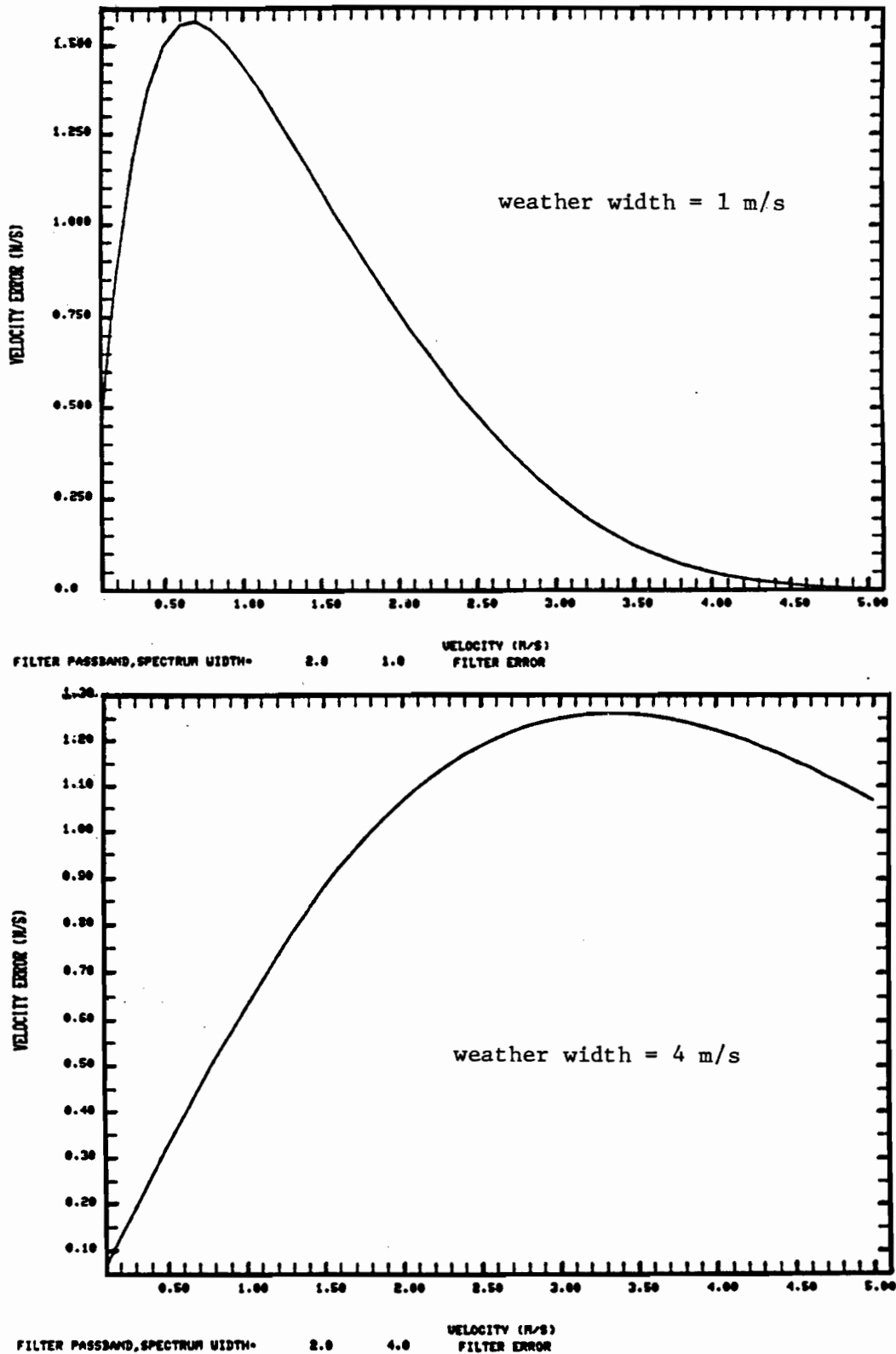


Fig. 3-11. Mean Velocity Errors for 2 m/s Passband.

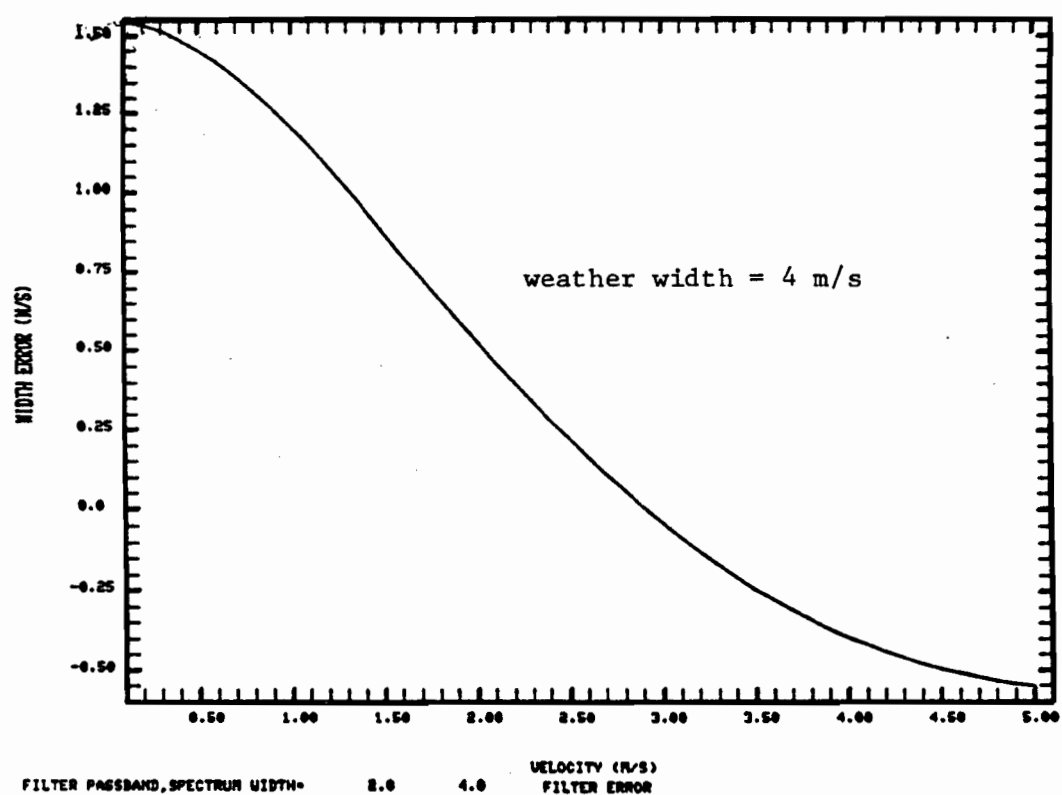
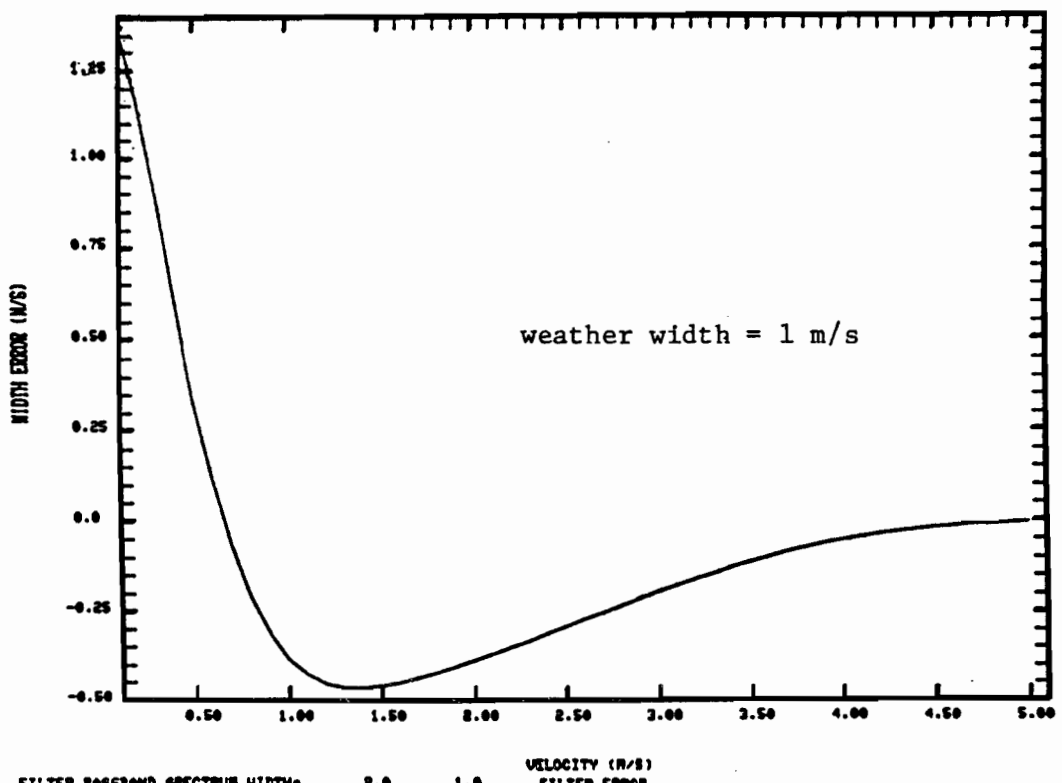
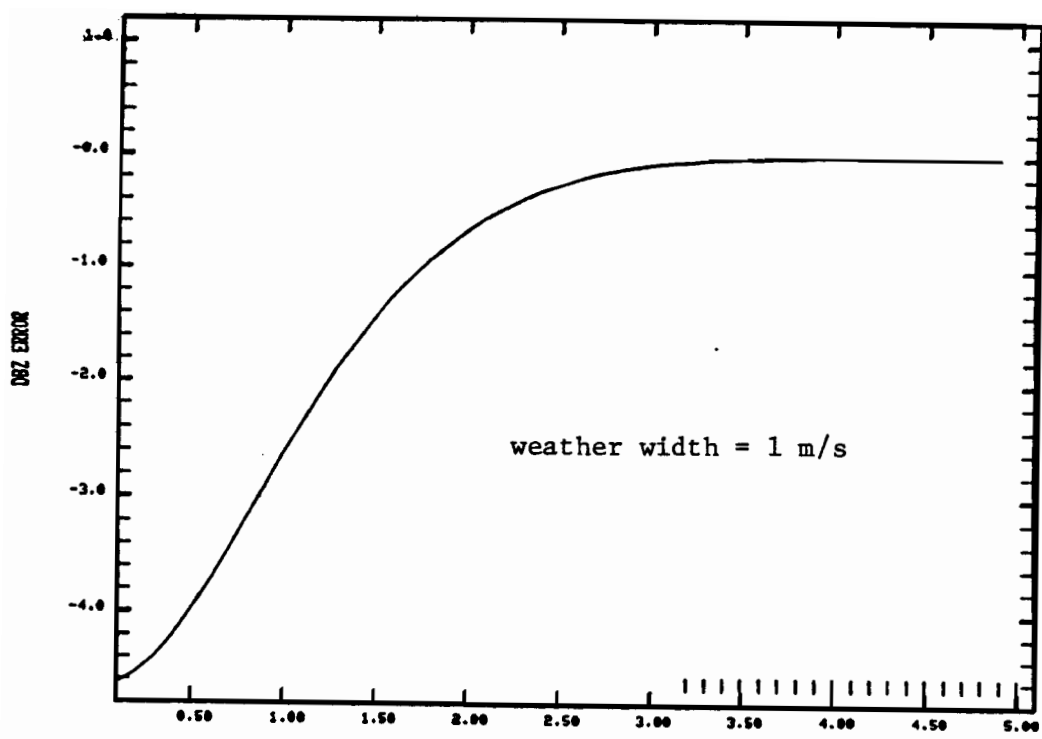
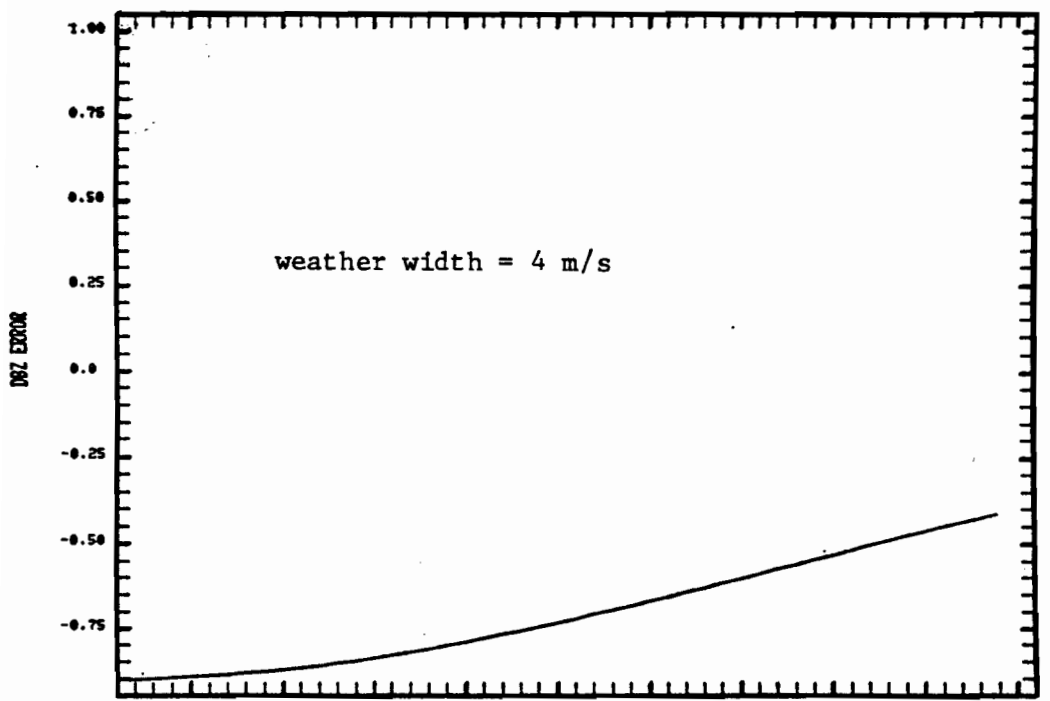


Fig. 3-12. Spectrum Width Errors for 2 m/s Passband.



FILTER PASSBAND,SPECTRUM WIDTH= 1.0 1.0 VELOCITY (M/S)
FILTER ERROR



FILTER PASSBAND,SPECTRUM WIDTH= 1.0 4.0 VELOCITY (M/S)
FILTER ERROR

Fig. 3-13. Reflectivity Errors for 1 m/s Passband.

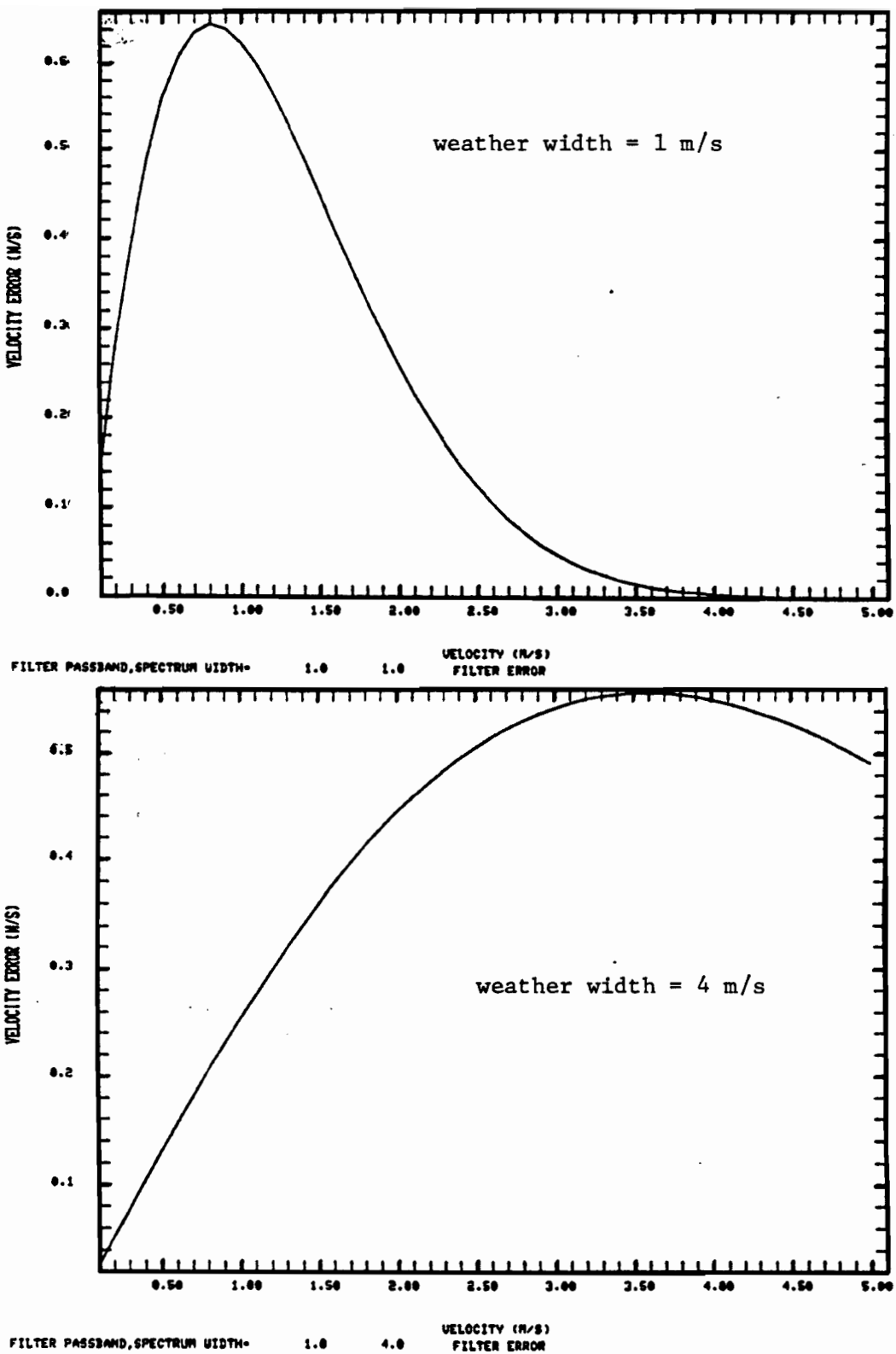


Fig. 3-14. Mean Velocity Errors with 1 m/s Passband.

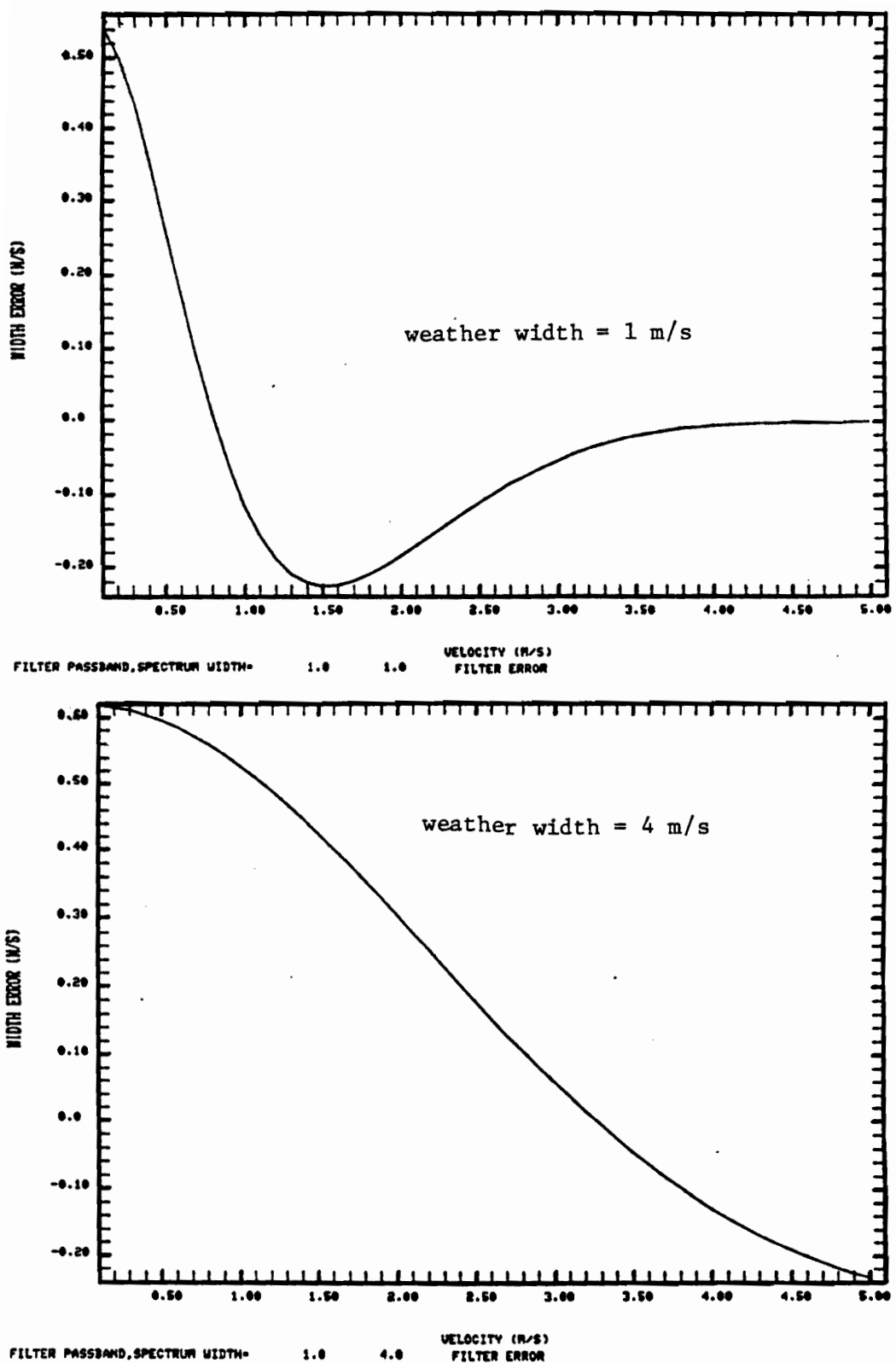


Fig. 3-15. Spectrum Width Errors with 1 m/s Passband.

To illustrate, with $V_p = 3$ m/s there is a 0.7 dB error at V_{av} when $\sigma_v = 1$ m/s and a 1.9 dB error when $\sigma_v = 4$ m/s. Thus, "worst case" σ_v for reflectivity rms errors is not "worst case" for bias errors due to the clutter filter.

(2) mean velocity estimation

The error at passband edge ($V_{av} = V_p$) is greater at large spectrum widths since more weather power is contained in the stopband. The pulse pair (PP) error is worse than that for Fourier analysis:

$$\begin{aligned}\text{error (Fourier)} &= \sigma_v / \sqrt{2\pi} \quad \text{for } \sigma_v \ll V_p \\ &= 0.40 \text{ m/s at } \sigma_v = 1 \text{ m/s}\end{aligned}\quad (3-8)$$

versus PP error of 0.75 m/s.

The error decreases for $|V_{av}| < V_p$. The worst case when $V_p = 3$ m/s is at larger widths (1.95 m/s error at $V_{av} = 4$ m/s when $\sigma_v = 4$ m/s).

(3) spectrum width estimation

With Fourier analysis (i.e., spectrum domain computation) of spectrum widths, the error for $V_{av} = V_p$ should be proportional to σ_v for $\sigma_v \ll V_p$. Specifically, for frequency domain estimation with $V_{av} = V_p$

$$\text{error in estimating } \sigma_v = 0.42 \sigma_v. \quad (3-9)$$

The pulse pair errors for $\sigma_v = 1.0$ agree fairly well with the expression above. For $\sigma_v \geq V_p$, the pulse pair errors are lower than the above expression.

There is no significant difference between the $R(0)/R(1)$ and $R(1)/R(2)$ estimators for σ_v in terms of clutter filtering error.

For $|V_{av}| > V_p$ the σ_v errors were all less than 1 m/s. The greatest extent of σ_v errors for $|V_{av}| \geq V_p$ is at the largest V_p , but the peak σ_v error appears to saturate at 0.75 m/s as V_p increases.

The weather parameter estimate biases due to clutter filtering must of course be traded off against the biases which arise when clutter is not suppressed. For reflectivity estimation, the bias error due to clutter, or clutter residue is simply

$$\begin{aligned}&= 10 \log_{10} (S+C) - 10 \log_{10} (S) \\ &= 10 \log_{10} (1 + C/S)\end{aligned}\quad (3-10)$$

where S = net signal power
 C = clutter (or clutter residue) power.

The error in mean velocity estimation due to clutter with a Gaussian spectrum (as computed by Zrnic' and Hamidi [1] is shown in Figure 3-16. This figure is approximately applicable to a linear time invariant clutter filter followed by pulse pair estimation for the following reasons:

1. the PP mean velocity error is given by:

$$\epsilon = (v_a/\pi) \text{ angle } [R_c(T_s) + R_w(T_s)]$$

where $R_c(\cdot)$ = clutter or clutter residue autocorrelation
 $R_w(\cdot)$ = weather autocorrelation

2. since the clutter spectrum and the clutter filter are symmetrical about zero frequency, the imaginary part of $[R_c(T_s)]$ is zero in either case.
3. by Fourier theory [13]:

$$R_c(0) \geq R_c(T_s) \geq R_c(0) - 2\pi T_s \int |f| S_c(f) df \quad (3-11)$$

where $S_c(f)$ is the clutter (or clutter residue) spectrum. If we assume that $S_c(f) = 0$ for $f > f_0$, then

$$R_c(0) \geq R_c(T_s) \geq R_c(0) (1 - 2\pi T_s f_0) \quad (3-12)$$

Taking $f_0 = 10\sigma_c/\lambda$, $\sigma_c = 0.3$ m/s and $T_s = 0.001$ sec, we obtain

$$R_c(0) \geq R_c(T_s) \geq 0.73 R_c(0).$$

The upper bound means that one can use the signal-to-clutter residue power ratio in Figure 3-16 to compute the errors while the lower bound says that the signal-to-clutter residue ratio should be increased by 1.4 dB before determining the error from Figure 3-16.

Figure 3-17 shows the corresponding errors for spectrum width bias error as a function of S/C ratio as determined by Zrnic' and Hamidi [1]. The argument above for mean velocity error can be applied in this case to reach the conclusion the use of signal-to-clutter residue ratio in Figure 3-17 will at worst overbound the error by approximately 1.5 dB in effective S/C ratio for weather widths ≤ 4 m/s.

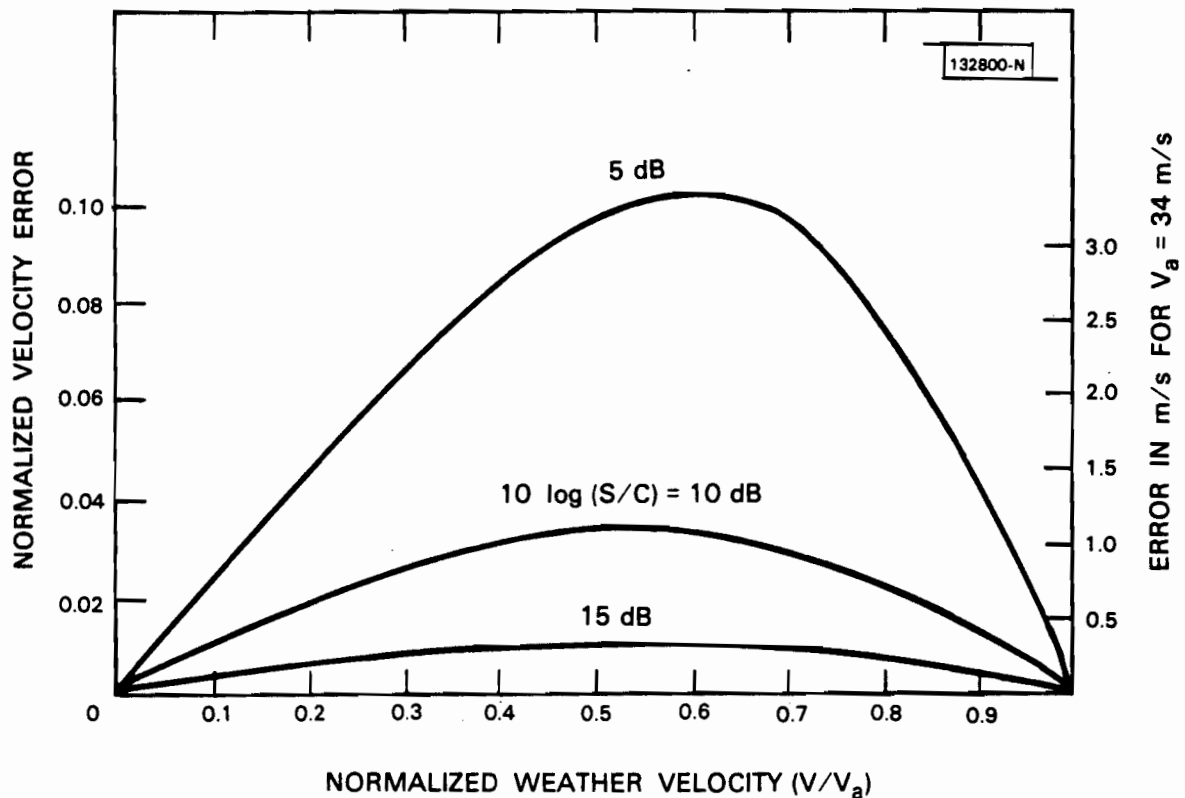


Fig. 3-16. Magnitude of the normalized velocity error versus the magnitude of the signal mean velocity. Signal-to-clutter power ratio is indicated, and the curves are strictly correct for $\sigma_c < \sigma_v \ll v_a$.

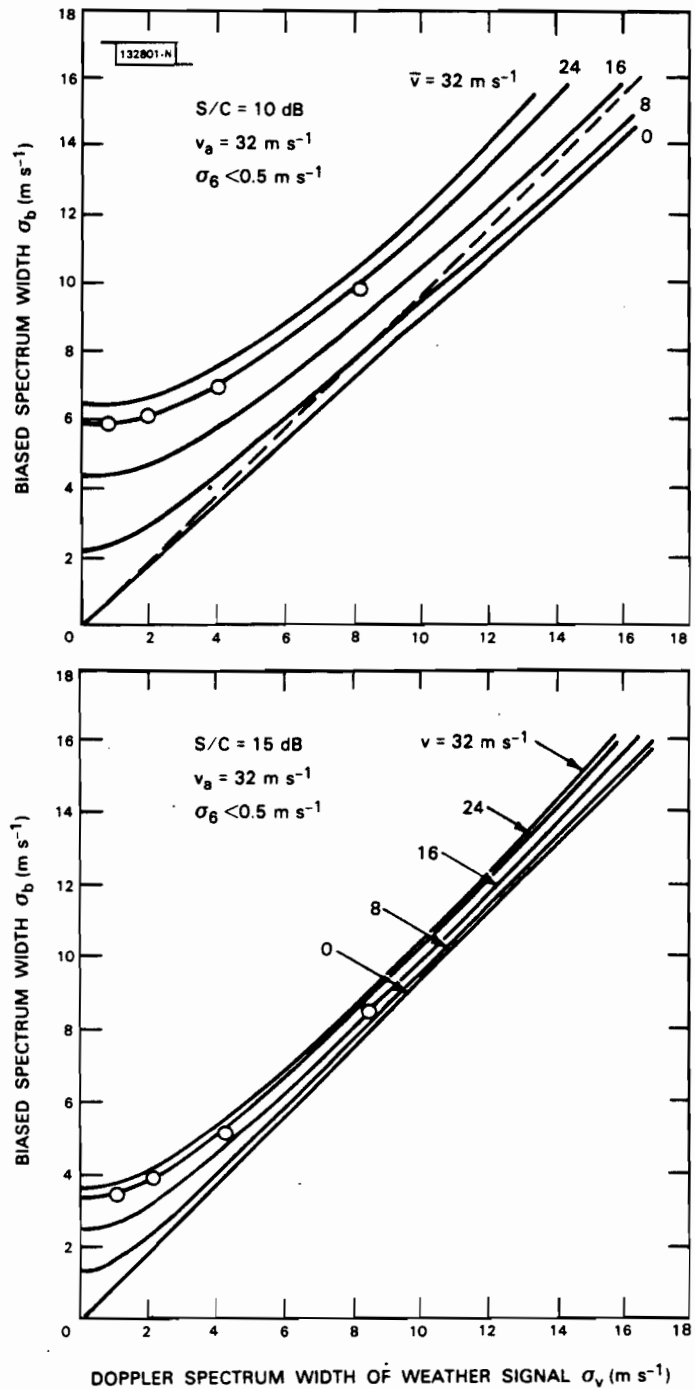


Fig. 3-17. Biased spectrum width when signal and clutter are present. The clutter spectrum width is less than $.5 \text{ m}\cdot\text{s}^{-1}$ and unambiguous velocity is $32 \text{ m}\cdot\text{s}^{-1}$. Mean velocities are indicated and results of simulations for $\bar{v} = 24 \text{ m}\cdot\text{s}^{-1}$ are superimposed. Dashed line is at 45° . To obtain values for any other unambiguous velocity v_a , divide the scale by 32 and multiply with v_a .

IV. CLUTTER SUPPRESSION CAPABILITY

In this section, we present the recommended clutter suppression requirements and the supporting rationale. Our objective here was to achieve a functional performance specification which:

- (1) matches as closely as possible the performance implied in the system definition phase RDA specification (Table 1-1) without specifying a particular form of clutter suppression,
- (2) has quantitative measures of capability which can directly be related to weather parameter estimates, and
- (3) relates directly to the characteristics of the clutter as they would be observed with a NEXRAD sensor.

Table 4-1 shows the specification text developed from the current study. Tables 4-2 and 4-3 provide additional specification details while Figs. 3-6 and 3-7 alluded to in Table 4-1 are Figs. 3-16 and 3-17 in the preceding chapter. Tables 3-7 and 3-8 alluded to in Table 4-1 are Tables 4-2 and 4-3 in this report.

In the remainder of this section, we describe the rationale for the various paragraphs in Table 4-1.

A. General Approach to Specification Development

In the preceding chapter, we have seen that a key issue in clutter suppression is the tradeoff between weather parameter errors due to clutter suppression and those due to the clutter residue. Paragraph #1 addresses this by separately specifying the maximum allowable errors in weather parameter estimates due to:

- (1) the clutter suppression technique when no clutter is present, and
- (2) the clutter residue as a function of the input signal-to-clutter power ratio and desired improvement factor.

In an operational radar, these two errors will be present simultaneously. However, since error (2) is clutter level dependent, it was felt that the disadvantage of complexity* in a simultaneous error specification would far outweigh advantage of better approximation to an actual clutter situation.

*A combined error specification would have to describe the allowable error as a function of 3 independent variables (weather velocity, width and S/C ratio).

TABLE 4-1

RECOMMENDED CLUTTER SUPPRESSION CAPABILITY SPECIFICATION TEXT

	<u>3.7.1.7 Ground Clutter Suppression</u>	
# 1	<p>The objective of the clutter suppression capability is to improve the capability to measure the weather return parameters in the presence of clutter. Clutter suppression capability is characterized in terms of an improvement in the equivalent signal/clutter (S/C) ratio. The weather return parameter errors when clutter is present are the sum of (a) the error which arises from the effects of the clutter suppression technique (e.g., a clutter filter) on the weather return, and (b) the S/C ratio dependent error which arises from the clutter residue. Bounds on error contribution (a) are defined in Tables 3-7 and 3-8, while those for contribution (b) are defined below and in Figures 3-6 and 3-7.</p>	# 4
# 2	<p>The RDA shall include ground clutter suppression for the reflectivity and Doppler channels meeting the requirements shown in Tables 3-7 and 3-8, respectively, when the RDA clutter suppression capability is characterized by the improvement in the ability to measure the weather return parameters at a nominal 2.8 GHz for a standard Gaussian random process weather return model in the presence of each of the following clutter models. Clutter model A is a Gaussian random process with a Gaussian spectrum centered at zero mean velocity. The spectrum rms width is the root sum square of 0.1 ms^{-1} and the rms width due to the antenna rotation rate at the bottom two elevation angles. Clutter model B represents a scattering echo from a point target, and consists of a complex waveform with random phase and an amplitude envelope which is a replica of the two-way antenna pattern.</p>	# 5
# 3	<p>At an S/C power ratio of $(X - I)$ dB, the weather return parameter errors due to clutter for the standard weather return model shall be less than or equal to that shown in Figure 3-6 for radial velocity and in Figure 3-7 for spectrum width. The bias error of the reflectivity measurement shall be less than</p> $-10 \log_{10} \left(\frac{R}{1 + R} \right)$ <p>where: $R = \text{antilog} (0.1(X - I))$ is the equivalent signal to clutter power ratio</p> <p>X is the input signal to clutter power ratio in dB</p> <p>I is the ground clutter suppression capability in dB (at least 30 dB for reflectivity data, or the requirement stated in Table 3-8 for radial velocity or spectrum width data.)</p>	# 6
		<p>If clutter suppression is accomplished by a linear time invariant filter followed by a conventional weather return parameter estimation scheme (e.g., pulse pair algorithm), the clutter rejection capability can be characterized by the ratio of the filter output power to filter input power for the various clutter models, as illustrated in Figure 3-8.</p> <p>The Government will supply: (a) a site peculiar elevation angle independent clutter suppression map which specifies those ranges and azimuths at which clutter suppression will be applied, and (b) a site peculiar table indicating the amount of clutter suppression (selected from Table 3-8) to be applied at each elevation angle in accordance with (a).</p> <p>Where the clutter suppression is off, there shall be no degradation in the weather return parameter accuracy with respect to Sections 3.7.1.2.3.1 and 3.7.1.2.3.2. In addition, capability shall be provided for Government access to the clutter suppression control lines.</p>

TABLE 4-2
MAXIMUM ALLOWABLE BIAS IN REFLECTIVITY ESTIMATES
DUE TO THE USE OF CLUTTER SUPPRESSION

Weather Spectrum Width ms^{-1}	Bias Error With High S/C Ratio (dB)	
	Clutter Model A	Clutter Model B
1	10	10
2	2	2
3	1	1
>3	< 1	< 1

Any bias of reflectivity estimates when clutter suppression is applied shall be systematic.

The reflectivity estimate bias is systematic if predictable from mean velocity and/or spectrum width parameters of the standard weather model.

TABLE 4-3
CLUTTER SUPPRESSION FOR RADIAL VELOCITY AND
SPECTRUM WIDTH ESTIMATES

Minimum Usable* Weather Return Velocity, v_{min} , in ms^{-1}	Required Ground Clutter Suppression Capability (I) in dB Required for Two Lowest Elevation Levels	
	Clutter Model A	Clutter Model B
2	20	20
3	28	30
4	50	50

*The weather return is deemed usable if, with the clutter suppression technique operating at a high S/C ratio, the mean velocity and spectrum width estimate biases and standard deviations are each less than 2.0 ms^{-1} at a signal to noise ratio of equal or higher than 5 dB for standard weather model returns with a mean velocity magnitude $\geq v_{min}$ and a spectrum width between 1.0 ms^{-1} and 4.0 ms^{-1} . The assumed carrier frequency is 2.8 GHz.

The rationale used to bound the type (1) errors in the accompanying tables was a function of the particular weather parameter and will be discussed in the following two sections. One general problem here was that the system definition phase NTR (NEXRAD Technical Requirements) specification did not directly specify allowable bias errors. However, since the effects of a bias error and twice the NTR rms errors will be similar for most NEXRAD applications, twice the rms errors were used as maximum allowable bias errors in Tables 4-2 and 4-3.

The use of two clutter models for performance assessment in paragraph #2 in Table 4-1 was motivated by the desire to emulate the principal features of ground clutter. Much of the rationale for the particular models used was discussed in Chapter III and more will be presented in the next chapter.

The exact meaning of the numerical clutter suppression capability in the original specification was unclear. The Groginsky-Glover paper [2] discusses the ratio of peak amplitude into an infinite impulse response (IIR) filter to the peak amplitude out of the filter as the antenna scans by a fixed discrete scatterer. Informal discussions with some of the participants in the original drafting group indicate that the rejection figure specified in the original NTR specification would correspond to the clutter filter notch depth at zero mean velocity.

Neither of these interpretations was fully satisfactory because of the following:

1. the clutter (and clutter residue) from a point scatter is a time varying quantity whose average power (i.e., energy) over the period of weather parameter integration is the key quantity in determining the error due to the clutter. Also, it was unclear how discrete scatterer rejection would be related to rejection of distributed clutter.
2. specification of a filter by the notch depth at zero frequency and the half-power passband edges does not provide an adequately tight bound on the clutter power reduction. Since it is the S/C ratio which determines the error, it was essential to either add a stop-band width specification to the original specification or, phrase the suppression in terms of equivalent clutter power reduction. The latter course was viewed as the only appropriate choice if a functional performance specification was to be developed.

Thus, in paragraph #3 of Table 4-1, the reduction in effective clutter-to-signal power (energy) ratio is used to quantitatively characterize the amount of clutter suppression.

It was essential to determine that the required amount of clutter power reduction shown in Tables 4-2 and 4-3 could be achieved by representative clutter suppression techniques. This was accomplished by the simulation studies described in Chapter VII.

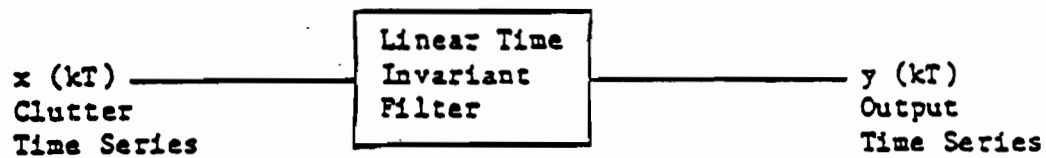
One difficulty with the use of the effective clutter power reduction concept in paragraph #3 of Table 4-1 and the accompanying error bounds is the need for a large number of simulations to explore the various weather mean velocity and spectrum width parameter combinations.

When the clutter suppression is accomplished by the use of a linear time invariant (LTI) filter followed by conventional (e.g., pulse pair) weather parameter estimation, the capability assessment in the presence of clutter can be determined from filter input-output power relationships which give equivalent results (recall Chapter III) with much less effort. Thus, paragraph #4 in Table 4-1 calls for the use of a filter input-output power ratio in such cases. It is implicitly assumed in paragraph #4 that the LTI filter has unity gain in the passband region so that the change in clutter power equals the change in S/C ratio for weather with a mean velocity greater than V_{usable} . Figure 3-8 referred to in paragraph #4 is Fig. 4-1 of this chapter.

Since achieving greater clutter suppression will introduce the possibility of greater weather parameter errors when the weather mean velocity is near zero, it is important that the clutter suppression capability be used only in those regions in which it is needed. Paragraphs #5 and #6 in Table 4-1 provide the capability for achieving a degree of control in the clutter filtering. The text shown here represents a tradeoff between optimization of clutter cancellation, hardware considerations, and the desire not to deviate from an earlier concensus of the principal users. In particular:

1. the degree of clutter suppression does not change as a function of azimuth at a given range and elevation angle (to simplify processing with IIR clutter filters at constant PRF),
2. the amount of clutter suppression to be used at a given elevation angle is constant so that suppression parameters (e.g., filter coefficients) need not change in processing a given azimuth - elevation ray, and
3. it was assumed that accomplishing no clutter suppression at a given azimuth range bin could be easily accomplished by bypassing (or paralleling) the clutter suppression operation. In such a case, the weather parameter accuracy should be identical to that if no clutter suppression were in use.

The term of "government access to the clutter control lines" was retained since it represented the results of an earlier principal users consensus.



T = Pulse Repetition Time

Clutter Model

Algorithm for Computing Clutter Suppression Capability: I

A

$$I = 10 \log_{10} [\langle |x(kT)|^2 \rangle / \langle |y(kT)|^2 \rangle]$$

B

$$I = 10 \log_{10} [C / \max \langle |y(kT)|^2 \rangle]$$

C = peak power return from the fixed scatterer

$\langle \rangle$ denotes time average over weather parameter estimation interval

FIGURE 4-1

CLUTTER SUPPRESSION CAPABILITY CHARACTERIZATION
FOR LINEAR TIME INVARIANT CLUTTER FILTERING

B. Rationale for Doppler Parameter Specification

The clutter suppression capability for the weather mean velocity and spectrum width estimates was developed by interpreting the NTR specification [11] in the context of the work by Groginsky and Glover [2]. In particular:

1. the +1 dB ripple in the clutter filter passband for the Doppler channel was developed from a goal of +1 m/s velocity error [2]. However, the velocity error induced by a clutter filter passband ripple depends on the filter ripple period, as well as the ripple amplitude (as will be shown in Chapter VII). Thus, the new specification directly specifies the maximum allowable velocity error due to the clutter filter.
2. similarly, the original specification discusses filter stopbands, whereas what is desired is accurate weather parameter estimates whenever the weather mean velocity is above some minimum velocity. Thus, we specify here a minimum "usable" velocity which corresponds to the velocity at which weather parameter estimates would have met the desired accuracies with the clutter filter passbands as specified in the original earlier NTR.

The error which arises due to weather spectrum "notching" depends on the exact clutter filter shape which was loosely specified in the earlier specification. However, to a first approximation, the passband width is the major determinant of this error. Thus, the idealized filter results of the preceding chapter were used as the basis for determining the usable velocity-tolerable error specification.

C. Rationale for Reflectivity Estimate Specification

The clutter specification for the weather reflectivity estimate was developed from the earlier NTR through discussions with users [especially those associated with the National Weather Service (NWS)]. There is a particular NWS need for accurate reflectivity estimates at all mean radial velocities; consequently, the concept of minimum usable velocity was not appropriate. On the other hand, it was recognized that accurate estimation of zero mean radial velocity weather in the presence of clutter could only be accomplished when the weather spectrum width was larger than that of the clutter.

Thus, it was viewed as appropriate to bound the errors due to the clutter suppression technique as a function of weather spectrum width. The particular bounds shown in Table 4-2 were obtained by considering the following suppression techniques:

- (a) signal variability processors under study by D. Sirmans (NSSL) and K. Shreeve (NWS), and
- (b) the linear filter - PP processor errors at zero mean velocity which are presented in Chapters III and VII.

Both of these techniques gave essentially identical results. It should be noted that the errors with technique (b) at non-zero weather mean radial velocities will be considerably smaller than those for technique (a). On the other hand, technique (a) does not require the use of a wide dynamic range linear receiver in the reflectivity channel.

The bounds on reflectivity error in the presence of clutter are the difference between the signal-and-clutter (residue) power versus the signal power which was given in Eq. (3-10).

V. CLUTTER MODELS

In this chapter, we discuss modeling of clutter for the purpose of clutter suppression specification and testing. Historically, the principal emphasis in clutter modeling has been on homogeneous distributed clutter from a random scattering surface because of:

- (1) ease of theoretical analysis, and
- (2) its utility in predicting clutter performance in practical applications such as sea clutter or land clutter as seen from aircraft.

However, it has been recognized that land clutter illuminated at the near-grazing angles characteristic of NEXRAD operation is not adequately characterized by such a model, especially in the presence of man-made objects.

Section A discusses the classical distributed model considered by Hamidi and Zrnic' [1] and the difficulties encountered in applying this model to represent actual radar sites. Section B considers a discrete scatterer model, while section C addresses measured clutter data from existing S-band radars as a model more typical of the actual NEXRAD environments.

A. Homogeneous Distributed Clutter

1. Received Power Levels

The received clutter power, P_C , in a radar measurement cell can be found by the classic radar equation:

$$P_C = \frac{P_T G^2 \lambda^2 \sigma}{(4\pi)^3 R^4} \quad (5-1)$$

where

P_T = power transmitted
 G = antenna gain
 λ = wavelength
 R = range
 σ = radar cross section for the cell

For scattering by a large number of random, homogeneous scatterers (e.g., ocean waves, trees, cornstalks, etc.), the radar cross section is given by:

$$\sigma = A_i \sigma_o \quad (5-2)$$

where σ_o = scattering cross-section/unit area
 A_i = area illuminated
 $= 0.5R \theta c\tau \sec \phi$
 θ = antenna beamwidth
 τ = pulse duration
 c = velocity of propagation
 ϕ = angle of incidence on surface.

Combining equations (5-1) through (5-3), we obtain:

$$P_c = \frac{P_t G^2 \lambda^2}{128\pi^3 R^3} \theta c\tau (\sigma_o \sec \phi). \quad (5-4)$$

The elevation angle dependence of σ_o is an important factor. If the terrain could be modeled as a single layer of isotropically scattering spheres which did not shadow one another, then σ_o would be independent of ϕ . However, it has been found empirically (see pages 75-77 of Long [18]) that the relationship:

$$\sigma_o = \gamma \sin \phi \quad (5-5)$$

where γ is independent of ϕ provides a much better fit to the observed data.

Substituting (5-5) into (5-2) and (5-3), we obtain:

$$\sigma = \gamma 0.5 \theta R c\tau \tan \phi \quad (5-6)$$

At the low elevation angles characteristic of NEXRAD mainlobe clutter:

$$\tan \phi \approx h/R \quad (5-7)$$

where h is the height of the antenna phase center above the scattering objects. Using the approximation of Eq. (5-7) in (5-6) we obtain:

$$\sigma \approx 0.5 \gamma h c \tau \theta \quad (5-8)$$

which is now independent of R and ϕ , and

$$P_c = \frac{P_t G^2 \lambda^2}{(4\pi)^3 R^4} \gamma (0.5 h c \tau \theta). \quad (5-9)$$

Eq. (5-9) shows that low NEXRAD phase center heights are advantageous for clutter mitigation (albeit disadvantageous from the viewpoint of achieving a line-of-sight to weather at low elevation angles. For "typical" values of $\tau = 1\mu s$, $\theta = 1^\circ$, and $h = 10m$, the product $0.5 h c \tau \theta = 24 m^2 = +14 dB$ with respect to $1 m^2$.

Tree-covered surfaces probably represent the most likely case of a land-based homogeneous, random clutter source which would provide appreciable clutter returns. Figs. 5-1 and 5-2 show the results of clutter measurements by Raytheon [17] at S- and X-band on heavily wooded hills near Harvard, MA. We see that γ at the angles of incidence of concern for NEXRAD (typically $<2^\circ$) was not significantly affected by frequency, but did decrease near-grazing incidence for trees without leaves.

A γ level of -15 dB with the "typical" $\tau\theta h$ product above corresponds to a σ of $0.8 m^2$. In Fig. 5-3 we compare the signal return from clutter with cross sections of $0.01 m^2$ and $1 m$ with representative weather reflectivities. We see that the returns from clutter with such cross sections could be of significant concern out to substantial ranges. Fortunately, the situation is not as bad as suggested by Fig. 5-3 since earth curvature* and/or shadowing by intervening objects will mitigate much of the tree clutter under normal propagation conditions.

Table 5-1 shows some other examples of land clutter reflectivity (σ_0) values at low grazing levels. Reflectivity levels of -30 dB correspond to a σ of $+1.0 m^2$ for typical NEXRAD parameters at a range of 10 km; hence we can see that other types of homogeneous terrain as well as trees may represent a significant clutter problem if illuminated by the NEXRAD radar, especially when anomalous propagation (AP) occurs.

2. Amplitude Distribution of Distributed Clutter

The above discussion has shown that distributed scatterers such as trees can produce large enough signals to be of concern for NEXRAD. Theoretically, the net return from such scatterers should be a complex Gaussian process (i.e., a Rayleigh distributed net power) as long as there are a large number of scatterers in a radar resolution cell.

Examination of the validity of Gaussian distribution model has generally been proceeded by two approaches:

*If the NEXRAD antenna phase center is Δh feet above the surrounding trees, the radio horizon with normal refraction will be at a range of $2.7 \sqrt{\Delta h} km = 12 km$ for $\Delta h = 50$ feet.

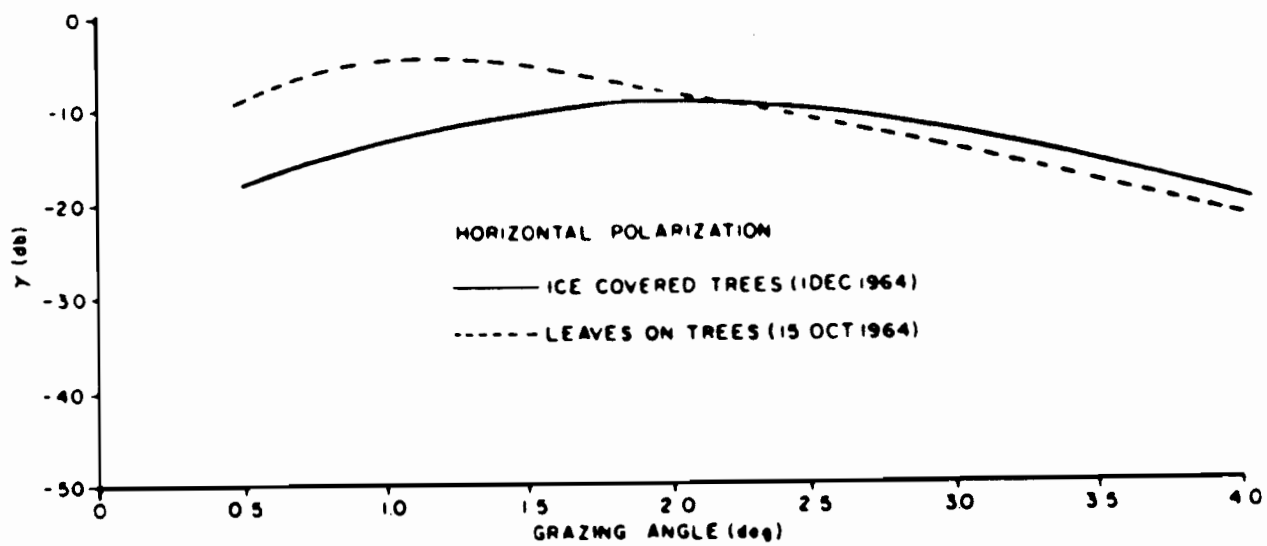


Fig. 5-1. Backscatter Coefficients vs. Grazing Angle at 2750 MHz (from [17]).

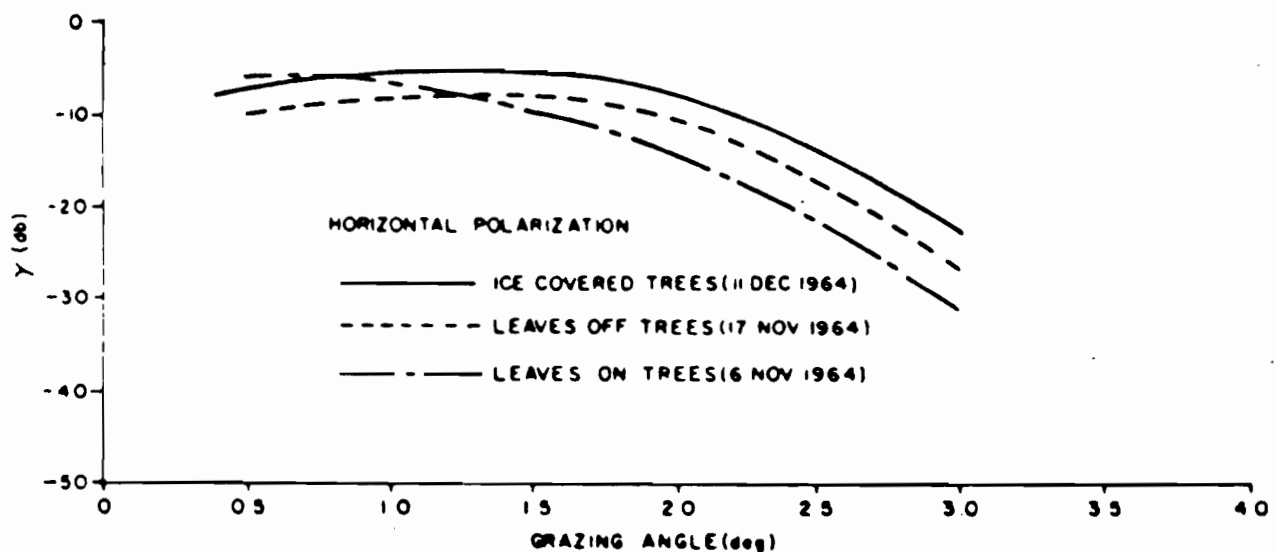


Fig. 5-2. Backscatter Coefficient vs. Grazing Angle at 9405 MHz (from [17]).

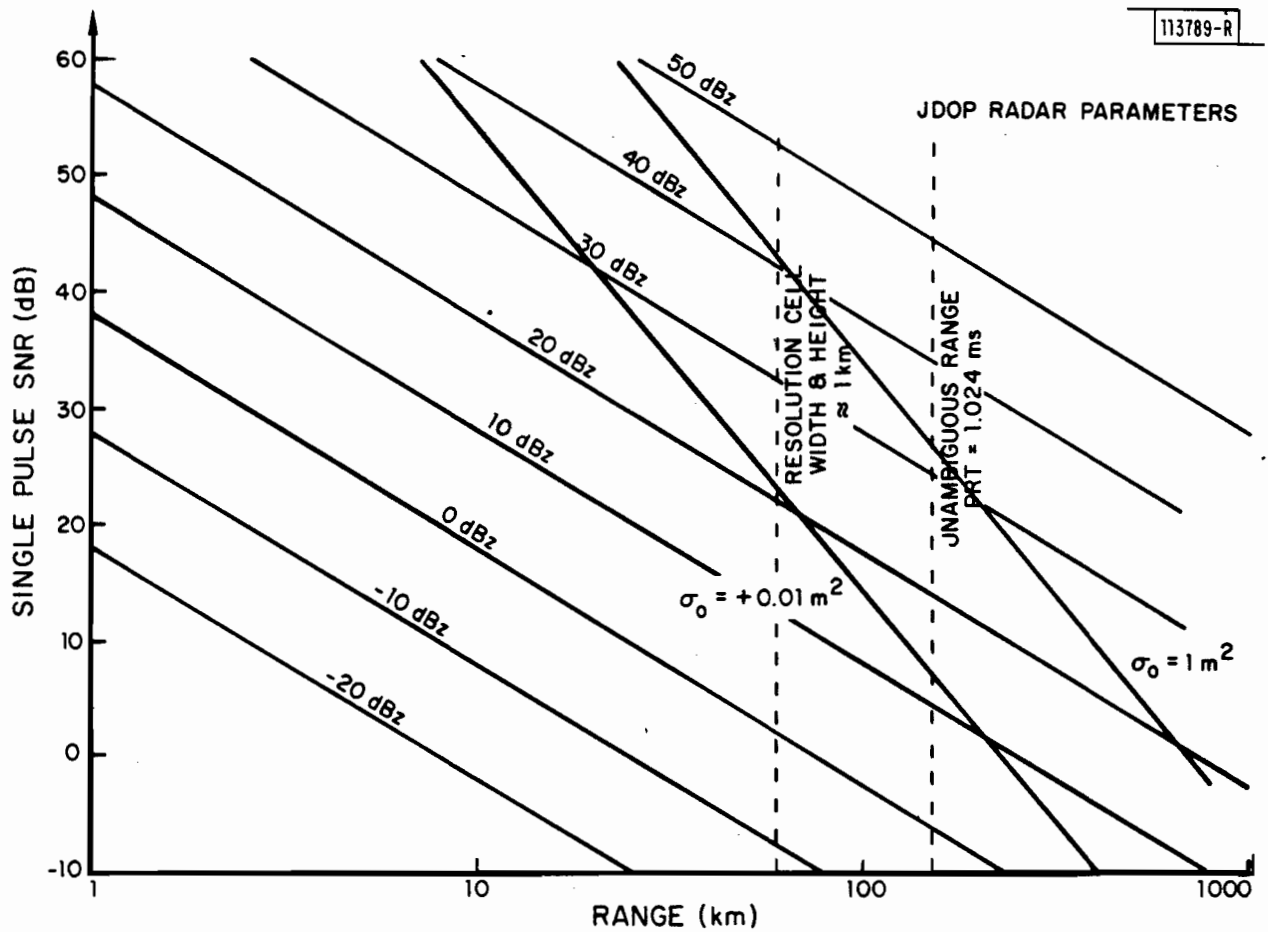


Fig. 5-3. Comparison of weather return SNR with clutter returns.

TABLE 5-1. LAND CLUTTER REFLECTIVITY (0 to 1.0° INCIDENT ANGLE) (FROM [5]).

Terrain type	Reflectivity, dB, below 1 m ² /m ² at indicated carrier frequency, GHz						
	UHF 0.5	L 1.2	S 3.0	C 5.6	X 9.3	K _u 17	K _a 35
	σ_m, σ_{84}	σ_m, σ_{84}^*	σ_m, σ_{84}				
Desert		45.35	-.31		38.30		
Cultivated land	30,- 28,-	32V,-		38.30	36.30		23H, 15H 18V, 10V
Open woods		34H,-	33.26		30.22		
Wooded hills	24.18 34,-	35.20 45.27	32.24 47.29	-.27	30.20 36.28		21H, 13H 13V, 8V
Small house Districts			35.26	35.26	30.24 36,-		
Cities	22,- 30,-	30.20			24.14		

Average of both polarizations except where noted.

σ_m = median backscatter coefficient in decibels below 1 m²/m²

σ_{84} = coefficient that 84 percent of the cells are below
pulse length \approx 1 μ sec
beamwidth \approx 2°

- (1) comparison of the distribution of received power from different cells with a Rayleigh distribution, and
- (2) determination of various statistics ratios such as the ratio of the average cross section to the median cross section (=1.45 for a Rayleigh process).

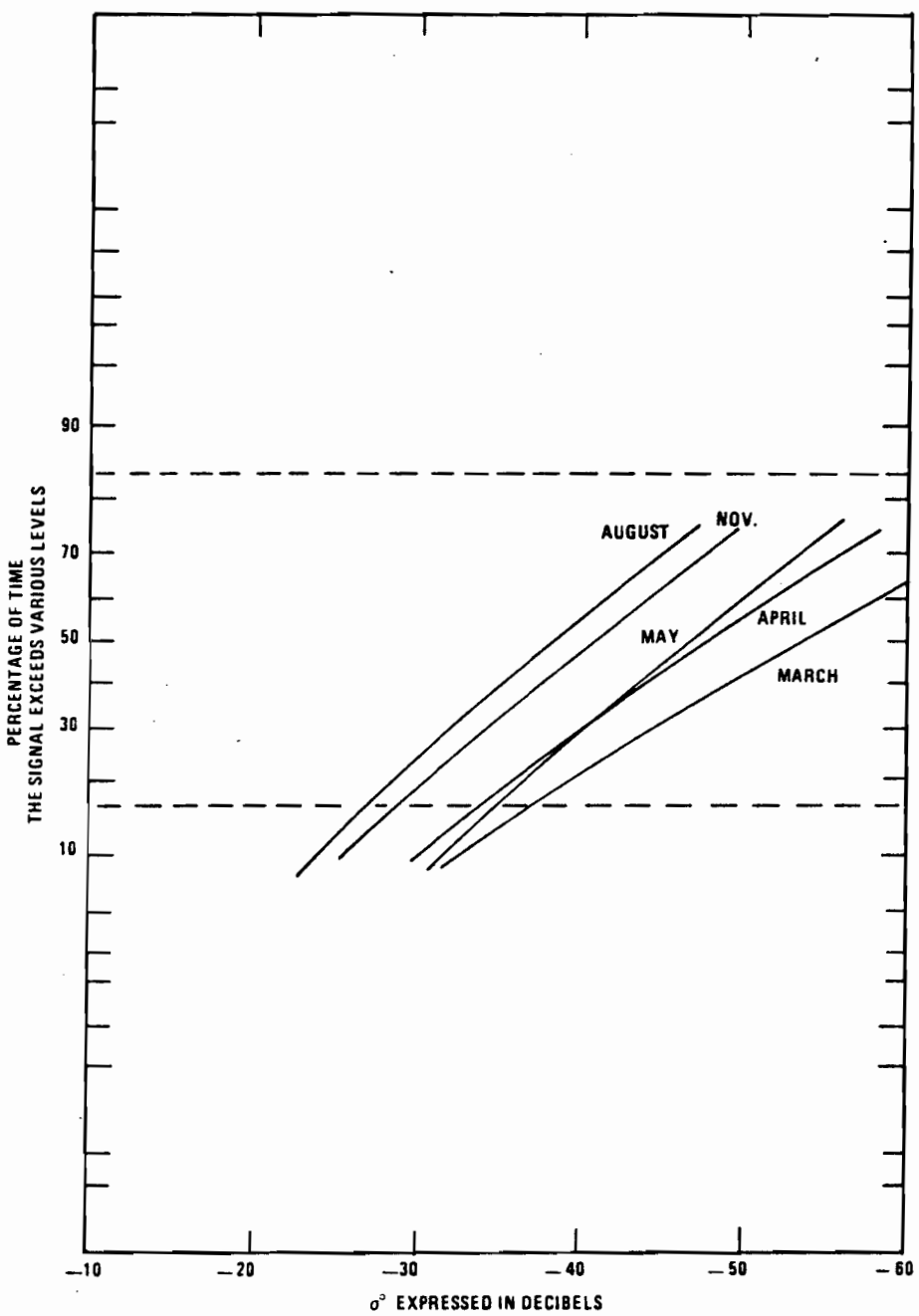
Directly applicable data at S-band is scarce. Fig. 5-4 shows an example of the distribution of σ for cultivated terrain at X-band. In this case, the σ_0 distribution is more nearly log normal than Rayleigh. At higher elevation angles, the distributions at X-band were more nearly Rayleigh. On the other hand, Long [17] describes C-band forest measurements as being nearly Rayleigh distributed.

3. Spectral Characteristics of Distributed Clutter

Perhaps more important from the NEXRAD modeling viewpoint is the time fluctuation of the cross section for vegetated terrain as a function of wind speed since this will determine how much clutter can be suppressed by a high-pass filter (or its equivalent). Hamidi and Zrnic' [1] suggested that the clutter spectrum is Gaussian distributed with a width determined by the wind velocity and the antenna scan rate. This model may encounter difficulties at very low scan rates or, when the antenna is motionless. It is generally accepted [18,19] that at low wind velocities a substantive portion of the echo from a single ground patch does not fluctuate, i.e., the return appears to be a dc component with a fluctuating component which depends on the wind velocity. At higher velocities, this dc component vanishes, but the resulting spectrum appears to have broader than expected "tails" which are attributed to scatterer rotation combined with random movement. Fig. 5-5 shows a measured X-band fluctuation spectrum rms width for heavily forested terrain in a strong wind. We see that the spectrum tails drop off more slowly than a Gaussian model.

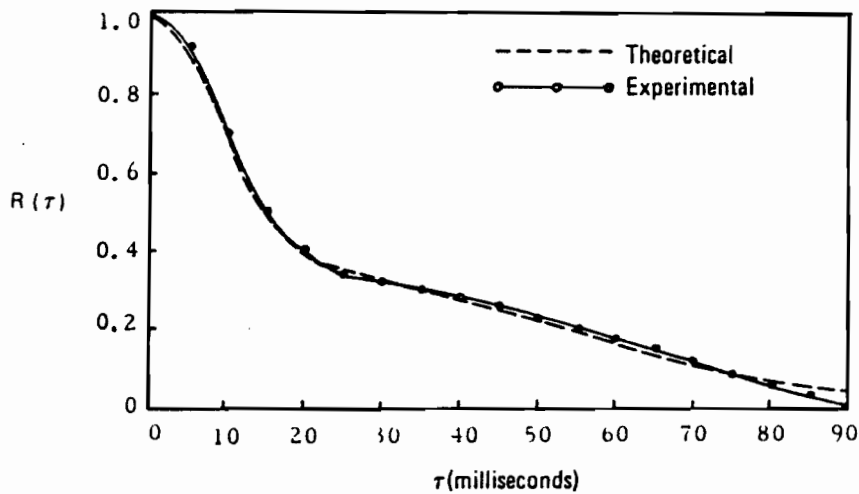
The "saving grace" in modeling distributed clutter from vegetation in the NEXRAD context is that the principal contribution to spectrum width will generally come from antenna rotation as was shown in Fig. 3-2. The spectrum of clutter for a scanning antenna is the convolution of the antenna scan spectrum with the clutter spectrum due to wind. The antenna scan spectrum (recall Fig. 3-4) is approximately Gaussian near its peak, but has tails which drop off faster than a Gaussian distribution. Consequently, the convolution is probably well approximated as Gaussian although the spectrum tails may still drop off more slowly than a Gaussian distribution at high wind velocities*.

*The S-band spectrum measurements at NSSL in [1] obtained at low wind velocities show no evidence of a substantial deviation from a Gaussian spectrum.



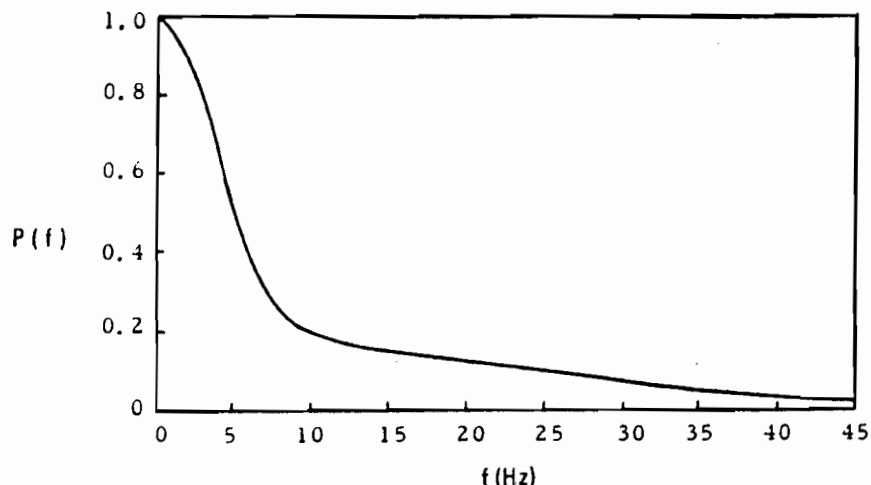
Source: Linell (1963).

Figure 5-4. σ^2 at X Band for Cultivated Terrain at Different Times of the Year. Depression Angle 1.25° (from [18]).



Source: Wong, Reed, and Kaprielian (1967).

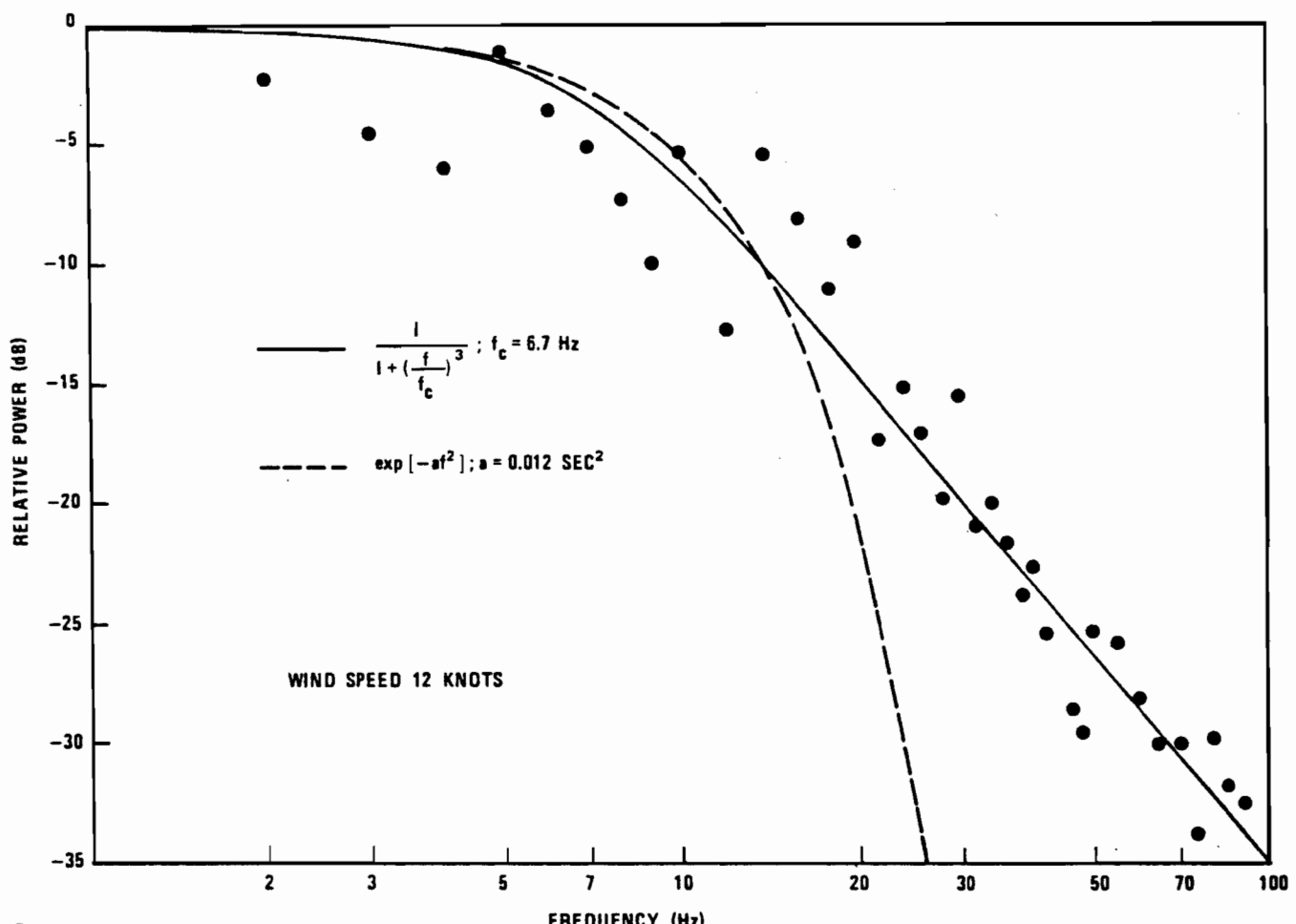
- a. Correlation Function for Ground Clutter at 9.2 cm. (Heavily wooded terrain at wind speeds of 50 mph.)



Source: Wong, Reed, and Kaprielian (1967).

- b. Power Frequency Spectrum for Ground Clutter at 9.2 cm. (Heavily wooded terrain at wind speeds of 50 mph.)

Fig. 5-5. Characteristics of X Band Ground Clutter (from [18]).



Source: Fishbein, Graveline, and Rittenbach (1967).

Each solid circle represents a power spectrum measurement.

Fig. 5-5. Characteristics of X-Band Ground Clutter (Cont.) (from [18]).

4. Principal Problems with the Distributed Clutter Model

Although the distributed clutter models of Equations (5-4) and (5-9) with the Gaussian spectrum assumption [Equation 3-4] are quite commonly used in radar system design (see e.g., [5]), it has been long recognized that the model is generally not applicable to all land clutter situations. For example, Nathanson and Reilly (in [6]) state that:

"It is well known that the reflectivity (σ_0) of both natural and man-made objects on the surface of the earth is generally much higher than that for sea clutter. However, there are considerable differences in the land clutter models used to determine performance of MTI, pulse-Doppler, pulse compression techniques, etc. A considerable portion of the discrepancy results because the spatial distribution of land clutter deviates from a Rayleigh distribution at low grazing angles.

Most land clutter measurements have been made from airplanes where the returns are averaged over large spatial areas having fluctuating scatterers, and the depression angle is large so that there is little masking or shadowing. As a result, the difference between the measured mean and median values of σ_0 are within a few dB of each other. With a surface radar the distribution functions of σ_0 are highly skewed and frequently fit a log-normal distribution more closely than a Rayleigh distribution. In other words, the logarithm of the reflectivity (σ_0 in dB) is approximately normally distributed. In the land clutter studies that have been made with surface radars, the mean value of reflectivity (σ_0) is frequently 20 dB above the median value (σ_m). The mean value is dominated by a few strong reflectors such as buildings, water towers and mountain cliffs. The median value is highly dependent on the masking or shadowing by the contours of the terrain."

Thus, it was necessary to develop an alternative clutter model which would take into account the factors discussed above.

B. Discrete Scatterer Model

Observations of clutter with narrow beams and short pulses [9,19] at L-band and S-band have shown that much of the stronger clutter appears to be confined to single radar resolution cells which suggest discrete scatterers are a principal contributor. Similarly, Ward (in [6]) recommends that land clutter be represented by point reflectors with radar cross sections from 10 to 10^4 m^2 uniformly distributed in area out to 40 km in range.

Thus a discrete scatterer model represents an important complement to the distributed clutter model described earlier. The key issues to be addressed are:

- (1) phase stability of discrete scatterer returns, and
- (2) how many discrete scatterers should be assumed to be present in a given radar resolution cell.

Phase variation during the reception of signals from a discrete scatterer could arise from a variety of sources including:

- (a) phase instabilities in the transmitter/receiver electronics
- (b) phase center offset from the axis of rotation for the antenna, and/or
- (c) variation in the propagation path refractive index.

System instabilities are discussed in Chapter IV. These were not incorporated in the clutter model since they are very hardware dependent and, can be assessed best experimentally.

Figure 5-6 shows the amplitude and phase of the received signal as the MIT radar scanned by a tower at a range of approximately 60 km. The symmetrical phase variation with scan angle suggests that source (b) above was the principal contributor to phase variation for this system. Since mechanism (b) is also hardware dependent, it was not incorporated into a "universal" clutter model*.

The number of discrete scatterers in a radar resolution volume is not a critical issue for clutter suppression by linear time invariant filters as long as practical non-linearities such as improper AGC setting do not arise. This is because the clutter residue from several discrete scatterers is the sum of the individual discrete scatterer residues. What is important† is that the discrete scatterer angular location be allowed to have an arbitrary position relative to the radar cell centroid since the discrete scatterer return is non-stationary in the time domain.

When two sizeable discrete scatterers are in a given radar cell with relative phases differing by 180° , it is possible to have situations in which the received signal power level changes very rapidly in a small azimuth sector. This rapid change could produce difficulties for some AGC schemes; however, the likelihood of this is probably small. For example, Ward's model (in [6]) for discrete scatterers yields an average of 0.25 scatterers per NEXRAD Doppler product resolution cell, and a 5% probability of two or more scatterers in a given cell.

*Also, the phase variation in Fig. 5-6 is quite slow.

†Especially, in the case of clutter suppression and weather parameter estimation on blocks of time series data.

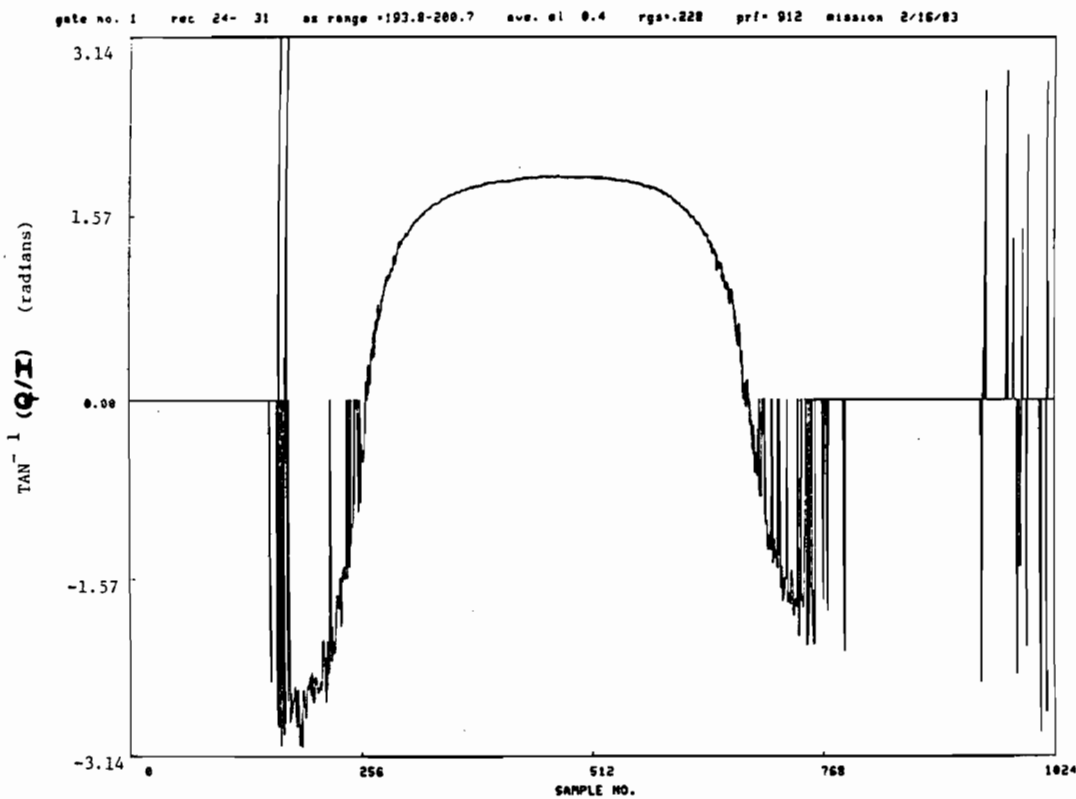
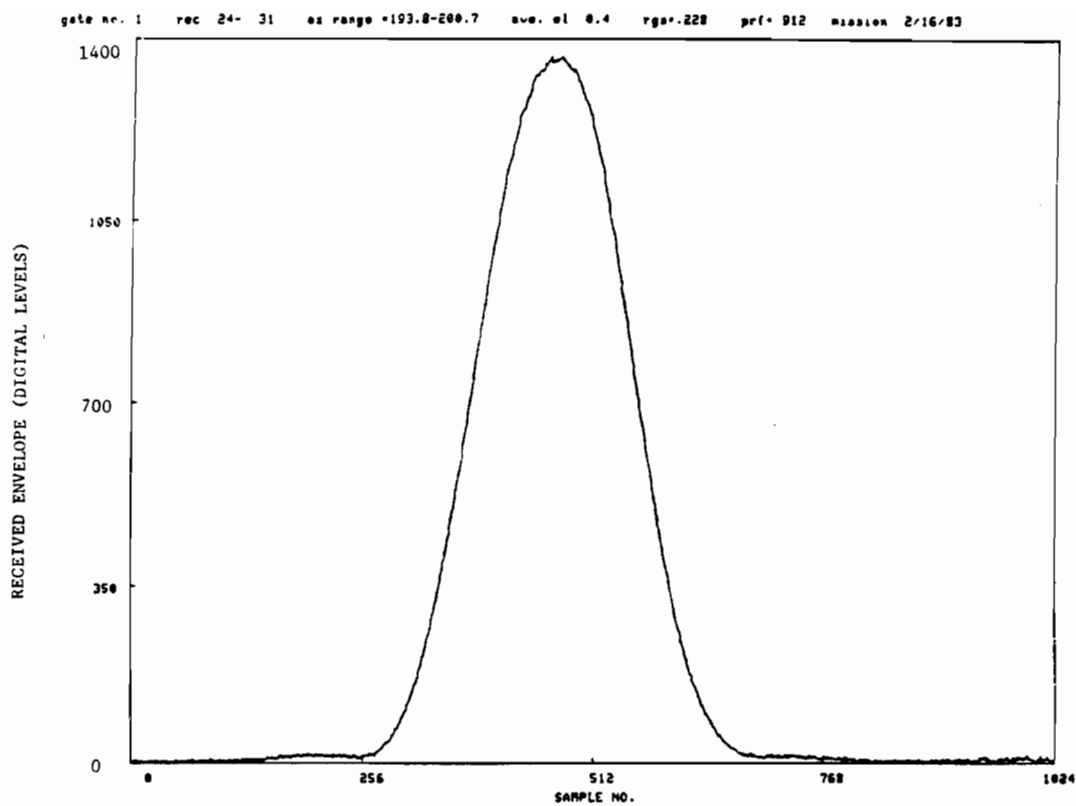


Fig. 5-6. Phase Variation As MIT Radar Scans by Radio Tower.

Since the actual density of discrete scatterers can only be resolved by experimental measurements, it is probably more reasonable to simply use actual recorded clutter time series to address performance when multiple discrete scatterers are present.

C. Recorded Clutter Time Series

The use of recorded clutter time series data has a number of advantages:

- (1) a variety of combinations of discrete and distributed clutter, and
- (2) representative spatial variation in clutter characteristics.

Thus, at the outset of this study, it had been hoped that recorded clutter time series could be used as one of the clutter models for system specification and quality assurance testing.

However, a number of difficulties were encountered:

- (1) digital recording of I,Q time series data is essential if the recorded data is to have the dynamic range and linearity consistent with demonstrating clutter suppression in excess of 40 dB. Unfortunately, several appropriate weather radars (e.g., those used in the JAWS project) can not make such digital recordings at this time,
- (2) the clutter suppression capability of existing radars is often limited by transmitter/receiver instabilities to a level below that called for in the specification (e.g., the MIT and NSSL radars). These instabilities typically reflect the fact that these radars were designed for weather parameter estimation without clutter filtering (in which case considerable phase and amplitude variation can be tolerated [20]), and
- (3) a significant fraction of the clutter at some of the sites (e.g., MIT and NSSL) arises from moving objects (e.g., cars) and hence will not be suppressed by techniques which assume that the clutter is centered about zero velocity. Although these clutter sources are an important part of the NEXRAD clutter environment, it is not expected that they will be suppressed as indicated in Chapter III. Hence, their existence would make the measured clutter data inappropriate for testing a suggested clutter technique against the specification.

In conclusion, although measured clutter data has many advantages for assessing the final NEXRAD integrity, it does not seem appropriate at this time to include performance against such data as part of the NEXRAD section 3.7.1.7 specification at this time.

VI. RECOMMENDED HARDWARE TESTS FOR QUALITY ASSURANCE

The tests to be performed by the contractors to demonstrate that the various performance criteria are achieved is an important part of the overall specification. Table 6-1 describes the clutter suppression quality assurance text developed from the present study and subsequent comments from potential users.

Since much of the clutter suppression will be accomplished by digital processing of digitized I,Q samples from the radar, it was reasonable to have much of the demonstration accomplished by digital simulation. Section A discusses the rationale for the digital simulation tests discussed in paragraph #2 of Table 6-1. It is also necessary that the RDA (i.e., transmitter and receiver) also have the requisite stability and linearity if the clutter suppression goals are to be achieved in practice. Section B presents the rationale for the tests described in paragraphs #3 and #4 of Table 6-1.

A. Digital Simulation Tests

The clutter models and performance criteria discussed in the clutter specification text are quite straightforward to simulate. Hamidi and Zrnic' [1] and Zrnic' [3] discuss how time series may be generated with a Gaussian spectrum of specified spectrum width centered about a mean radial velocity. Although this approach will give insight into the clutter suppression statistics, it does require a substantial number of Monte Carlo simulations to determine the suppression capability.

We anticipate that the evaluation of distributed clutter suppression and weather parameter errors for clutter suppression by a linear time invariant (LTI) filter followed by pulse pair estimation would be accomplished by the method used in Chapters III and VII:

1. determine the input spectrum
2. multiply the input spectrum by the squared filter frequency response
3. inverse transform to obtain the output autocorrelation function, and
4. obtain the weather clutter parameters estimates by the usual PP algorithms.

B. Hardware Tests

The instability residue power test described in paragraph #3 of Table 6-1 is a necessary, but not sufficient, condition for achieving the desired 50 dB of clutter rejection in the Doppler velocity parameter estimates. The instability residue of principal concern corresponds to frequencies which would be in the usable velocity region (e.g., outside the stopband of the clutter filters).

TABLE 6-1. RECOMMENDED QUALITY ASSURANCE TEST
ASSOCIATED WITH CLUTTER SUPPRESSION.

4.2.5.2.1 RDA Performance Tests

- #1 The RDA performance testing of the preproduction system shall consist of a series of tests using the operating parameters established for the site, and using live and recorded weather data. The contractor shall perform tests to verify the performance of the radar and its associated signal processor in the presence of ground clutter and various weather phenomena.
- #2 Demonstration of the ground clutter suppression capability shall be accomplished by processing of simulated digitized samples from individual range gates and by the tests described below. For purposes of simulation, the system front end noise may be ignored, but quantization noise and arithmetic precision effects shall be considered. The clutter suppression capability simulation studies will use clutter models A and B, and simulated weather data with various mean velocities and spectrum widths.
- #3 The integrated instability residue power measured in the frequency domain shall be at least 50dB below the peak signal power as measured with a normal prt on a point target with the antenna in a fixed position.
- #4 The signal return from a fixed discrete scatterer (e.g., a corner reflector) in the antenna far field (using the normal radome and at the PRF to be used at low elevation angles) shall be used to provide a clutter model B signal. The suppression of this signal (characterized in accordance with Section 3.7.1.7) shall be no worse than that shown for clutter model B in Tables 3-7 and 3-8 with 5 dB degradation allowed for range testing imperfections.

For example, if the LTI clutter filter stopband width is 1 m/s with the bulk of the clutter energy at velocities \leq 0.25 m/s, one is principally concerned about the instability residue spectrum at frequencies $>$ 13 Hz equals (i.e., velocities above 0.75 m/s). The measurement of power at such frequencies without contamination by the large component at zero frequency has been discussed in the literature (see e.g., references [14] and [15]). The key factors to be considered are:

1. use of a sufficiently long time interval for Fourier analysis so that the mainlobe of the zero velocity signal does not extend into the frequency band of interest,
2. use of an appropriate time window and choice of frequencies for spectrum computation so that the sidelobes of the zero frequency signal do not bias the instability residue power, and
3. averaging in the time domain to achieve stable estimates.

Fig. 6-1 shows a field measurement (at Fort Sill, OK) of the Doppler spectrum on a stationary C-band radar using a TWT transmitter*. The spectrum was computed by an FFT using a uniform time window whose nulls occur at the evaluation frequencies (thus, the high sidelobes due to the zero velocity peak do not appear). The integrated instability residue power assuming all non-zero frequency bins are of concern can be computed as follows:

Relative Power Level (dB)	$10^5 \times$ Relative Power	Number of Frequencies (NF)	$NF \times 10^5 \times$ Relative Power
-60	0.1	1	0.1
-62	0.06	2	0.13
-65	0.03	3	0.09
-67	0.02	2	0.04
-73	0.01	56	<u>0.28</u>
Total Power			0.64

$$\text{Integrated instability residue} = -52 \text{ dB}$$

Fig. 6-2 shows the stationary antenna power spectrum measured at 1000 Hz PRF on the S-band Doppler radar at MIT [16]. This radar uses an FPS-18 klystron with a solid state Stable Local Oscillator (STALO) and the original (noisy) exciter chain. By computations similar to those above, we find that the integrated instability residue power for this radar is -44 dB, so

*Klystrons such as are used in the S-band ASR-8 would show a lower instability residue than a TWT.

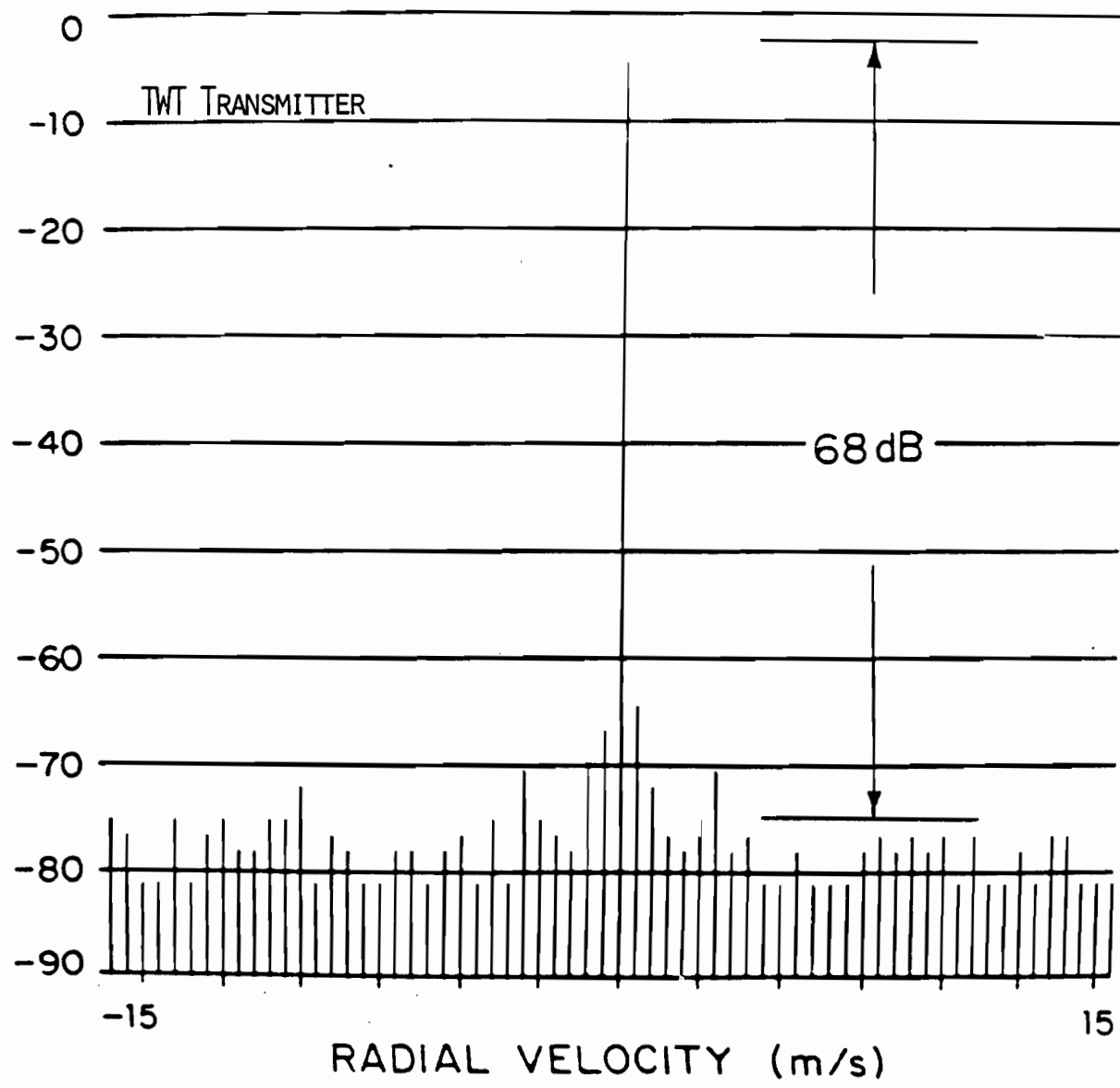


Fig. 6-1. Instability Residue for C-Band Surveillance Radar.

DATE NO. 3 NREC 500- 699 AZ=196.8 EL= 0.5 RGS=.228 PRF= 912 MISSION 11/10/82

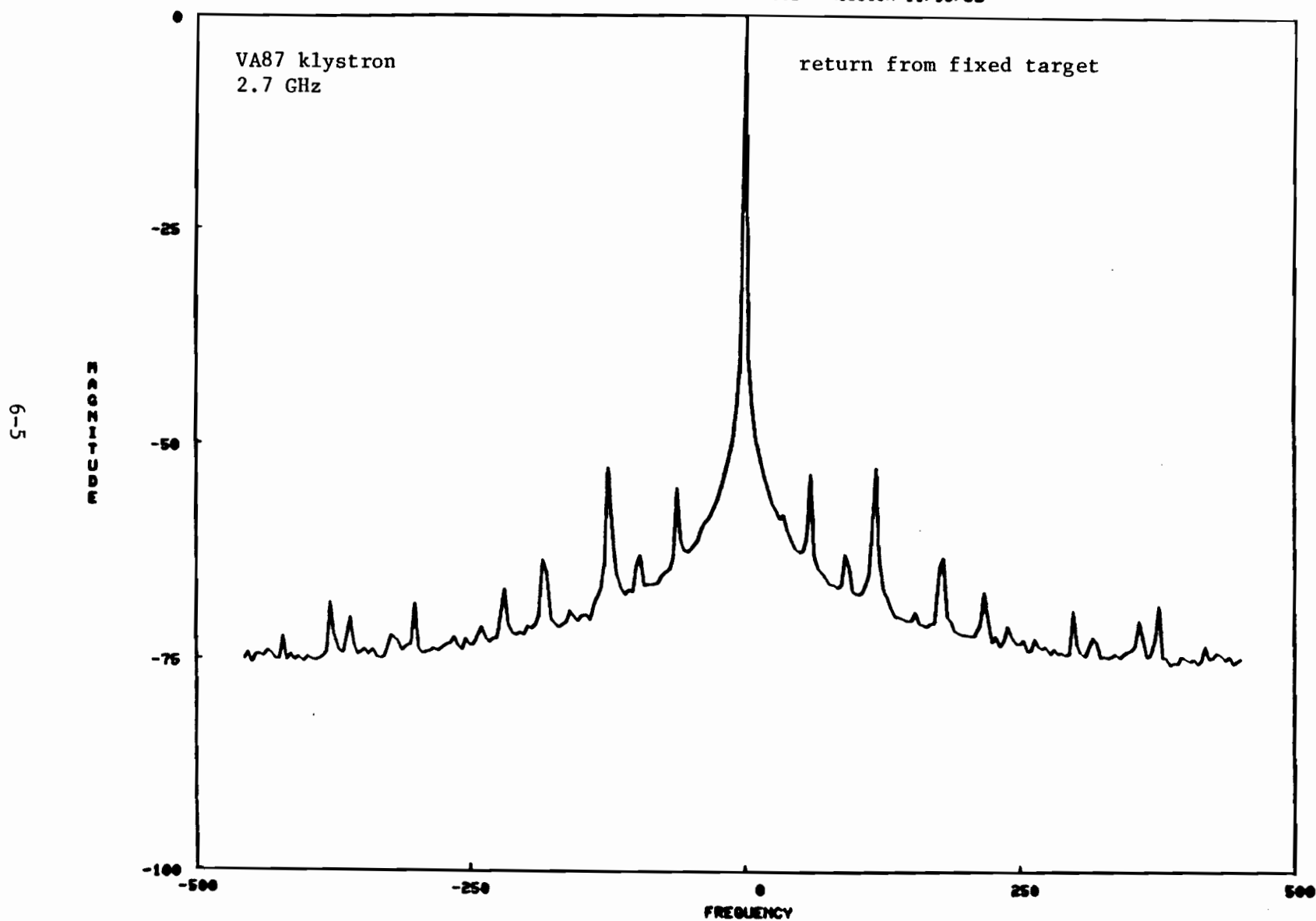


Fig. 6-2. Instability Residue Spectrum on MIT Meteorology Dept. Radar.

that this radar with its current hardware cannot achieve 50 dB of clutter power suppression. By replacing the exciter chain and improving the power supply, it would be possible to reduce the MIT radar instability residue to less than -50 dB.

The measurement of instability residue power involves a very small portion of the overall system linear dynamic range. It is thus necessary to have an additional test which exercises a much greater portion of the system dynamic range.

The use of the signal return from a fixed scatterer as the antenna scans to furnish a clutter model B-like target in paragraph 4 of Table 6-1 is intended to accomplish such a test. Figures 6-3 and 6-4 show an example of the output from nearby range gates as the MIT radar was scanned by a radio tower at a range of approximately 30 nmi. Calculation shows that the return from a range bin 1/4 nmi away from the range bin containing the tower is some 45 dB below the tower peak level. This relative level difference suggests that the rejection of this clutter from the radio tower* will be limited by the radar system instability and by front-end noise, but not by clutter from objects near the ground level.

Figure 6-5 shows a representative stationary antenna power spectrum measured on the NSSL radar at Norman, OK. The spectrum here drops off quite differently in frequency from the MIT radar so that the instability residue levels are a function of the clutter suppression stopband. For a 1 m/s stopband, the NSSL residue level is approximately -29 dB while a 3 m/s stopband has an instability level of approximately -41 dB.

*Experimental results on rejection of this clutter signal are described in Chapter VII.

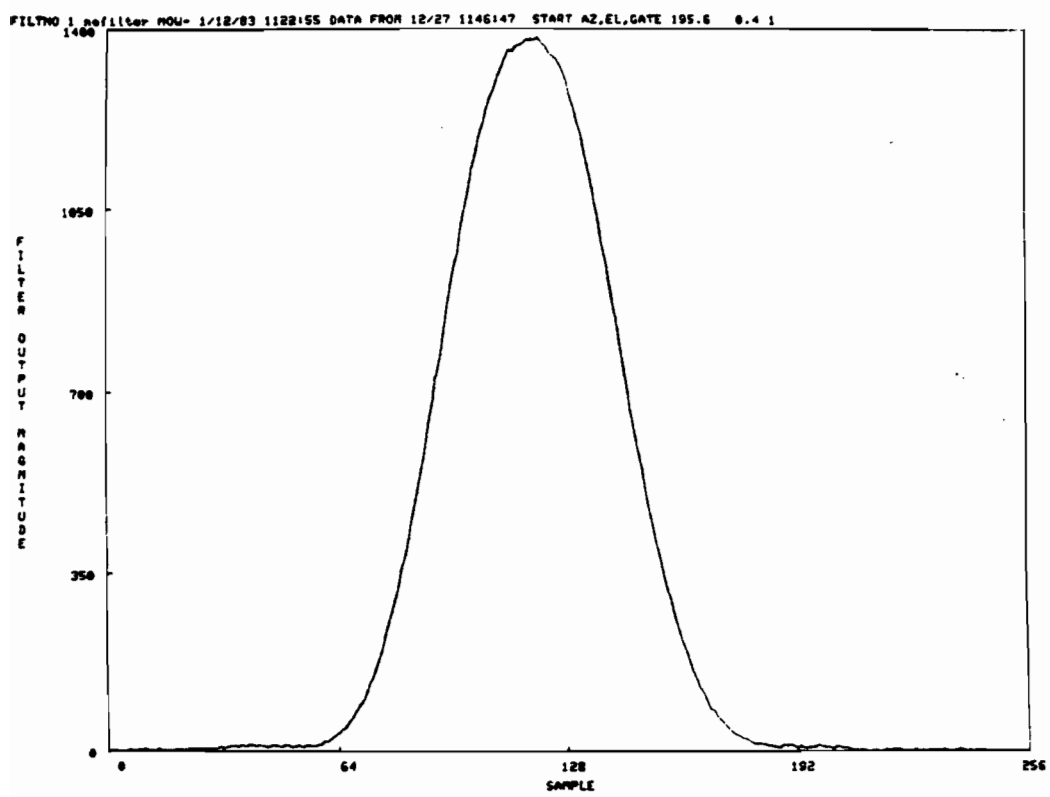


Fig. 6-3. Envelope From Range Gate with Radio Tower.

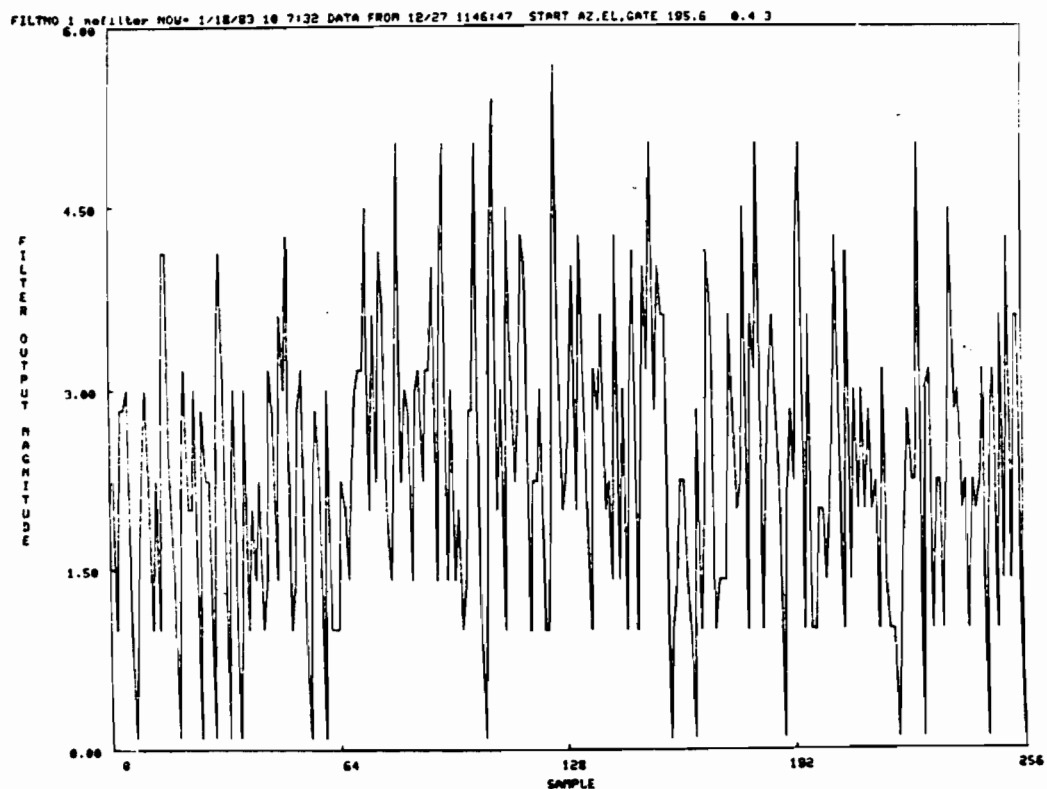


Fig. 6-4. Envelope From Range Gate 0.25 nmi Away
From Gate in Fig. 6-3.

GATE NO. 1 NREC1999-2053 AZ=354.8 EL= 0.600 START RANGE(KM)= 4.200 GATSPC= 0.6 PRF=1302 DAY 216 ISPLS 1
FFT PERFORMED ON 128 VALUES AT A TIME 4 GROUPS OF SPECTRUM VALUES ARE AVERAGED CR1 = -30.80450 CR3 = -41.77500

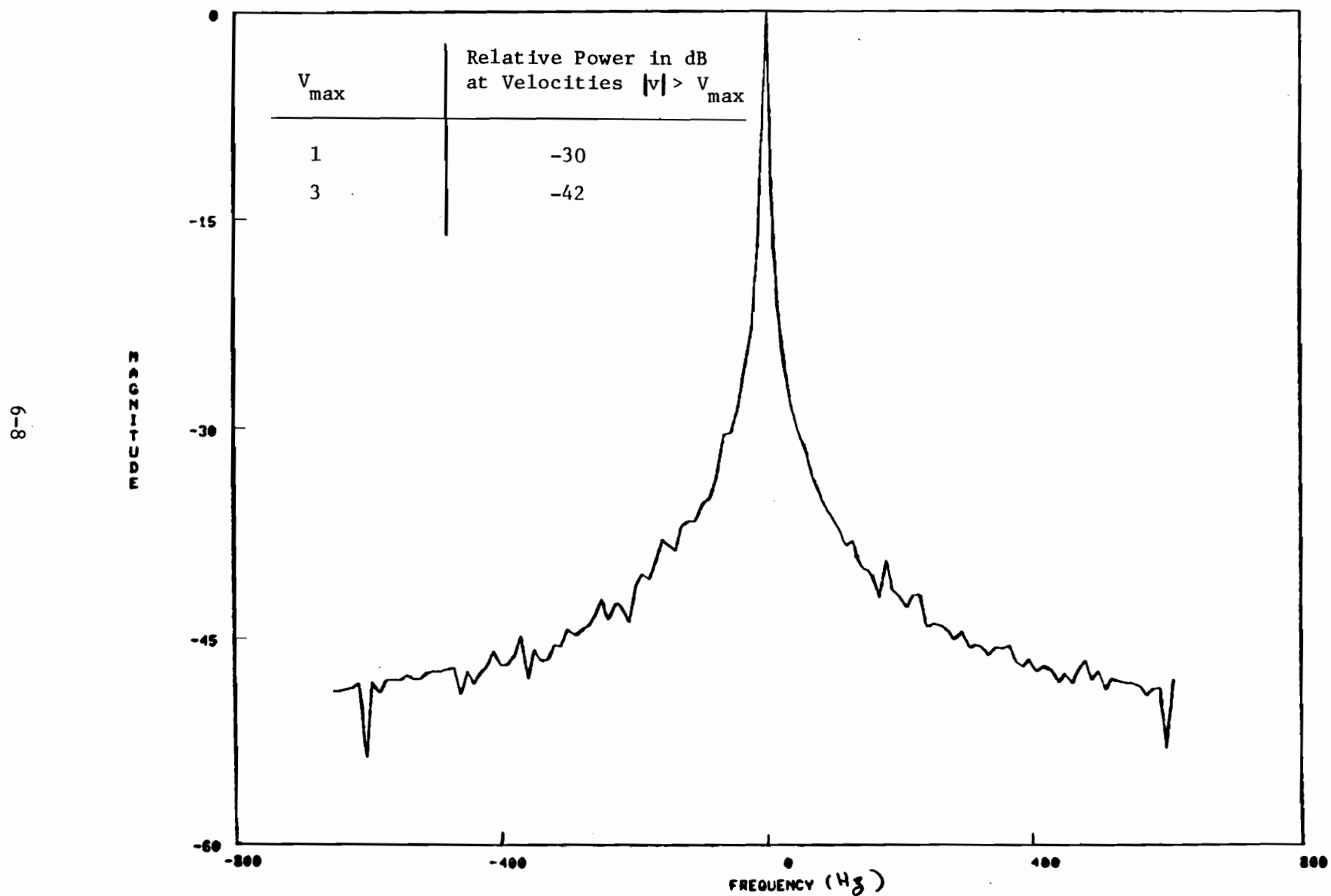


Fig. 6-5. Power Spectrum of Data From NSSL Radar.

VII. CLUTTER SUPPRESSION PERFORMANCE OF REPRESENTATIVE FILTERS ON MODEL AND MEASURED CLUTTER DATA

In this section, we present numerical results for clutter suppression and weather parameter errors using several representative techniques against 1) the various clutter and weather models, and 2) measured clutter time series from the MIT and NSSL S-band weather radars. The objective of these computations was to demonstrate that the numerical values in the specification are practically achievable.

In all cases, the clutter suppression technique considered was an LTI filter followed by pulse pair estimation. Two types of LTI filters were considered:

- (1) a 39-point finite impulse response (FIR) equiripple design using the Parks-McClelland procedure [22], and
- (2) elliptical 3-pole infinite impulse response (IIR) filters such as were considered by Groginsky and Glover [1].

Each of these filter types has its merits for the present exercise: the FIR filters provide a direct tradeoff between stopband and passband width with deviations from the desired shape while IIR filters require fewer multipiles and less data storage as well as offering somewhat greater notch depths. Section A considers the performance of FIR filters on synthetic data while in Section B we assess the IIR filter performance on the same data sets. in Section C shows examples of applying the FIR filter designs to measured clutter time series.

A. Finite Impulse Response Filter Results For Weather and Clutter Models

Four FIR filter designs were considered with the parameters shown in Table 7-1. Filters 1-3 were chosen to correspond to the clutter filter passband widths discussed in the original NTR specification while filter 4 was designed to meet the reflectivity clutter rejection specification.

Figure 7-1 shows the filter frequency response* for filter 1. We see that the filter has a deep notch at zero velocity (approximately -50 dB) and ripples of +2 dB in the passband. Figure 7-2 shows the suppression for clutter model A as a function of the clutter spectrum width. We see that although the notch depth is over 50 dB, the clutter suppression is only 30 dB for a motionless antenna (clutter "intrinsic" width of 0.1 m/s) and approximately 20 dB for a more typical NEXRAD width of 0.25 m/s. The possibility of such large differences between notch depth and actual suppression capability was one of our major concerns with the original NTR specification (recall the discussion in section A in Chapter IV).

*The computer-generated frequency scale in this (and all subsequent frequency response plots) is in terms of the fractional Nyquist rate. To facilitate conversion to meteorologically significant terms, we have indicated salient velocities assuming an unambiguous Doppler velocity of 30 m/s.

TABLE 7-1. PARAMETERS FOR FINITE IMPULSE RESPONSE CLUTTER FILTERS.

Filter #	Stopband Width (m/s)	Passband Width (m/s)	Stopband Ripple/ Passband Ripple Weighting	Peak Ripple (dB) in Stopband	Peak Ripple (dB) in Passband
1	0.33	1.0	5:1	-21	2.0
4	0.50	1.5	12:1	-30	2.8
2	0.67	2.0	20:1	-37	2.10
3	1.0	3.0	40:1	-51	1.0

filter impulse response length = 39 samples

assumed unambiguous velocity = 60 m/s

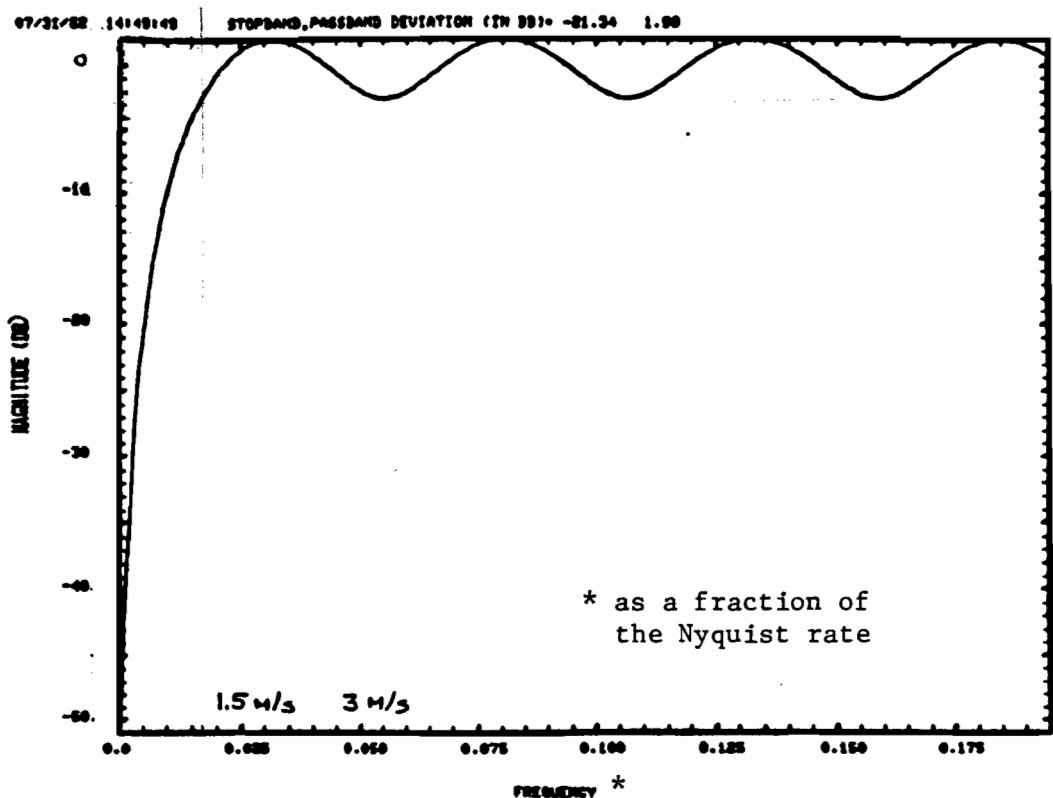


Fig. 7-1. Frequency response for FIR filter 1.

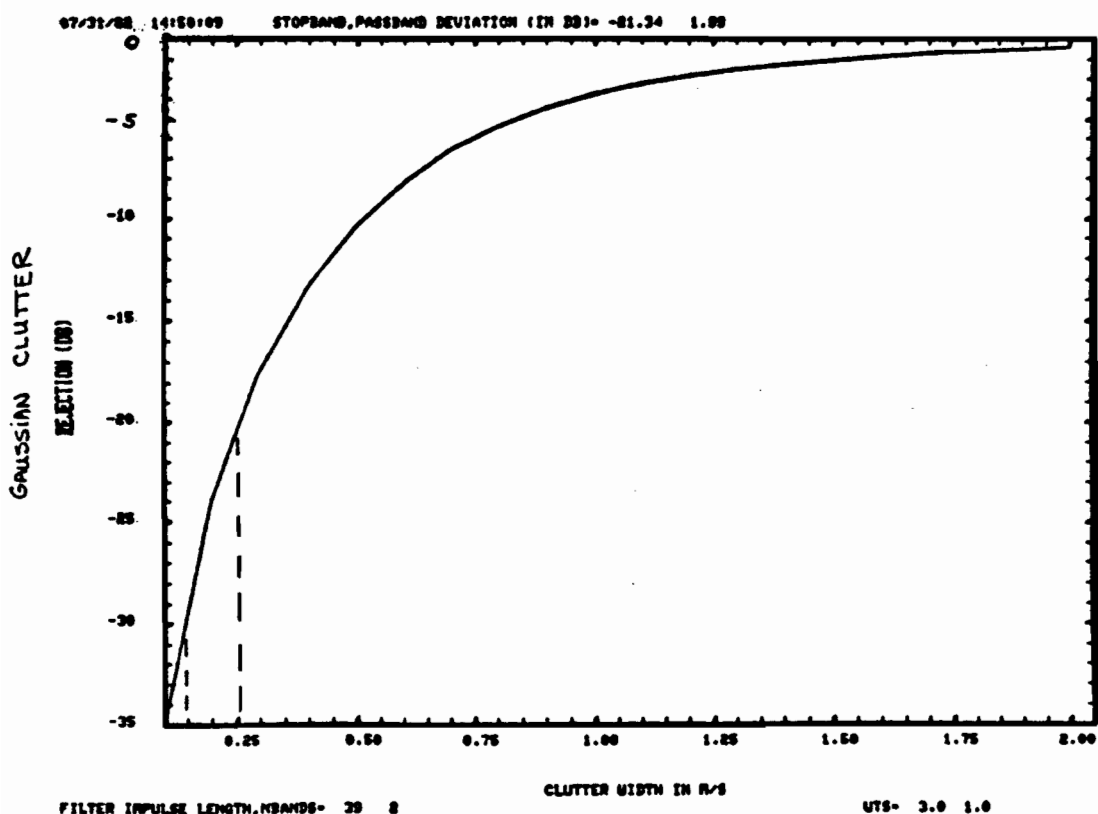


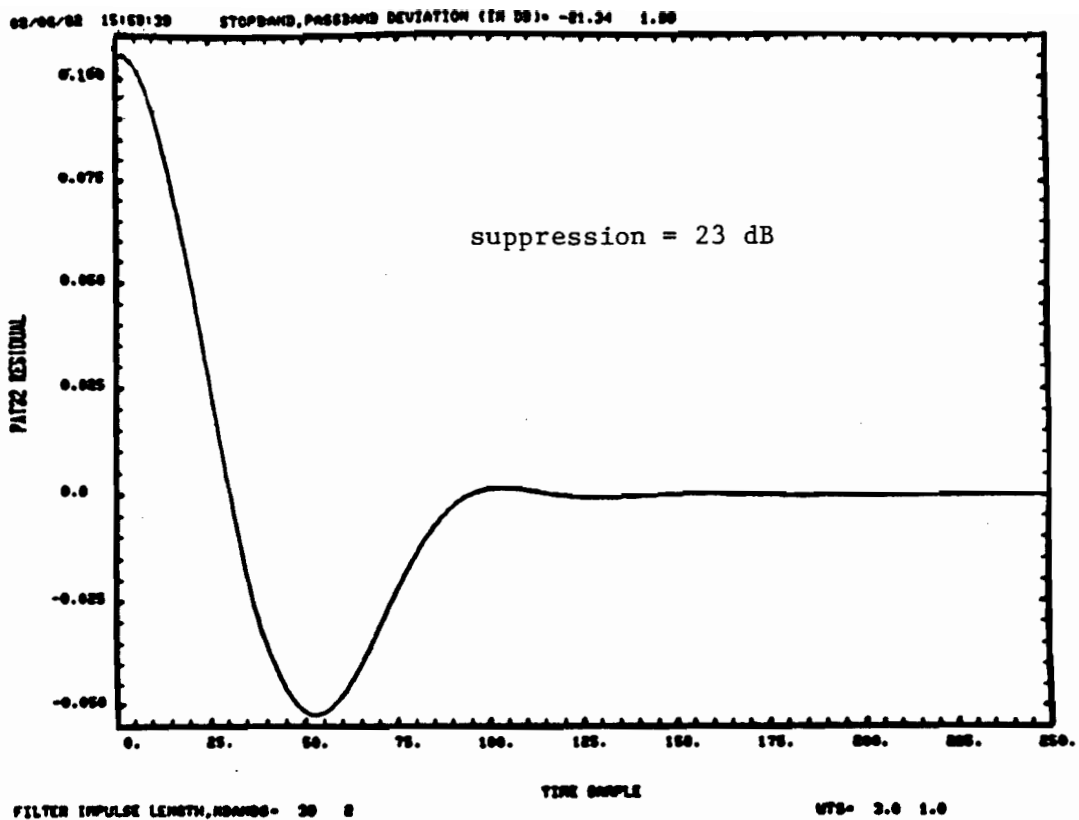
Fig. 7-2. FIR filter #1 suppression for clutter model A.

Figure 7-3 shows the filter output for clutter model B at two antenna scan rates. Since the filter coefficient and clutter model are symmetrical, only half of the clutter residue is plotted. In this case, the peak residue coincides with the beam peak. The suppression at 3.2 rpm is slightly better than for clutter model A while the suppression at 1.6 rpm is several dB better than that for clutter model A at the corresponding width.

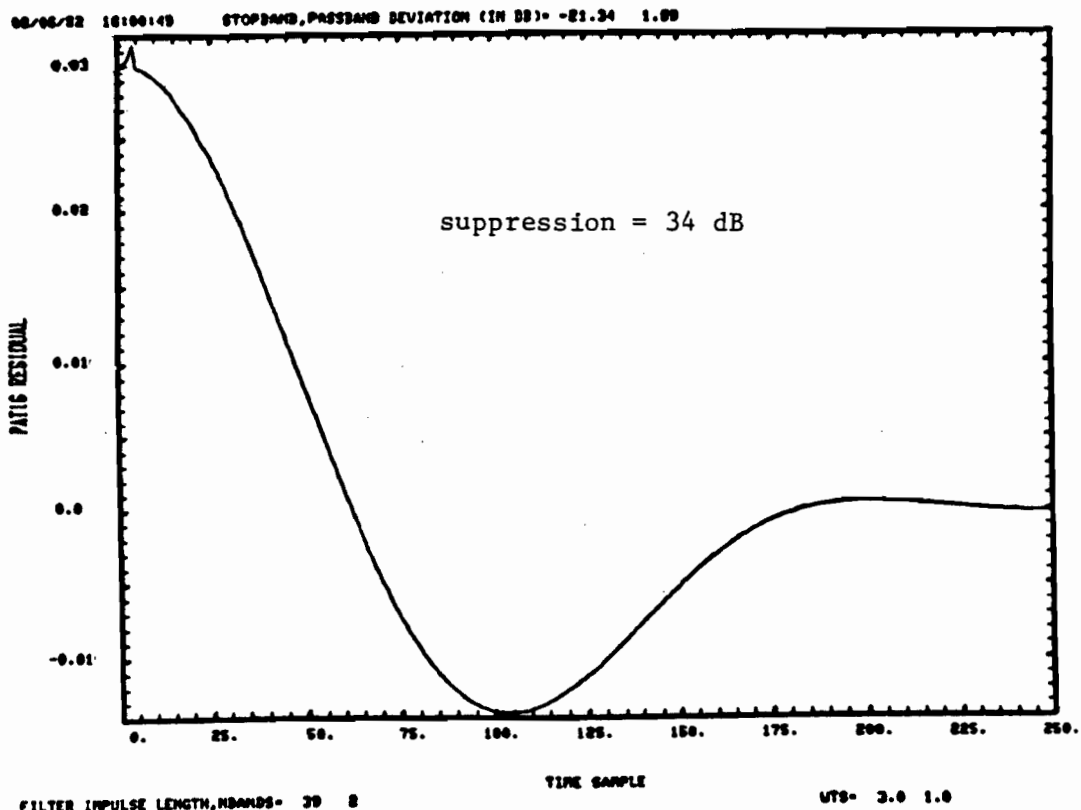
Figure 7-4 shows the weather parameter errors for this filter as a function of weather mean velocity for a weather width of 1 m/s. The errors near the passband edge are seen to be somewhat smaller than those for the idealized filter (Figures 3-13 to 3-15). For example, the FIR filter reflectivity error at 1 m/s is 1.75 dB whereas the idealized filter error was 2.6 dB. The passband ripples cause the periodic errors seen at larger weather velocities. Although the ripples are 4 dB peak-to-peak, the weather parameter errors are seen to be small for weather velocities \geq 2 m/s. In particular, we see that the mean velocity error due to the ripples is less than 0.15 m/s whereas the analysis in [2] would suggest errors on the order of 2 m/s. The difference arises because the period of the ripples here is small enough relative to the weather widths that averaging over ripples occurs to a significant extent. This effect becomes even more pronounced at wider weather widths as will be seen when we discuss the other two FIR filters.

Figures 7-5 to 7-8 are the corresponding plots for FIR filter #2. This filter has a notch depth of -37 dB at zero velocity with a -60 dB notch at approximately 0.5 m/s. We see that although the notch depth at zero velocity is less than that for FIR filter #1, the clutter suppression for a "typical" clutter width of 0.25 m/s is some 17 dB better than that for FIR filter #1. For clutter model B, we see that the suppression at 3.2 rpm is greater than that at 1.6 rpm because of the stopband peak ripple at zero velocity. The weather parameter errors for this filter at a weather width of 2 m/s arise almost completely from the notch effects. Simulations with a 1 m/s weather width gave errors due to the passband ripples which were virtually identical to those shown in Fig. 3-4.

Figures 7-9 to 7-12 are the corresponding results for FIR filter #3 which is designed to provide the 50 dB of clutter suppression with a 3 m/s passband edge and 1 dB passband ripples called for in the original NTR specification. We see that over 50 dB of clutter suppression is provided against clutter model A for clutter widths up to 0.35 m/s as well as for clutter model B. The weather parameter errors are dominated by the filter notch rather than the passband ripples. Fig. 7-13 shows an expanded view of the error due to passband ripples for a weather width of 1 m/s. We see that the velocity errors are less than ± 0.08 m/s, an order of magnitude less than suggested by Groginsky and Glover [2]. Figure 7-14 shows the errors with a weather width of 0.3 m/s. At such a narrow width, the reflectivity error tracks the passband ripples; but the velocity (and

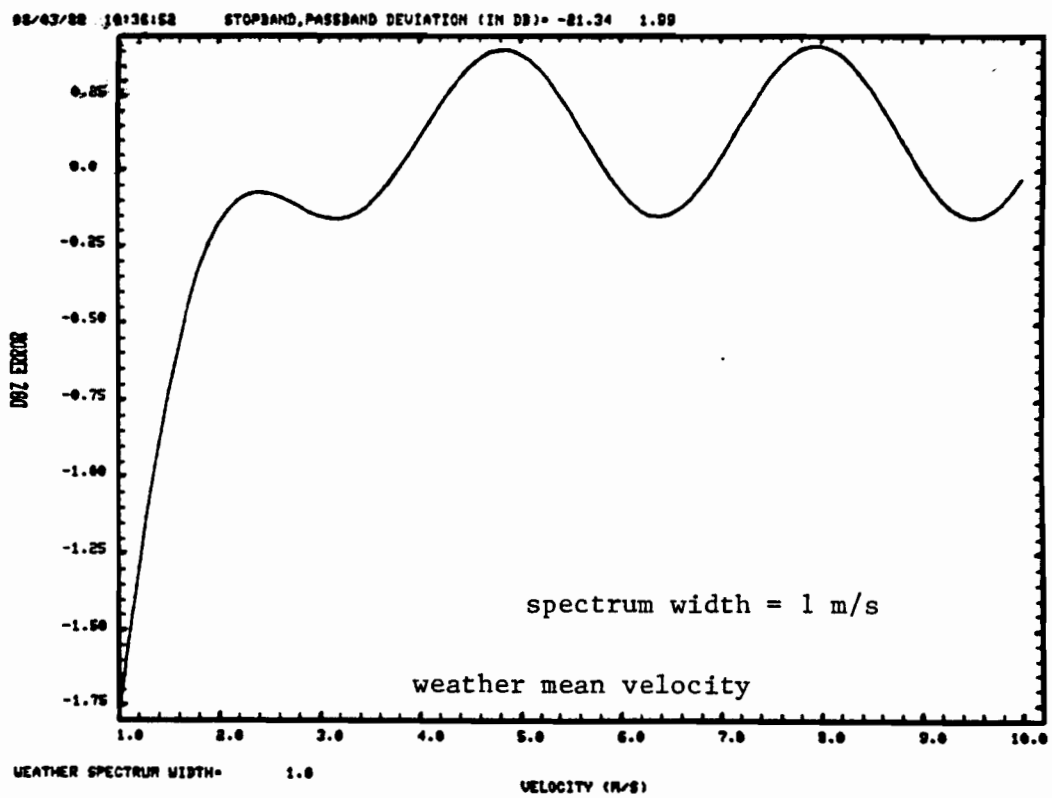


(a) 1° beamwidth at 3.2 rpm.



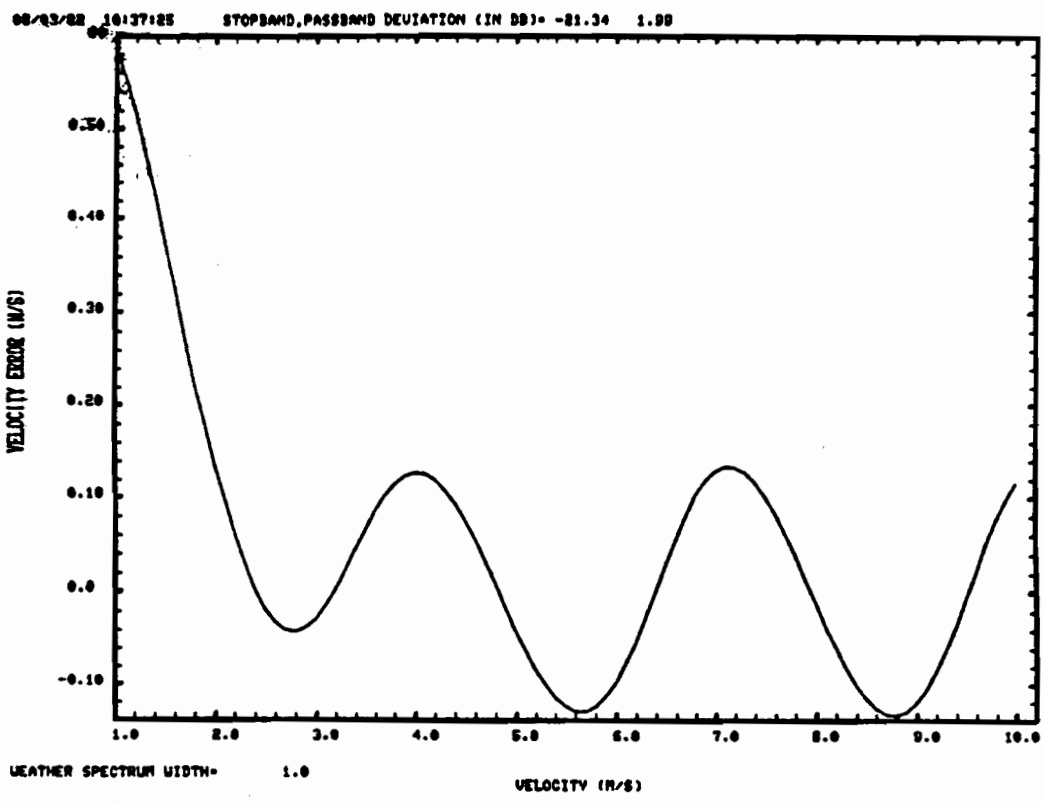
(b) 1° beamwidth at 1.6 rpm.

Fig. 7-3. FIR filter #1 suppression for clutter model B.

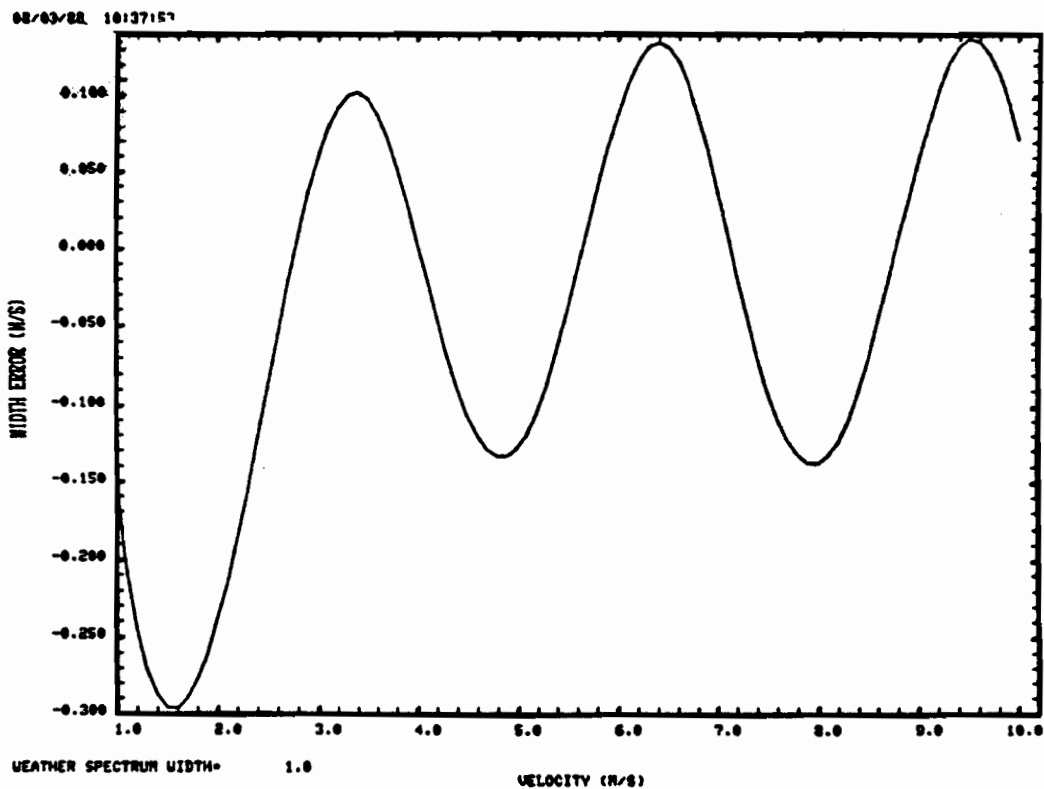


(a) Reflectivity error.

Fig. 7-4. Weather parameter errors with FIR filter #1.



(b) Mean velocity error.



(c) Spectrum width error.

Fig. 7-4. Weather parameter errors with FIR filter #1 (con't).

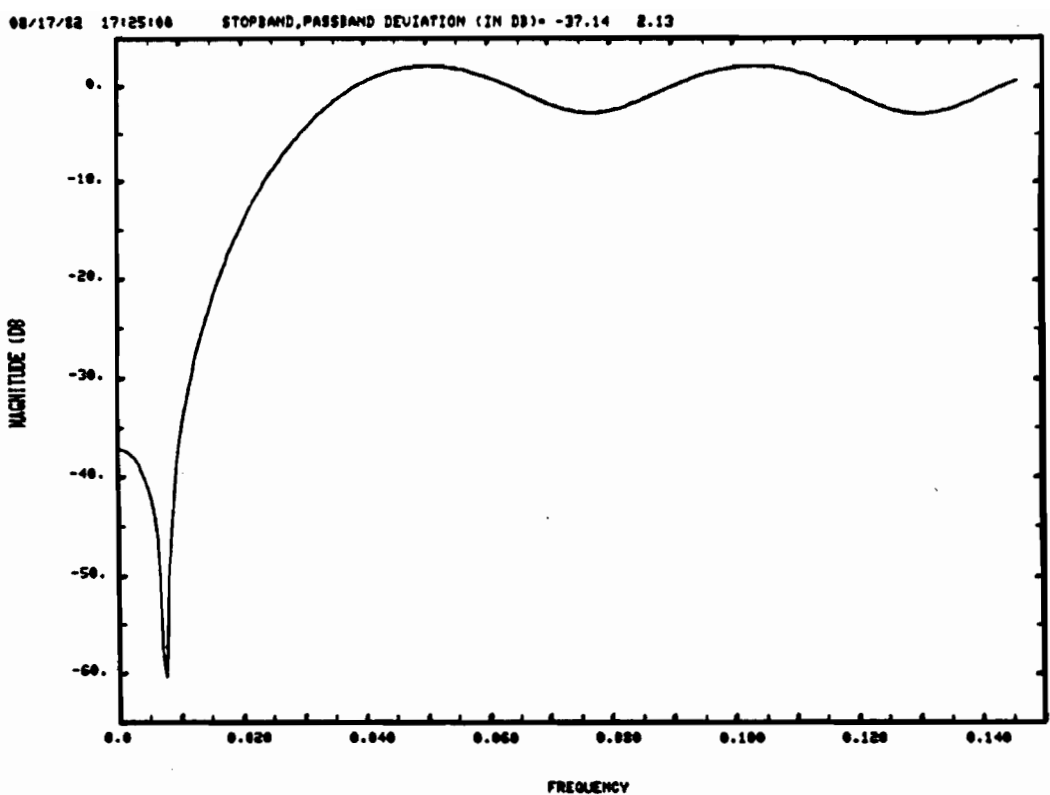


Fig. 7-5. Frequency response for FIR filter #2.

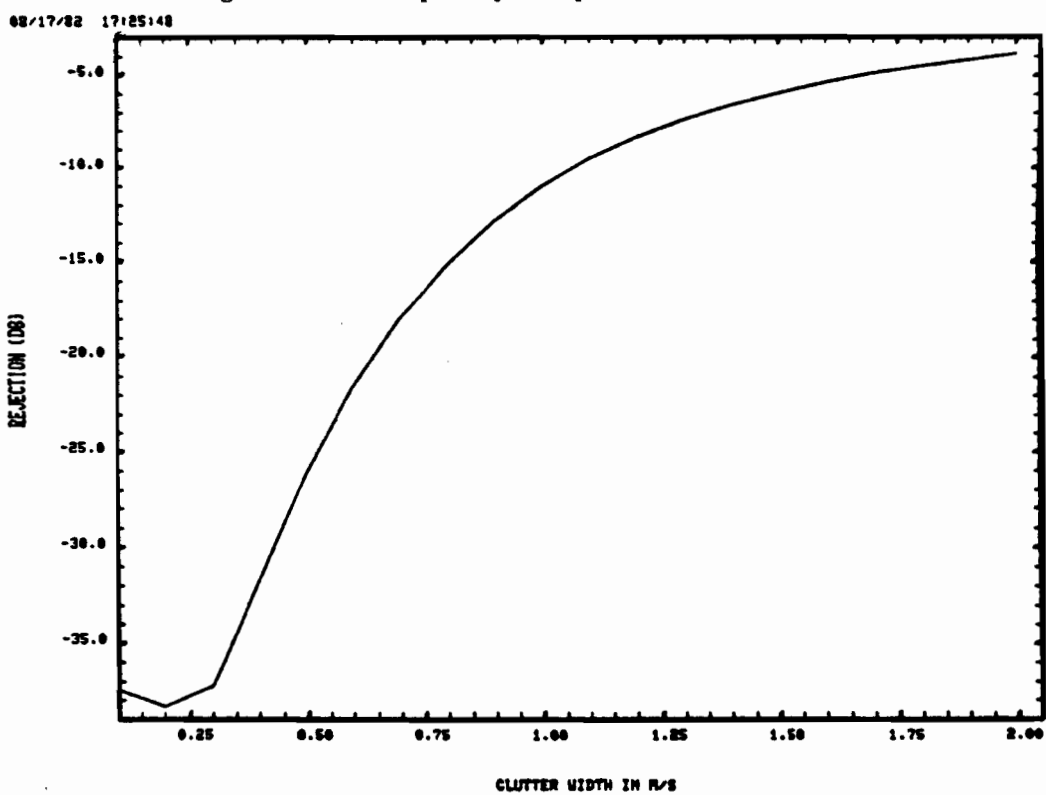
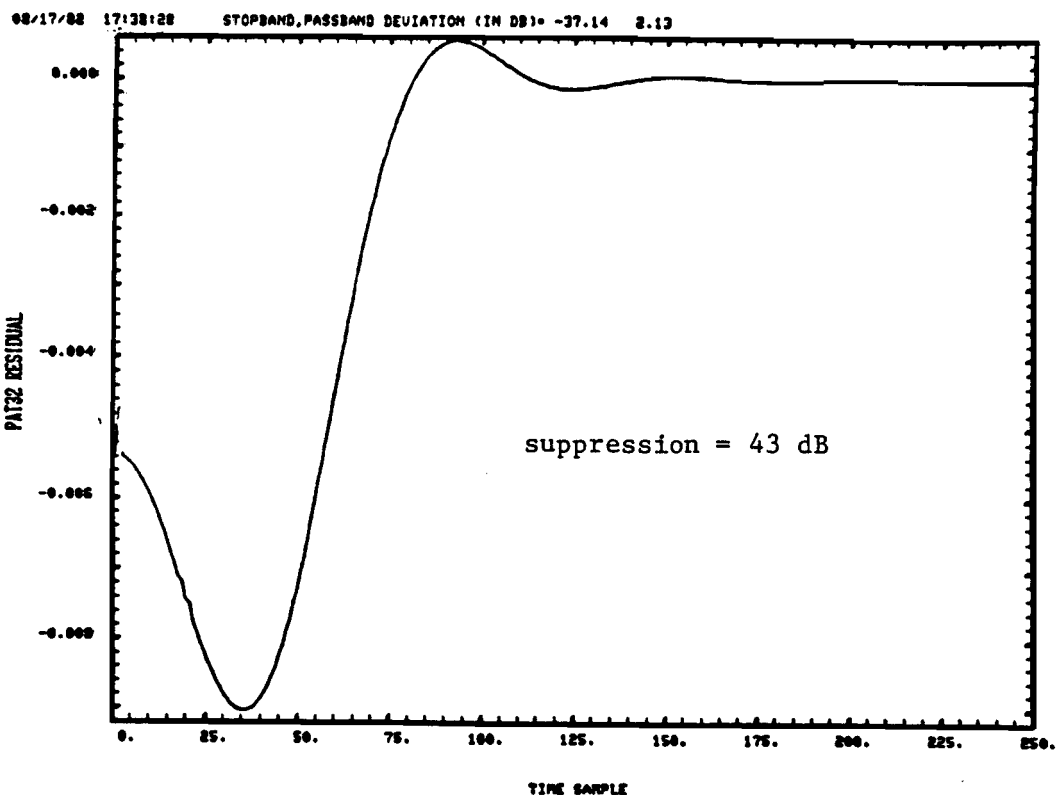
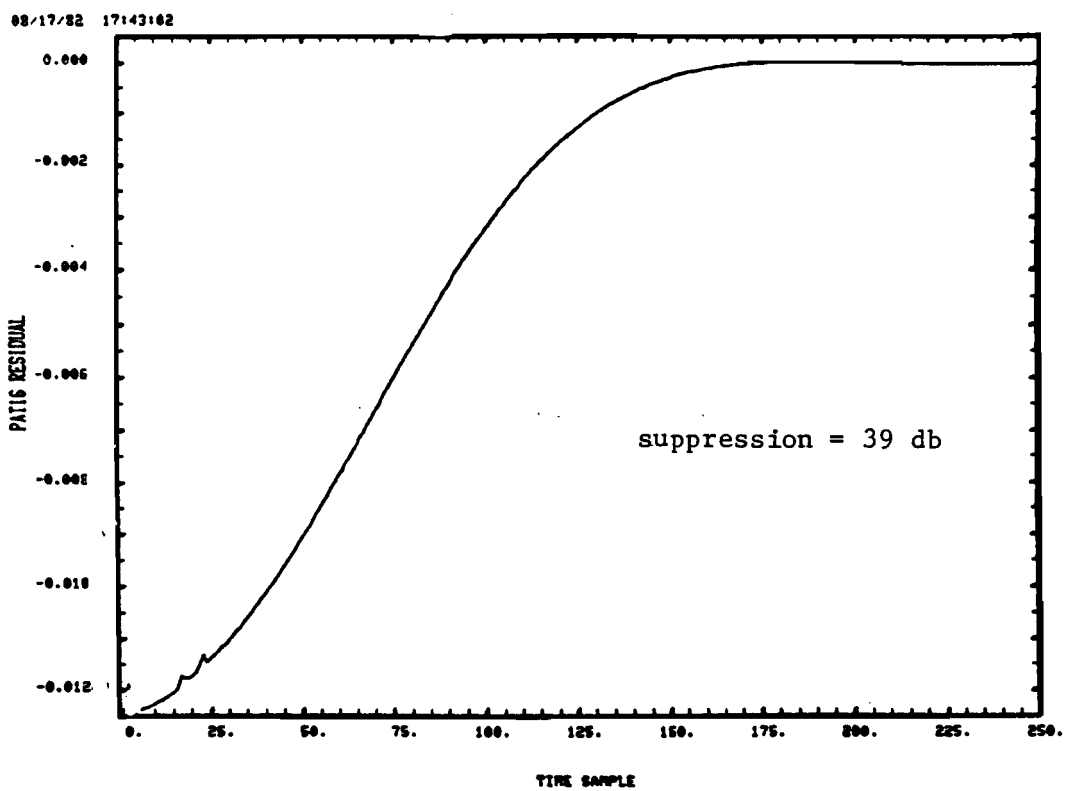


Fig. 7-6. FIR filter #2 suppression for clutter model A.

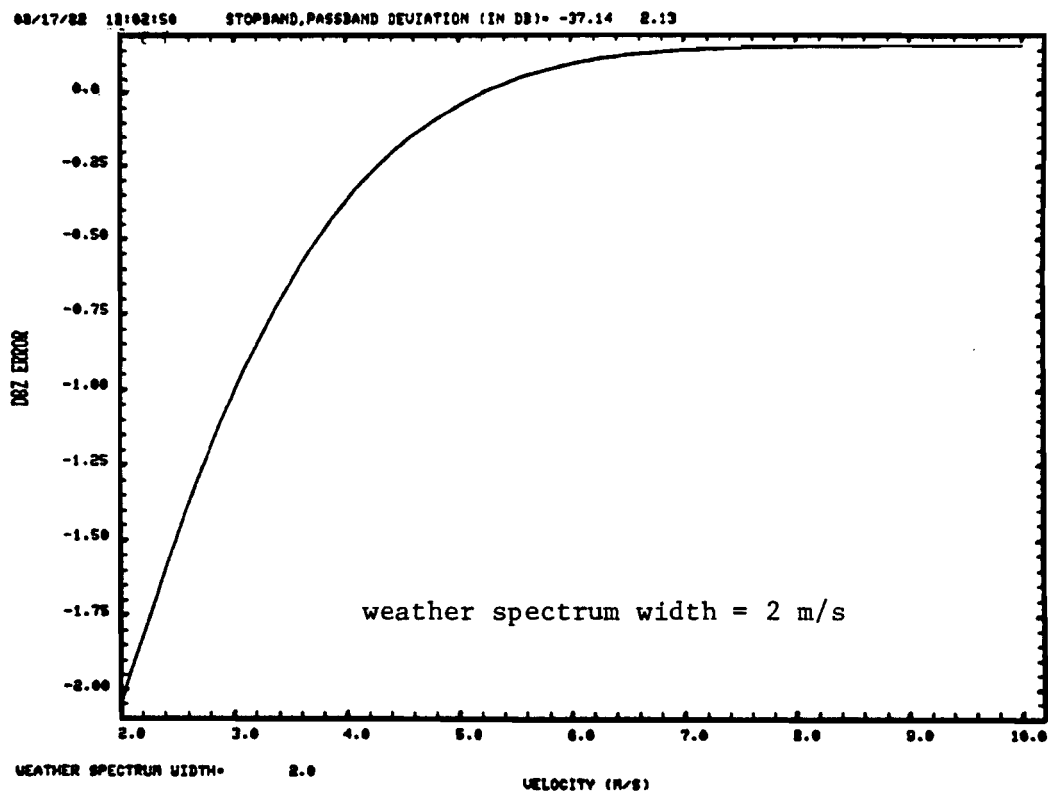


(a) 1° Beamwidth at 3.2 rpm.



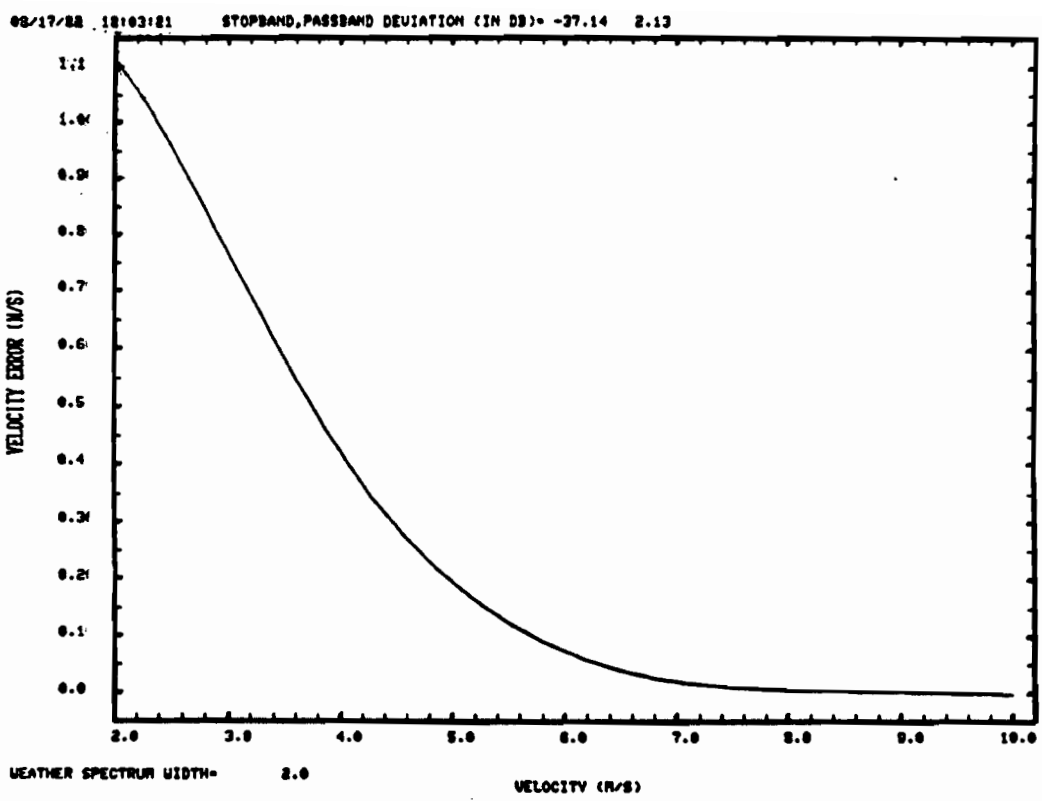
(b) 1° Beamwidth at 1.6 rpm.

Fig. 7-7. FIR filter #2 suppression for clutter model B.

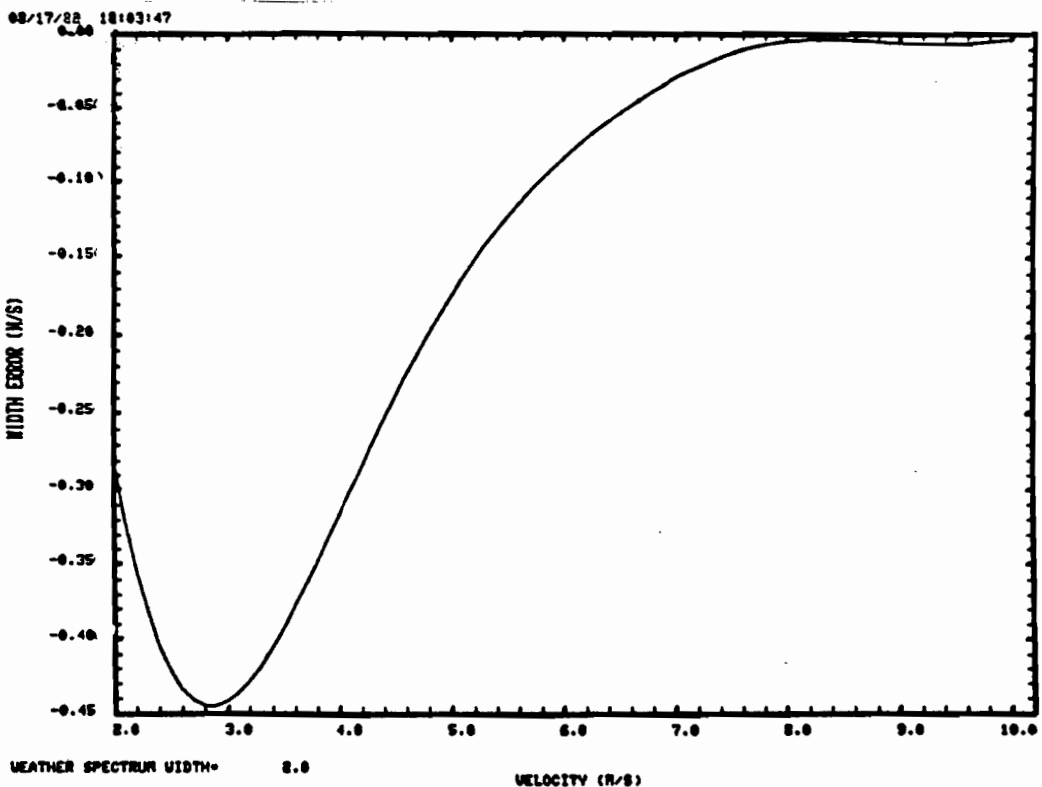


(a) Reflectivity error.

Fig. 7-8. Weather parameter errors for FIR filter #2.



(b) Mean velocity error.



(c) Spectrum width error.

Fig. 7-8. Weather parameter errors for FIR filter #2. (cont.)

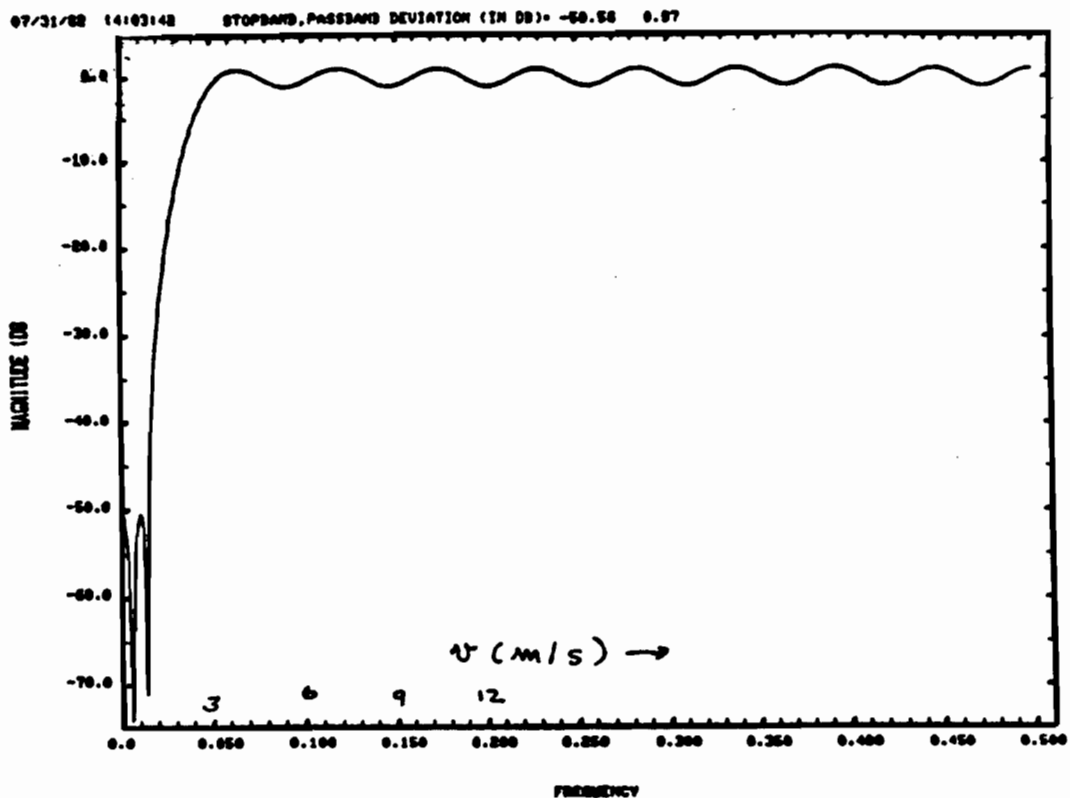


Fig. 7-9. FIR filter #3 frequency response.

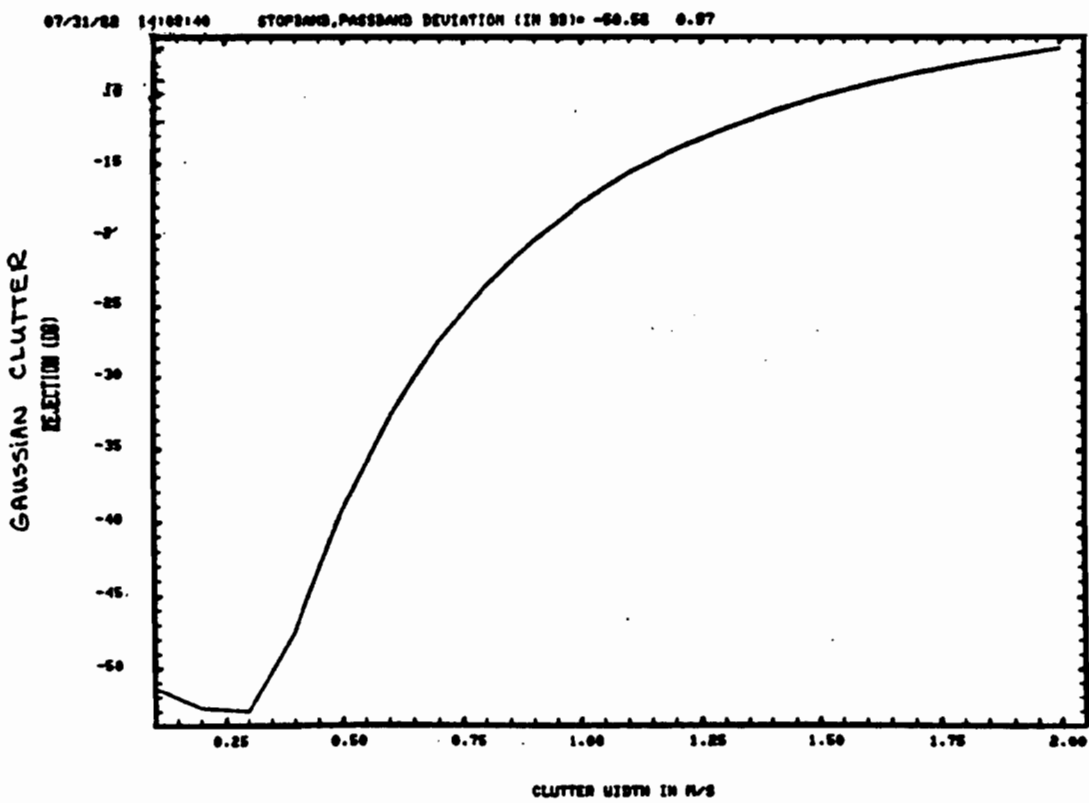


Fig. 7-10. FIR filter #3 suppression for clutter model A.

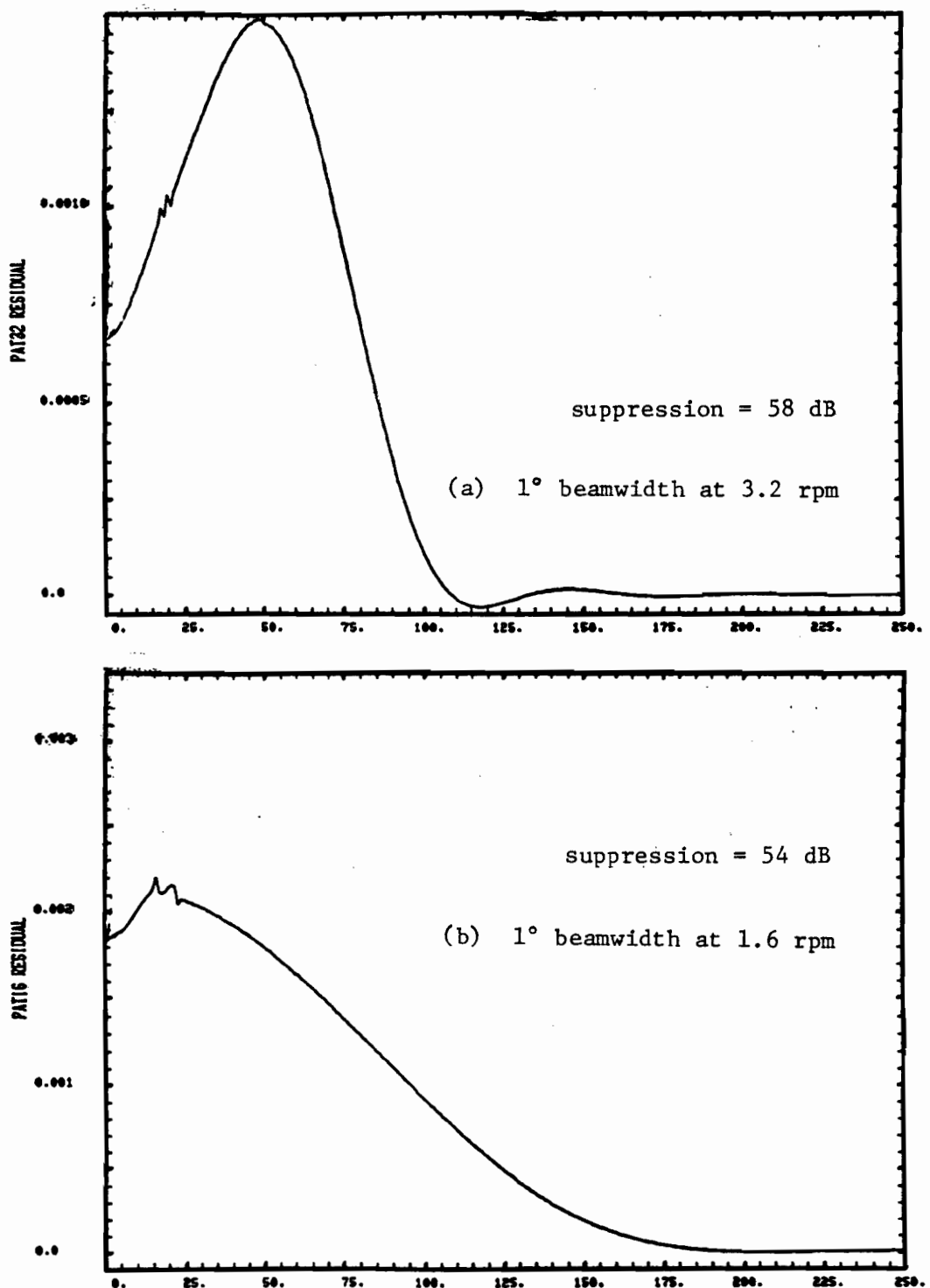
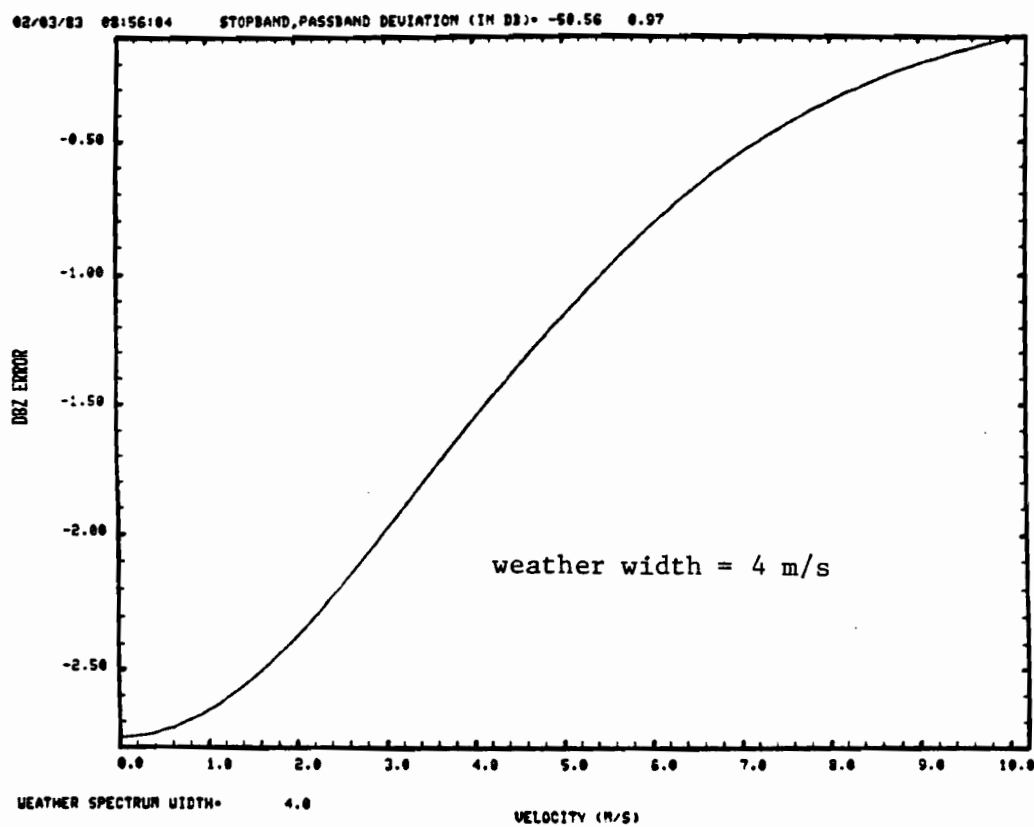
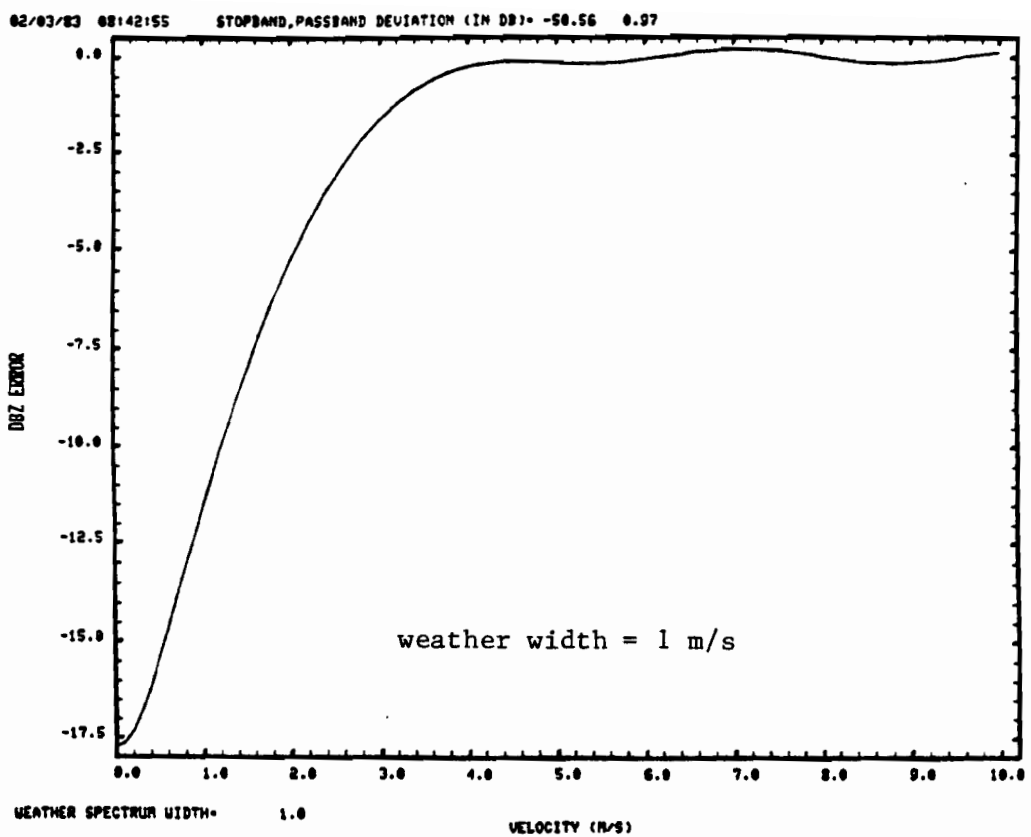
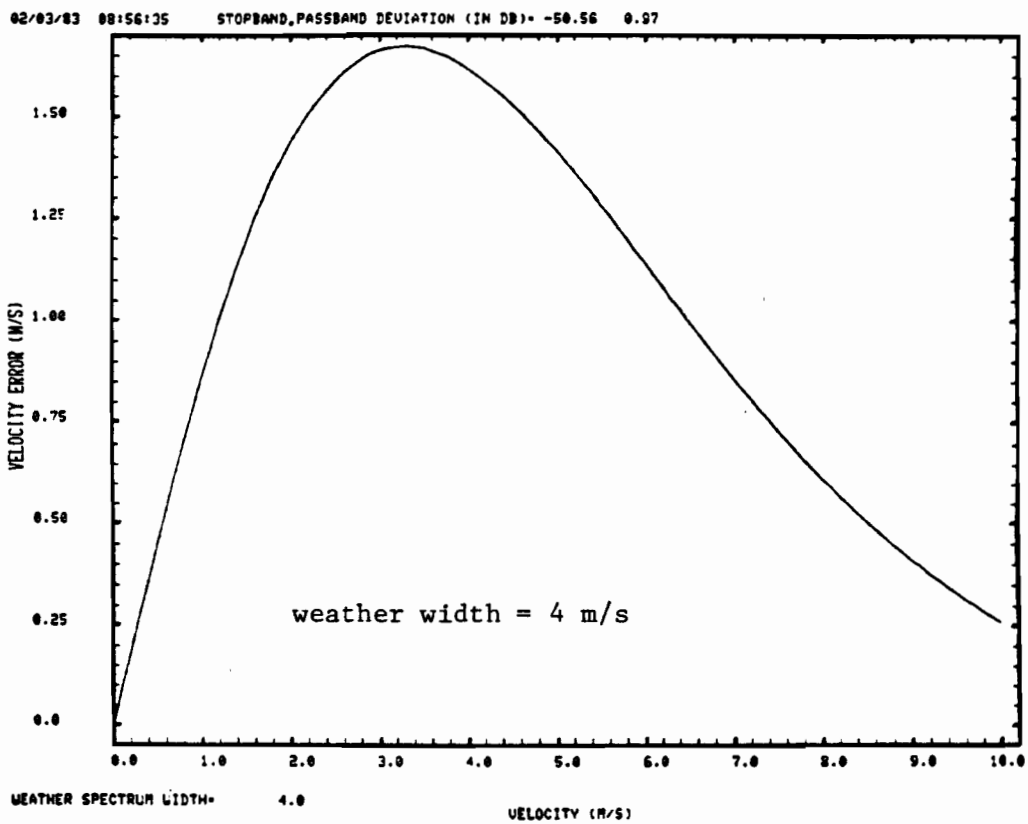
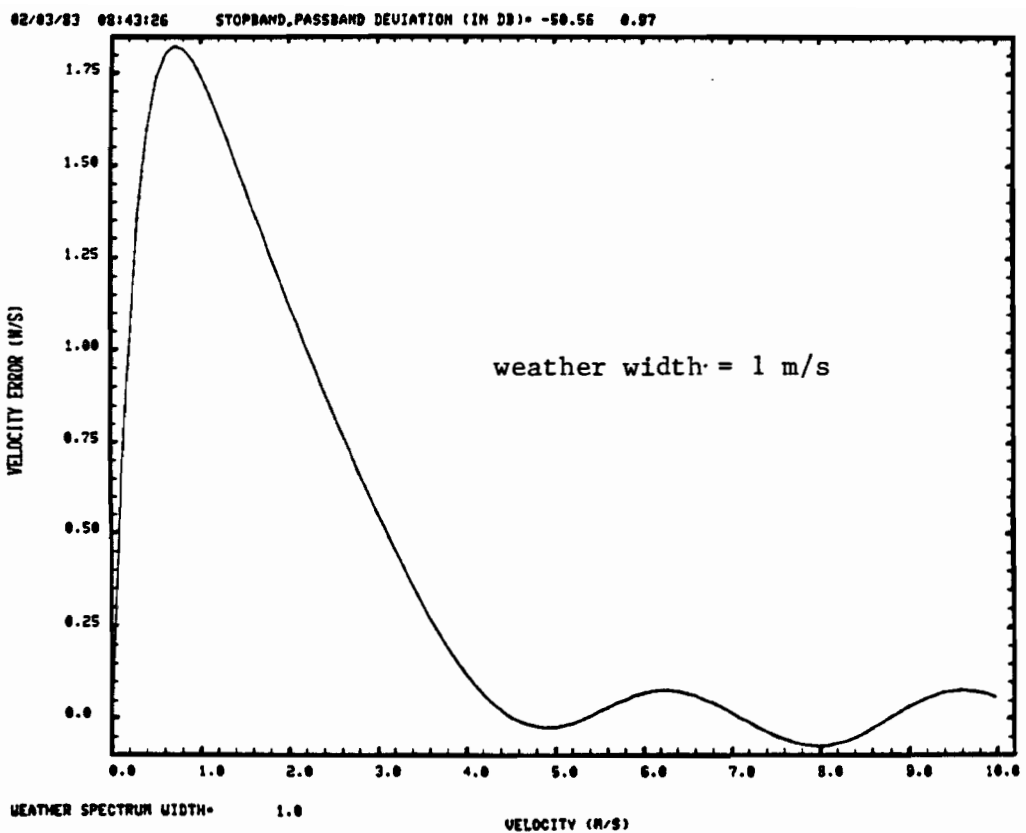


Fig. 7-11. FIR Filter #3 Suppression for Clutter Model B.



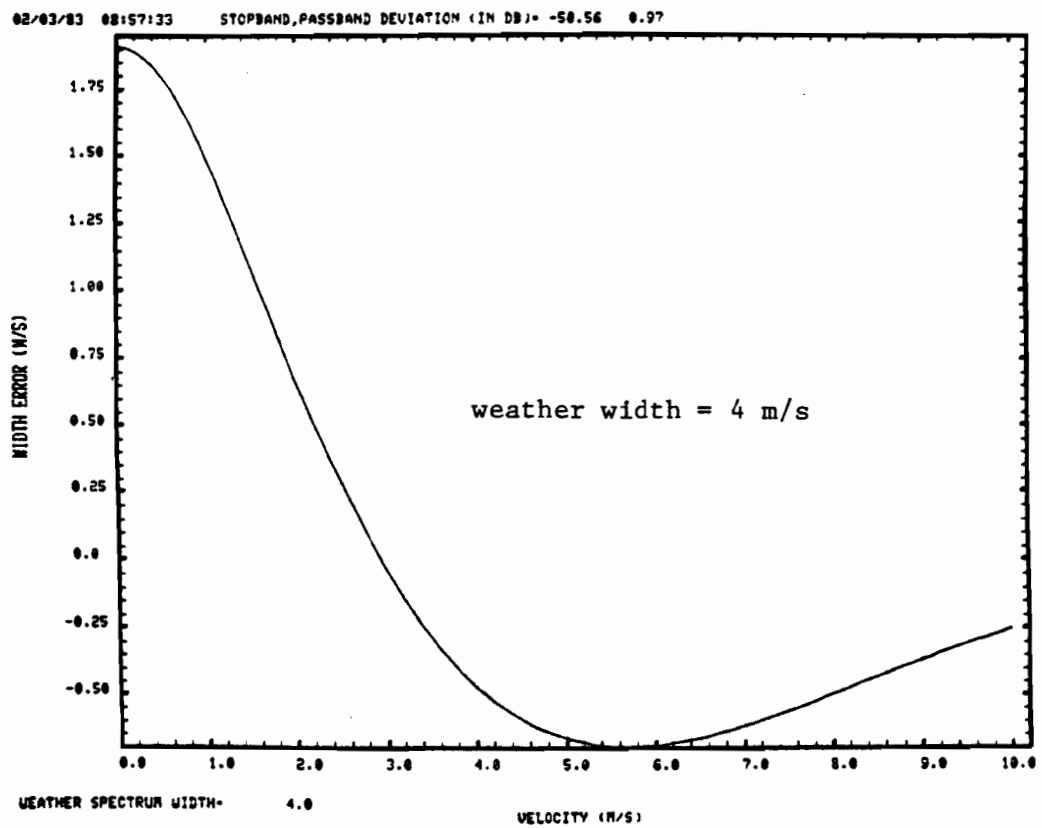
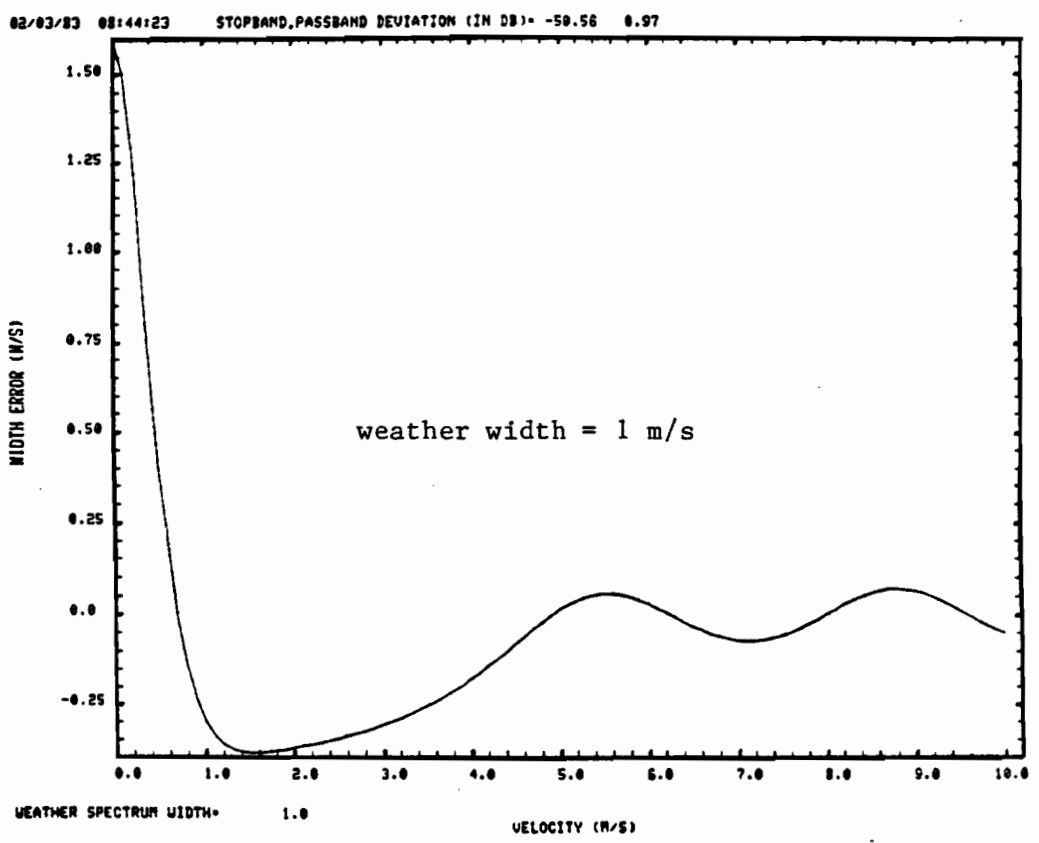
(a) Reflectivity errors.

Fig. 7-12. Weather parameter errors with FIR filter #3.



(b) Velocity errors.

Fig. 7-12. Weather parameter errors with FIR filter #3. (Cont.)



(c) Spectrum width errors.

Fig. 7-12. Weather parameter errors with FIR filter #3. (Cont.)

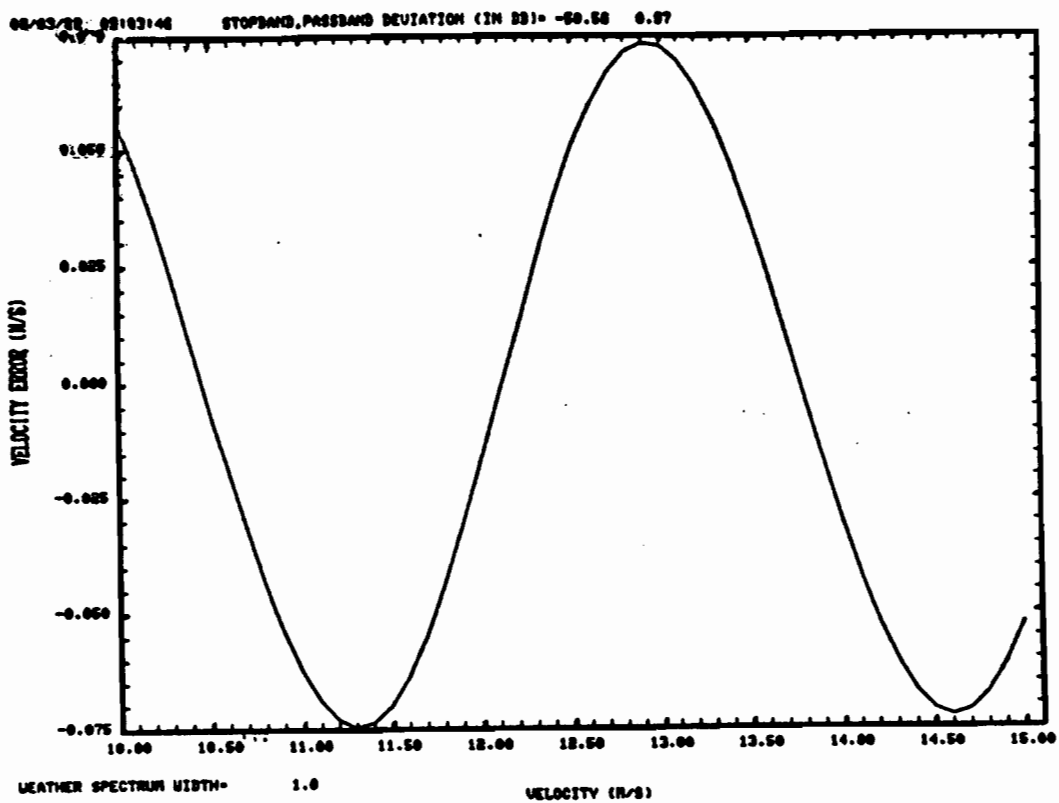
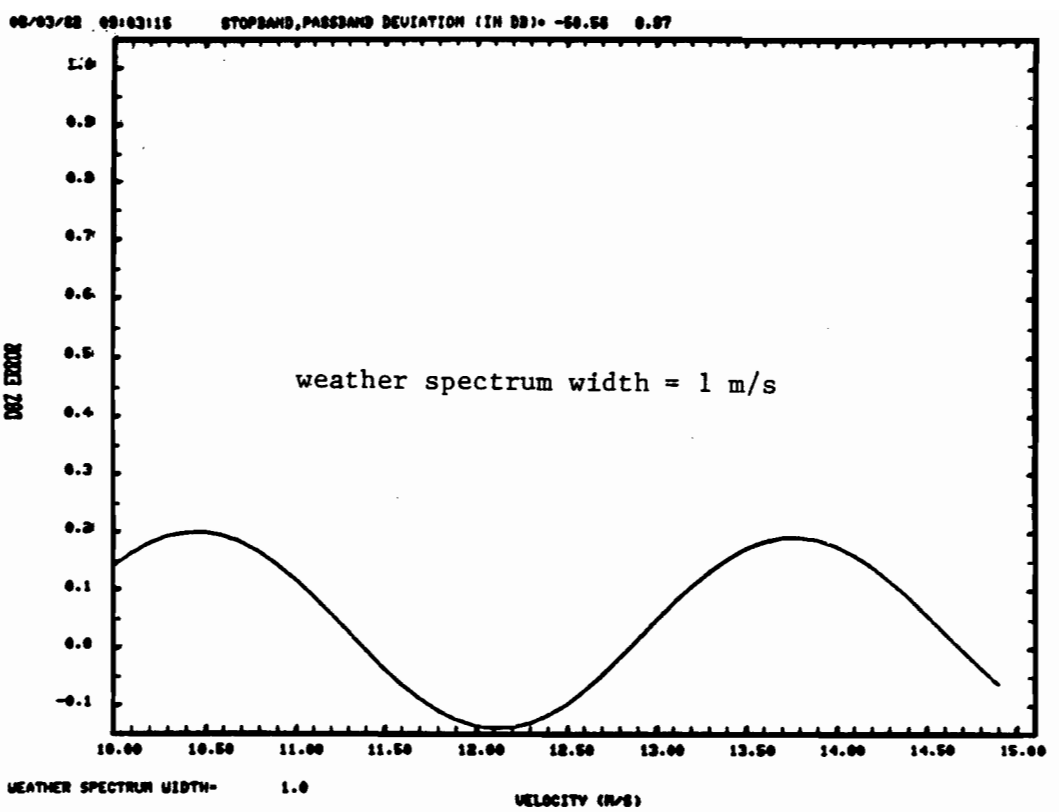


Fig. 7-13. FIR filter #3 weather parameter errors due to passband ripples.

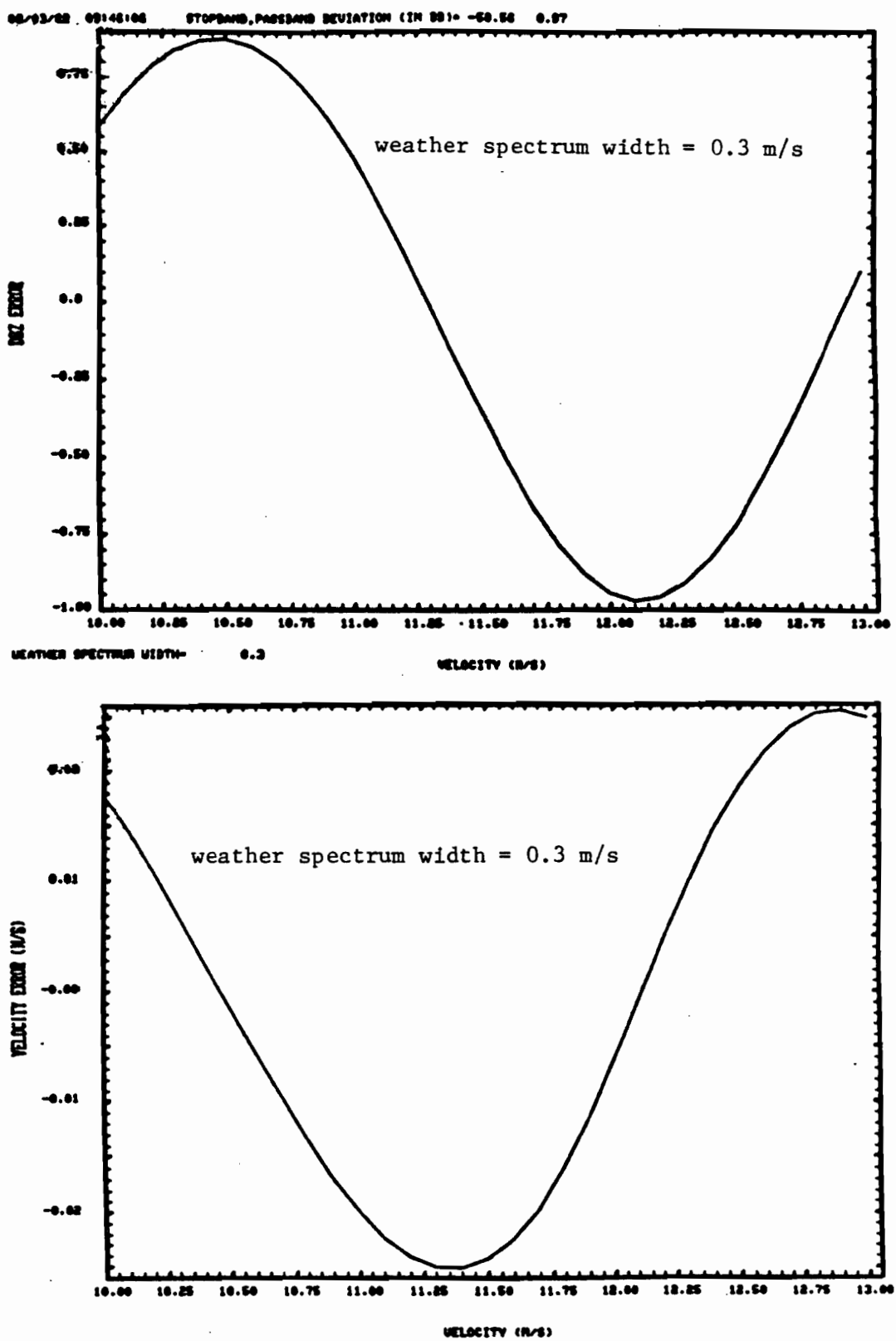


Fig. 7-14. FIR filter #3 weather parameter errors due to passband ripples.

spectrum width) errors are very small. If such narrow widths were operationally of concern, the reflectivity error due to passband ripples could be compensated by use of a lookup table.

Figures 7-15 to 7-17 show the frequency response and clutter suppression for FIR filter #4 which is a first cut at a design to meet the reflectivity clutter suppression specification. Based on the experience with passband ripples in the other FIR filters, this filter was allowed to have ± 2.8 dB passband ripples so as to minimize the passband width. The clutter suppression with both clutter models is in excess of 30 dB for clutter widths up to 0.25 m/s. Figure 7-18 shows the reflectivity error for this filter as a function of mean velocity at various weather spectrum widths. The errors at zero mean velocity are comparable to those shown in Table 4-1 while the errors at larger mean velocities are much less than the values shown in Table 4-1. The approximately constant bias error at large mean velocities arises from averaging the squared sinusoid frequency response:

$$H^2(v) \approx (1 + a \cos kv)^2 \quad (7-1)$$

$$\overline{H^2(v)} = 1 + a^2/2 \quad (7-2)$$

Thus, if $a = 0.28$ (corresponding to a 2.8 dB ripple),

$$1 + a^2/2 = 1.05 \Rightarrow 0.16 \text{ dB.}$$

This bias is strictly predictable from the clutter filter characteristic and hence removable.

B. Infinite Impulse Response (IIR) Filter Results for Weather and Clutter Models

Since the 3-pole elliptical filters described by Groginsky and Glover [2] were used as the basis for the augmented NTR specification, it was important to assess the performance of such filters against the recommended specification. Three such filters were considered:

- (1) a Groginsky-Glover [2] design for 919 Hz PRF with a 1.5 m/s passband,
- (2) a Groginsky-Glover [2] design for 1.5 m/s passband at 525 Hz PRF being used to furnish a 3 m/s passband at 1050 Hz, and
- (3) a Hamidi-Zrnic' [1] design to yield 3 m/s passband at 1280 Hz.

In the case of filter #2, the filter coefficients were quantized to 12 bits as indicated in Groginsky and Glover [2] so as to provide (by comparison with filter #3) some insight into quantization sensitivity.

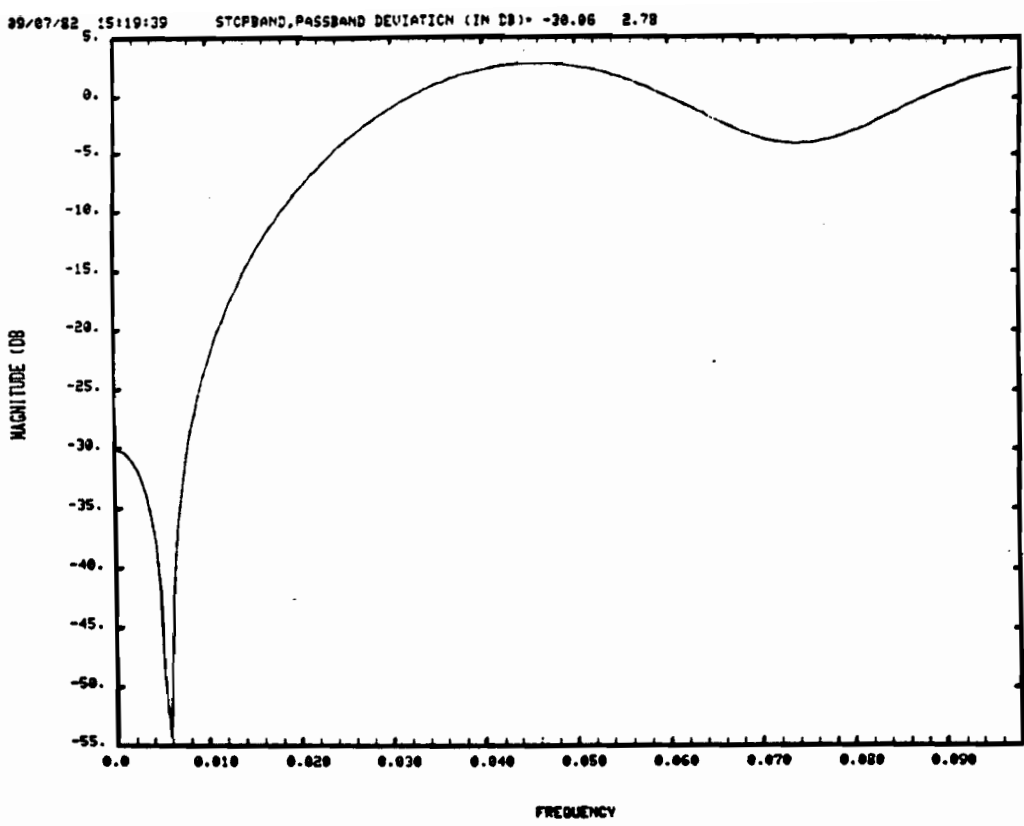


Fig. 7-15. Frequency response for FIR filter #4.

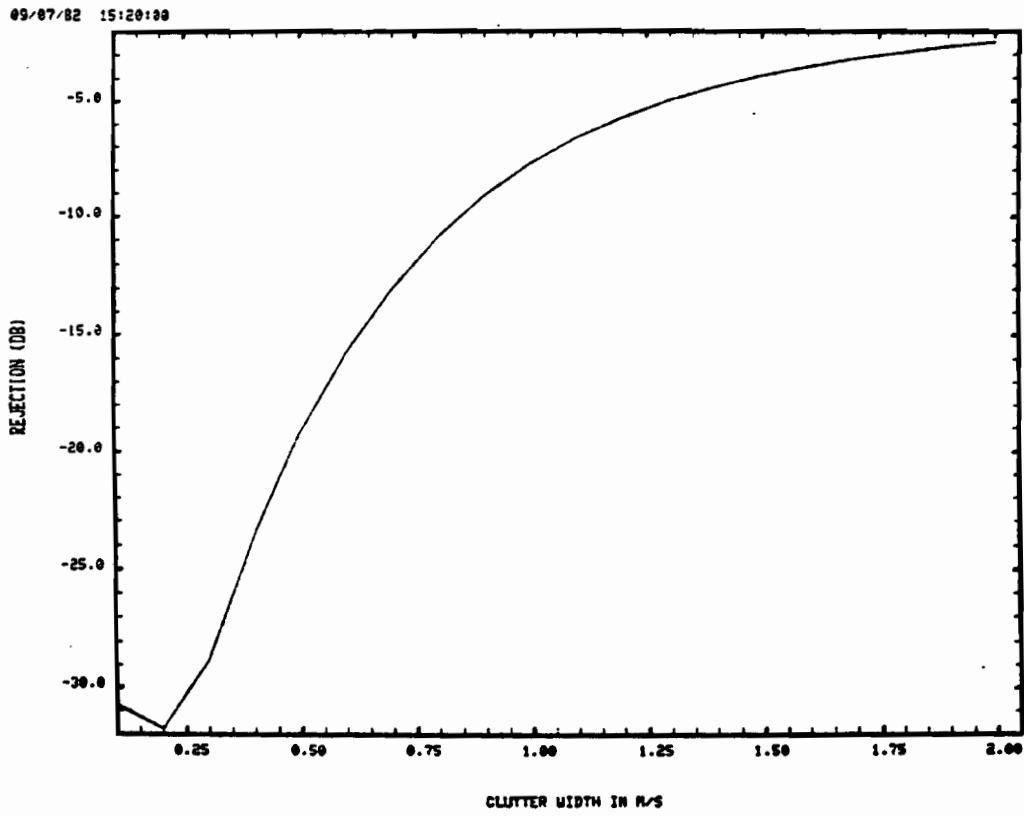
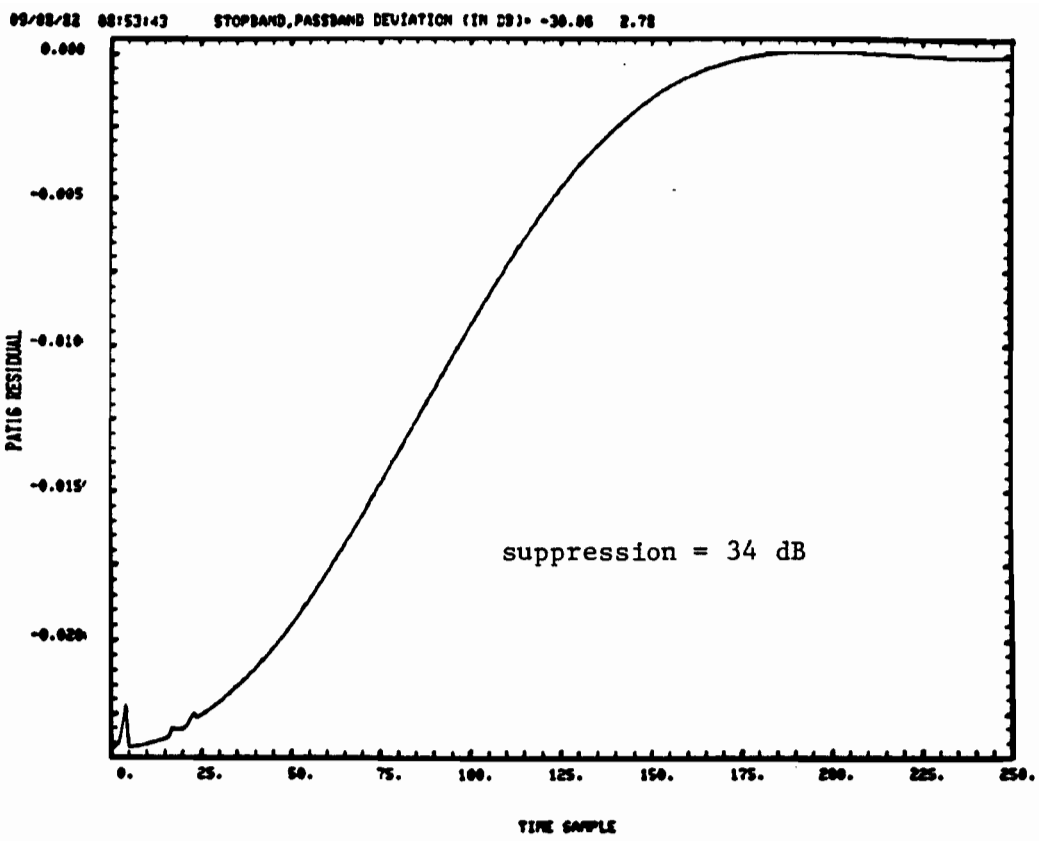
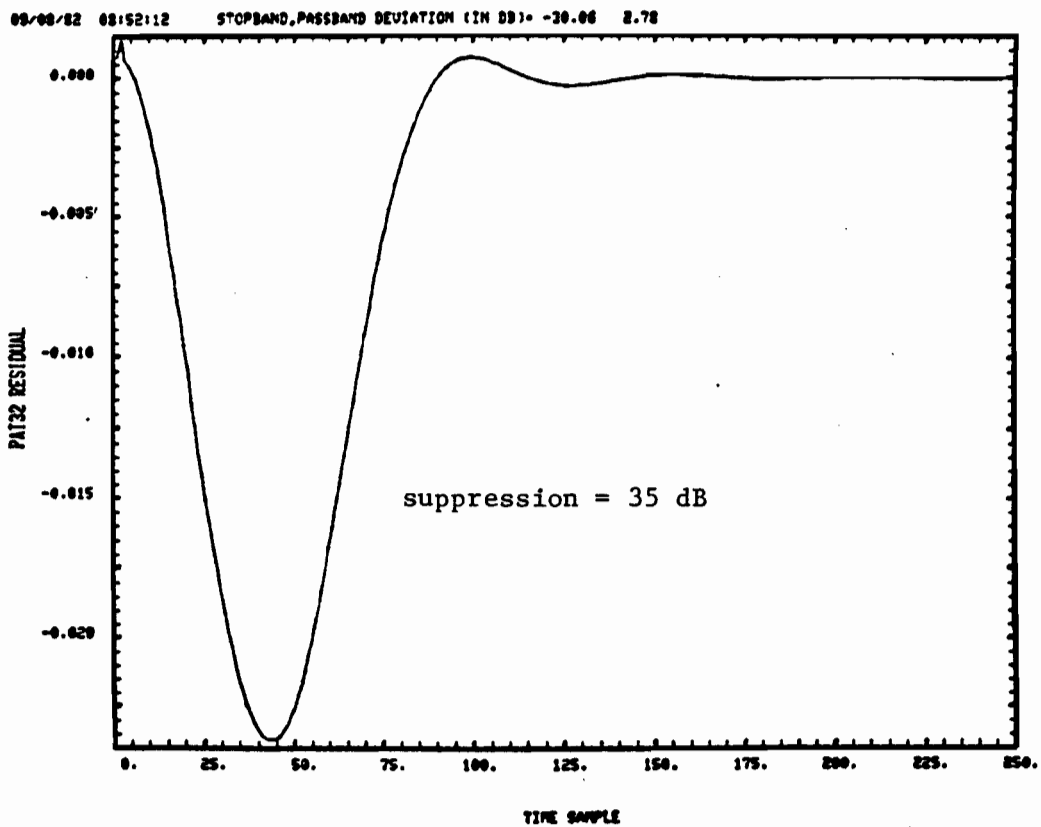


Fig. 7-16. FIR filter #4 suppression for clutter model A.

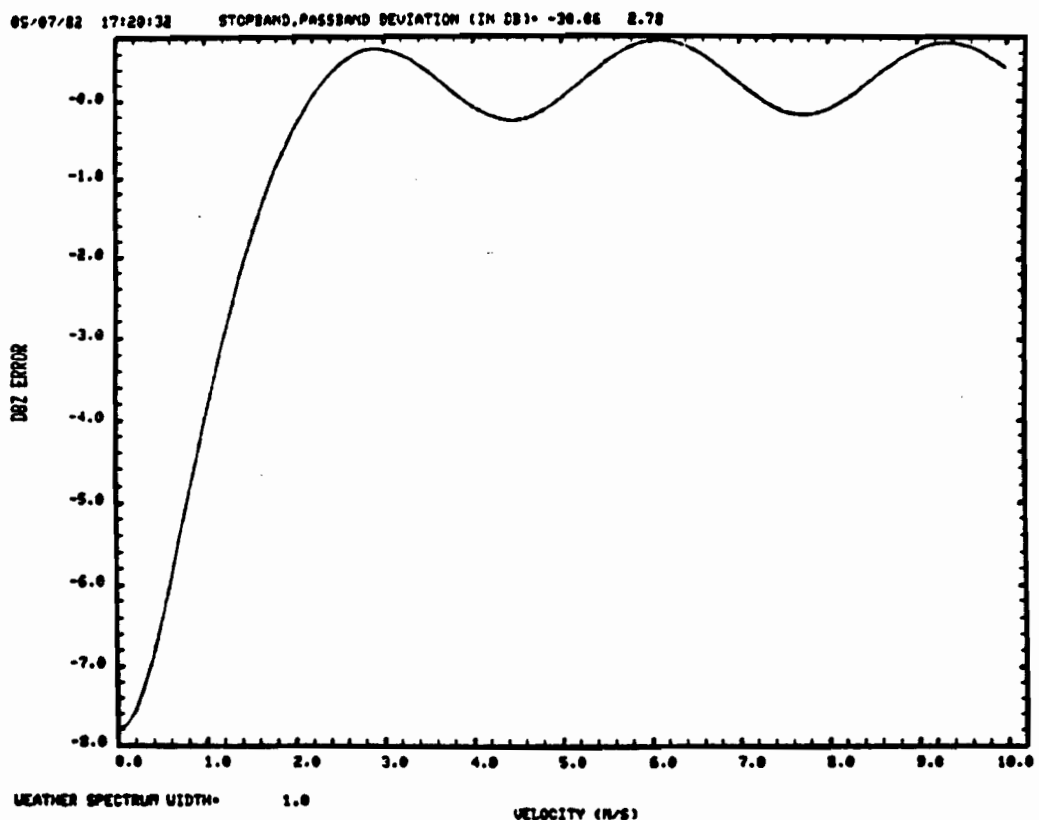


(a) 1° Beamwidth at 3.2 rpm.



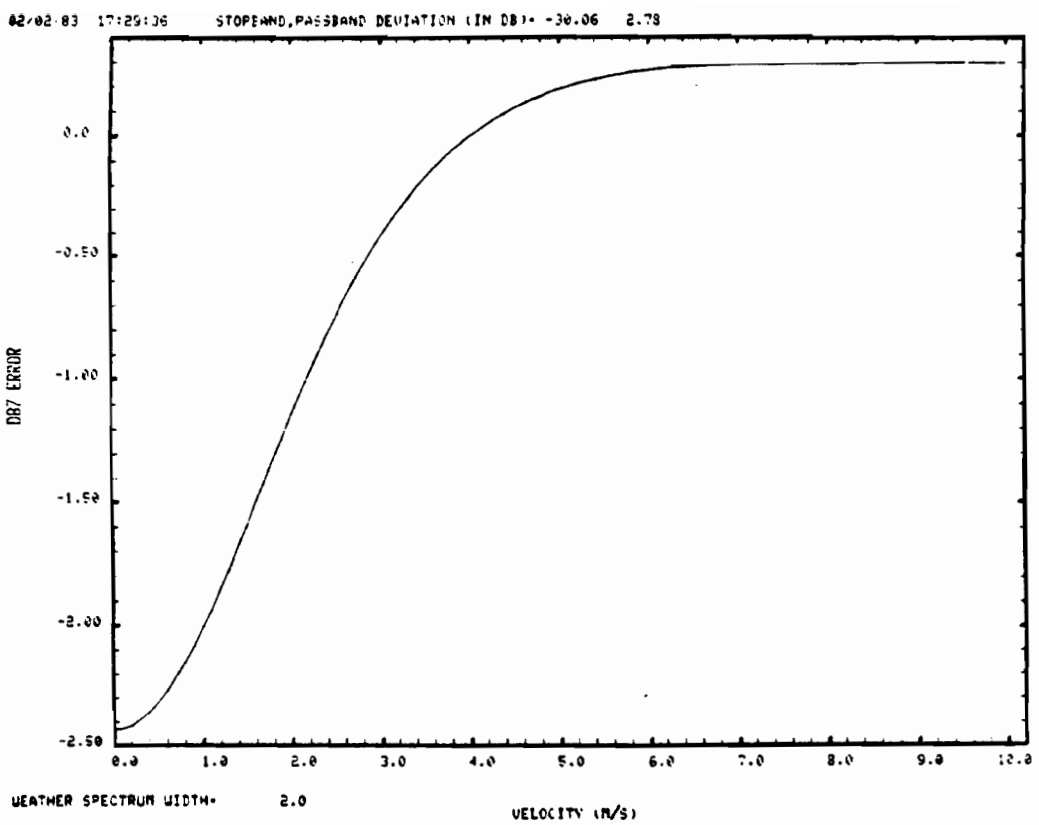
(b) 1° Beamwidth at 1.6 rpm.

Fig. 7-17. FIR filter #4 suppression for clutter model B.

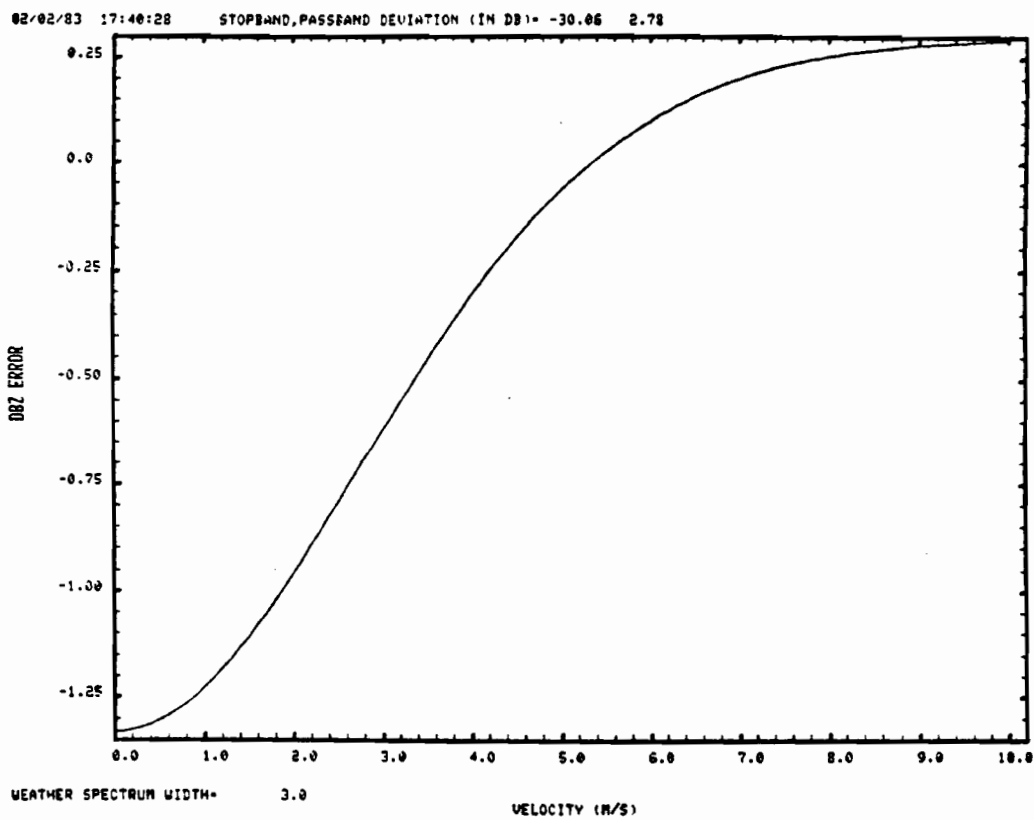


(a) Weather spectrum width = 1 m/s.

Fig. 7-18. Reflectivity errors with FIR filter #4.



(b) Weather width = 2 m/s.



(c) Weather width = 3 m/s.

Fig. 7-18. Reflectivity errors with FIR filter #4 (con't).

Figures 7-19 to 7-21 show the frequency response and clutter suppression capability* for IIR filter #1, while Figures 7-22 to 7-24 show the weather errors due to this filter when clutter is not present. This filter is seen to provide substantially better suppression (e.g., 43 dB at a clutter model A width of 0.25 m/s versus 34 dB for FIR filter #4) for both clutter models than did FIR filter #4. On the other hand, the reflectivity bias error at zero mean weather velocity is somewhat greater than that of FIR filter #4 for spectrum widths > 1 m/s.

This filter (suitably scaled for PRF) would be a strong candidate for clutter suppression in the reflectivity channel (if clutter filtering were used in the reflectivity channel).

Figures 7-25 to 7-30 and 7-31 to 7-36 show the corresponding results for IIR filters #2 and #3 which have nominally the same passband of 3 m/s. The Hamidi-Zrnic' design [1] with very high accuracy coefficients is seen to provide slightly better clutter suppression capability at the expense of slightly larger weather velocity estimate errors when no clutter is present. Comparing these IIR results with those for the FIR filter #3 which had a similar passband, we note that:

- (1) both filter types are essentially identical in terms of the maximum clutter model A spectrum width to yield 50 dB suppression as well as weather reflectivity and spectrum width estimate errors due to the filter
- (2) the IIR filters provide greater suppression at small clutter widths (especially, clutter model B at 1.6 rpm), while
- (3) the FIR filter yields somewhat lower weather velocity errors when the weather velocity is well above the passband edge.

C. FIR Filter Results for Measured Clutter Data

Experiments with measured clutter data were conducted on two types of clutter data:

- (1) returns from a discrete scatterer (e.g., a radio tower) which emulates clutter model B, and
- (2) returns from regions with a variety of clutter sources.

1. MIT Data

Figures 7-37 to 7-39 show examples of clutter suppression by FIR filters 1-3 on radio towers illuminated by the MIT radar while Table 7-2 contains

*All three of the IIR filters have a passband gain of +2 to +3 dB which was not removed in the computations of clutter suppression nor reflectivity bias error.

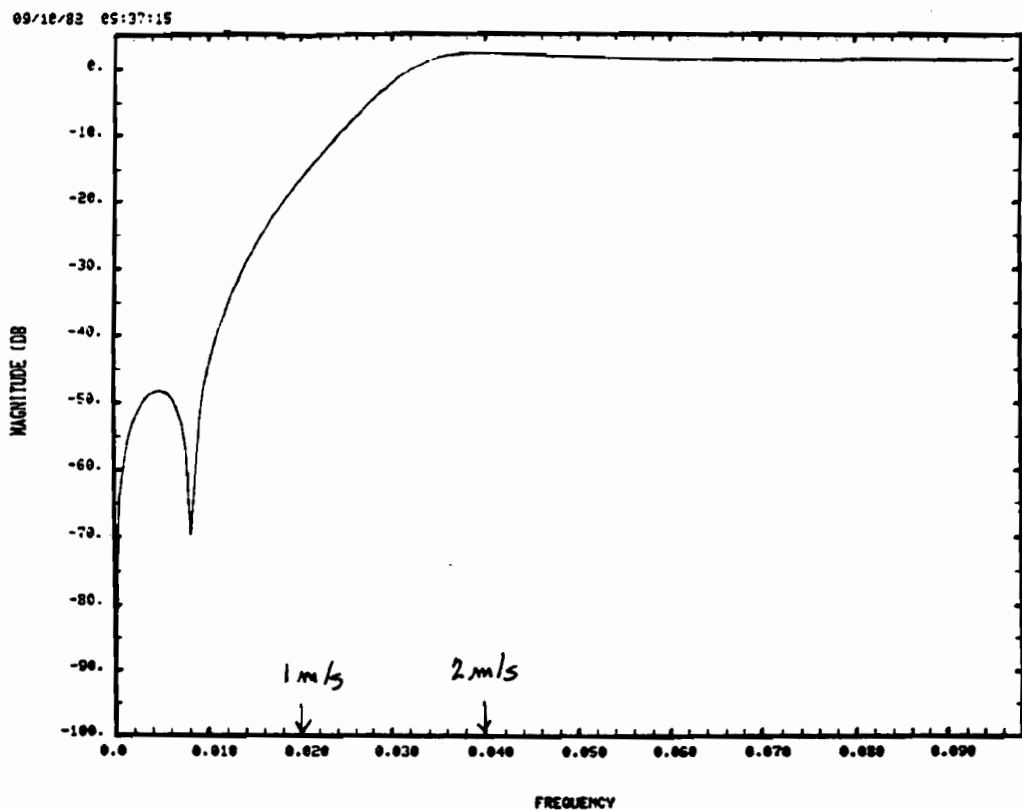


Fig. 7-19. Frequency response for IIR filter #1.

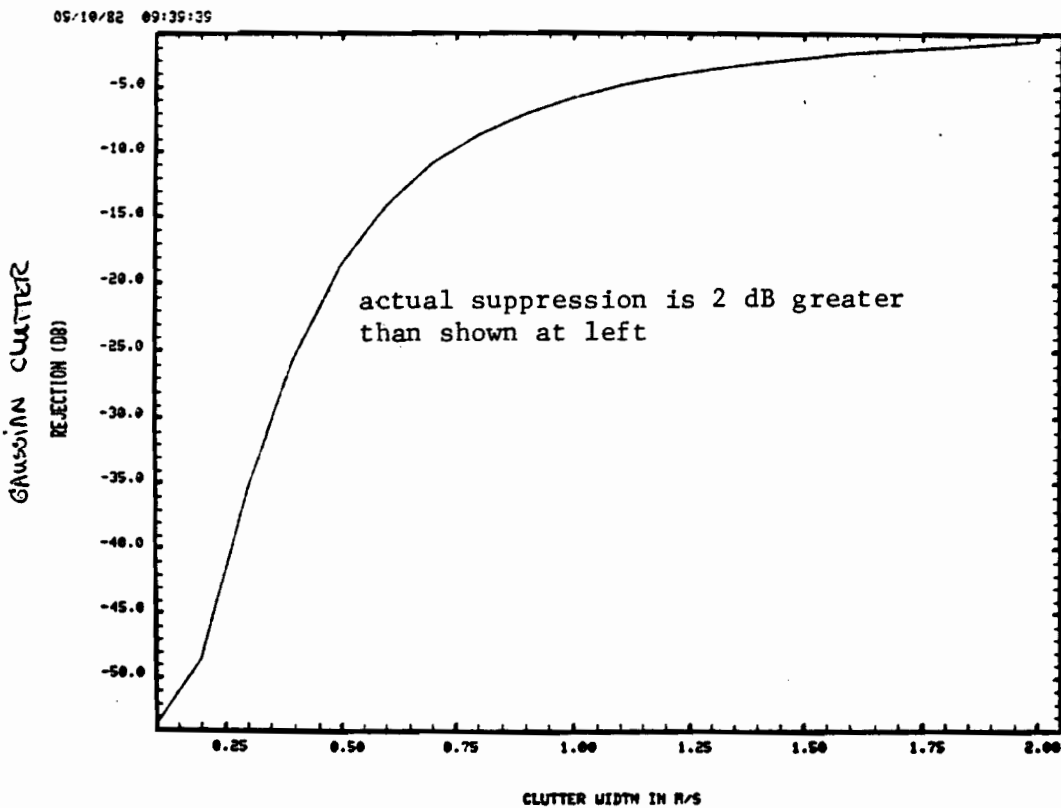
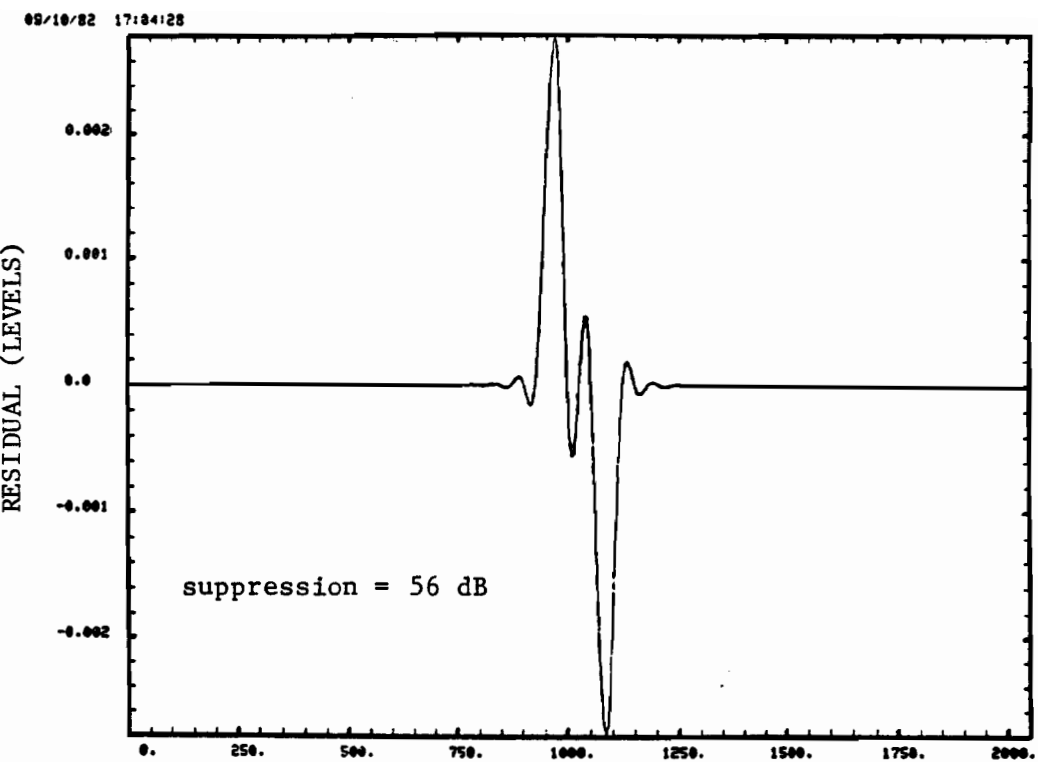
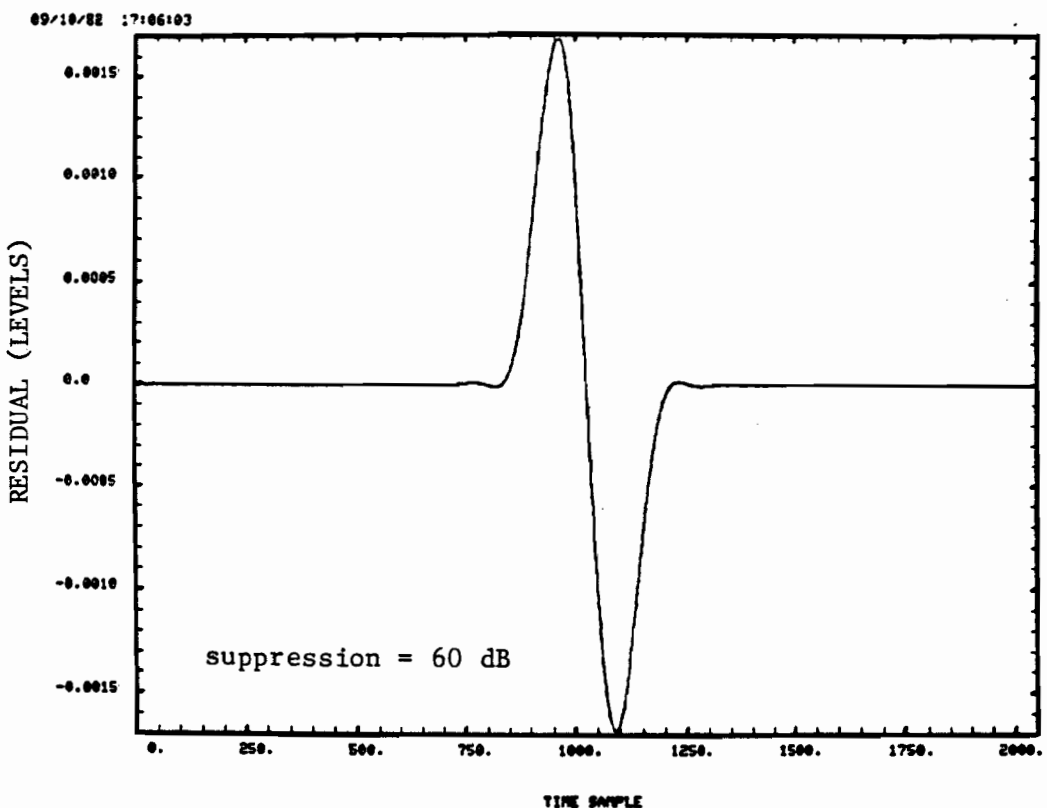


Fig. 7-20. IIR filter #1 suppression for clutter model A.



(a) 1° Beamwidth at 3.2 rpm.



(b) 1° Beamwidth at 1.6 rpm.

Fig. 7-21. IIR filter #1 suppression for clutter model B.

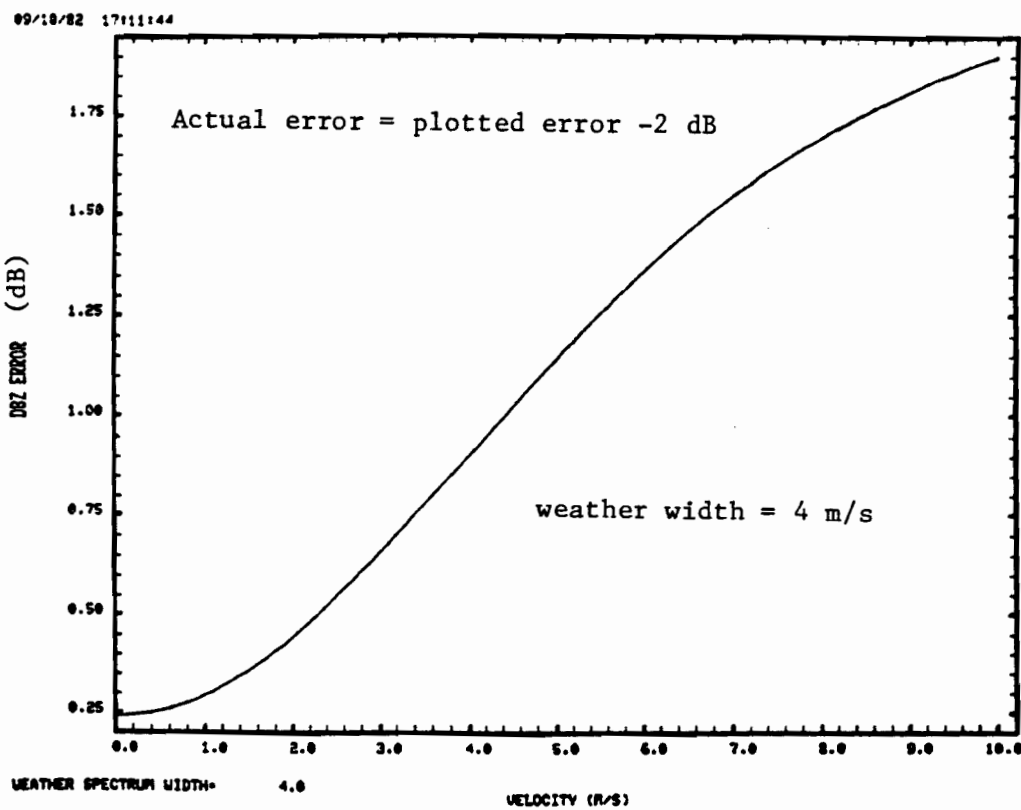
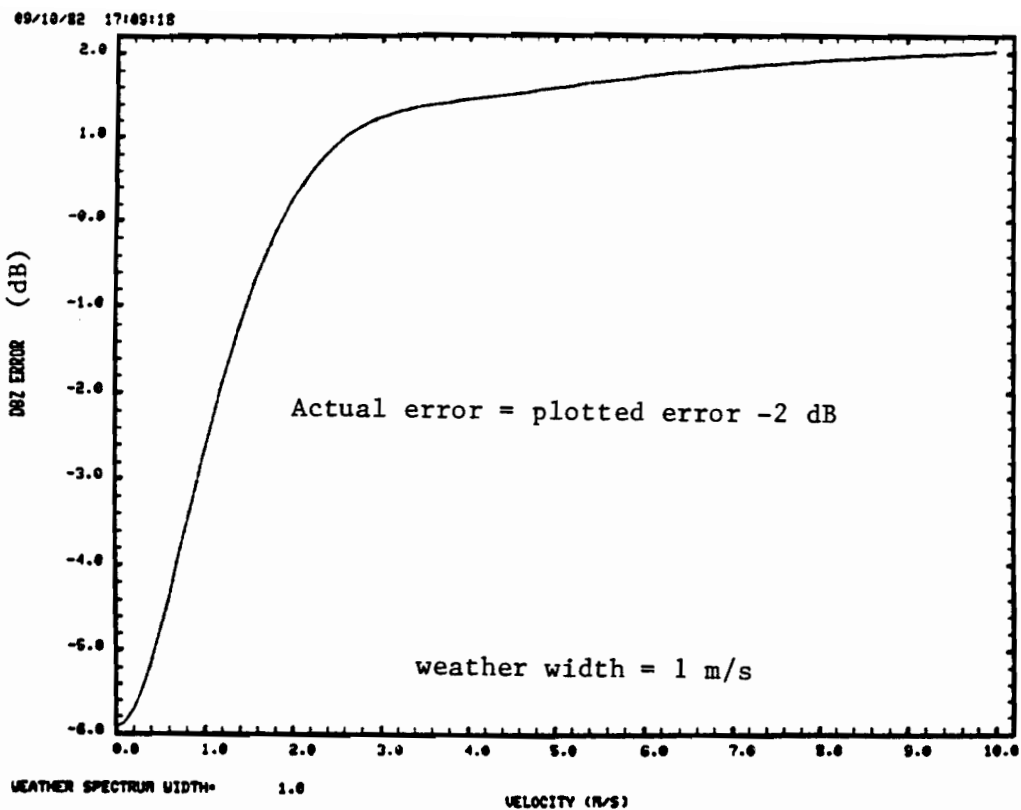


Fig. 7-22. Reflectivity error with IIR filter #1.

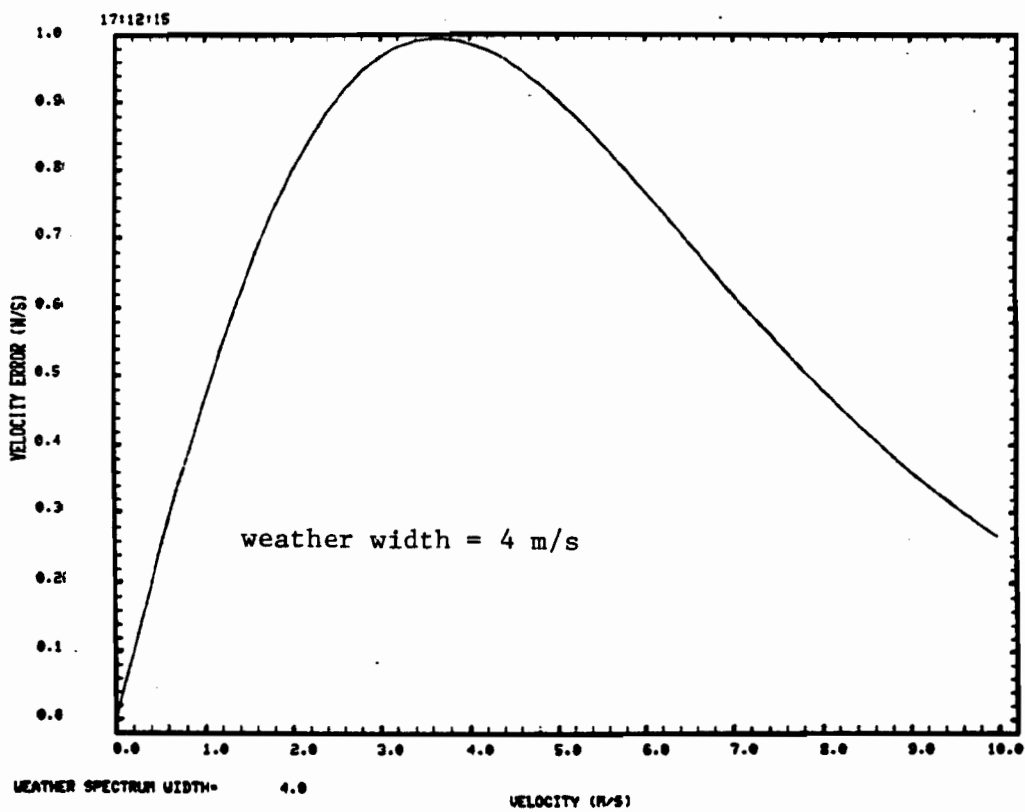
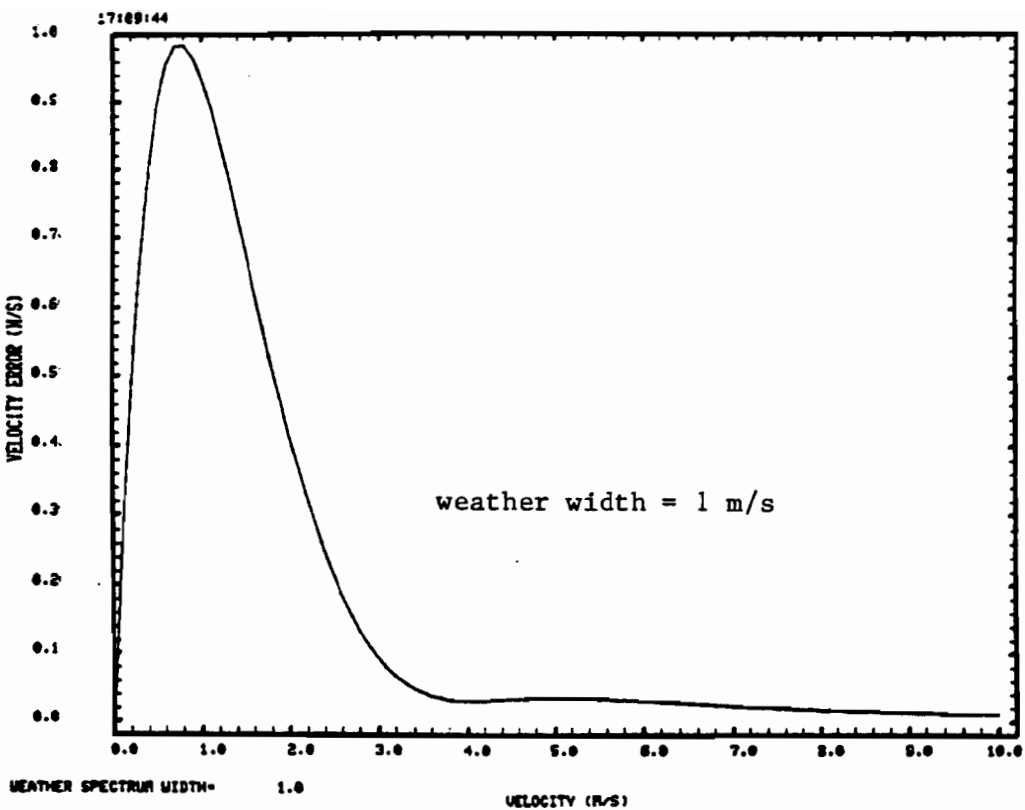


Fig. 7-23. Weather mean velocity error with IIR filter #1.

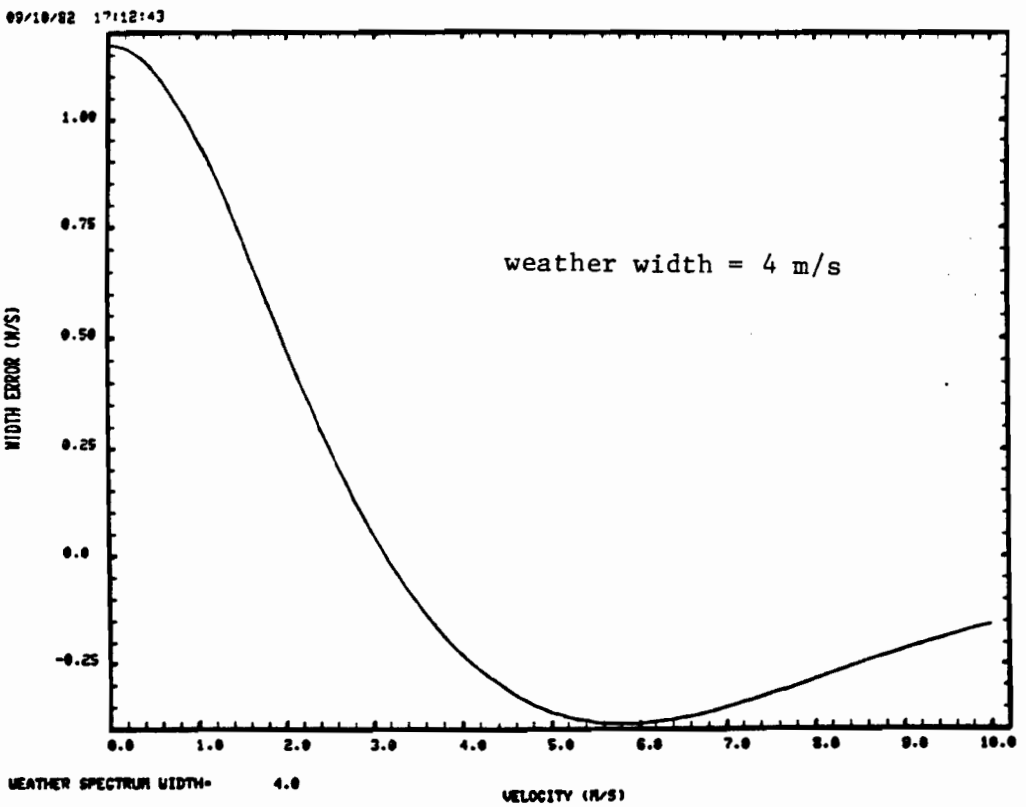
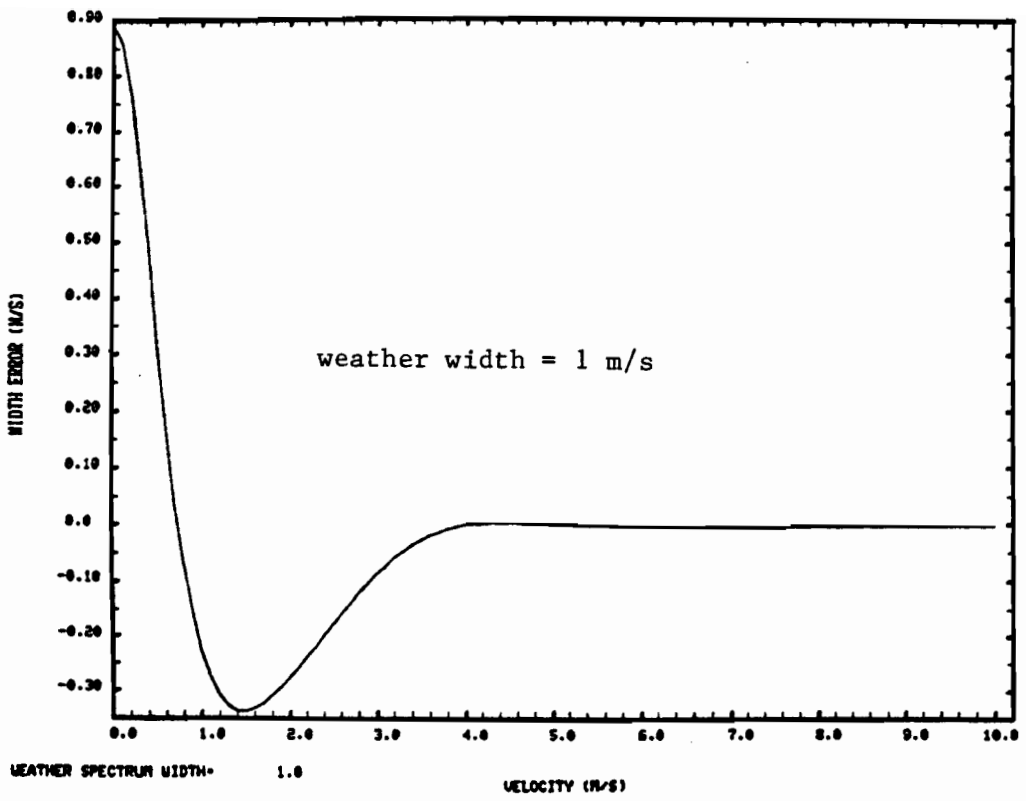


Fig. 7-24. Weather spectrum width error with IIR filter #1.

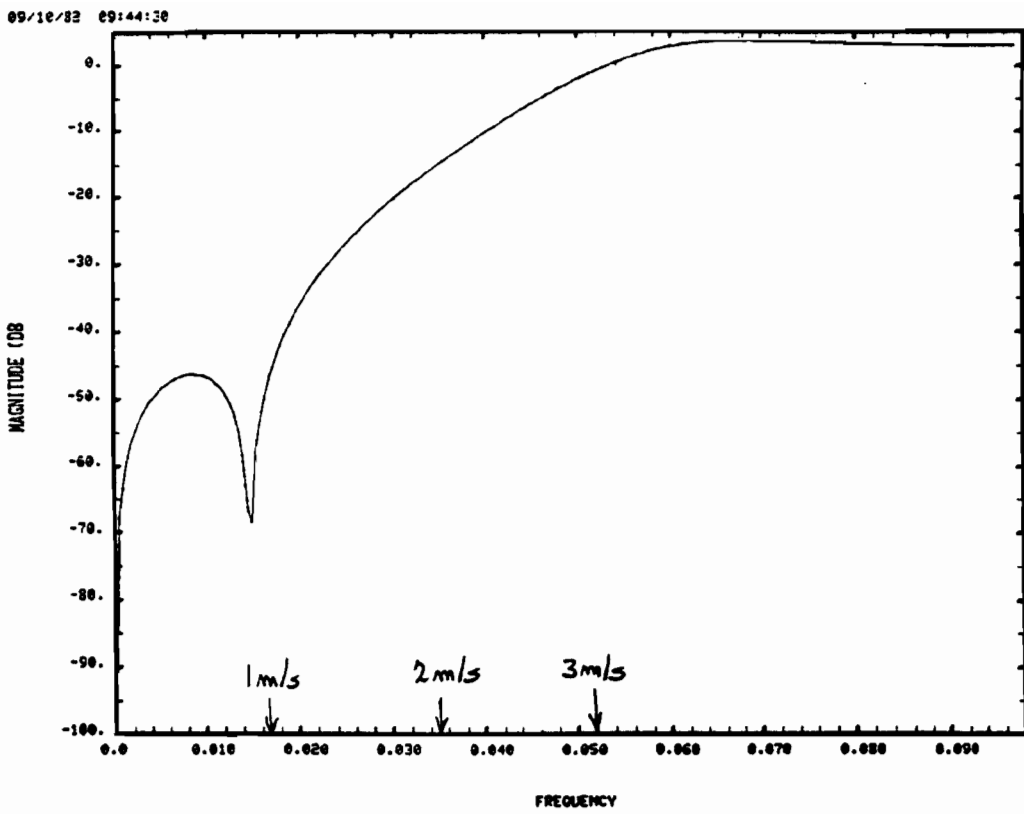


Fig. 7-25. Frequency response for IIR filter #2.

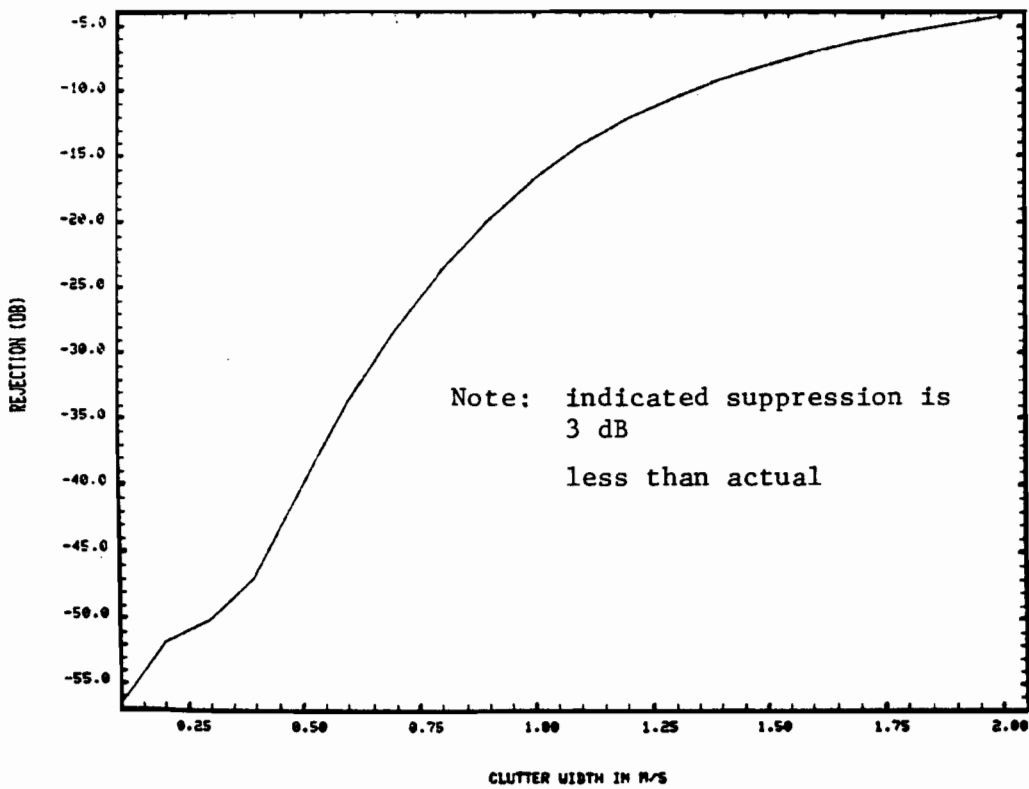
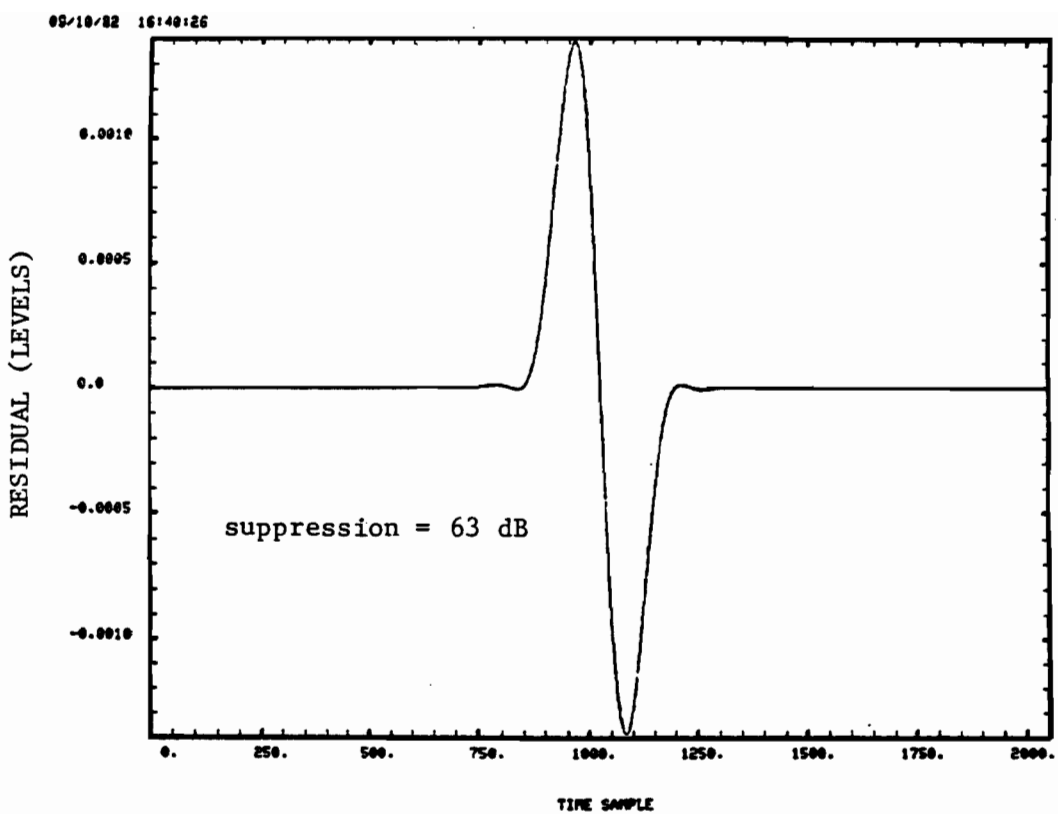
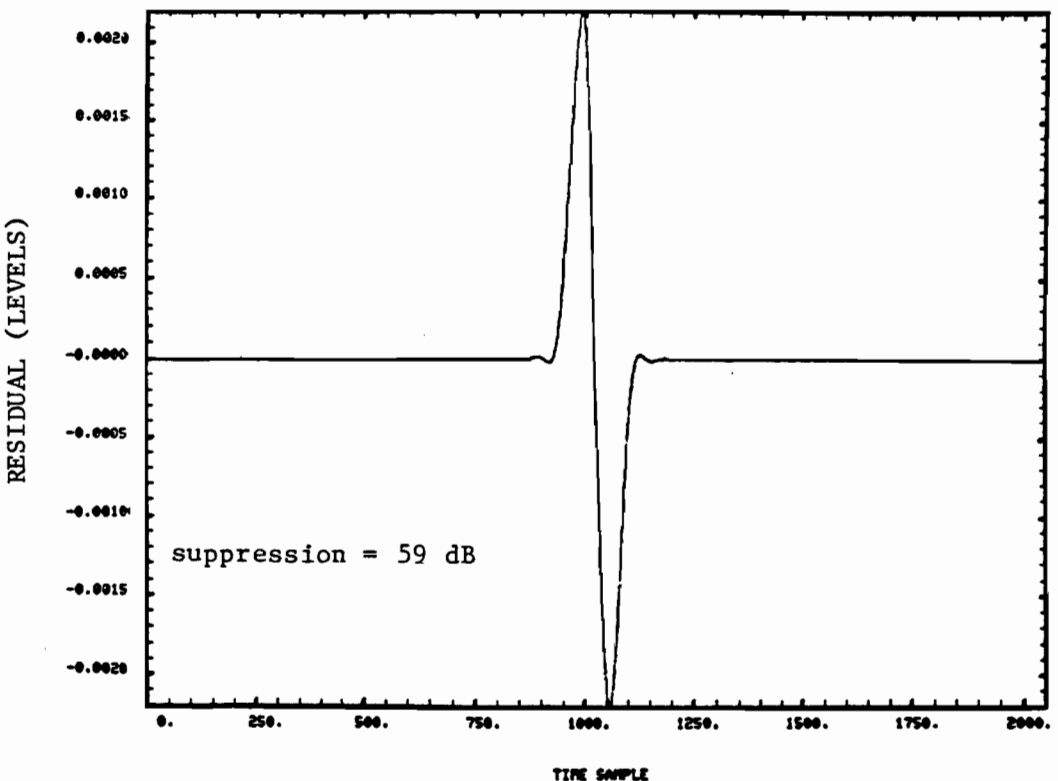


Fig. 7-26. IIR filter #2 suppression for clutter model A.



(a) 1° Beamwidth at 1.6 rpm.



(b) 1° Beamwidth at 3.2 rpm.

Fig. 7-27. IIR filter #2 suppression for clutter model B.

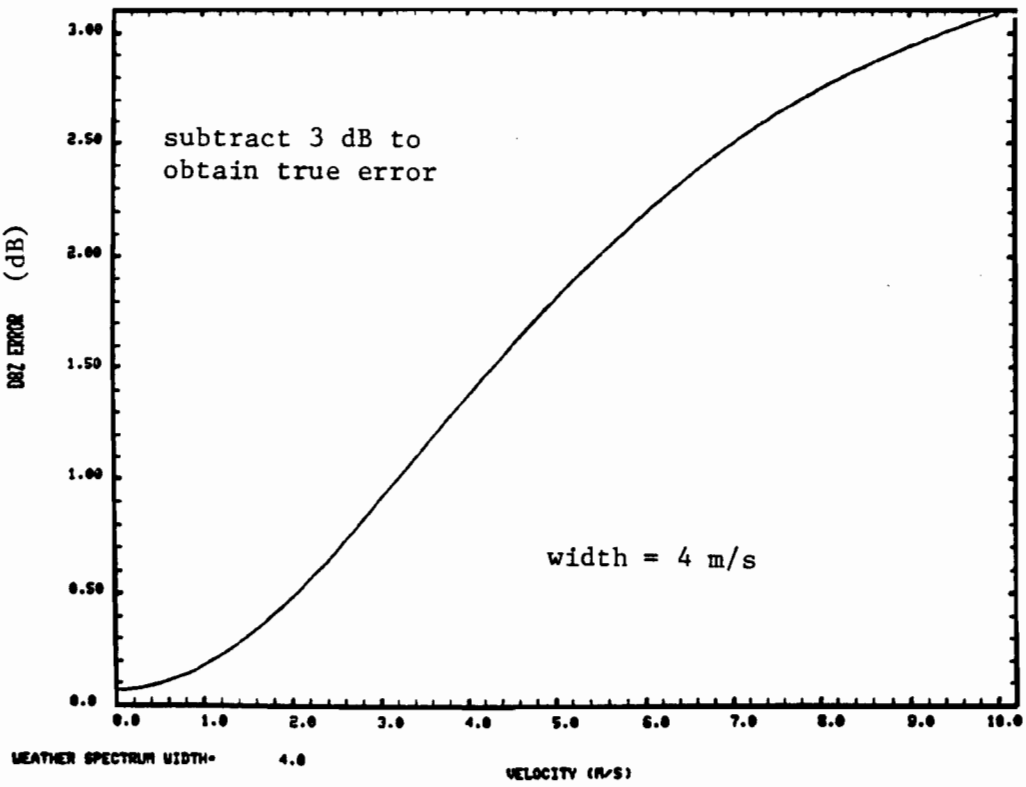
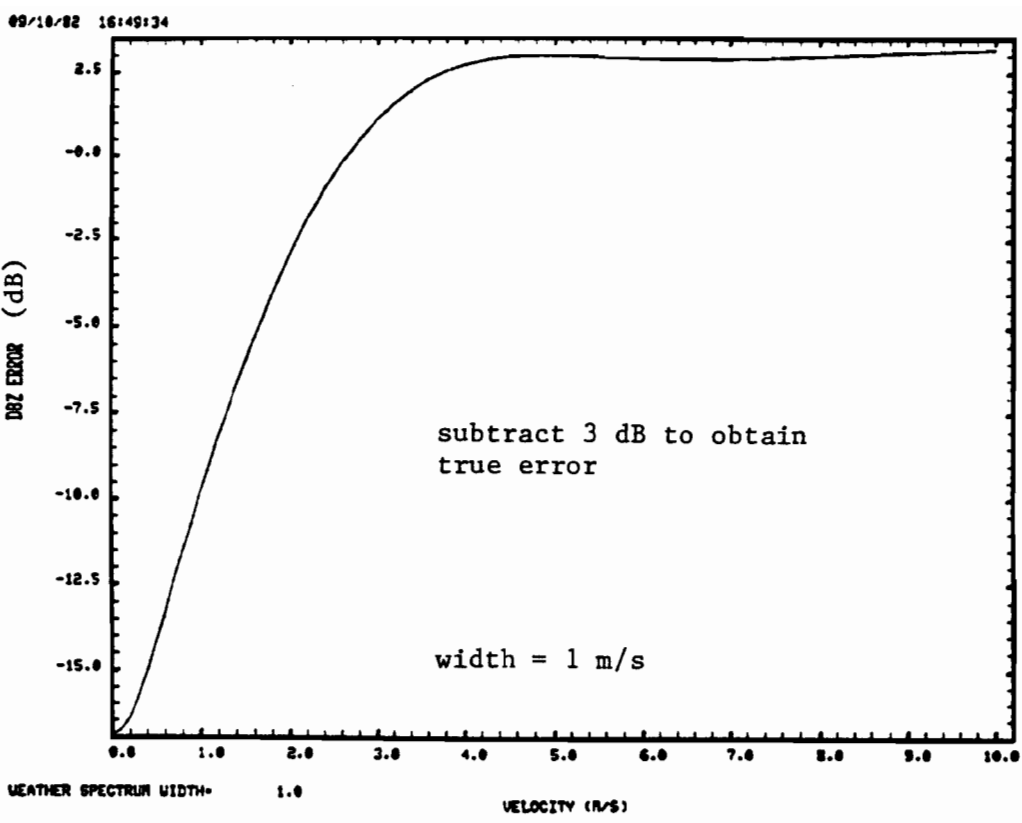


Fig. 7-28. Weather reflectivity errors for IIR filter #2.

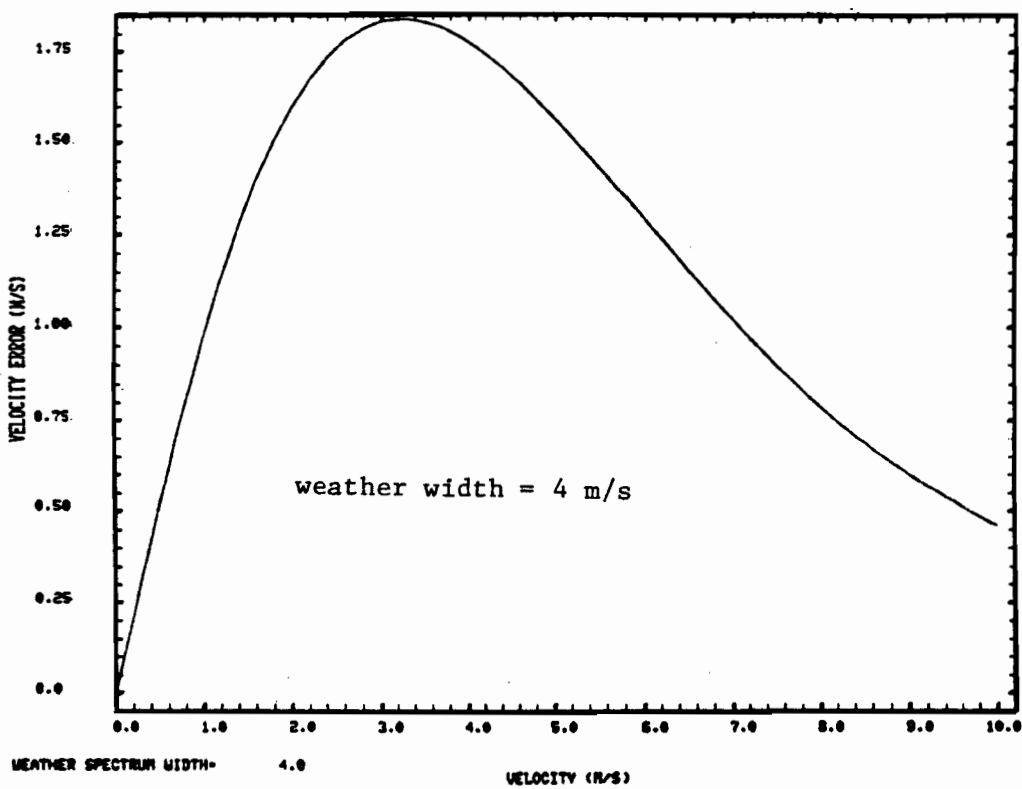
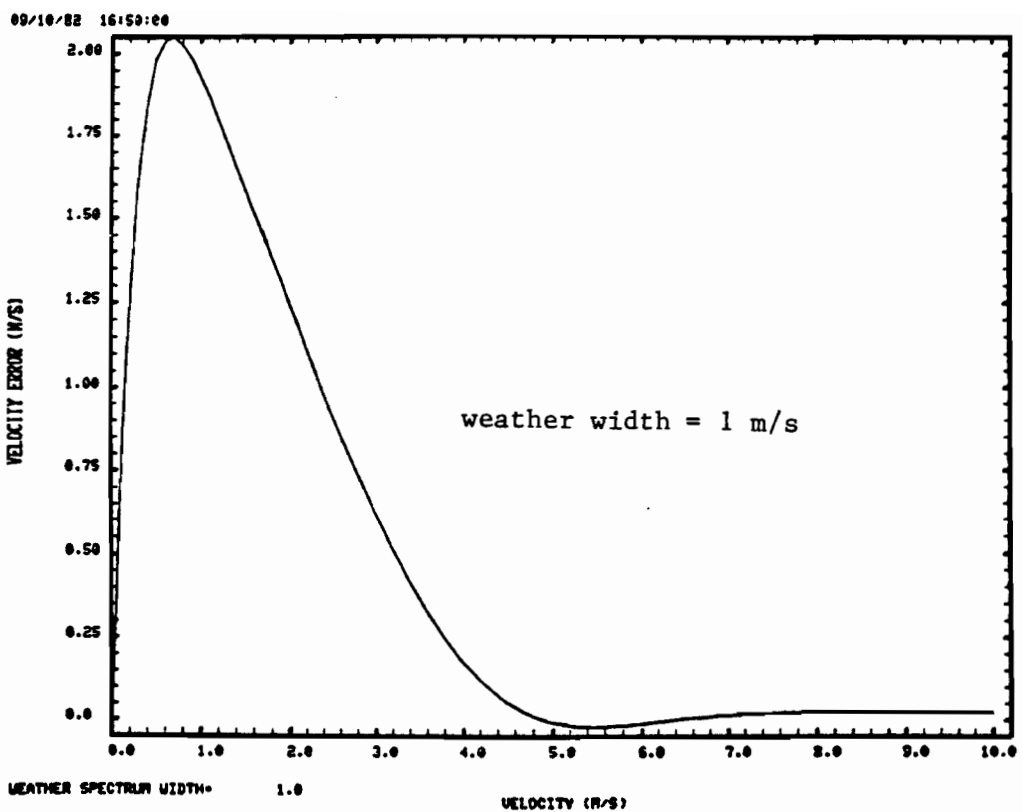


Fig. 7-29. Weather velocity errors for IIR filter #2.

09/18/82 16:50:28

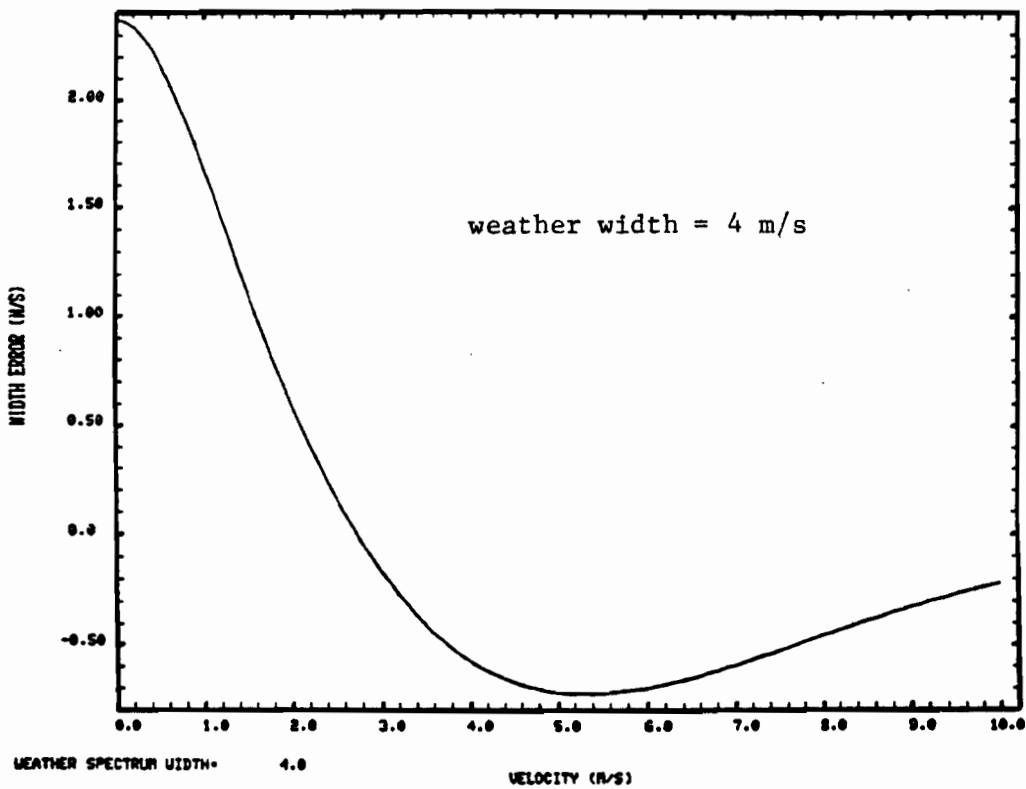
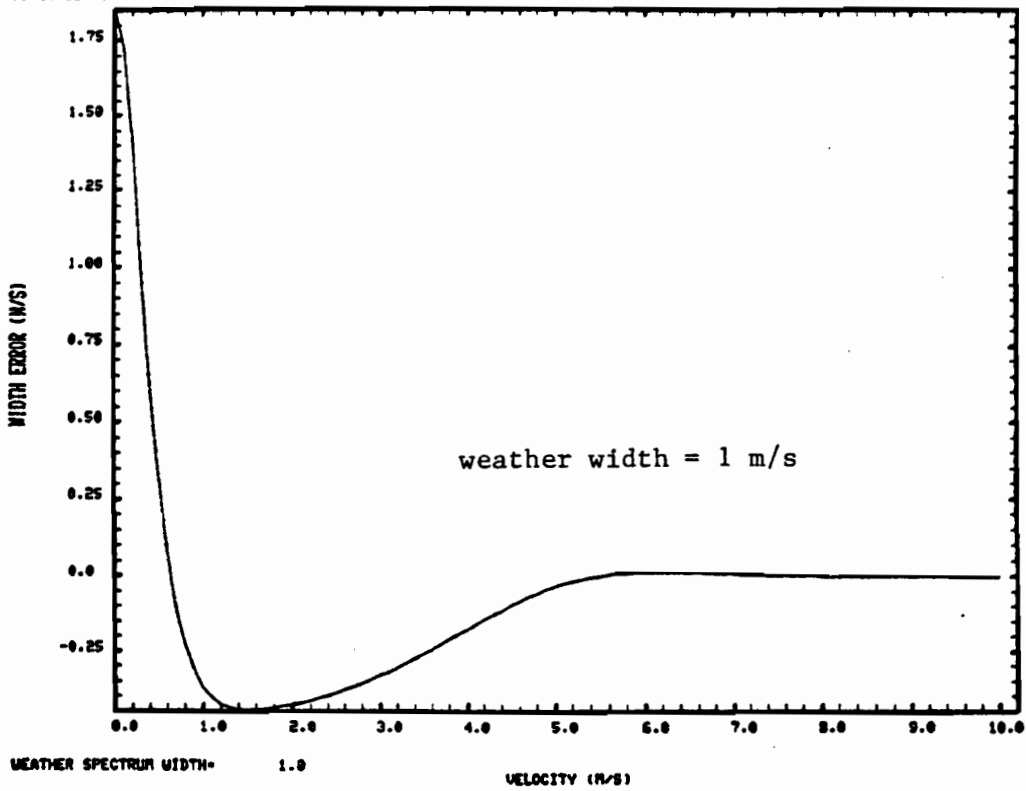


Fig. 7-30. Weather spectrum width error with IIR filter #2.

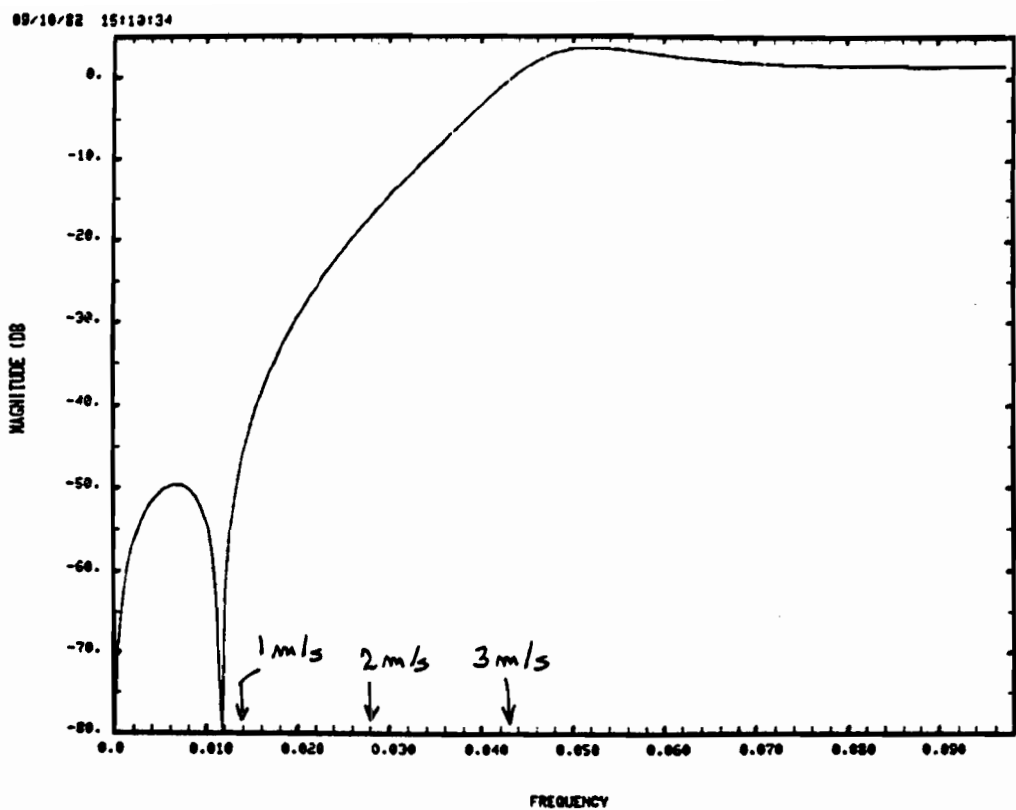


Fig. 7-31. Frequency response for IIR filter #3.

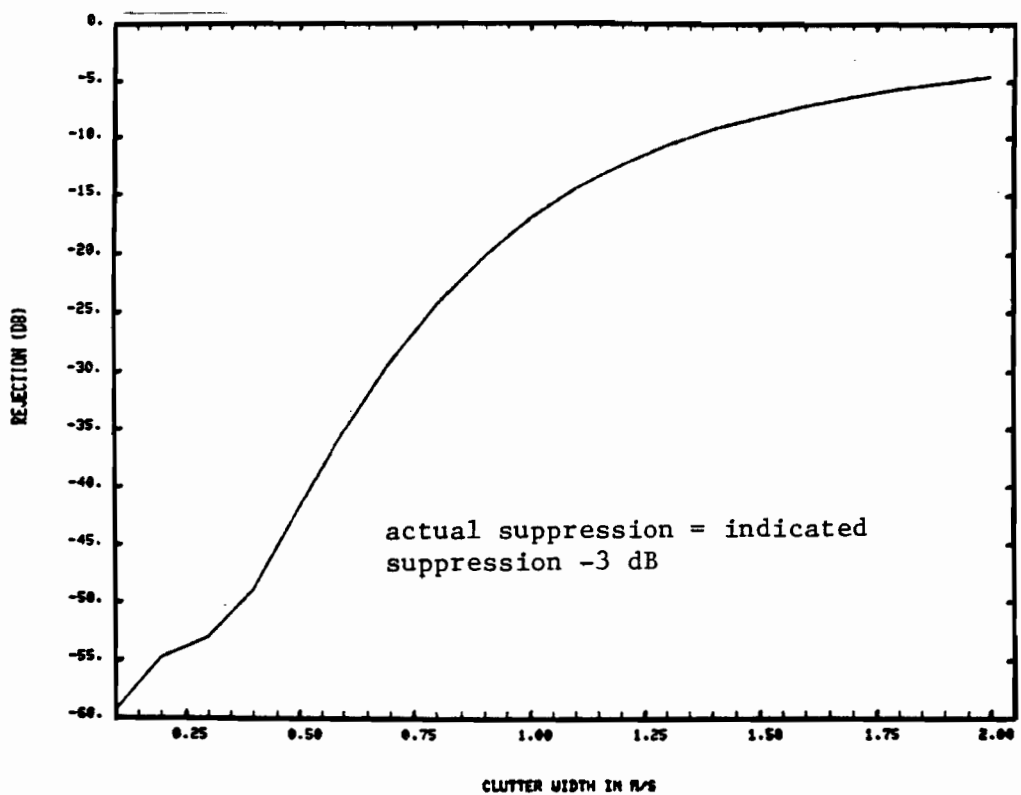
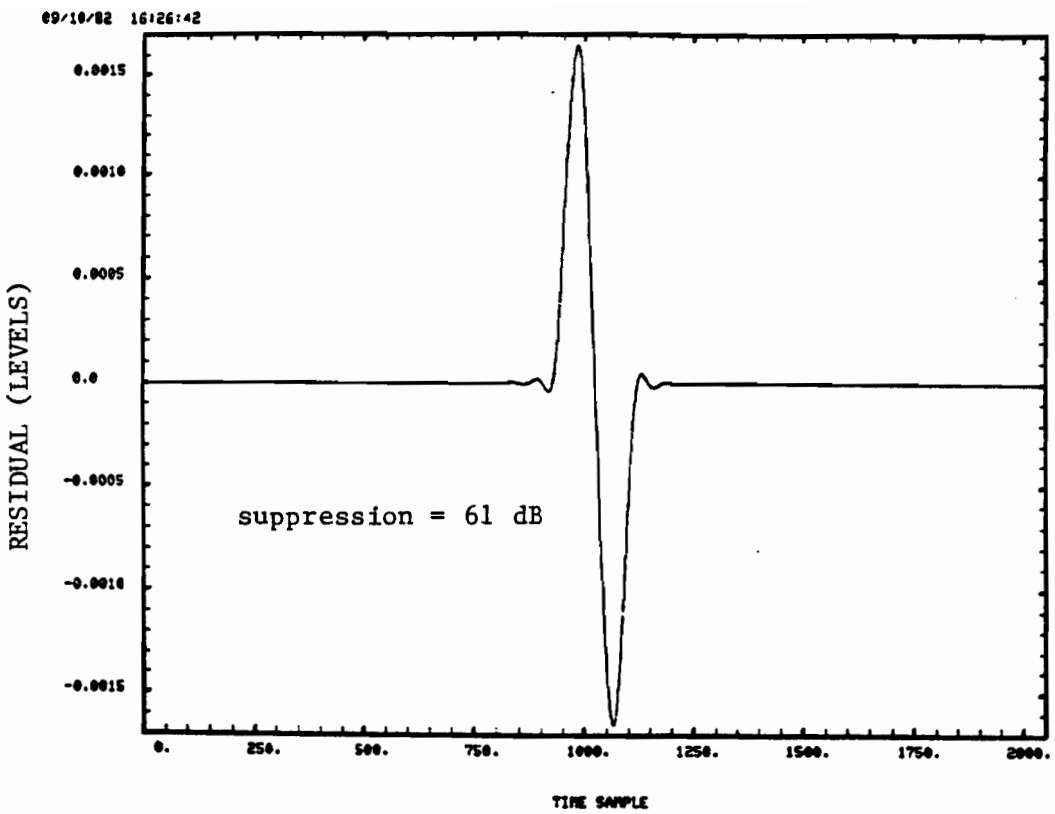
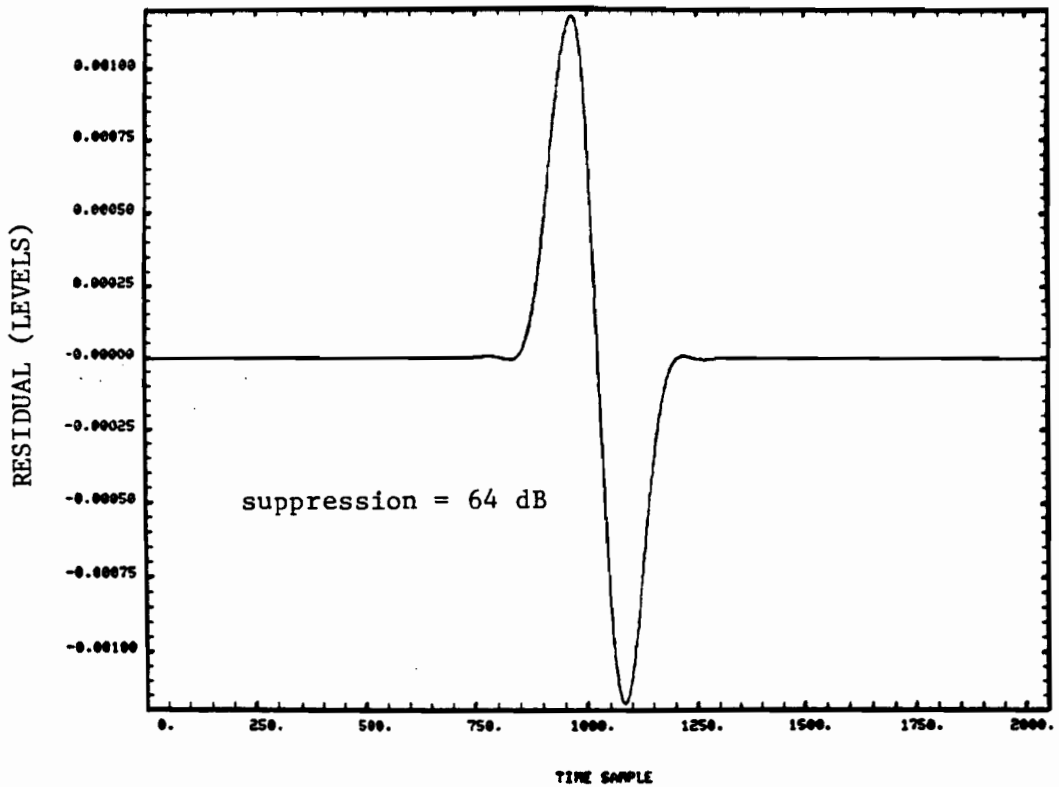


Fig. 7-32. IIR filter #3 suppression for clutter model A.



(a) 1° Beamwidth at 3.2 rpm.



(b) Beamwidth at 1.6 rpm.

Fig. 7-33. IIR filter #3 suppression for clutter model B.

09/10/82 16:18:55

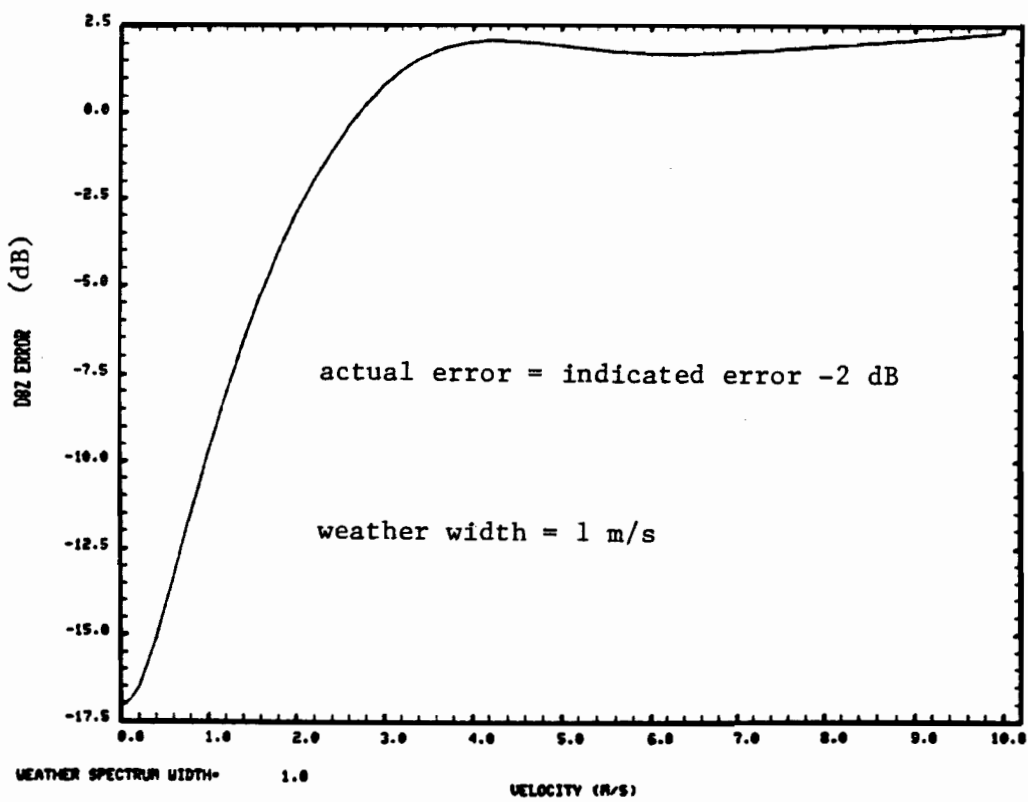
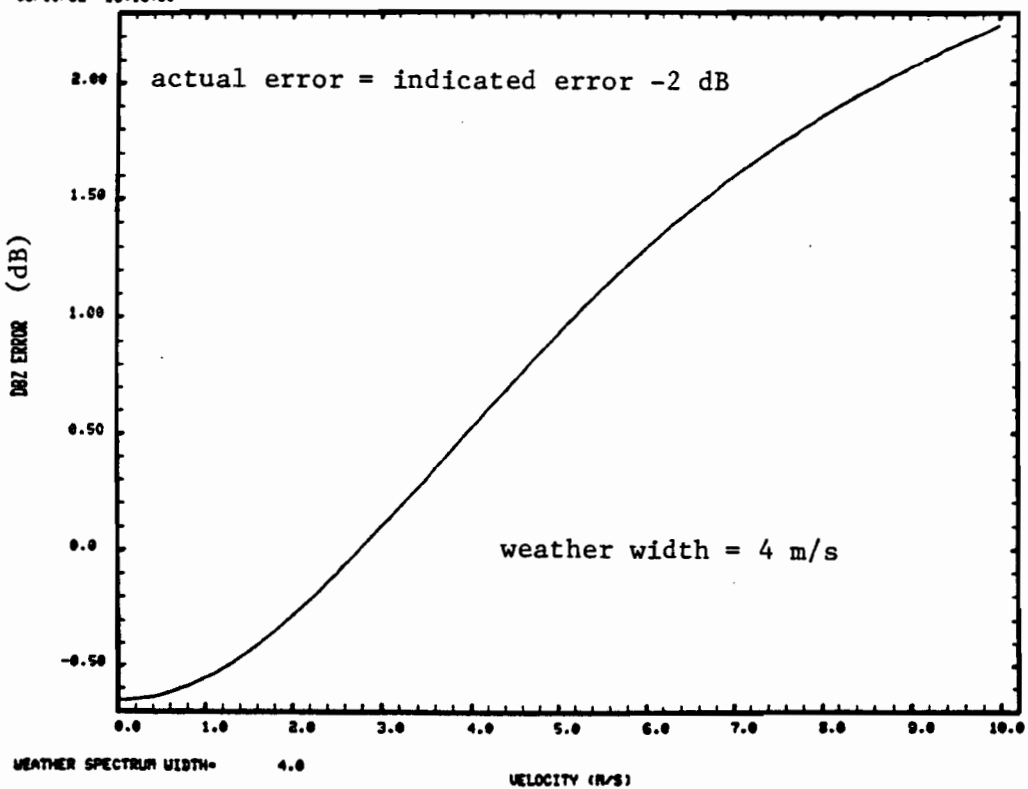


Fig. 7-34. Reflectivity error with IIR filter #3.

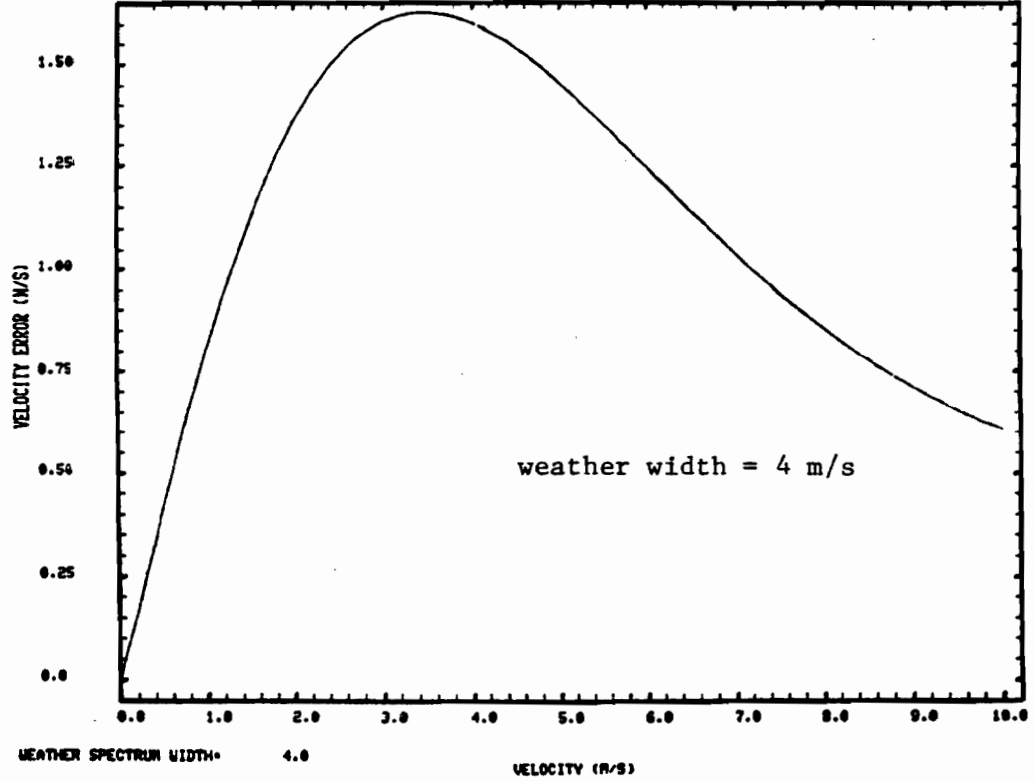
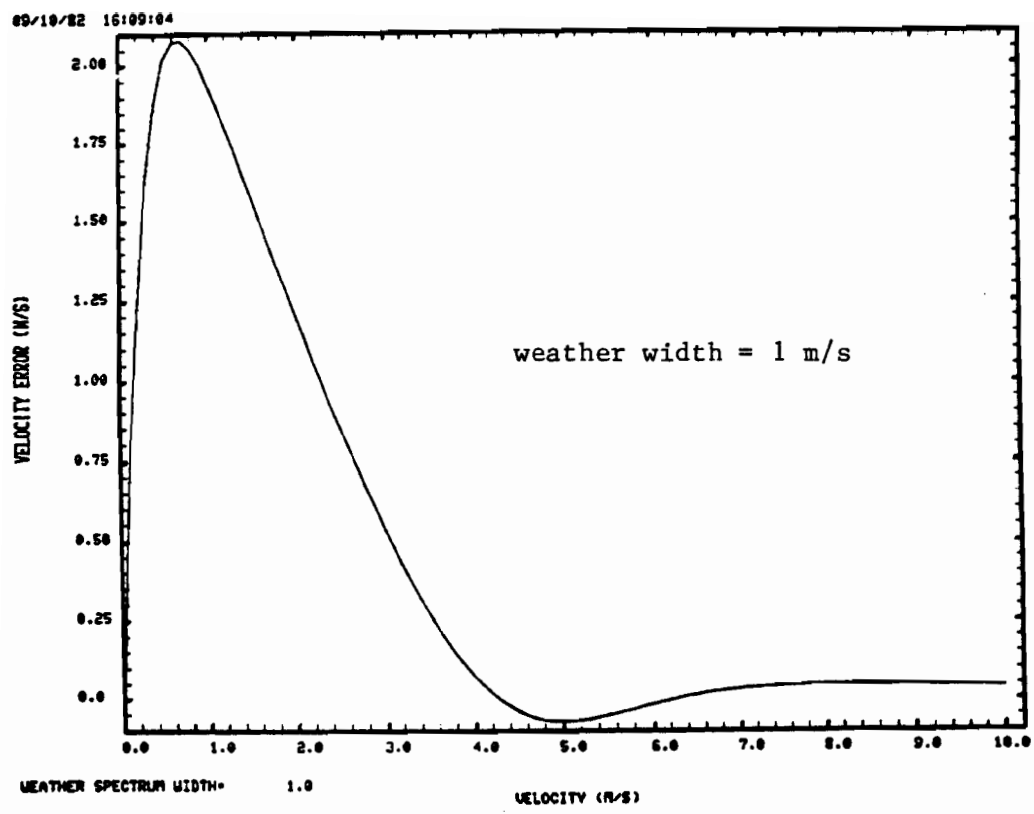


Fig. 7-35. Weather mean velocity error with IIR filter #3.

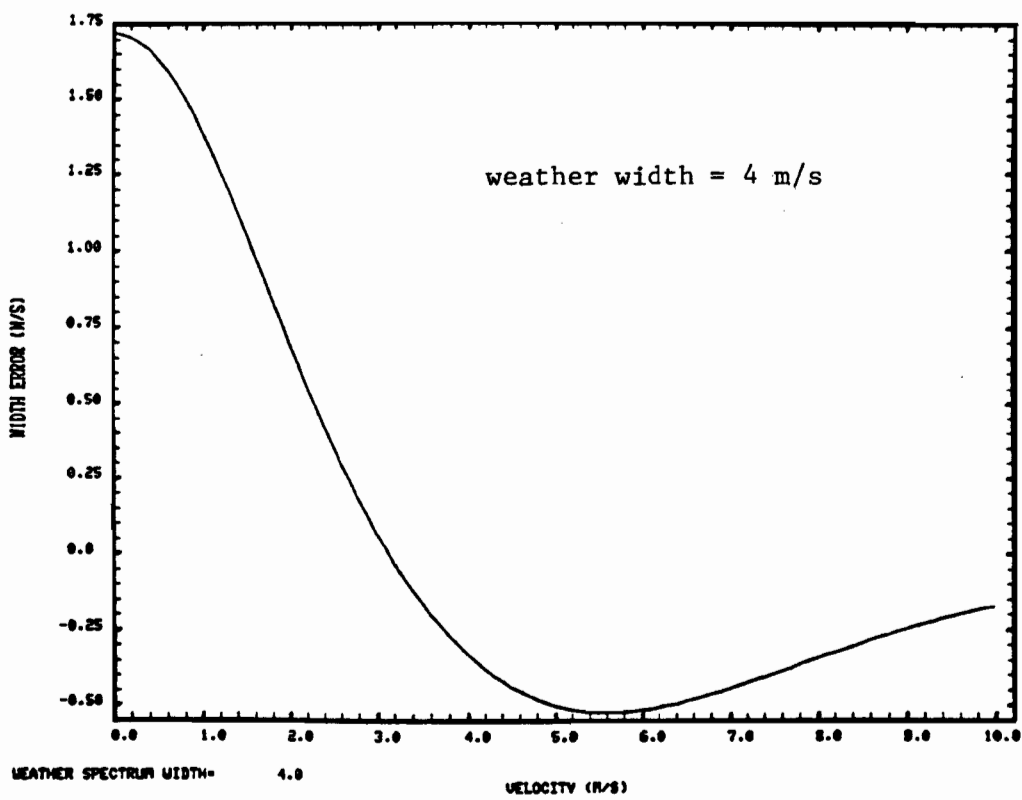
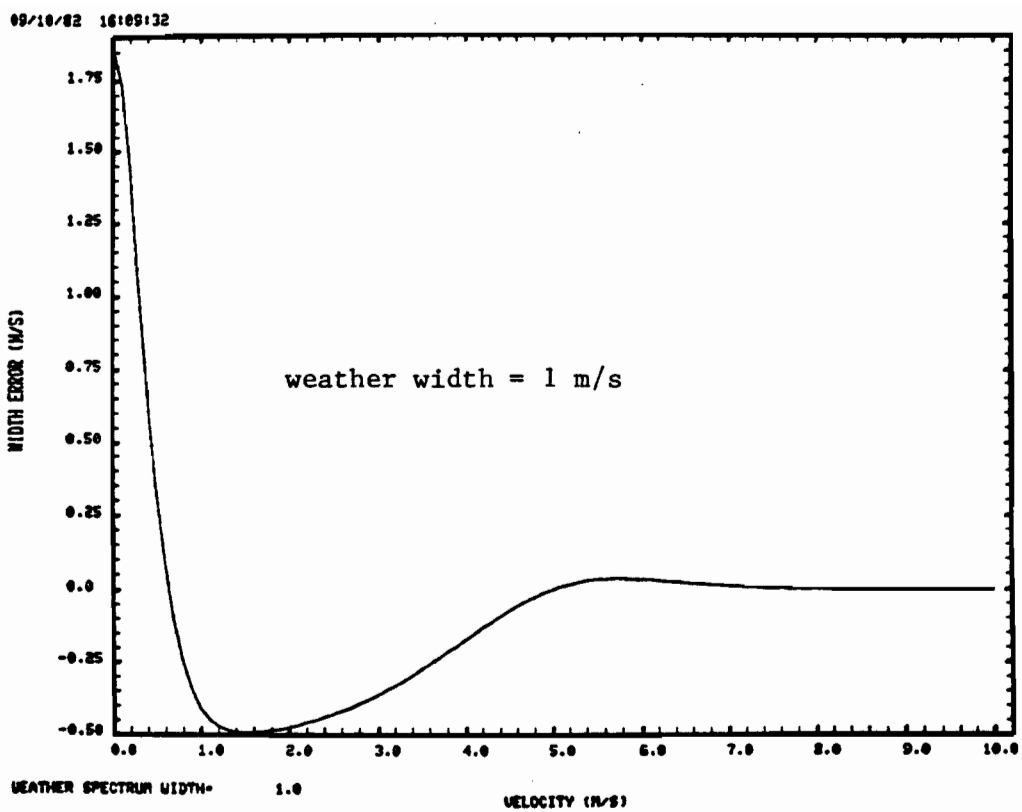


Fig. 7-36. Weather spectrum width error with IIR filter #3.

horizontal and vertical scales identical for both plots

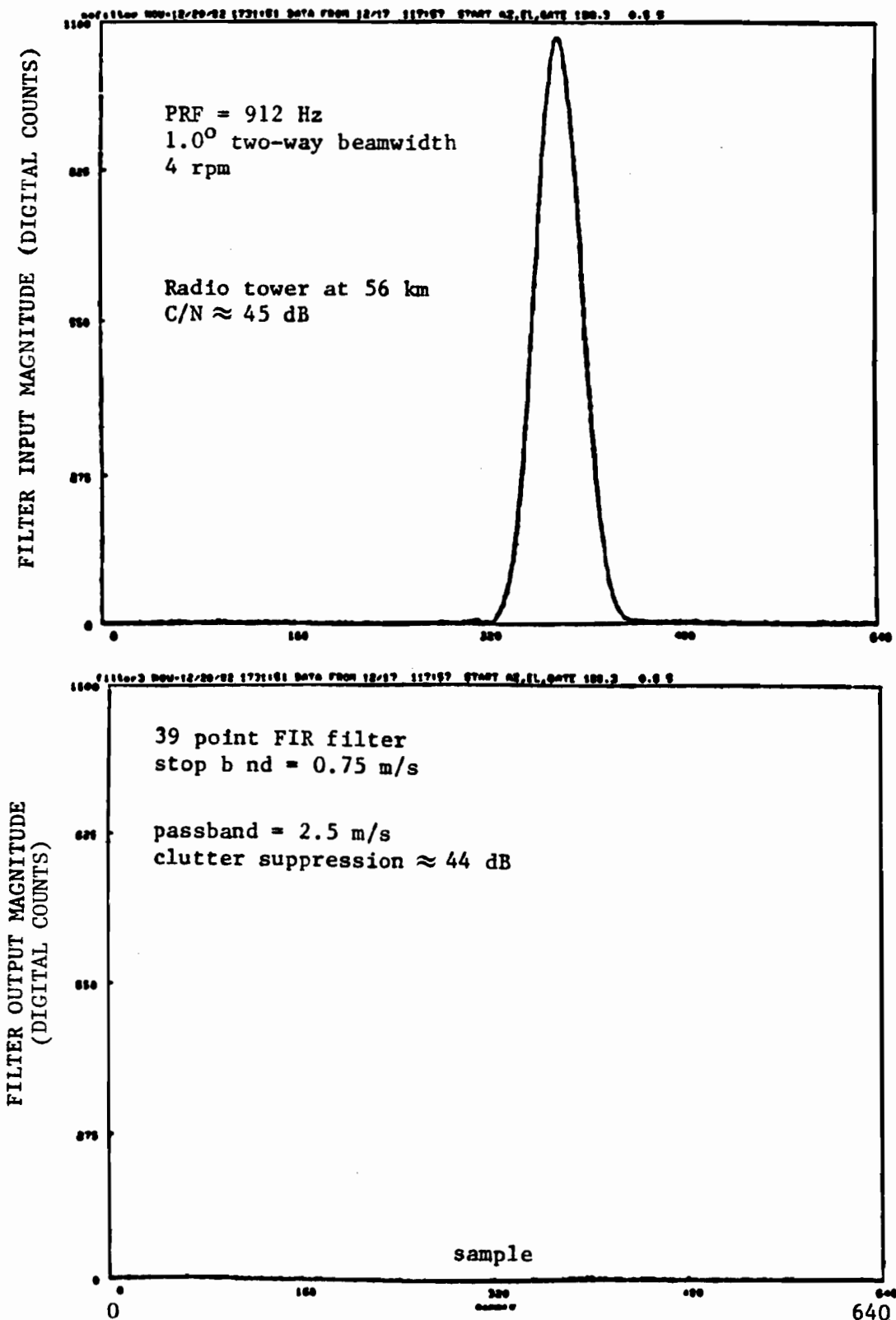


Fig. 7-37a. MIT Point Clutter Suppression by 2.5 m/s Stopband FIR Filter.

horizontal and vertical scales same for both plots

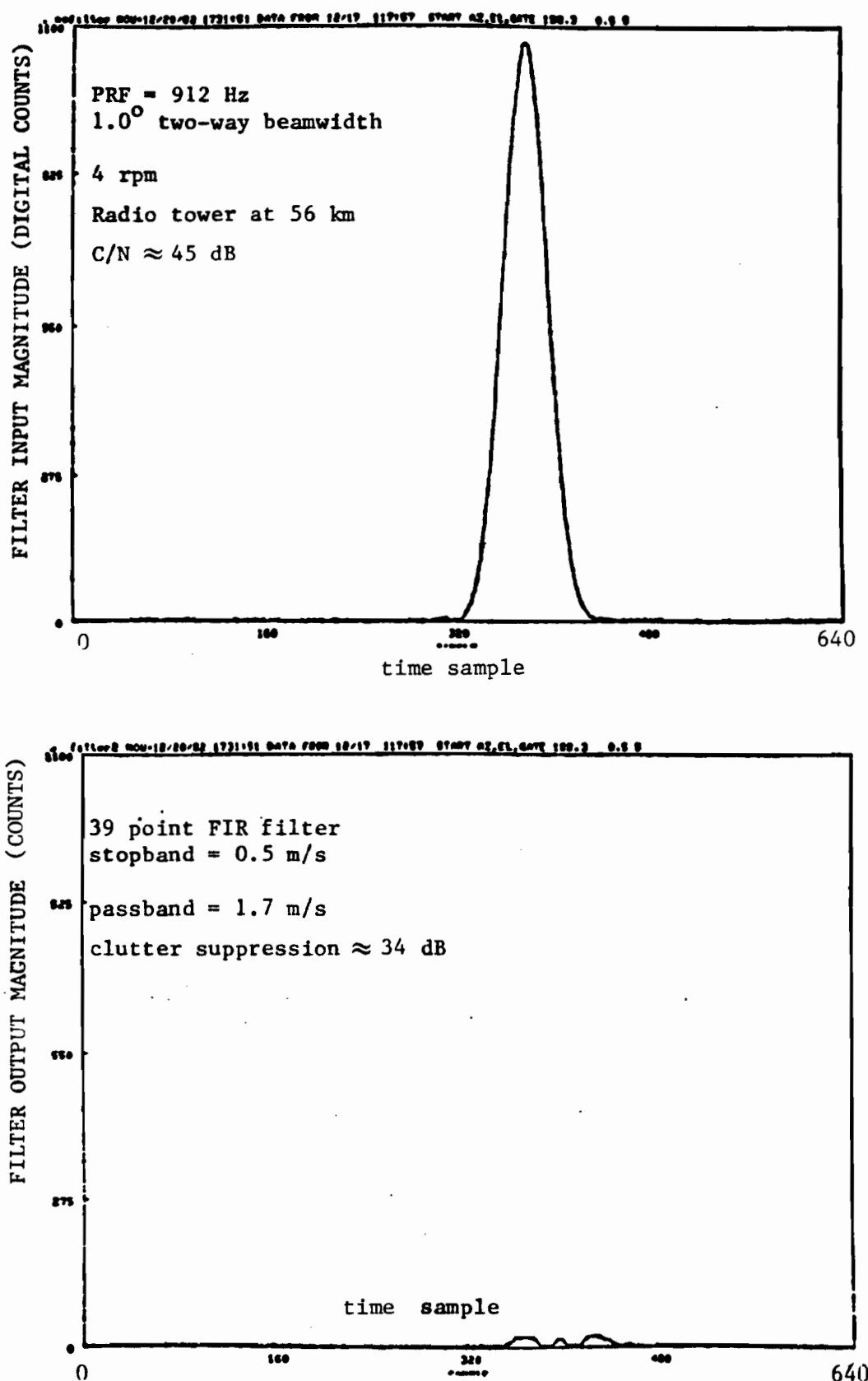
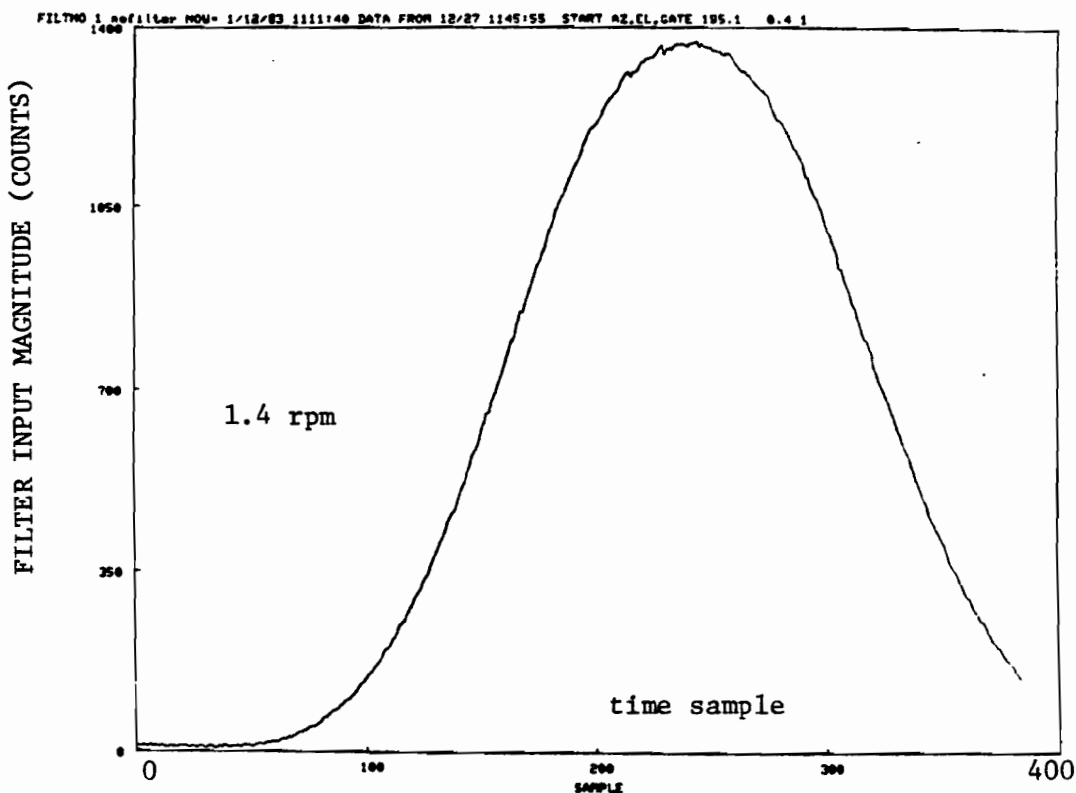
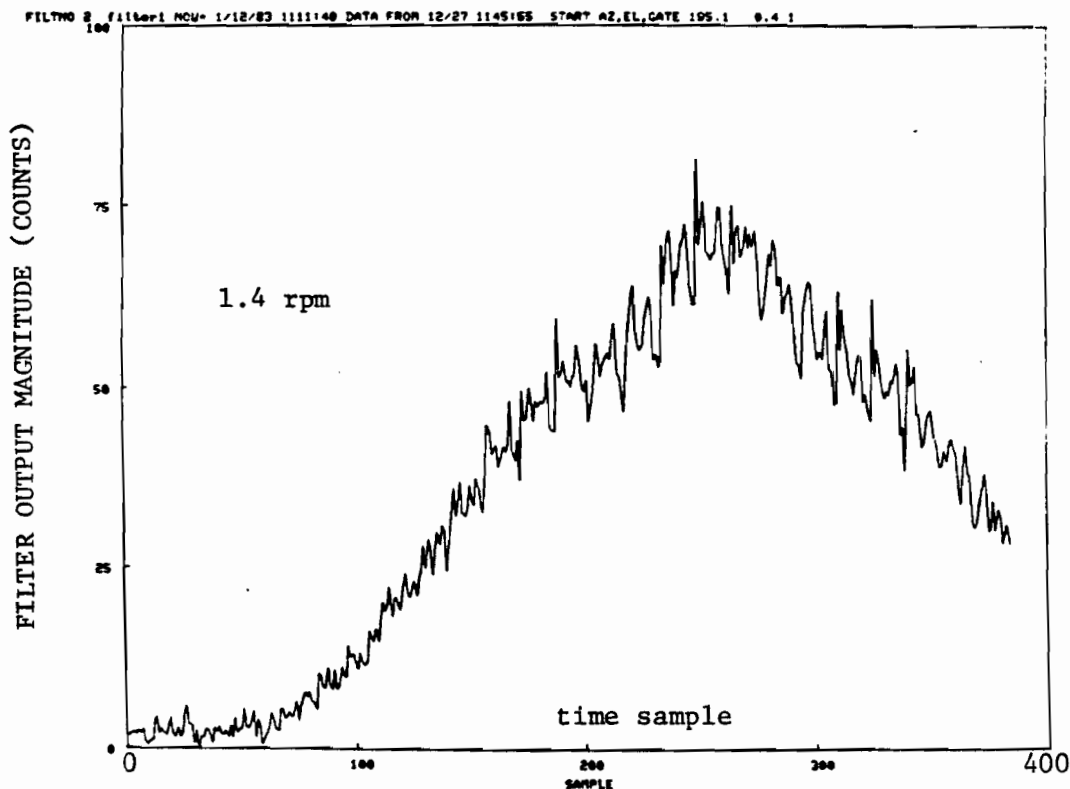


Fig. 7-37b. MIT Point Clutter Suppression by 1.7 m/s Stopband FIR Filter.

VERTICAL SCALE NOT SAME FOR BOTH PLOTS

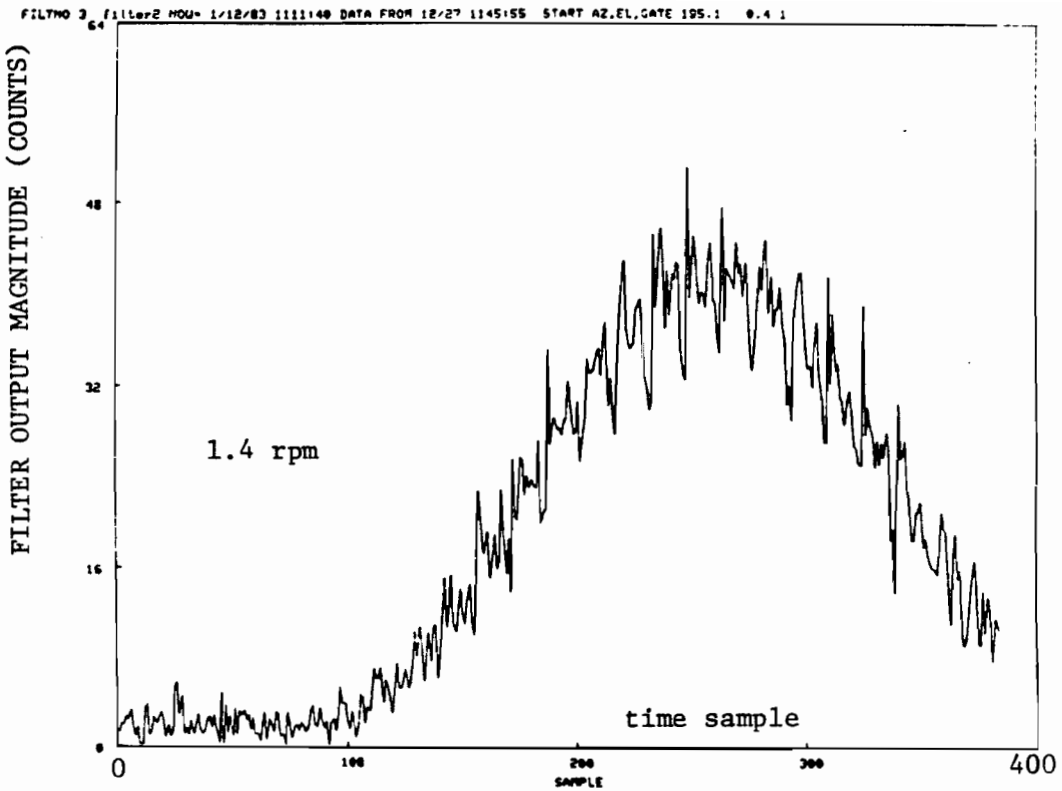


(a) Clutter Waveform

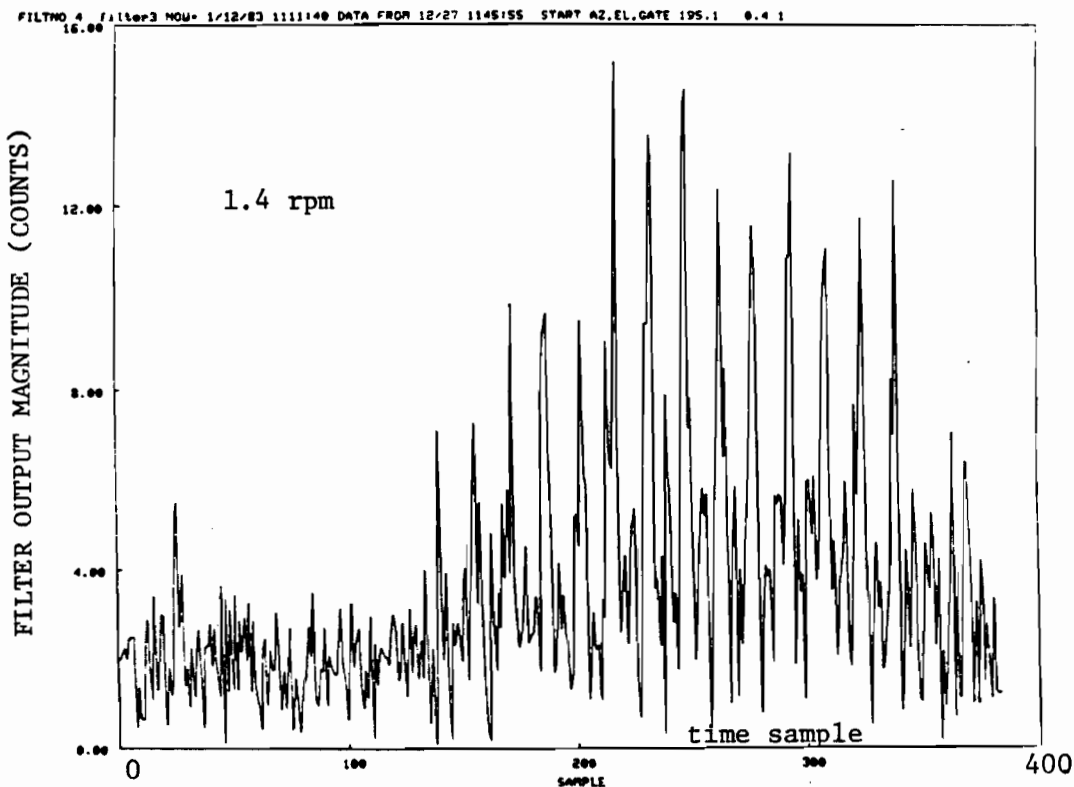


(b) Output of 1 m/s Stopband Filter

Fig. 7-38. Example of Suppression of Radio Tower Clutter from MIT Radar.



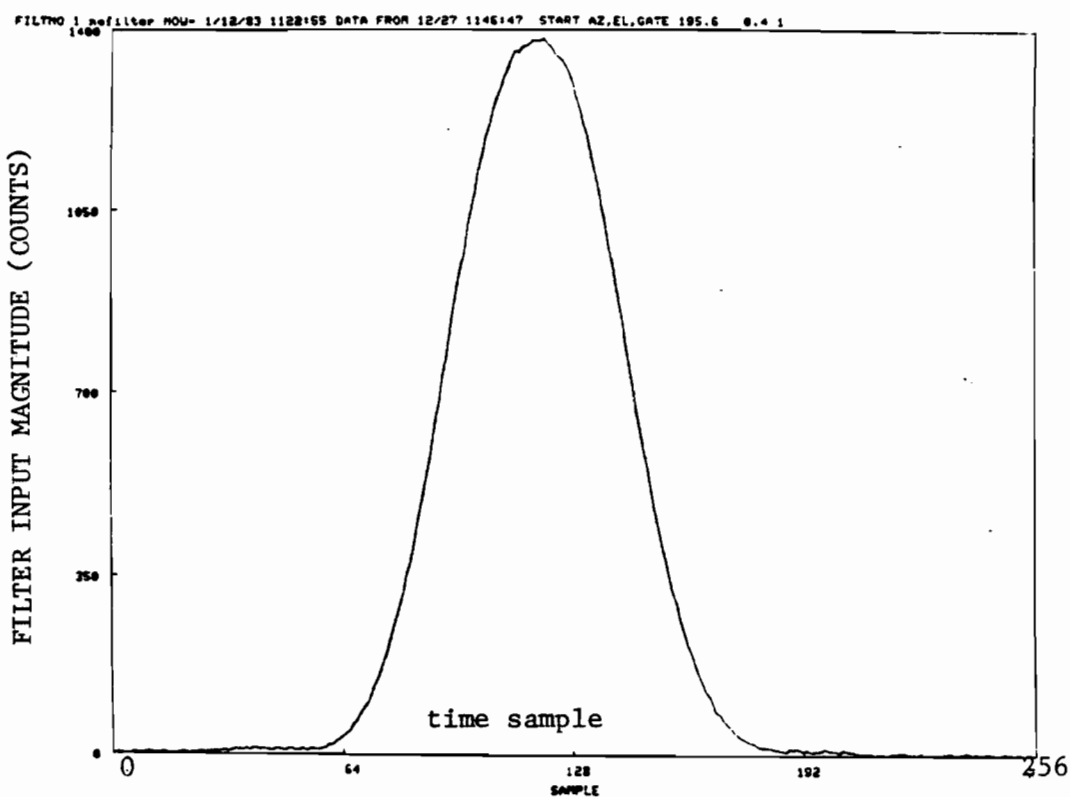
(c) Output of 2 m/s Stopband Filter



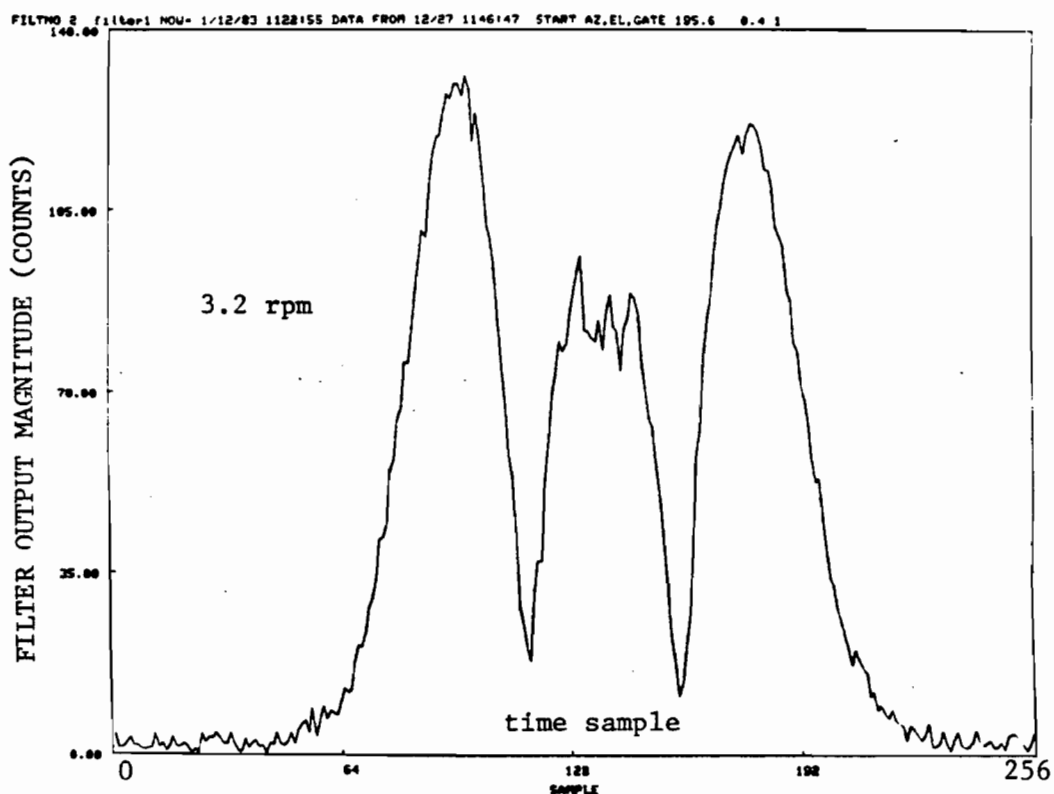
(d) Output of 3 m/s Stopband Filter

Fig. 7-38. Example of Suppression of Radio Tower Clutter from MIT Radar (Cont).

VERTICAL SCALE NOT SAME FOR BOTH PLOTS

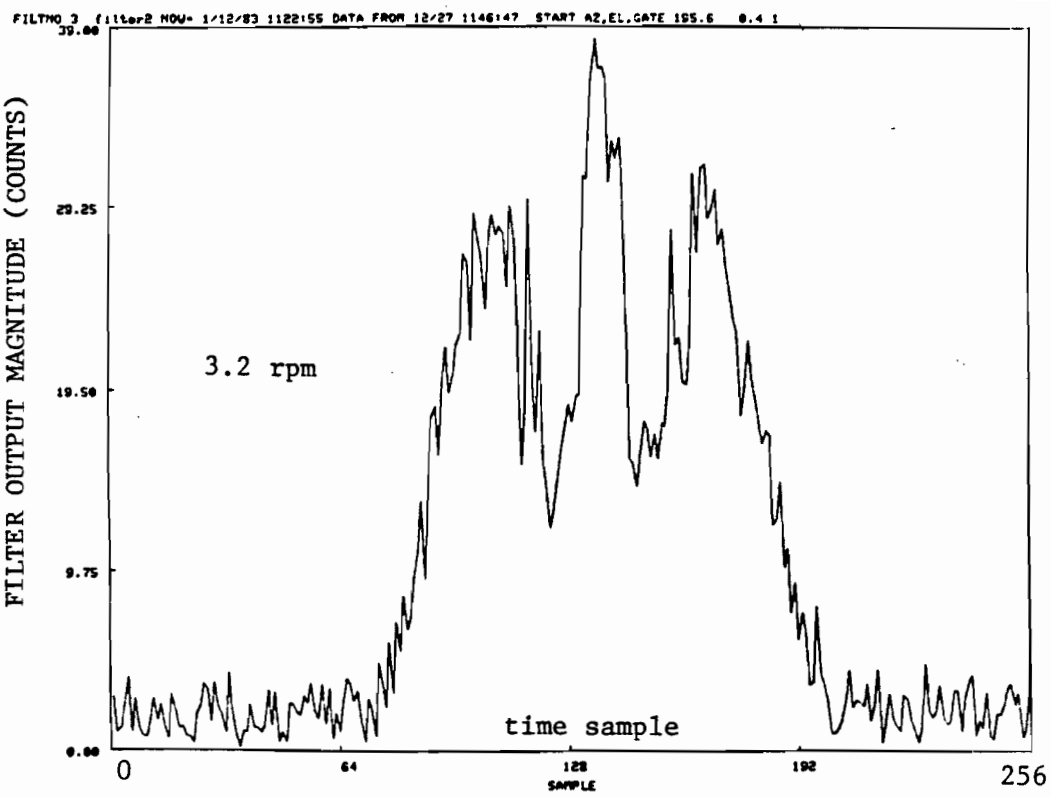


(a) Clutter Waveform

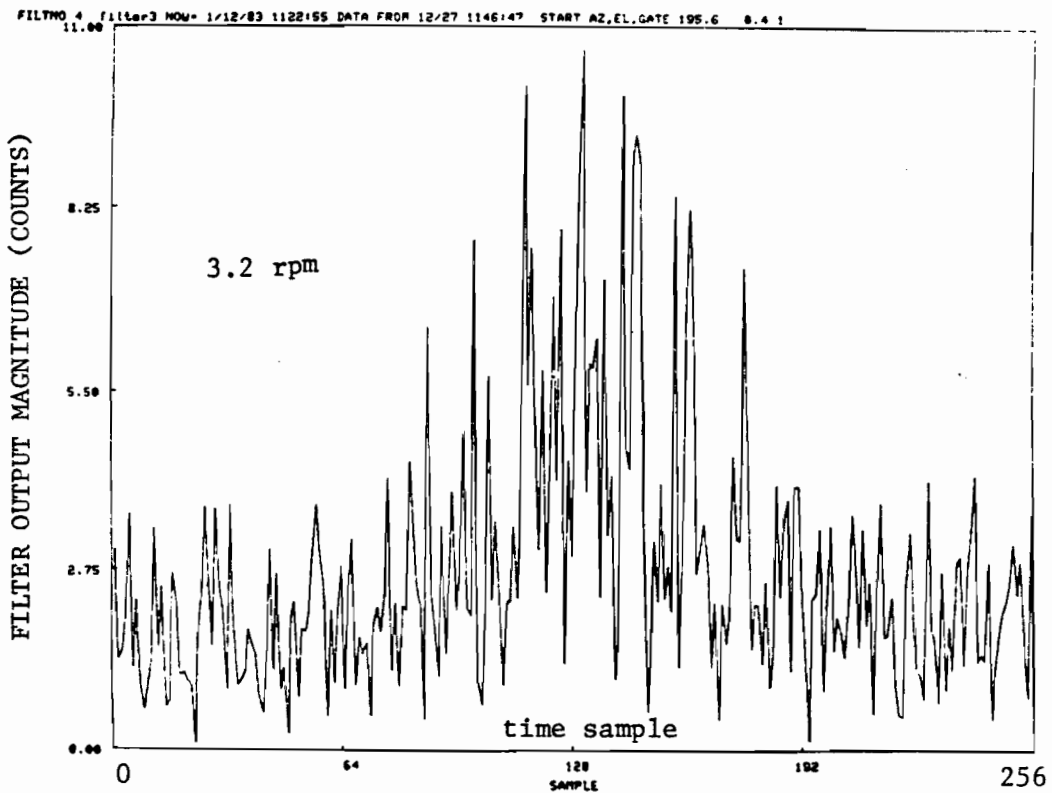


(b) Output of 1 m/s Stopband Filter

Fig. 7-39. Example of Suppression of Radio Tower Clutter from MIT Radar.



(c) Output of 2 m/s Stopband Filter



(d) Output of 3 m/s Stopband Filter

Fig. 7-39. Example of Suppression of Radio Tower Clutter from MIT Radar (Cont.)

TABLE 7-2. SUMMARY RESULTS ON SUPPRESSION OF DISCRETE SCATTERER CLUTTER WITH MIT S-BAND WEATHER RADAR.

Date	Time	Scan Rate (rpm)	90% Quantile Pair Reduction (dB)		
			Filter 1	Filter 2	Filter 3
12/27/82	1145:55	1.4	26.3	30.4	46.7
	1146:47	4.2	20.5	32.7	47.7
12/29/82	1021:11	4.2	20.0	33.2	44.0
	1021:42	1.4	26.3	30.4	43.1
	1056:26	1.4	26.3	30.4	44.0
	1056:46	4.2	20.4	33.6	44.9
1/3/83	1111:03	1.4	20.8	33.5	46.2
	1111:29	4.2	26.4	30.4	45.0

Weather and Terrain Cover:

12/27/82	clear, calm	bare ground
12/29/82	hazy, 17 knot wind	bare ground
1/3/83	clear, 1 knot wind	bare ground

<u>Filter #</u>	<u>Passband (m/s)</u>
1	1
2	2
3	3

statistics on the data sets. We see that the suppression with FIR filter #3 is close to the 45 dB level predicted by the instability residue results in Chapter VI. Examination of the filter #3 residue (Figs. 7-38 and 7-39) shows that much of the residue has a period of 16 ms (= 1/60 Hz).

Despite the stability limitations of the MIT radar, we see that the quality assurance test for clutter model B (paragraph #4 of Table 6-1) was fully met by filters 1 and 2. Filter #3 met the quality assurance test objective on the low wind days, but fails some 1 dB short on the windy day. As noted earlier, this failure to achieve suppression greater than 45 dB on the radio tower signal is primarily due to the instability residue of the radar.

Tables 7-3 to 7-5 show examples of the input-output statistics from filtering full "rings" of MIT clutter data at ranges of approximately 4, 9 and 15 km, respectively. The median 90% quantile values are viewed as most representative of the clutter suppression capability since the recording system may effectively saturate on the highest level clutter* and, suppression on low level clutter is biased downward by receiver noise effects. Figure 7-40 compares the suppression achieved with the three principal Doppler filters as a function of range for several different days. We see that the filter 3 clutter suppression for this data is substantially (e.g., 8-10 dB) lower than that for the discrete scatterer signal, but that the other two filters achieve suppressions fairly close to the discrete scatterer results and the specified capability in Table 4-1. The decrease in suppression at the longest range for all filters is principally due to the lower input clutter to noise level at that range.†

Tables 7-6 to 7-9 show the results of pulse pair estimation of the MIT site clutter velocity parameters on a day with light winds. We see that a substantial fraction of the clutter at this site is moving at a high mean velocity or has a much larger spectrum width than would be expected for a day with light winds. We believe that the motor vehicles are a major cause of this moving clutter. Since this clutter is little affected by the clutter suppression filters, the result is that the spatially averaged clutter suppression is lower than would have been the case with clutter from fixed scatterers.

*12-bit A/D converters were used with a R^{-2} STC law which results in 1 quantization level corresponding to a reflectivity level of +10 dBz for the ranges shown here. The IF amplifiers smoothly limit at the upper range (see Appendix A) so the A/D converter does not saturate and to preserve mean velocity information.

†Since the filter output power is lower limited by the front-end noise power, the apparent clutter suppression of input power/output power will be biased downward whenever the residual clutter power is \leq the front-end noise power.

TABLE 7-3. FILTER STATISTICS FOR RANGE RINGS CORRESPONDING
TO FIG. 7-41.

OUTPUT FROM CLUTTER FILTER PROGRAM = TSCLT

MISSION DATE = 1/ 3/83 FILE = 15 STARTING RECORD = 1 STARTING AZ. = 358°
EL = 0.6 START TIME = 11:35:51 RGS = 0.228 NO. OF SAMPLES = 13530

FILTER 1 = NULL

RANGE GATE	MEAN(DB)	MEDIAN(DB)	90 % QUANTILE(DB)
1	49.3	19.1	47.2
2	45.5	15.9	45.4
3	46.3	14.5	43.6
4	43.1	15.0	38.6
5	45.5	13.6	38.1
6	46.0	14.5	34.9

FILTER 2 = 1 M/S 929 NPTS = 39 STOPBAND = 0.326 PASSBAND EDGE = 0.978
WTS = 3.00 1.00

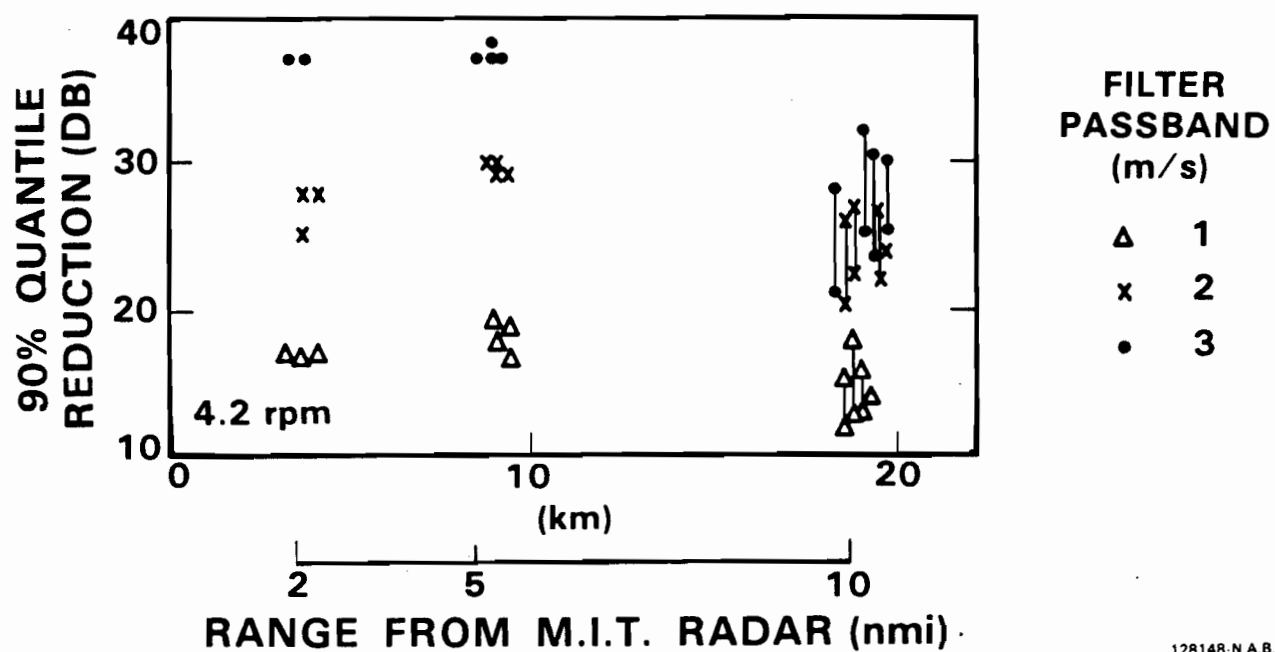
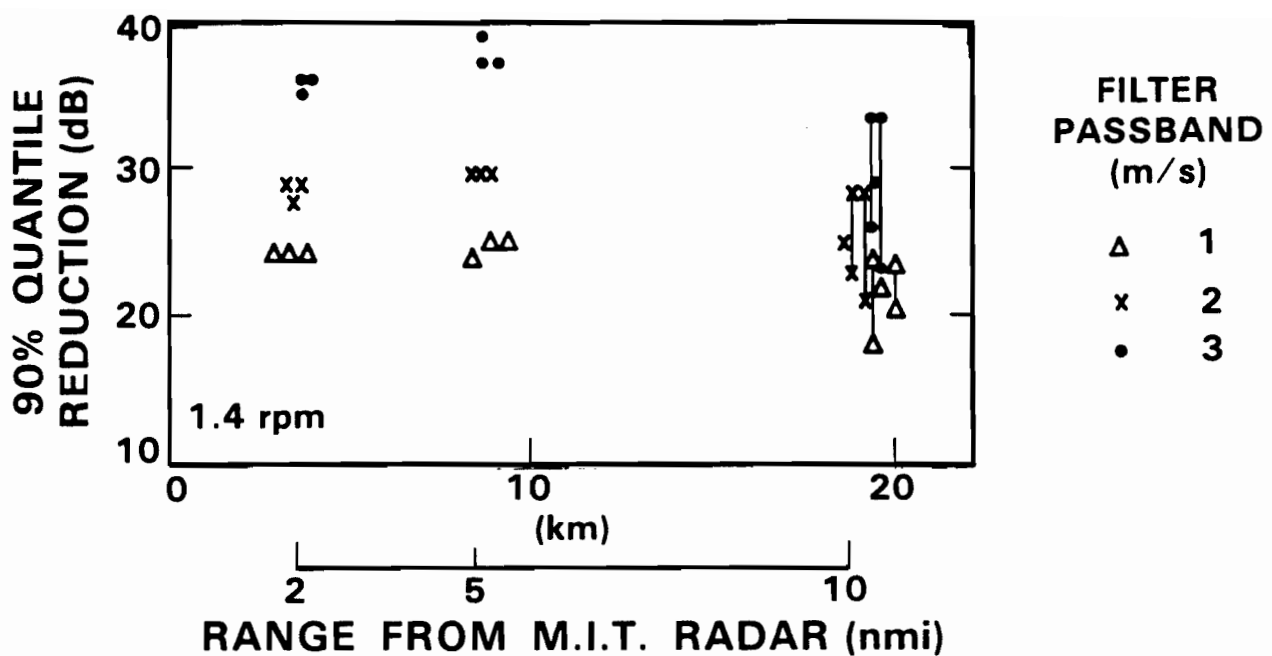
RANGE GATE	MEAN(DB)	MEDIAN(DB)	90 % QUANTILE(DB)
1	32.9	9.5	32.2
2	28.7	8.6	30.0
3	29.9	7.7	30.9
4	27.0	7.3	25.0
5	25.9	6.3	25.0
6	27.1	7.3	23.1

FILTER 3 = 2 M/S 929 NPTS = 39 STOPBAND = 0.652 PASSBAND EDGE = 1.956
WTS = 5.00 1.00

RANGE GATE	MEAN(DB)	MEDIAN(DB)	90 % QUANTILE(DB)
1	27.9	5.9	20.9
2	18.5	5.9	20.4
3	19.0	5.4	19.1
4	24.4	5.0	15.4
5	16.3	4.5	14.1
6	18.2	5.0	15.4

FILTER 4 = 3 M/S 929 NPTS = 39 STOPBAND = 0.978 PASSBAND EDGE = 2.934
WTS = 40.00 1.00

RANGE GATE	MEAN(DB)	MEDIAN(DB)	90 % QUANTILE(DB)
1	28.2	5.0	16.3
2	15.2	5.0	16.8
3	13.9	4.5	15.4
4	22.9	4.1	13.2
5	10.9	4.1	11.3
6	14.7	4.5	12.7



128148-N.A.B.C

Fig. 7-40. Measured clutter suppression in 1.5-nmi rings at MIT site.

Table 7-6. DISTRIBUTION OF M.I.T. CLUTTER' SPECTRUM WIDTHS
AT VERY CLOSE RANGE

REFLECTIVITY (dBz)	PERCENTAGE WITH SPECTRUM WIDTH (m/s)					
	0-1	1-2	2-3	3-5	5-10	>10
<20	84.6	12.5	1.1	0.7	0.9	-
20-40	86.3	9.9	2.1	0.9	0.6	-
40-60	91.6	8.0	0.1	-	0.1	-
>60	98.7	1.2	-	-	-	-

RANGE < 5 nm

Table 7-7. DISTRIBUTION OF M.I.T. CLUTTER MEAN VELOCITIES
AT VERY CLOSE RANGE

REFLECTIVITY (dBz)	PERCENTAGE WITH MEAN VELOCITY (m/s)					
	0 - 1	1 - 2	2 - 3	3 - 5	5 - 10	>10
<20	97.4	1.5	-	-	-	0.2
20 - 40	97.4	1.1	0.7	0.4	0.4	-
40 - 60	99.3	0.2	0.1	-	-	0.2
>60	99.4	0.2	-	0.1	-	0.2

RANGE ≤ 5 nm

Table 7-8. DISTRIBUTION OF M.I.T. CLUTTER SPECTRAL WIDTHS
AT CLOSE RANGE

REFLECTIVITY (dBz)	PERCENTAGE WITH SPECTRUM WIDTH (m/s)					
	0 - 1	1 - 2	2 - 3	3 - 5	5 - 10	>10
<20	46.9	27.6	12.3	12.0	5.9	0.3
20 - 40	70.6	20.5	4.1	3.3	1.5	-
40 - 60	86.2	13.6	0.1	-	-	-
>60	94.5	-	-	-	-	-

5 nm < RANGE < 10 nm

Table 7-9. DISTRIBUTION OF M.I.T. CLUTTER MEAN VELOCITIES
AT CLOSE RANGE

REFLECTIVITY (dBz)	PERCENTAGE WITH MEAN VELOCITY (m/s)					
	0 - 1	1 - 2	2 - 3	3 - 5	5 - 10	>10
<20	70.0	11.6	6.1	5.6	4.9	1.7
20 - 40	91.4	2.2	2.1	1.9	1.5	0.8
40 - 60	99.7	0.1	0.1	-	-	-
>60	100.0	-	-	-	-	-

5 nmi < RANGE < 10 nmi

Further indication of this can be obtained by comparing the respective filter output envelopes with the input envelope for a portion of a given range ring. Figures 7-41 to 7-43 show several examples of these envelopes. Figure 7-41 is an example of clutter principally from large discrete scatterers in which the suppressions are typically within 5 dB of that for the radio towers. Figure 7-42 is an intermediate case in that good suppression is obtained against most of the clutter, but two azimuths have noticeably poorer suppression. Figure 7-43 shows more azimuths with poor suppression. These are characterized by scalloping in the input envelope which suggests that several moving scatterers are located at the cells with poor suppression.

2. NSSL Results

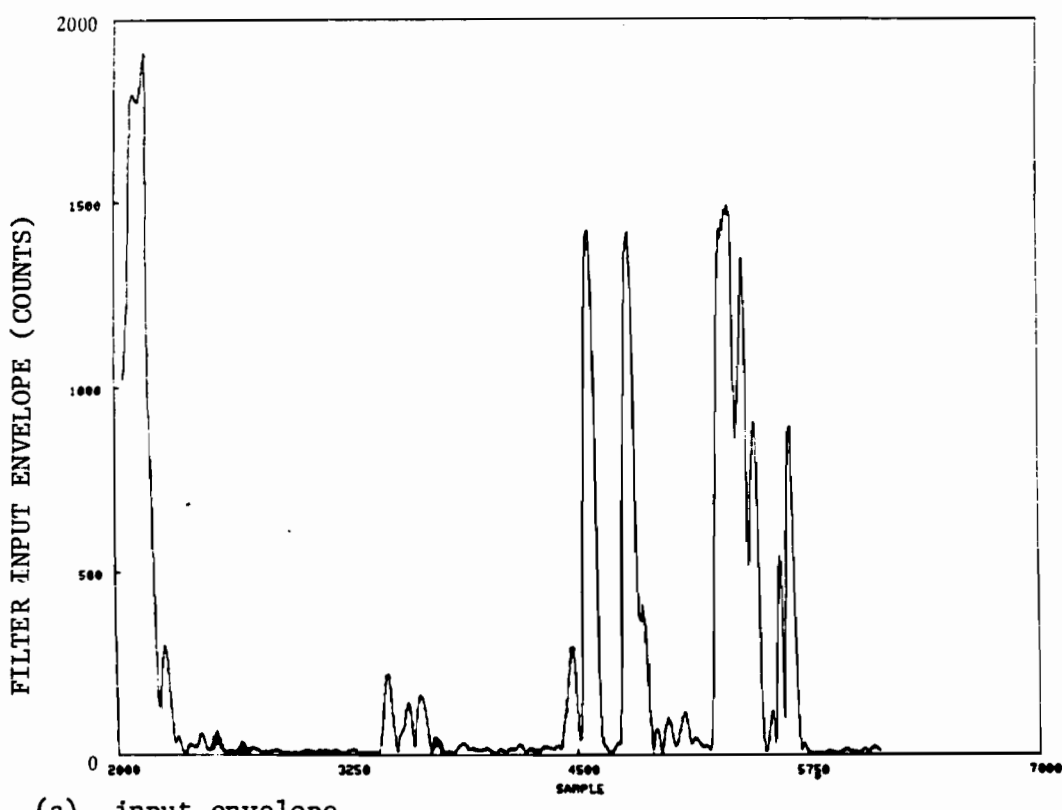
The NSSL data set consists of clutter from two ranges, neither of which contains a fixed target analogous to Figures 7-37 through 7-39. Some insight as to achievable suppression with the NSSL radar can be achieved by considering suppression with a stationary antenna. Figure 7-44 shows the input and output envelope from one such measurement. The large oscillations in input amplitude suggest that the antenna was slowly rotating (corresponding experiments on the MIT radar gave a peak-to-peak amplitude variation of 0.3 dB). Table 7-10 shows the results of filtering these data. Given the noise-like nature of the residue and close correspondence between the input mean and median values, suppression should probably be defined in terms of the change in the median value. A wide variation in clutter levels and suppression results is evident between the various range bins. However, it appears that 40 dB suppression is achievable in some of the range bins*, which is in line with the NSSL instability residue results shown in chapter VI.

Figures 7-45 and 7-46 show representative filter input and output envelopes for two ranges at the NSSL site while Tables 7-11 and 7-12 show the corresponding filter output statistics. The relatively poor suppression on the data at 4.2 km is probably due to a combination of receiver saturation (as manifested in the steps at the beginning of the filter output time series) and moving clutter (near the 2000th time sample). Receiver saturation results in constant I or Q outputs, i.e., a dc level. Thus, the size of the steps in the filter output is directly related to the suppression at zero frequency. At the 15 km range, there is a lesser amount of saturation† evident, but the moving clutter near the 2600th time sample stands out vividly in the filter outputs.

*A similar test with MIT radar data from 2/16/83 yielded 46-47 dB suppression.

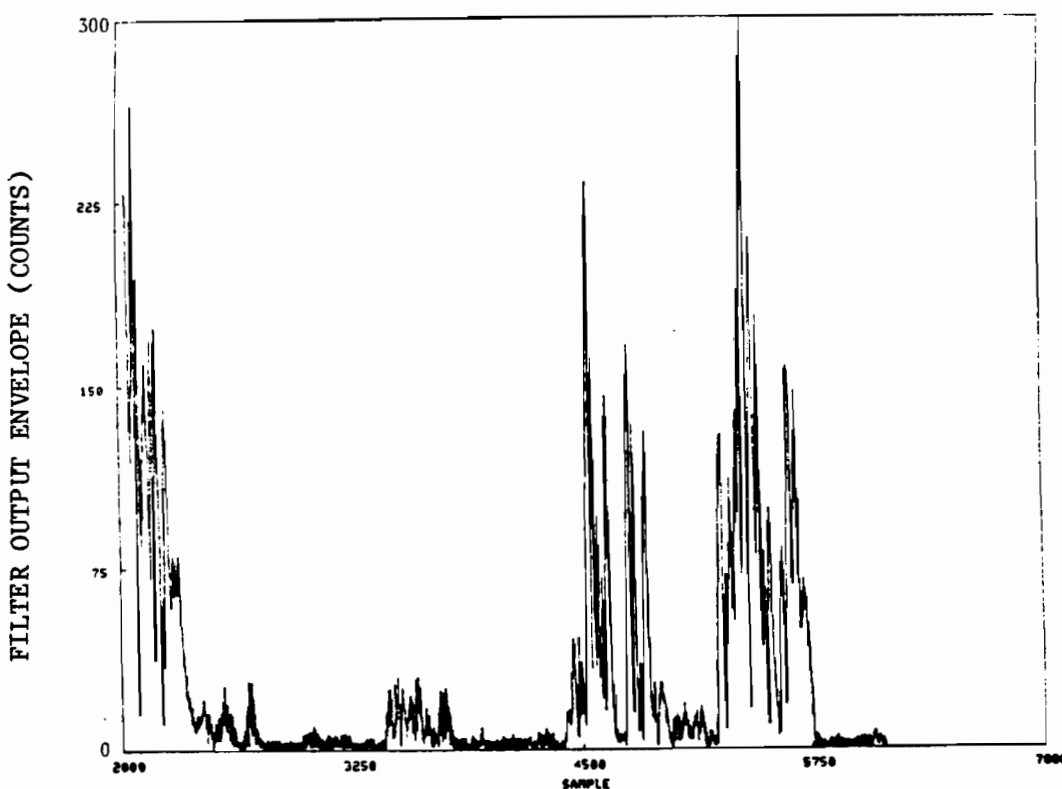
†The AGC nominally used at NSSL for weather measurements was disabled for these measurements so that time series data could be recorded continuously.

FILTRN 1 no filter NOW= 3/29/83 10:25 :18 DATA FROM 1/ 3/83 11:35:51 START AZ,EL,GATE 358.0 0.6 1 PLOT AZ= 53
STARTING RANGE = 18.675 GATE SPACING = 0.225



(a) input envelope

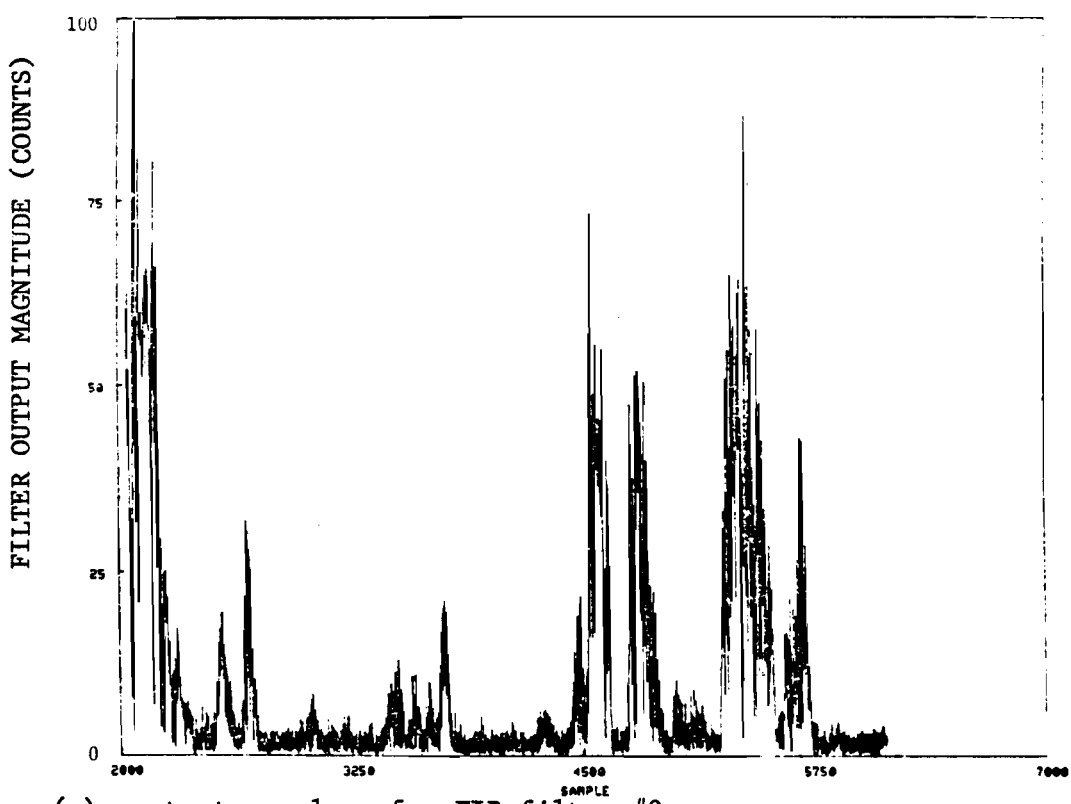
FILTRN 2 /filter1 NOW= 3/25/83 10:25 :18 DATA FROM 1/ 3/83 11:35:51 START AZ,EL,GATE 358.0 0.6 1 PLOT AZ= 53
STARTING RANGE = 18.675 GATE SPACING = 0.225



(b) output envelope for FIR filter #1

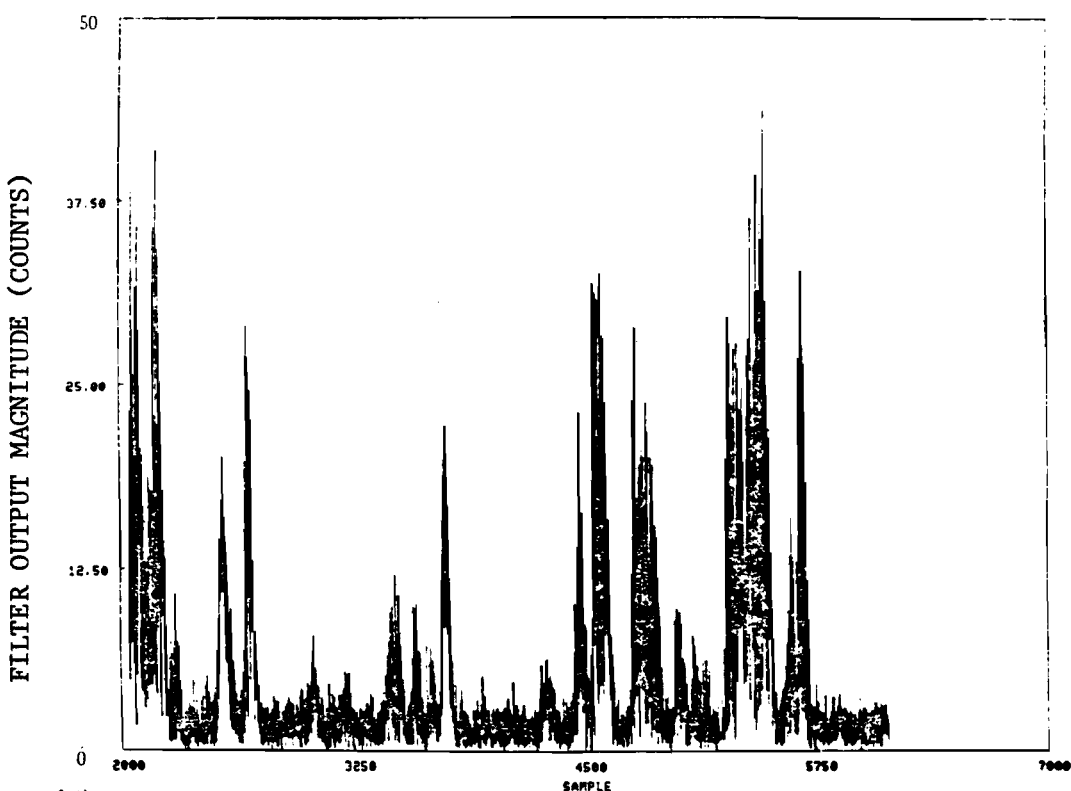
Fig. 7-41a. Suppression of MIT Site Clutter
at 19 km Range.

FILTNO 3 filter2 MOD= 3/29/83 10:25 :18 DATA FROM 1/ 3/83 11:35:51 START AZ,EL,GATE 358.0 0.6 1 PLOT #2+ 53
STARTING RANGE = 18.675 GATE SPACING = 0.225



(c) output envelope for FIR filter #2

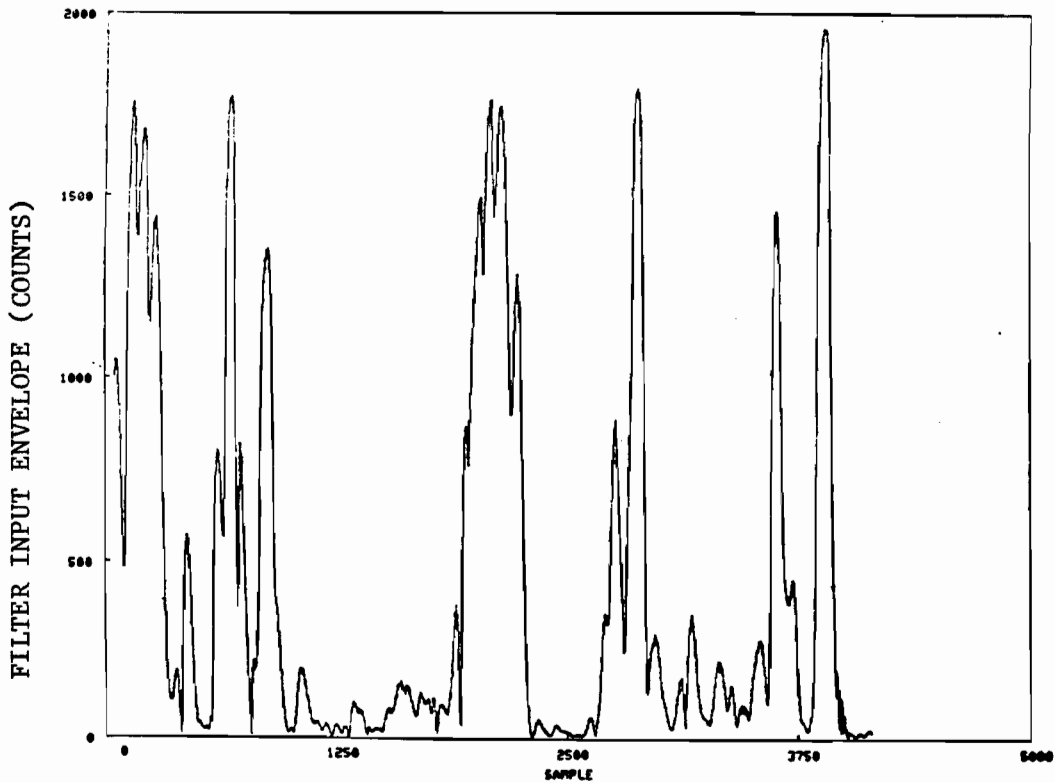
FILTNO 4 filter3 MOD= 3/29/83 10:25 :18 DATA FROM 1/ 3/83 11:35:51 START AZ,EL,GATE 358.0 0.6 1 PLOT #2+ 53
STARTING RANGE = 18.675 GATE SPACING = 0.225



(d) output envelope for FIR filter #3

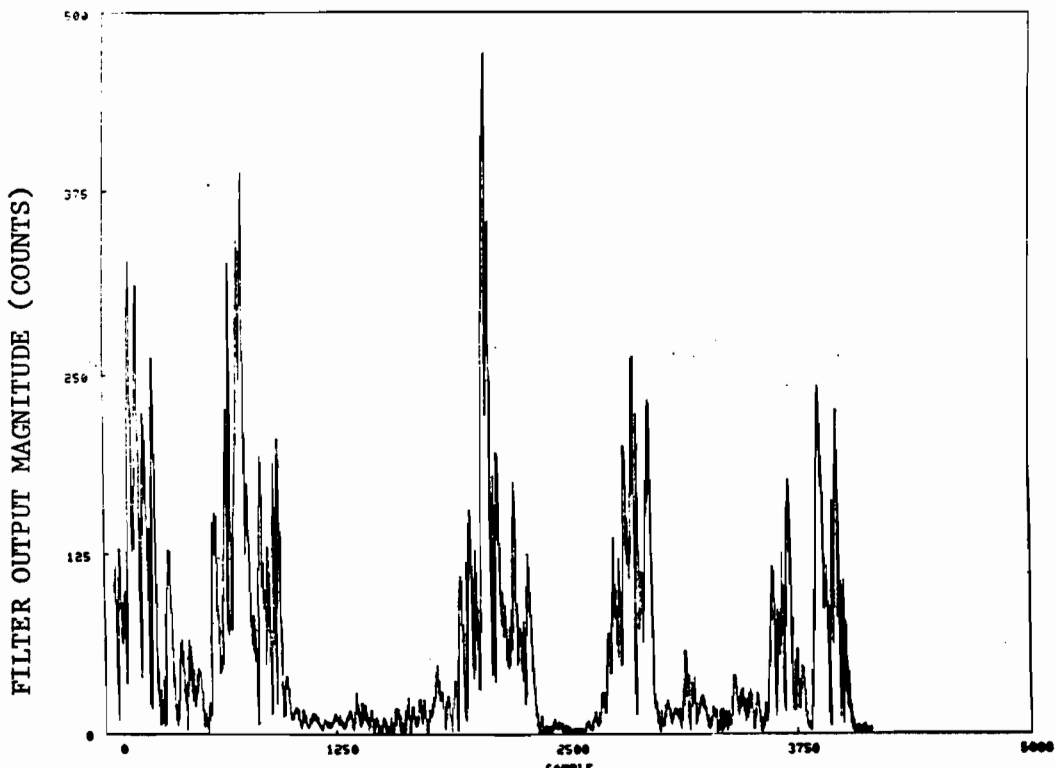
Fig. 7-41b. Suppression of MIT Site Clutter
at 19 km Range.

FILTHO 1 refilter NCU= 3/21/83 18:12 :31 DATA FROM 2/16/83 11:59:56 START AZ,EL,GATE 1.3 0.4 1 PLOT AZ- 1
STARTING RANGE = 8.550 GATE SPACING = 0.225



(a) input envelope

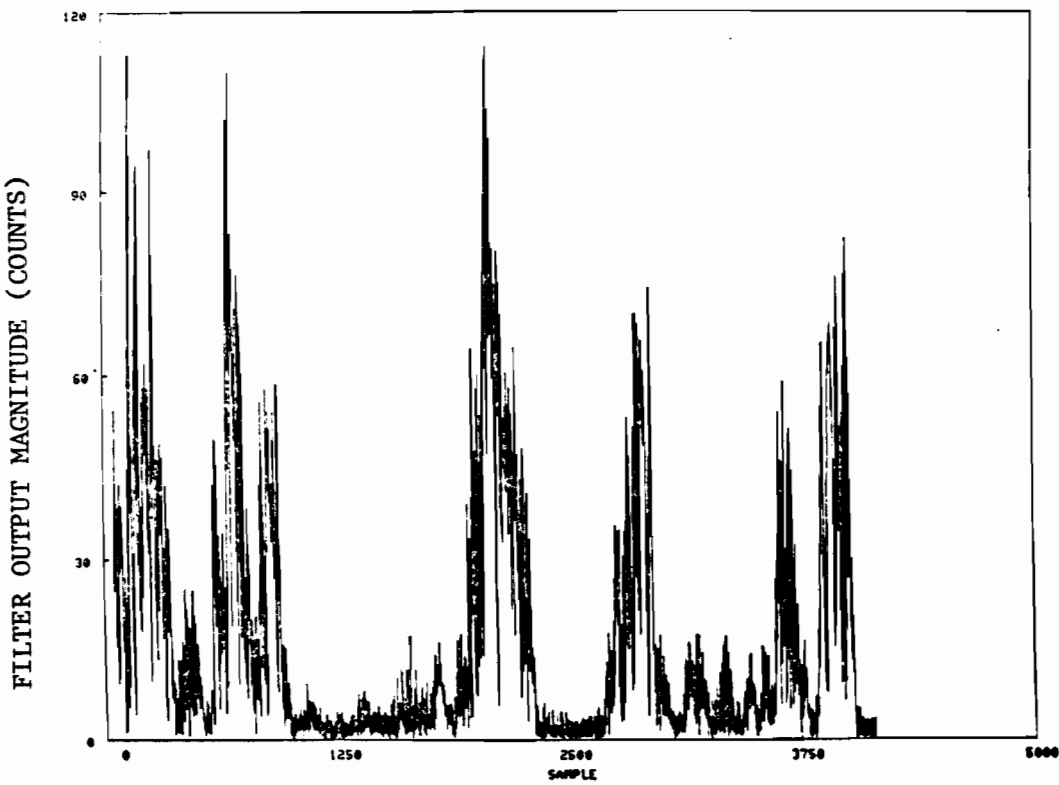
FILTHO 2 filter1 NCU= 3/21/83 18:12 :31 DATA FROM 2/16/83 11:59:56 START AZ,EL,GATE 1.3 0.4 1 PLOT AZ- 1
STARTING RANGE = 8.550 GATE SPACING = 0.225



(b) output envelope for FIR filter #1

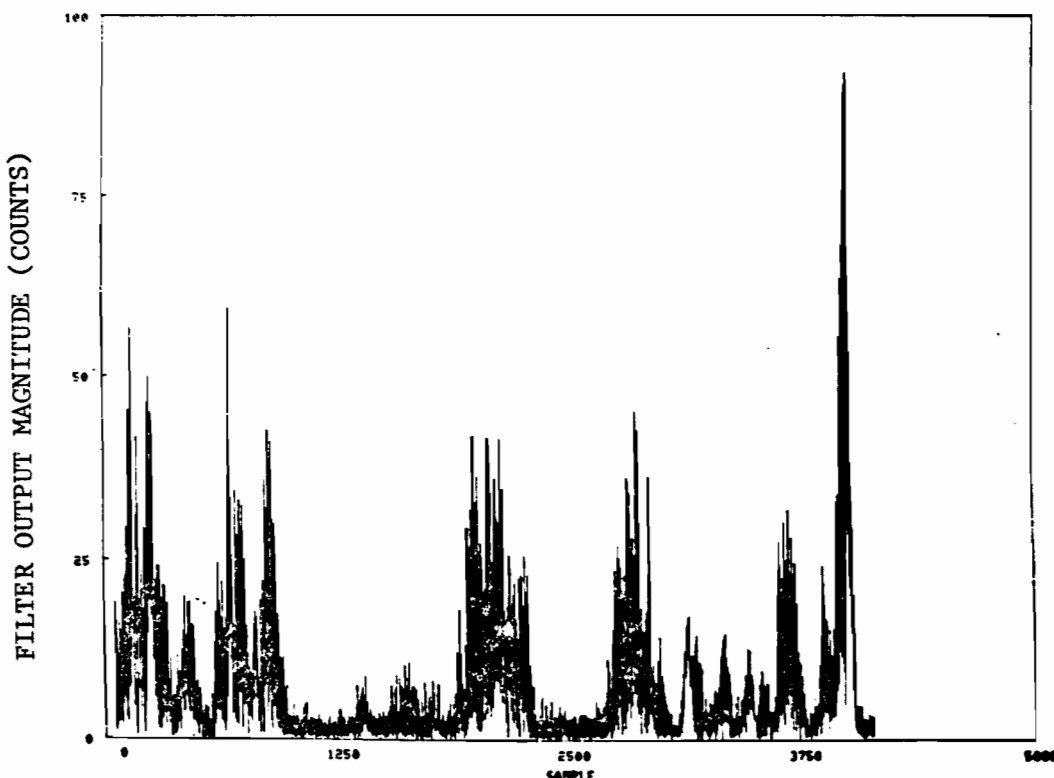
Fig. 7-42. Suppression of MIT Site S-Band Clutter at 8 km Range.

FILTNO 3 filter2 NOw= 3/21/83 18:12 :31 DATA FROM 2/16/83 11:58:56 START AZ,EL,GATE 1.3 0.4 1 PLOT AZ+ 1
STARTING RANGE = 8.550 GATE SPACING = 0.225



(c) output envelope for FIR filter #2

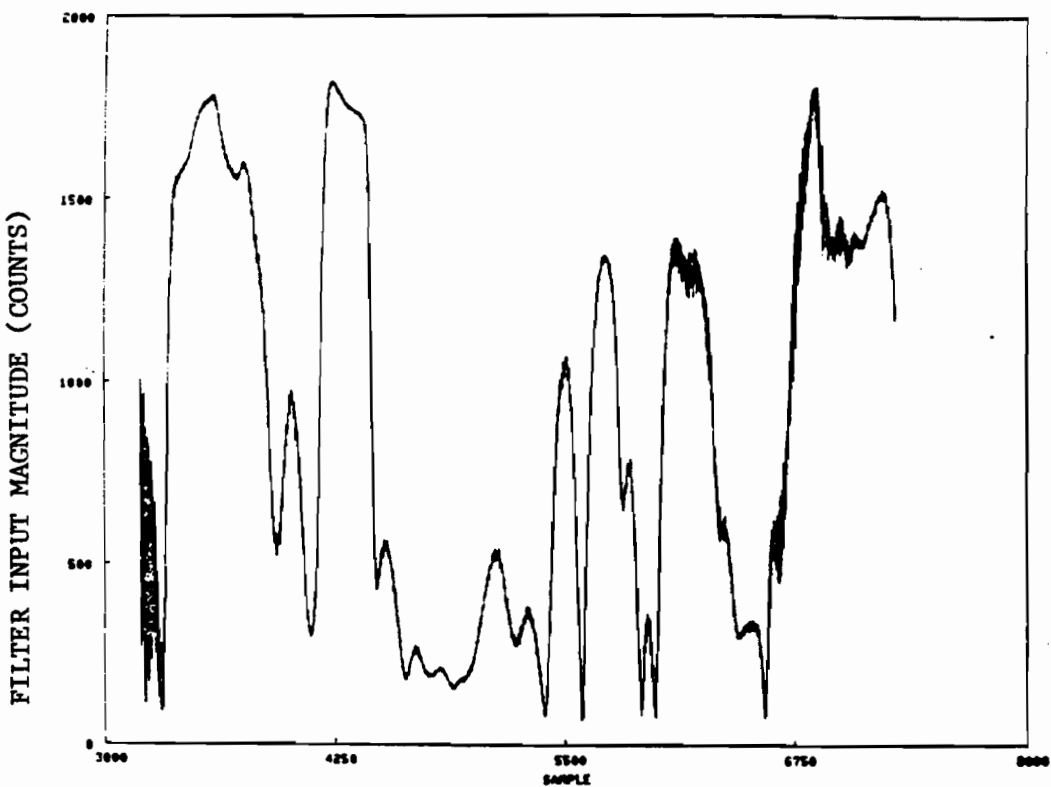
FILTNO 4 filter3 NOw= 3/21/83 18:12 :31 DATA FROM 2/16/83 11:58:56 START AZ,EL,GATE 1.3 0.4 1 PLOT AZ+ 1
STARTING RANGE = 8.550 GATE SPACING = 0.225



(d) output envelope for FIR filter #3

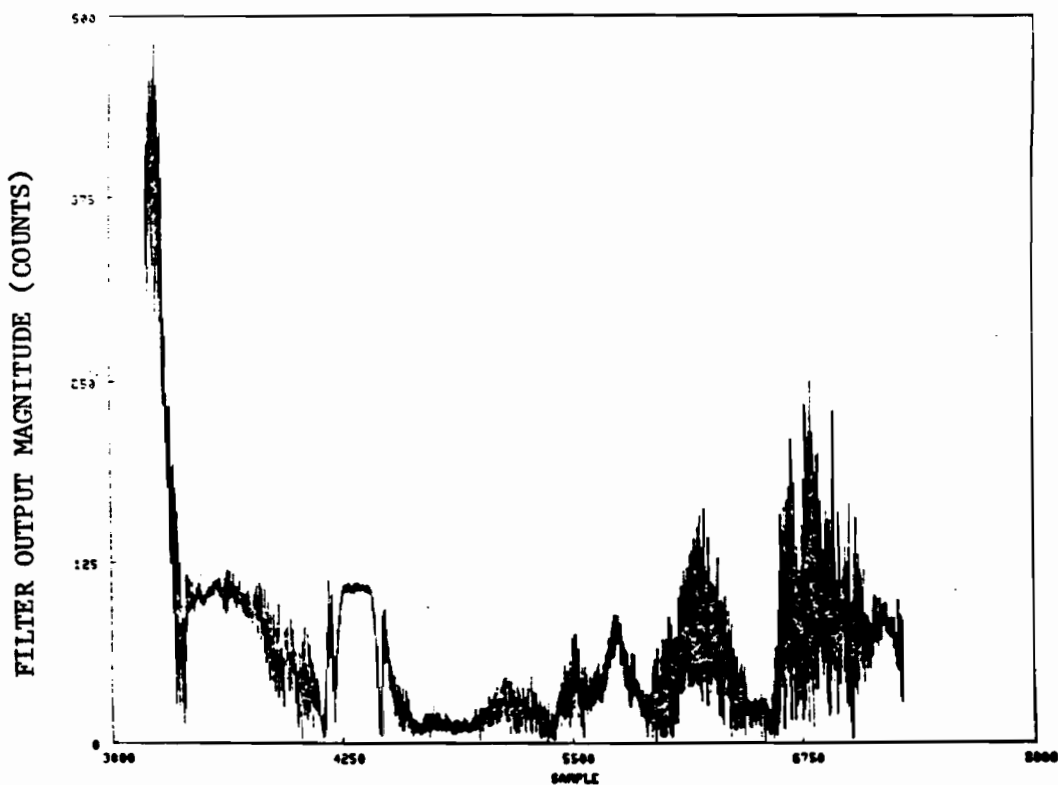
Fig. 7-42. Suppression of MIT Site S-Band Clutter at 8 km Range (Cont.)

FILTNO 1 filter NOU= 3/22/83 9:48 :25 DATA FROM 2/16/83 11:55:27 START AZ,EL,GATE 359.1 0.4 1 PLOT AZ= 25
STARTING RANGE = 3.600 GATE SPACING = 0.225



(a) input envelope

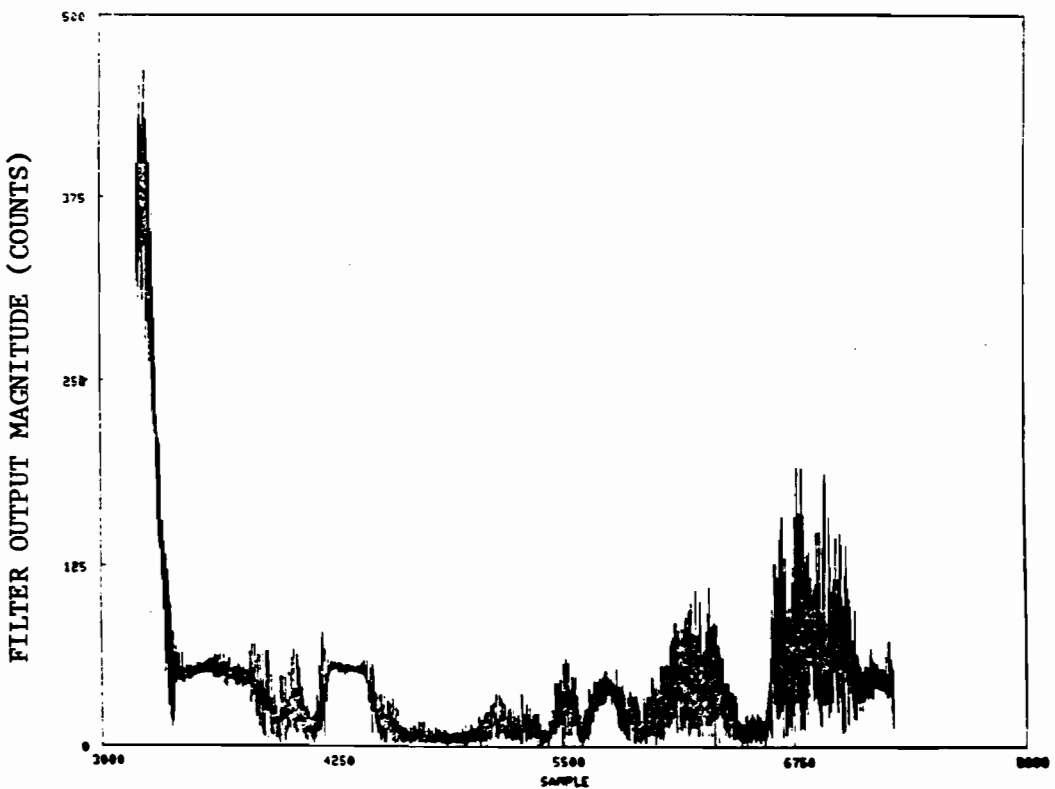
FILTNO 2 filter NOU= 3/22/83 9:48 :25 DATA FROM 2/16/83 11:55:27 START AZ,EL,GATE 359.1 0.4 1 PLOT AZ= 25
STARTING RANGE = 3.600 GATE SPACING = 0.225



(b) output envelope for FIR filter #1

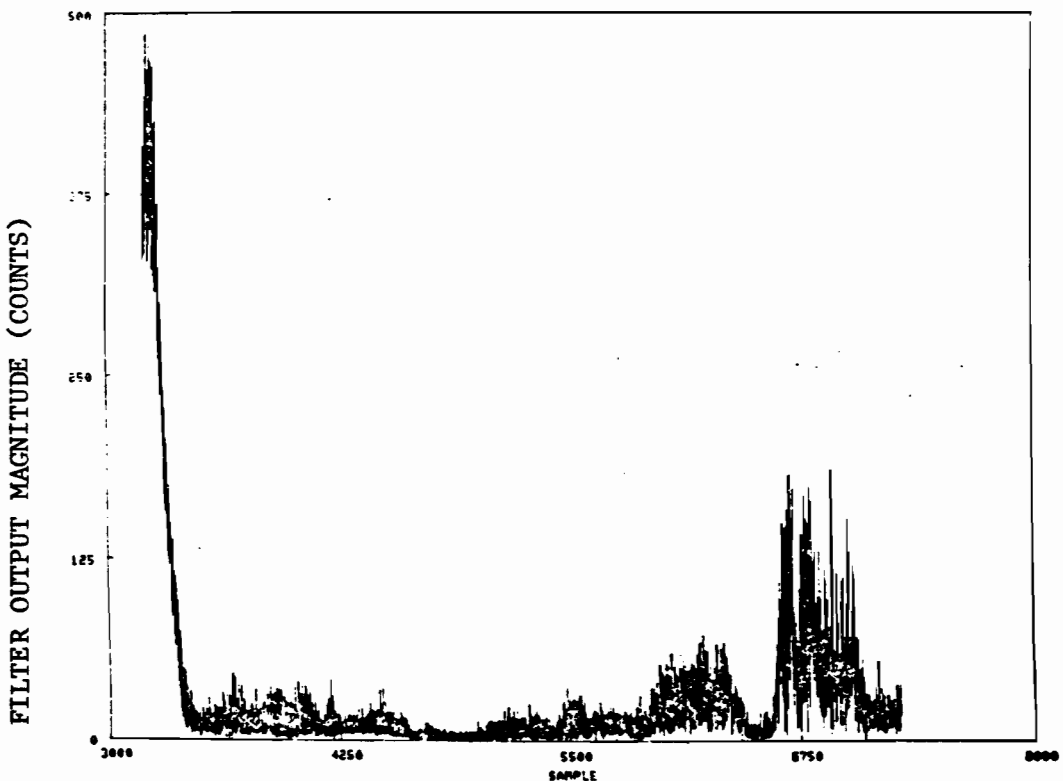
Fig. 7-43. Suppression of MIT Site S-Band Clutter at 4 km Range.

FILNO 3 Filter2 NOU 3/22/83 9:43 :25 DATA FROM 2/16/83 11:55:27 START AZ,EL,GATE 350.1 0.4 I PLOT AZ+ 25
STARTING RANGE = 3.600 GATE SPACING = 0.225



(c) output envelope for FIR filter #2

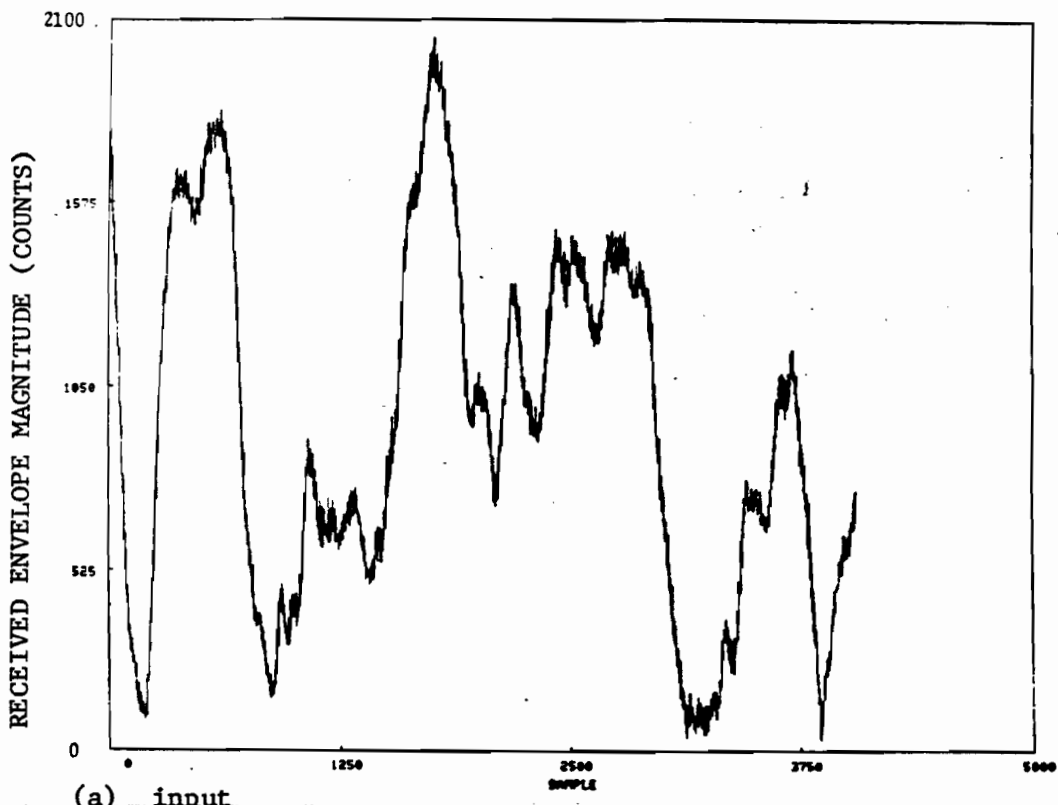
FILNO 4 Filter3 NOU 3/22/83 9:48 :25 DATA FROM 2/16/83 11:55:27 START AZ,EL,GATE 350.1 0.4 I PLOT AZ+ 25
STARTING RANGE = 3.600 GATE SPACING = 0.225



(d) output envelope for FIR filter #3

Fig. 7-43. Suppression of MIT Site S-Band Clutter at
4 km Range (Cont.).

FILTNO 1: refilter HOU= 4/ 4/83 12:14 :45 DATA FROM 0/ 0/ 0 12:25:40 START AZ,EL,GATE 354.8 0.0 1 PLOT AZ= 354
STARTING RANGE = 4.200 GATE SPACING = 0.600



FILTNO 2: filter1 HOU= 4/ 4/83 12:14 :45 DATA FROM 0/ 0/ 0 12:25:40 START AZ,EL,GATE 354.8 0.0 1 PLOT AZ= 354
STARTING RANGE = 4.200 GATE SPACING = 0.600

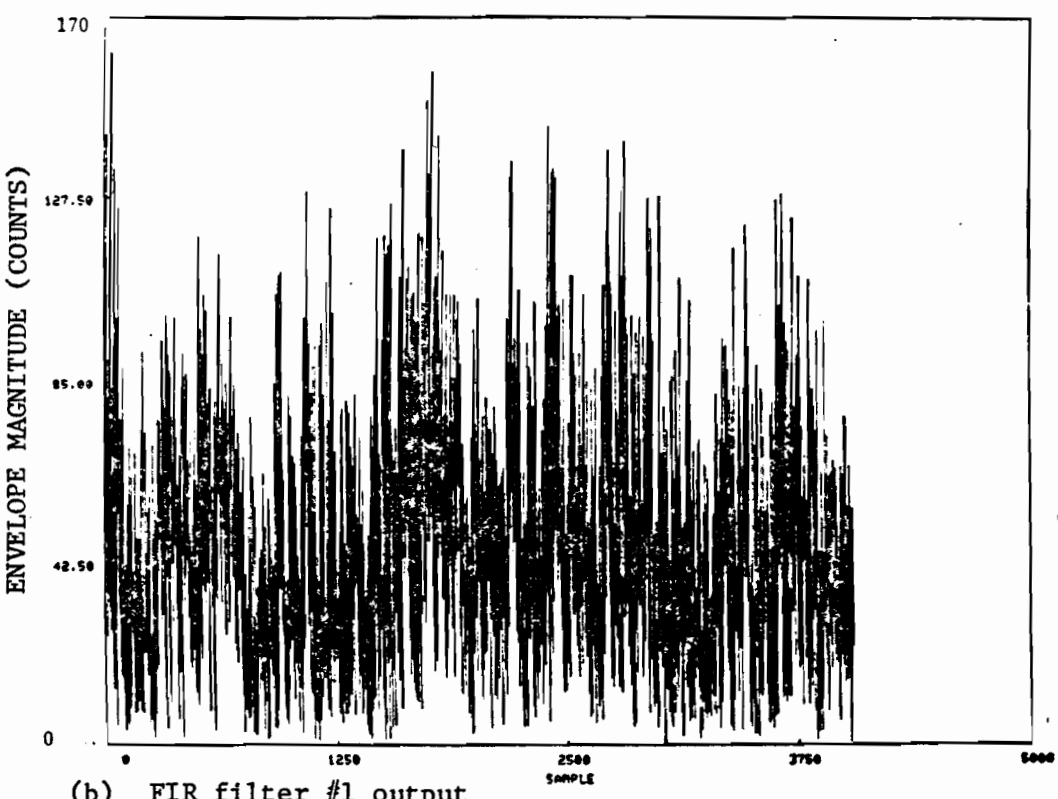
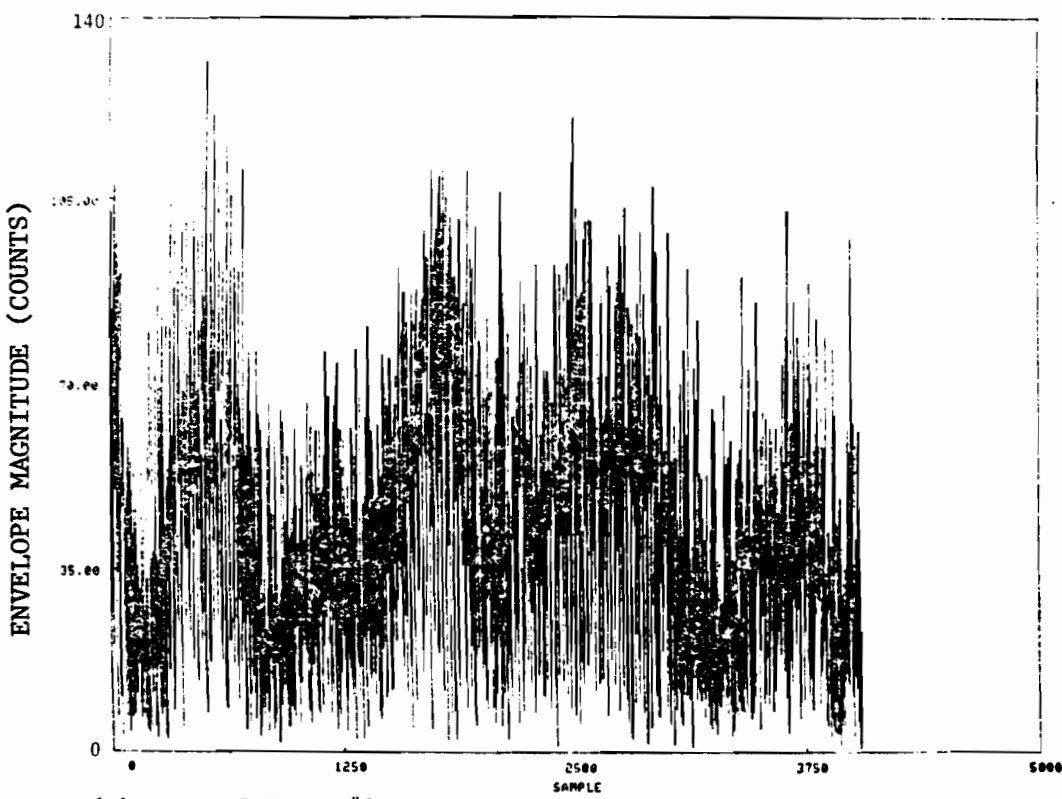


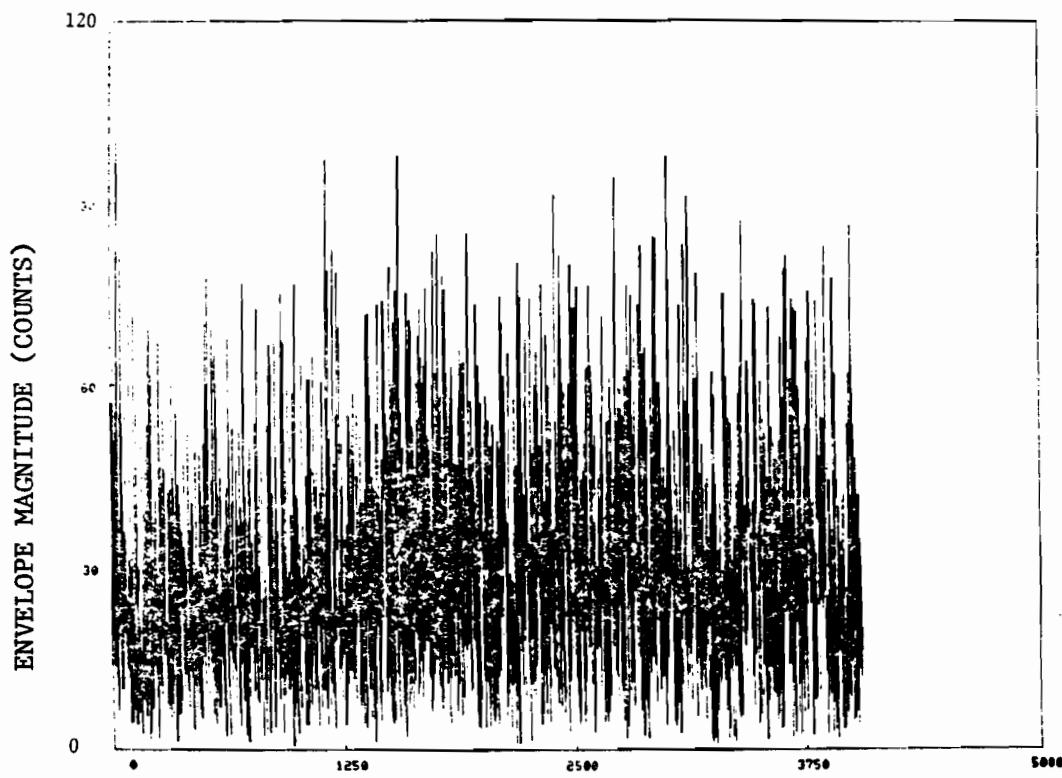
Fig. 7-44a. NSSL Site Clutter Suppression
With Stationary Antenna.

FILNO 3 filter2 NOB= 4/ 4/83 12:14:45 DATA FROM 8/ 8/ 8 12:25:40 START AZ,EL,GATE 354.8 0.0 1 PLOT AZ= 354
STARTING RANGE = 4.200 GATE SPACING = 0.600



(c) FIR filter #3 output

FILNO 4 filter3 NOB= 4/ 4/83 12:14:45 DATA FROM 8/ 8/ 8 12:25:40 START AZ,EL,GATE 354.8 0.0 1 PLOT AZ= 354
STARTING RANGE = 4.200 GATE SPACING = 0.600



(d) FIR filter #3 output

Fig. 7-44b. NSSL Site Clutter Suppression with Stationary Antenna

TABLE 7-10. RESULTS OF FILTERING NSSL DATA AT
RANGE OF 15 KM WITH ANTENNA STATIONARY

OUTPUT FROM CLUTTER FILTER PROGRAM = TSCLT
THIS TAPE IS FROM NSSL RADAR

TODAY = 4/4/83 12:14:45

MISSION DAY = 216 STARTING RECORD = 1999 STARTAZ = 354.8
EL 0.6 START TIME = 12:25:40 START RANGE(KM) = 4.200 RGS = 0.600

FILTER 1 = NULL

FILTER 3= 2 M/S 1302 NPTS = 39 STOPBAND = 0.573 PASSBAND EDGE = 2.048
WTS = 8.00 1.00

RANGE GATE	MEAN(DB)	MEDIAN(DB)	90 % QUANTILE(DB)
1	60.5	59.0	64.0
2	67.1	66.7	68.1
3	57.3	56.3	59.9
4	65.2	66.3	68.1
5	64.2	64.4	65.8
6	55.7	53.1	59.4
7	66.1	66.3	67.2
8	66.3	66.3	66.7
9	65.7	65.8	67.2
10	55.0	53.6	58.1
11	56.8	56.7	57.2
12	54.8	53.6	58.1
13	62.2	61.7	64.0
14	49.8	48.6	53.1
15	68.4	68.1	69.0
16	48.3	48.1	49.9

RANGE GATE	MEAN(DB)	MEDIAN(DB)	90 % QUANTILE(DB)
1	33.7	31.8	37.2
2	40.7	37.7	43.1
3	33.4	31.3	36.8
4	37.1	36.8	39.5
5	39.0	37.2	42.2
6	30.6	28.1	34.0
7	41.7	38.6	44.0
8	37.4	36.8	38.1
9	36.5	36.3	39.0
10	30.5	28.6	34.0
11	30.2	27.7	33.6
12	41.3	39.5	44.5
13	41.4	39.9	44.5
14	35.2	33.6	38.6
15	42.4	39.9	45.8
16	28.0	24.5	31.3

FILTER 2= 1 M/S 1302 NPTS = 39 STOPBAND = 0.286 PASSBAND EDGE = 1.003
WTS = 4.00 1.00

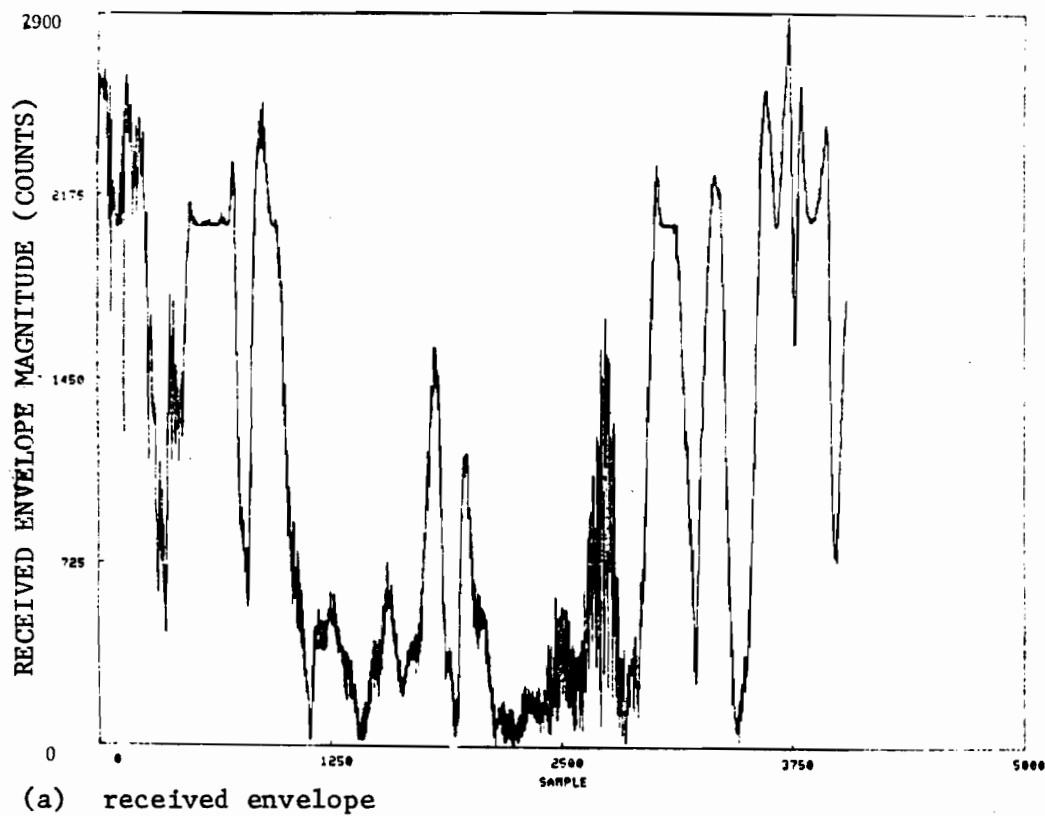
FILTER 4= 3 M/S 1302 NPTS = 39 STOPBAND = 0.788 PASSBAND EDGE = 3.072
WTS = 40.00 1.00

RANGE GATE	MEAN(DB)	MEDIAN(DB)	90 % QUANTILE(DB)
1	34.3	32.2	37.7
2	47.3	41.3	50.8
3	34.1	32.2	37.7
4	39.9	38.1	42.7
5	44.1	41.3	47.2
6	33.4	30.9	36.8
7	49.0	44.5	52.6
8	36.4	35.4	38.1
9	42.6	39.9	45.8
10	34.8	32.7	38.1
11	29.7	28.1	32.7
12	41.8	39.9	45.4
13	44.3	43.1	47.2
14	38.1	36.8	41.3
15	43.1	40.4	46.7
16	29.2	25.0	31.8

RANGE GATE	MEAN(DB)	MEDIAN(DB)	90 % QUANTILE(DB)
1	30.1	27.7	33.6
2	35.3	30.0	39.0
3	31.3	29.5	34.9
4	29.4	26.8	32.7
5	37.1	34.9	40.8
6	28.5	25.9	31.8
7	37.2	34.0	40.4
8	29.0	26.3	32.7
9	30.0	27.2	33.6
10	23.7	25.9	32.2
11	26.7	23.1	30.0
12	40.8	39.5	44.5
13	36.3	34.5	39.9
14	32.0	30.0	35.4
15	38.3	34.5	42.7
16	26.8	22.7	30.0

7-63

FILTNO 1 filter1 now= 4/ 4/83 17:25 :50 DATA FROM 8/ 8/ 8 12:36:18 START AZ,EL,GATE 14.5 0.0 1 PLOT #2= 14
STARTING RANGE = 15.150 GATE SPACING = 0.600



(a) received envelope

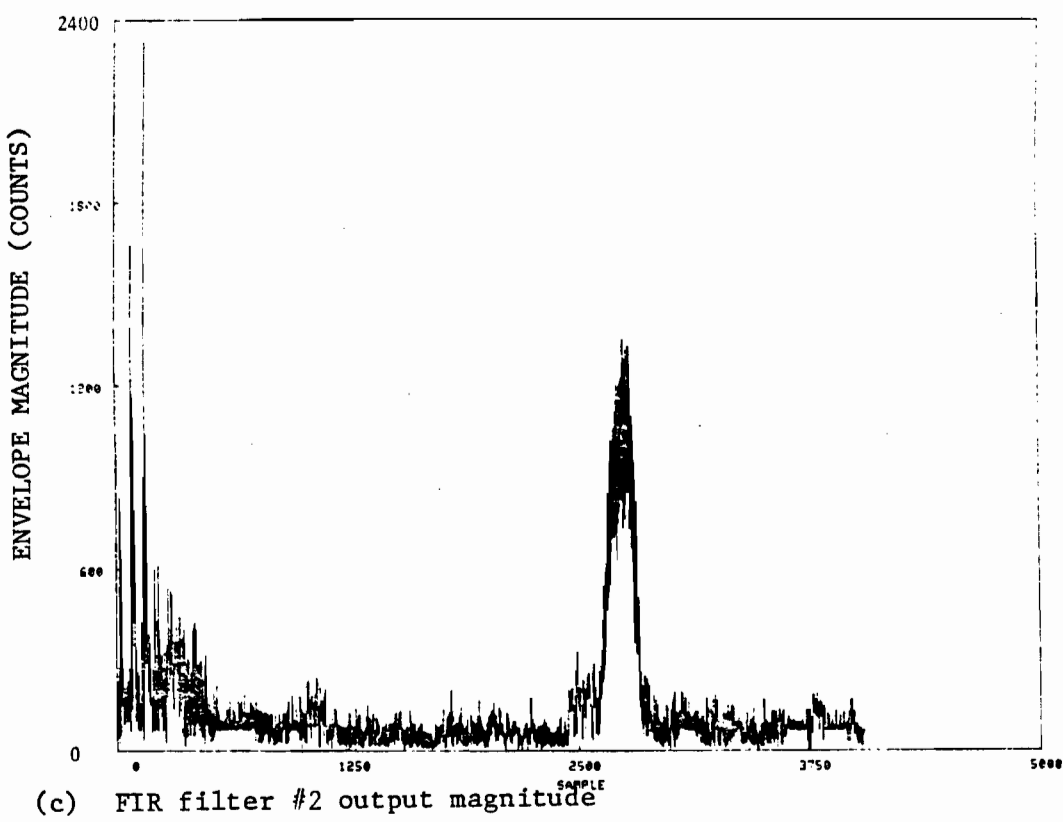
FILTNO 2 filter1 now= 4/ 4/83 17:25 :50 DATA FROM 8/ 8/ 8 12:36:18 START AZ,EL,GATE 14.5 0.0 1 PLOT #2= 14
STARTING RANGE = 15.150 GATE SPACING = 0.600



(b) FIR filter #1 output magnitude

Fig. 7-45a. Clutter Suppression of NSSL Site Clutter
at 15 km.

FILTNO 3 filter2 NOW= 4/ 4/83 17:25 :50 DATA FROM 8/ 8/ 0 12:36:18 START AZ,EL,GATE 14.5 0.0 1 PLOT AZ= 14
STARTING RANGE = 15.150 GATE SPACING = 0.600



FILTNO 4 filter3 NOW= 4/ 4/83 17:25 :50 DATA FROM 8/ 8/ 0 12:36:18 START AZ,EL,GATE 14.5 0.0 1 PLOT AZ= 14
STARTING RANGE = 15.150 GATE SPACING = 0.600

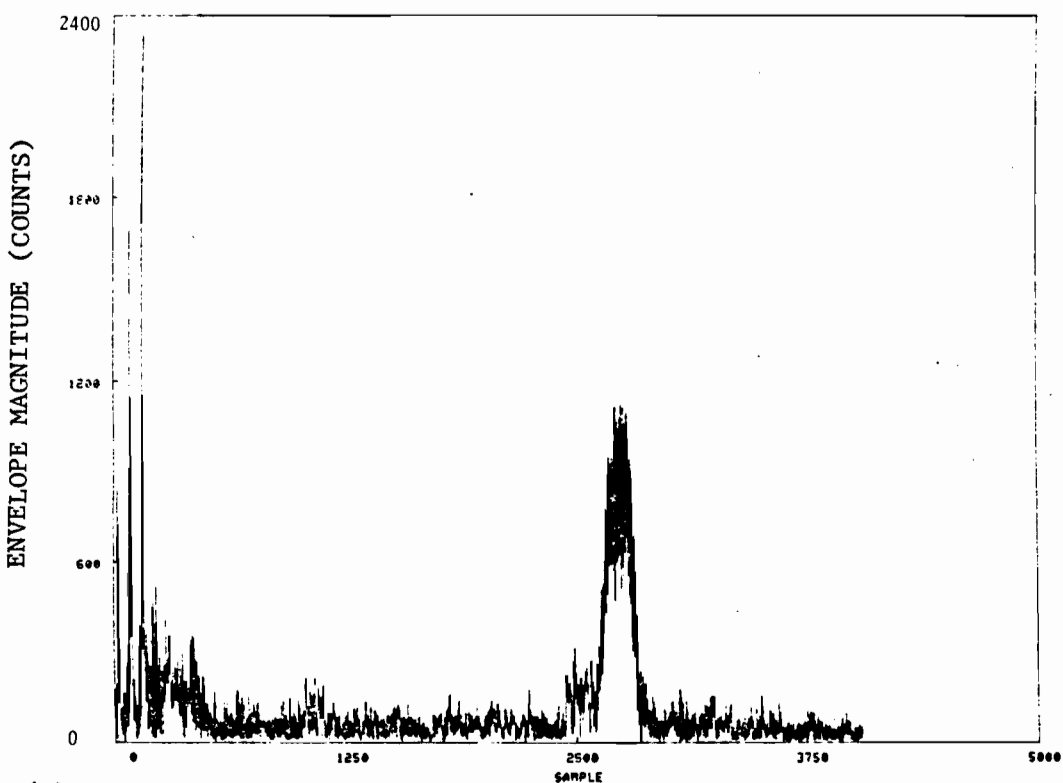
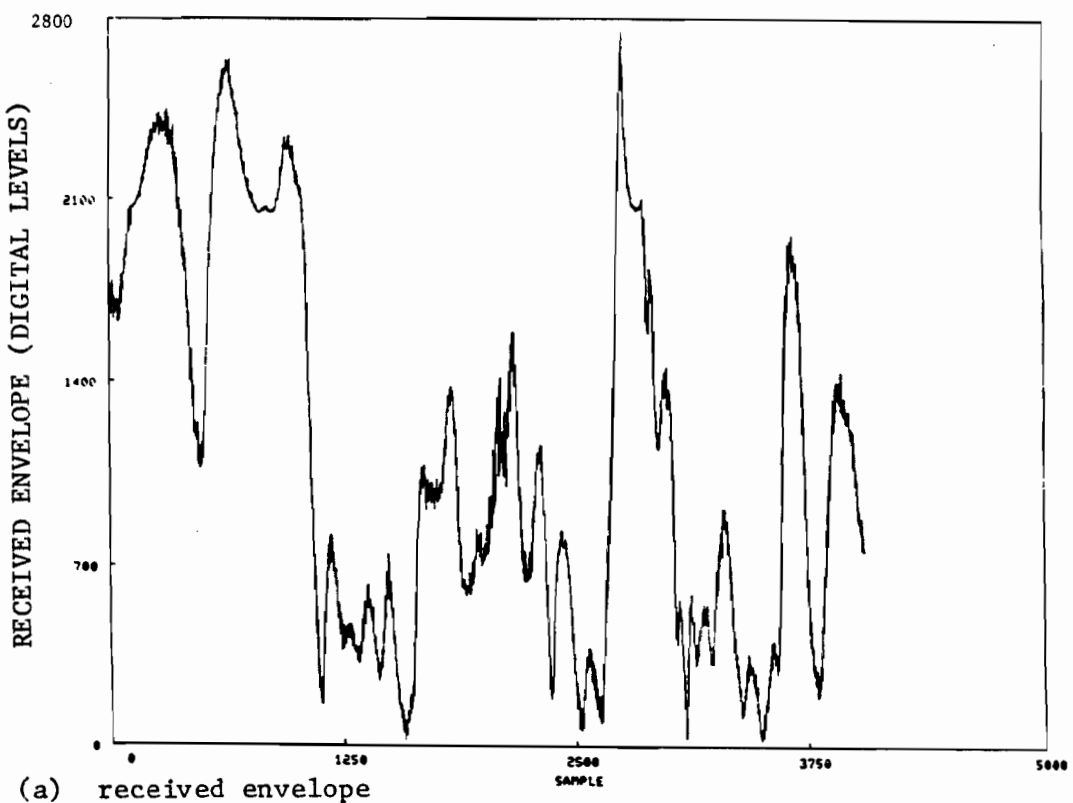


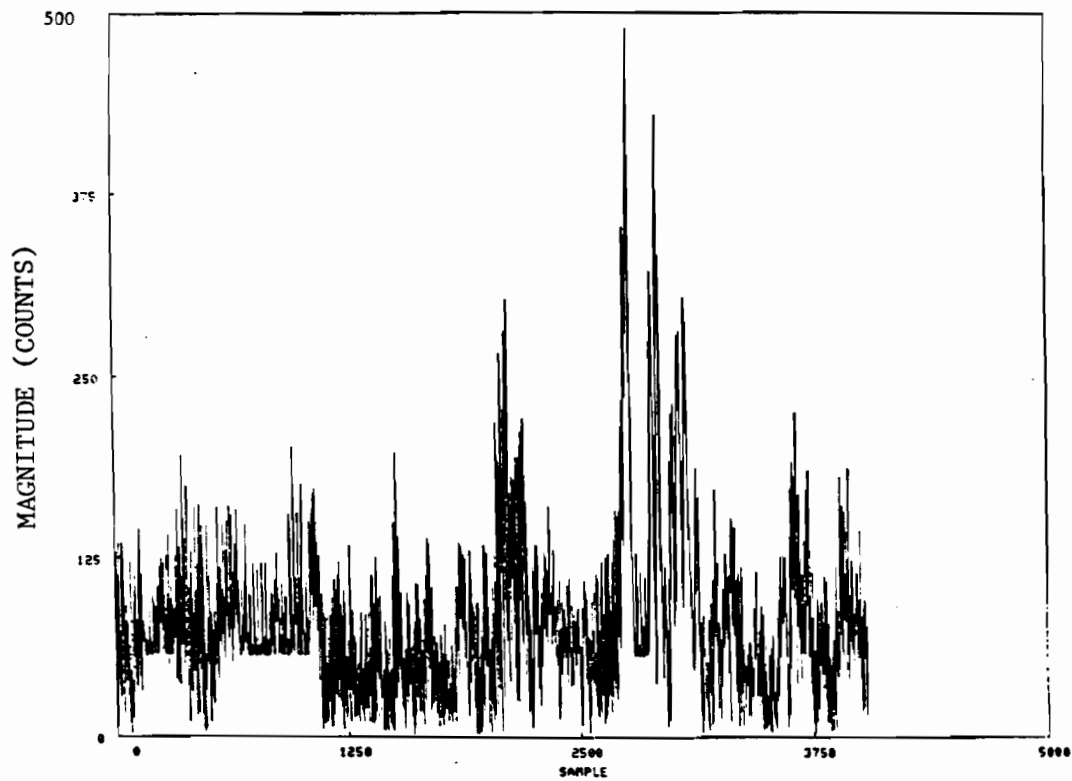
Fig. 7-45b. Clutter Suppression of NSSL Site Clutter
at 15 km

FILNO 1 nofilter NOU 4/27/83 15:20 :46 DATA FROM 0/ 0/ 0 12:25:54 START AZ,EL,GATE 354.8 0.0 1 PLOT AZ= 354
STARTING RANGE = 4.200 GATE SPACING = 0.600



(a) received envelope

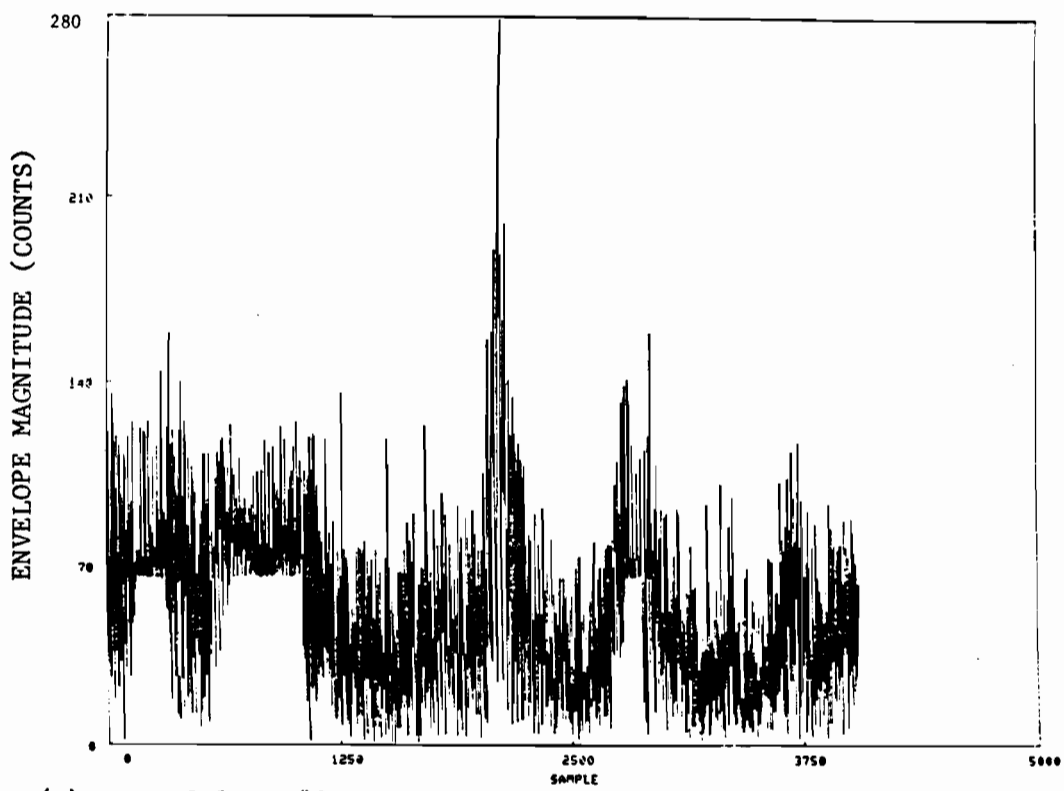
FILNO 2 filter1 NOU 4/27/83 15:20 :46 DATA FROM 0/ 0/ 0 12:25:54 START AZ,EL,GATE 354.8 0.0 1 PLOT AZ= 354
STARTING RANGE = 4.200 GATE SPACING = 0.600



(b) FIR filter #1 output magnitude

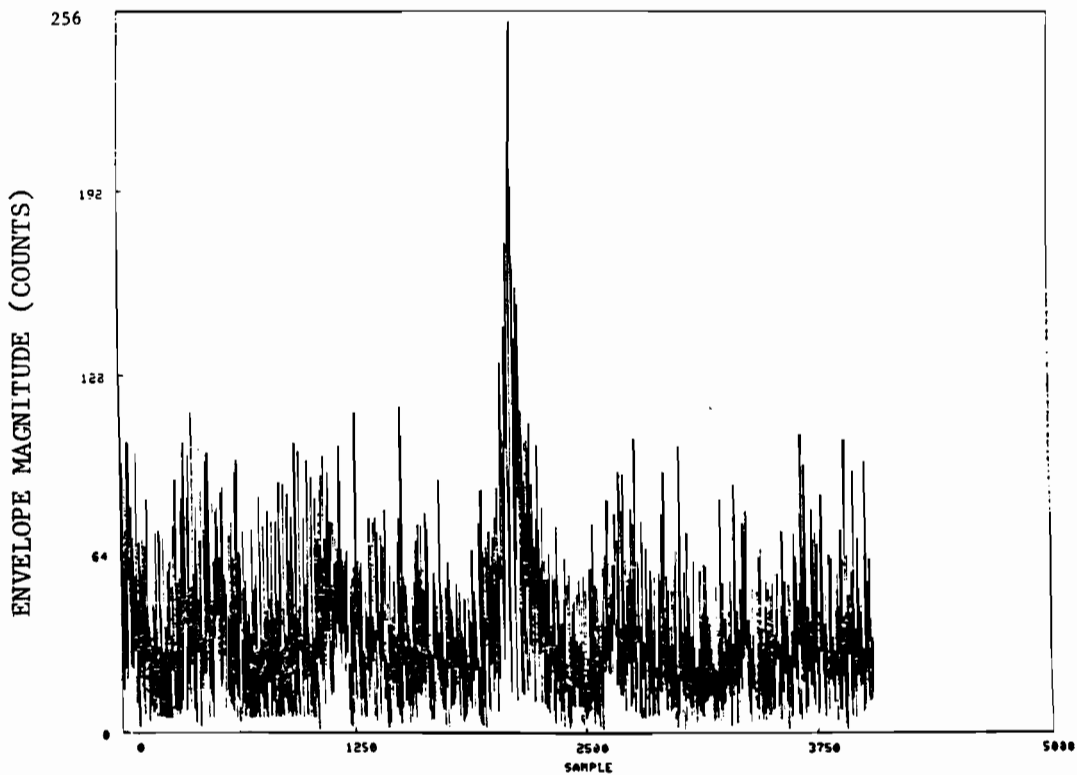
Fig. 7-46a. Results of Filtering NSSL Data
at Range of 4.2 km.

FILTNO 3 filter2 NOU= 4/27/83 15:20 :46 DATA FROM 0/ 0/ 0 12125154 START A2,EL,GATE 354.8 0.0 1 PLOT A2+ 354
STARTING RANGE = 4.200 GATE SPACING = 0.600



(c) FIR filter #2 output magnitude

FILTNO 4 filter3 NOU= 4/27/83 15:20 :46 DATA FROM 0/ 0/ 0 12125154 START A2,EL,GATE 354.8 0.0 1 PLOT A2+ 354
STARTING RANGE = 4.200 GATE SPACING = 0.600



(d) FIR filter #3 output magnitude

Fig. 7-46b. Results of Filtering NSSL Data at Range of 4.2 km

TABLE 7-11. RESULTS OF FILTERING NSSL DATA
AT 15 KM

OUTPUT FROM CLUTTER FILTER PROGRAM = TSCLT
THIS TAPE IS FROM NSSL RADAR

TODAY = 6/ 4/83 17:25:5

MISSION DAY = 216 STARTING RECORD = 1729 STARTAZ = 14.5
EL 0.6 START TIME = 12:36:18 START RANGE(KM) = 15.150 RGS = 0.600

FILTER 1 = NULL

RANGE GATE	MEAN(DB)	MEDIAN(DB)	90 % QUANTILE(DB)
1	61.3	51.7	66.3
2	60.9	49.5	66.3
3	60.6	48.1	66.3
4	60.4	48.1	66.3
5	60.3	47.7	66.3
6	59.6	45.8	65.8
7	58.9	45.4	65.3
8	60.7	48.1	66.3
9	58.4	45.4	64.4
10	55.7	41.3	59.9
11	55.7	41.3	59.0
12	55.9	40.8	59.4
13	53.8	40.8	55.4
14	54.8	39.0	57.2
15	52.7	39.9	54.9
16	53.3	37.7	53.6

7-
88 FILTER 2= 1 M/S 1302 NPTS = 39 STOPBAND = 0.286 PASSBAND EDGE = 1.003
WTS = 4.00 1.00

FILTER 3= 2 M/S 1302 NPTS = 39 STOPBAND = 0.573 PASSBAND EDGE = 2.068
WTS = 8.00 1.00

RANGE GATE	MEAN(DB)	MEDIAN(DB)	90 % QUANTILE(DB)
1	46.4	36.3	46.9
2	48.2	36.8	46.7
3	49.6	36.3	46.3
4	46.4	36.3	44.5
5	46.1	35.9	44.5
6	46.9	35.4	44.9
7	43.2	34.9	43.6
8	43.4	35.4	43.1
9	46.7	34.5	44.5
10	45.1	33.6	42.7
11	44.5	33.1	41.8
12	43.3	33.6	42.2
13	44.6	33.1	43.6
14	41.0	32.7	40.8
15	42.4	32.7	41.8
16	41.6	32.2	40.6

7-
89 FILTER 4= 3 M/S 1302 NPTS = 39 STOPBAND = 0.788 PASSBAND EDGE = 3.072
WTS = 40.00 1.00

RANGE GATE	MEAN(DB)	MEDIAN(DB)	90 % QUANTILE(DB)
1	45.2	34.0	44.0
2	47.2	34.9	45.4
3	49.0	34.5	45.4
4	45.5	34.0	43.1
5	44.8	33.6	43.1
6	45.5	33.6	43.6
7	42.2	33.1	42.2
8	42.3	32.7	41.8
9	45.9	33.1	43.6
10	44.4	32.2	41.8
11	43.8	32.2	41.3
12	41.8	32.2	41.3
13	43.6	32.2	42.7
14	40.6	31.8	39.9
15	41.5	31.8	40.8
16	40.6	31.8	39.5

These results from NSSL illustrate the need for:

- (1) careful design of the rf and analog components of a NEXRAD if clutter suppression capability inherent in the digital processor is to be achieved, and
- (2) subsequent processing (e.g., by the use of clutter map techniques) to reduce the effects of clutter from moving scatterers such as cars.

VIII. SUMMARY AND RECOMMENDATIONS FOR FUTURE WORK

In this section, we summarize the findings of the study and make suggestions for follow-on work to resolve the remaining uncertainties. This study focused on the development of the functional specification for clutter suppression which is described in Chapters IV and VI. This specification has been incorporated into the Validation Phase NEXRAD Technical Requirements.

We stress that this specification developed was constrained to be (1) consistent (to the maximum extent possible) with the systems definition phase specification, and (2) achievable in a time frame compatible with the NEXRAD schedule as opposed to "starting from scratch" to develop a new specification. Thus, important issues such as the operational utility of various levels of clutter suppression were not addressed in detail.

A. Summary

A key element in developing the functional specification was to review the clutter threat in terms of how clutter causes weather parameter errors and geometric situations where clutter will be of particular concern. It was concluded that:

- (1) in "normal" joint-use NEXRAD operations, overlap of first trip clutter with second trip weather in the Doppler channel represents a major challenge. This challenge is made more severe by the range advantage of the first trip clutter (Chapter II).
- (2) anomalous propagation (AP) will represent a significant challenge at long ranges (e.g., greater than 60 km) when it occurs, (Chapters II and V), and
- (3) detection of certain, more specialized weather phenomena (e.g., low level wind shear and prestorm convective boundary layer cells) involve a significant clutter challenge due to the need to measure weak signals at low elevation angles (Chapter II).

The next major issue was the handling of weather parameter errors due to the clutter suppression technique as opposed to those which are clutter level dependent. To avoid excessive complexity in the specification, it was decided to separately specify these two contributions. The suppression technique dependent error bounds were based on errors for a pulse pair processor preceded by a linear high-pass filter. Thus, the functional specification error bounds are consistent with the high-pass LTI filter/pulse pair processor technique implied in the original specification.

The clutter from areas with man-made objects (e.g., buildings) shows distinctive differences in time waveform and amplitude statistics from that associated with numerous, smaller scatterers. Thus, it was necessary to

define two different clutter models to address these differences in clutter behavior:

- (a) a distributed clutter model wherein the clutter width depends on scan rate and a wind velocity related parameter, and
- (b) a discrete scatterer clutter model whose time waveform represents the antenna power pattern.

Suppression performance capability for each of these models was lower bounded by the power suppression of representative FIR and IIR low-pass LTI filters.

The quality assurance tests were developed to verify:

- (1) transmitter/receiver stability alone
- (2) signal processor capability alone, and
- (3) suppression on a discrete scatterer clutter signal in a front-to-end test.

Since the required performance was functionally specified, the quality assurance test was easy to develop and short in length.

It was deemed important to demonstrate that the desired clutter suppression capability is in fact practically achievable. The signal processor capability was demonstrated by simulation studies on the two clutter models with a variety of linear filters. Table 8-1 summarizes the results of these simulations with respect to the specification requirements. We see that both filter types met the specification goals. This suggests that there are a variety of NEXRAD signal processor designs which are capable of achieving the desired suppression capability.

The transmitter/receiver capability to meet the most stringent overall clutter specification capability did not exist on either the two current Doppler weather radars for which we obtained actual clutter time series data. Table 8-2 shows that the achieved suppression against a type B clutter signal on the MIT radar met or at worse was within 2 dB of the quality assurance test criteria. The use of currently available stable S-band transmitter/receivers such as are used in the ASR-8 would have permitted demonstration of the desired suppression capability experimentally.

We conclude from these simulation tests using both the theoretical clutter and weather models described in the specification and measured S-band radar data from a discrete scatterer that the specification requirements and quality assurance tests developed are achievable with currently available technology.

TABLE 8-1. CLUTTER SUPPRESSION AGAINST THEORETICAL CLUTTER MODELS
CLUTTER SUPPRESSION (dB)

Function	Usable Velocity (m/s)	Clutter Model A			Clutter Model B		
		Spec.	FIR	IIR	Spec.	FIR	IIR
Doppler	2	20	21	NS	20	23	NS
Doppler	3	28	37	NS	30	39	NS
Doppler	4	50	51	53	50	58	59
Reflectivity	-	30	31	40	30	34	56

NS = not simulated

Spec = specification in Chapter IV

TABLE 8-2. CLUTTER SUPPRESSION AGAINST MEASURED POINT CLUTTER DATA FROM MIT SITE.

Function	Usable Velocity (m/s)	Quality Assurance Test Objective	Achieved Suppression (dB)
Doppler	1	15	20 - 26
Doppler	2	23	30 - 33
Doppler	3	45	43 - 48
Reflectivity	-	25	NS

NS = not simulated

B. Recommendations for Future Work

The clutter suppression capability described in the developed specification will make a very substantial increase in the capability of NEXRAD to successfully cope with the clutter challenges described earlier. However, it must be emphasized that:

- (1) certain clutter features could not be adequately defined in the context of the present study, and
- (2) additional clutter suppression features to handle moving and/or extremely high level clutter will be necessary if NEXRAD is to achieve the desired automatic weather hazard detection capability.

Below, we briefly describe the work which needs to be done in the near term so that updated NEXRAD specifications can be generated.

1. Clutter Environment Characterization

A number of problems were encountered in processing the NSSL clutter data (e.g., frequent saturation in the A/D converters, and lack of discrete scatterer data for system assessment). It would be very desirable to obtain new NSSL tapes taking into account the experience with the initial tapes. Also, it was hoped that data from the FAA Technical Center (FAATC) could be obtained, but equipment breakdown prevented that from occurring.

The time (spectral) characteristics of anomalous propagation data are of particular concern because such clutter can obscure major portions and even all of a given "trip". Unfortunately, it was not possible to obtain such data in the summer of 1982 although requests were made to the operators of the NSSL and FAATC weather radars.

Time series measurements of clutter from forested terrain in medium-to-high level winds is of interest because the spectral characteristics will play a key role in choice of usable weather velocities (e.g., filter pass bands). Data at S-band is sparse, and there are difficulties in extrapolating data at higher frequencies (e.g., X-band) to S-band.

Measured data from other representative sites (especially, those near forests, mountains, and airports) would be very useful in defining what clutter suppression features in addition to the current specification capability will be required.

2. Implementation Issues

A number of implementation related issues were addressed in the context of this study. However, there are several issues which merit some additional investigation. These include:

- (a) refinement of the LTI filter designs for reflectivity estimation. The filter designs considered did not consider compensation for filter characteristics in assessing the requisite filter features. Also, alternative designs (e.g., minimum phase FIR filters [25]) are capable of even narrower transition bands between the stopband and passband regions, and
- (b) validation and refinement of concepts for AGC operation in the presence of clutter also needs attention. The time series clutter data from this study will be provided to the contractors to facilitate the beginning of this process.

3. Data Editing for Clutter Residue Suppression

The experiments with measured I,Q data described in Chapter VII have shown that a substantial portion of the clutter is not rejected because the clutter sources are moving to a greater extent than implied by the model in Chapter III. Experience with ATC radars in the same frequency band (Refs. 7-8) have shown that maps bounding the clutter residue levels can be very effective at preventing such clutter from yielding erroneous results at the radar output. However, studies using measured data from NEXRAD-like radars will be necessary to develop the corresponding NEXRAD specification due to the differences between the desired target and nature of clutter*.

*e.g., the MTD clutter maps take advantage of the point nature of aircraft targets, and treat the weather as clutter.

REFERENCES

1. Zrnic', D.S., and Hamidi, S. "Considerations for the Design of Ground Clutter Cancellers for Weather Radar," Report No. DOT/FAA/RD-81/72 (Feb. 1981).
2. Groginsky, H.L., and Glover, K. "Weather Radar Canceller Design," Preprints, 19th Conf. on Radar Meteor., Am. Meteor. Soc., Boston, MA, 192-201 (1980).
3. Zrnic', D.S. "Simulation of Weatherlike Doppler Spectra and Signals," J. Appl. Meteor., 14, (4), 619-620 (1975).
4. Zrnic', D.S. "Estimation of Spectral Moments for Weather Echoes," IEEE Trans. on Geosci. Elec., GE-17, (4), Oct., 113-128 (1979).
5. Nathanson, F.E., Radar Design Principles. McGraw-Hill, New York, NY (1969).
6. Barton, D.K., Radar Volume 5: Radar Clutter, Artech House, Dedham, MA (1975).
7. Karp D. and Anderson, J.R., "Moving Target Detector (Mod II) Summary Report," Project Report ATC-95, MIT/Lincoln Laboratory, FAA-RD-80-77 (Nov. 1981).
8. Karp, D., "En Route Weather Data Extraction from ATC Radar Systems," Project Report ATC-113, MIT/Lincoln Laboratory, FAA-RD-82-5 (March 1982).
9. Anderson, J.R., "Evaluating Ground Clutter Filters for Weather Radars," Preprints, 20th Conf. on Radar Meteor., Am. Meteor. Soc., Boston, MA, 314-318 (Nov. 1981).
10. Doviak, R., Zrnic' D.S., and Sirmans, D., "Doppler Weather Radar," Proc. IEEE, Vol. 67, 1522-1553 (Nov. 1979).
11. "NEXRAD Technical Requirements (NTR)," NEXRAD JSPO document R400-SP201 (30 Sept. 1982).
12. Skolnik, M., Introduction to Radar Systems, McGraw-Hill, NY (1962).
13. Popoulis A., The Fourier Integral and Its Applications, McGraw-Hill, NY (1962).
14. Childers, D. (editor), Modern Spectrum Analysis, IEEE Reprint, New York, NY (1978).

REFERENCES (Continued)

15. Harris, F., "On the Use of Windows for Harmonic Analysis with the Discrete Fourier Transform," Proc. of IEEE, Vol. 66, 51-83 (Jan. 1978).
16. Laird, B. and Evans, J., "FAA Weather Surveillance Requirements in the Context of NEXRAD," Project Report ATC-112, MIT/Lincoln Laboratory, FAA-RD-81-111 (Jan. 1982).
17. H. Krason and G. Randig "Terrain Backscatter Characteristics at Low Grazing Angles for X- and S-band," Proc. of IEEE, 1965-66 (Dec. 1965).
18. M. Long, Radar Reflectivity of Land and Sea, Lexington Books, Lexington, MA (1975).
19. D. Barton and W. Shrader, "Interclutter Visibility in MTI Systems," IEEE Eascon, 294-297 (1969) (also in [6]).
20. R. Rauch, "A Comparison of Meteorological Doppler Radars with Magnetron and Klystron Transmitters," 20th Conf. on Radar Meteor., Am. Meteor. Soc., Boston, MA 211-214 (1981).
21. L. Hennington, "Reducing the Effects of Doppler Radar Ambiguities," 19th Conf. on Radar Meteor., Am. Meteor. Soc., Miami Beach, FL, 216-218 (1980).
22. T. Parks and J. McClellan, "Chebyshev Approximation for Nonrecursive Finite Impulse Response Filters," IEEE Trans. Circuit Theory, Vol. CT-19, 189-194 (Mar. 1972).
23. R. Passarelli, P. Romanik, S. Geotis and A. Siggia, "Ground Clutter Rejection in the Frequency Domain," 20th Conf. on Radar Meteor., Am. Meteor. Soc., Boston, MA, 295-300 (1981).
24. E. Hofstetter, A. Oppenheim and J. Siegel, "A New Technique for the Design of Non-recursive Digital Filters," Proc. 5th Annual Princeton Conf. Inform. Sci. Systems, 64-72 (1971).
25. O. Herrmann and W. Schuessler, "Design of Nonrecursive Digital Filters," Electronics Letters (May 1970).
26. B. Bean and E. Dutton, Radio Meteorology, Dover Publications, New York, NY (1968).
27. Final Report on the Joint Doppler Operational Project (JDOP) 1976-1978. NOAA Technical Memorandum ERL NSSL-86, March 1979.

APPENDIX A - TECHNICAL CHARACTERISTICS OF THE MIT RADAR

The S-band weather radar at the MIT Meteorology and Physical Oceanography Department was used to obtain the bulk of the clutter data presented in the preceding chapters. The radar is located atop the Green Building at MIT at an altitude of approximately 300 feet above ground level. Figures 2-2 to 2-6 show the site features. Table A-1 shows the principal technical characteristics. This radar was derived from an FPS-18 with no special measures taken to substantially reduce power line harm on the high voltage supply.

The clutter amplitude measurements shown in Figures 2-7 to 2-13 were accomplished by merging the pulse pair reflectivity estimates with a 10-bit A/D converter at several fixed receiver gains. The I,Q time series were measured with a (new) 12-bit A/D converter using an R^{-2} STC law which resulted in 1 digital level corresponding to +10 dBz reflectivity for all ranges shown here. To minimize the acute spectral broadening which can occur with "hard" clipping at the A/D converter upper and lower limits, an IF amplifier is used which smoothly limits the A/D inputs to ± 0.9 of the full A/D converter range. Figure A-1 shows the transfer function of this IF amplifier.

Since the MIT radar two-way beamwidth is 45% larger than the NEXRAD beamwidth, the I,Q time sample data was taken at scan rates which are 45% faster than the corresponding NEXRAD scan rates so as to keep the dwell times constant.

TABLE A-1. MIT TESTBED RADAR CHARACTERISTICS.

Antenna

Aperture	18 feet
Gain	42 dB
Sidelobe Levels	-26 dB minimum
Beamwidth	1.45° one-way
Polarization	horizontal
Maximum rotation rate	6 r.p.m. (both axes)
Height	312 ft. above m.s.l.

Transmitter

Source	VA87 klystron
Frequency	2705 MHz
Peak Power	1 MW
Pulse Width	1 microsecond
PRF	Variable (1200 Hz max.)

Receiver

Pre-selector	tunable cavity
RF amplifier	solid state
Noise figure	4 dB
STALO	crystal controlled
COHO	30 MHz crystal
Bandwidth	1.1 MHz
STC	PIN diode at RF
STC curve	Programmable
MDS	-103 dBm

Digital Signal Processor

A/D Converters	12 bits I; 12 bits Q
Range sample spacing	1/16, 1/8, 1/4, 1/2 n.m.
Number of range gates processed	288
Algorithm	pulse-pair processing
Processor output	0th, 1st, 2nd moments or I,Q time series

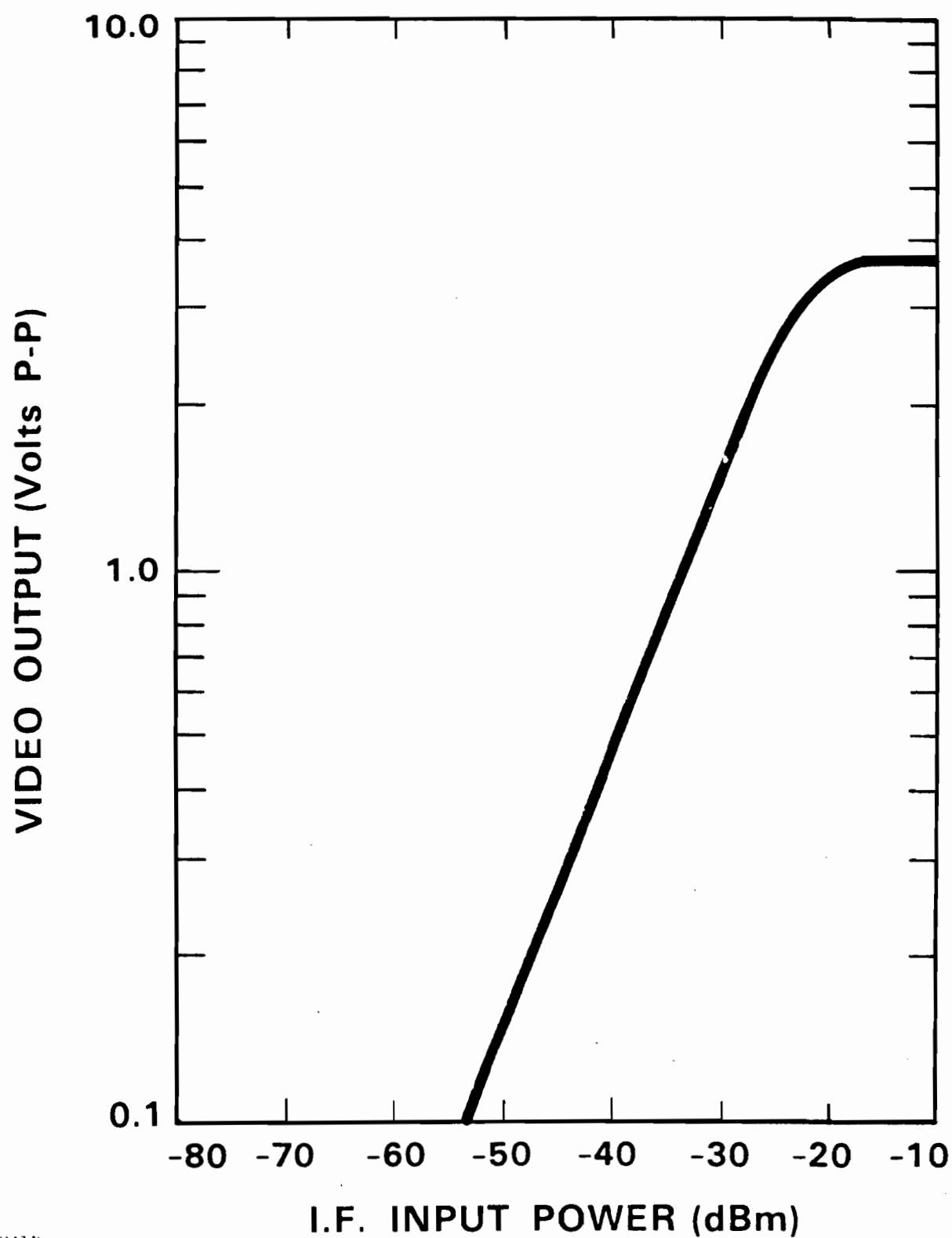


Fig. A-1. IF Amplifier Characteristic.